SOLVENT-INDUCED MODIFICATIONS OF THE MORPHOLOGY AND SOLID-STATE PROPERTIES OF IBUPROFEN

Jill M.E. Bunyan

A thesis presented for the degree of

Doctor of Philosophy

in the Faculty of Science of the

University of Strathclyde

Department of Pharmaceutical Sciences
School of Pharmacy and Pharmacology
University of Strathclyde
Glasgow

August 1992

To A.P.

without whom this would

not have been possible.

ABSTRACT

The effect of crystallisation solvent on crystal morphology and mechanical properties of ibuprofen was studied. Intermolecular potentials were calculated to assess the relative growth rates of crystal faces of ibuprofen. Comparison of the predicted morphology with solution-grown crystals clarified the interaction of solvent with the growing crystal. Single crystal dissolution and x-ray techniques indicated that crystals grown from non-polar solvents were more strained. In conjunction with solution NMR results (which showed differences in molecular association in solvents of varying polarity) this led to two different growth mechanisms being proposed. The crystal structure of resolved S(+) ibuprofen confirmed that enantiomeric dimers present in non-polar solvents could act as additives, selectively decreasing the growth rate at specific crystal faces, and introducing lattice strain. Deformation processes of ibuprofen did not appear to be changed by the solvent of crystallisation. However, crystals grown from non-polar solvents fractured readily. In conjunction with the unfavourable acicular morphology this is likely to be a source of processing problems of industrially produced crystals.

ACKNOWLEDGEMENTS

I thank the Science and Engineering Research Council for financial support, and providing time on the SRS at Daresbury Laboratory.

I would also like to thank: Dr.David Sheen, for supervision and advice; Dr.Andrew A. Freer, Department of Chemistry, Glasgow University, for carrying out single crystal x-ray diffraction work; colleagues and friends in the Physical Chemistry Department for their advice and support; my parents, Mr. and Mrs.G.J.Bunyan for their moral (and as always, financial!) support, and, in particular, Dr.Alan Pearson, who helped in far too many ways to mention.

SYMBOLS USED

a	Directional vector used to define crystal lattice
A	Area supporting applied tensile force
A_i	Area of face i
b	Directional vector used to define crystal lattice
$\underline{b}$	Burgers vector of a dislocation
c	Directional vector used to define crystal lattice
C	Concentration in bulk solution
C_i	Equilibrium concentration in interfacial layer
C_p	Polarisation factor
C_s	Equilibrium concentration in a saturated layer
d_{hkl}	Spacing between two consecutive lattice rows
d_{SF}	Sample to film distance
D	Diffusion coefficient
D_{elec}	Dielectric constant
E_{att}	Attachment energy
E_l	Line energy of a dislocation
E_{sl}	Slice energy
ΔE	Cohesive energy of solvent
ΔE_D	Contribution to ΔE from non-polar interactions
ΔE_H	Contribution to ΔE from hydrogen bonding
ΔE_p	Contribution to ΔE from permanent dipole interactions
F	Applied tensile force
F_{hkl}	Structure factor
h	Thickness of stationary layer around dissolving crystal

(hkl)	Crystal face or lattice plane
{hkl}	Crystal form, compromising all faces equivalent by symmetry to (hkl)
ΔH_f	Enthalpy of fusion
ΔH_s	Enthalpy of sublimation
ΔH_v	Enthalpy of vaporisation
k	Boltzmann constant
k_{obs}	Observed rate constant
k_r	Rate constant for surface reaction
k_t	Transport rate constant
KHN	Knoop hardness number
K_{obs}	Observed apparent rate constant
$\underline{l}$	Line direction of a dislocation
L	Change in free energy on crystallisation
n_s	Number of nearest neighbours in surface layer
n_t	Total number of nearest neighbours
N_C	Crystal density
N_s	Solubility
PBC	Periodic Bond Chain
q_i	Fractional charge on atom i
R	Gas constant
S	Surface area of solid
T	Absolute temperature
T_m	Melting point
T_R	Roughening temperature
u	Shear modulus of a dislocation
[uvw]	Crystal edge or zone axis or lattice row
<uvw>	All edges, zones axes or lattice rows equivalent

	by symmetry to [uvw]
V	Molar volume of solvent
V_c	Unit cell volume
V_{elec}	Electrostatic contribution to the intermolecular interaction
V_{VDW}	Contribution of Van der Waals interactions to the intermolecular interaction
$x_{s.eq}$	Ratio of solubility to crystal density
z	Number of asymmetric units per unit cell
α	Angle defining unit cell
α_J	Jackson a-factor
β	Angle defining unit cell
δ_D	Dipole parameter of solvent
δ_H	Hydrogen-bonding parameter of solvent
δ_P	Non-polar parameter of solvent
ξ_g	Extinction distance
γ	Angle defining unit cell
λ	Wavelength
η	Mosaic spread or lattice strain
ς	Crystallographic anisotropy factor
σ	Supersaturation
σ_i	Specific free energy of face i
Φ	Surface free energy
Φ_{inter}	Intermolecular contribution to crystallisation energy
Θ_B	Bragg angle
$d\Theta^{1/2}$	Rocking curve width

τ_e Resolved shear stress

τ_e' Effective resolved shear stress

μ Linear x-ray absorption coefficient

$(\mu_a)_i$ Atomic absorption coefficient of atomic species i

λ (eqn 2.11) Angle between tensile axis and slip direction

ϕ (eqn 2.11) Angle between tensile axis and slip plane

ψ (eqn 2.11) Angle between indenter facet and axis of rotation

γ (eqn 2.11) Angle between indenter facet and slip direction

CONTENTS

List of Figures

List of plates

List of Tables

INTRODUCTION

1 INTRODUCTION

It is increasingly recognised that solid-state properties of pharmaceutical materials are of great importance in determining their processing behaviour. In particular, with the development of high-speed tableting equipment, the selection of materials with good flowability and which compress readily to form strong compacts is of prime importance. In many cases, use of suitable excipients is possible, but where the drug compound is present in high proportions, the solid-state properties of the active material itself are critical.

The term "crystal engineering" has been coined to describe development of crystalline materials with morphological and mechanical properties appropriate to their required function. In general, manipulation of solid-state properties is carried out at the crystallisation stage, since it is at this point that properties such as polymorphic form, crystal morphology, and defect structure are determined. Later processing operations such as comminution can also be utilised to alter solid-state properties, but acquisition of the suitable qualities at the crystallisation stage eliminates the need for such additional steps.

Alteration of crystallisation conditions can therefore be used to manipulate crystal properties, for example by change of crystallisation temperature, solvent, or use of face-specific growth inhibitors for

habit modification. In order to do so in a controlled manner, the crystal structure must be studied and potential interaction sites determined. A recent patent stated "there are no known means of predicting which solvent would result in a given, desirable crystal habit" [1]. Other workers have however been successful in designing chemical additives which did alter crystal morphology in a predictable way [2,3,4]. There is therefore scope for extending this work to determine the effect of an alteration in crystallisation solvent on crystal morphology.

One drug compound associated with a number of processing problems which derive from its crystal morphology is ibuprofen, [2-(4-isobutylphenyl)propionic acid]. It is crystallised on an industrial scale from hexane, giving elongated acicular crystals. However, this shape is not well suited to tableting and there is a history of problems associated with compaction of ibuprofen. In general, crystals of a rod or needle-like habit exhibit poor flow characteristics, as does ibuprofen, which also may adhere to the faces of tablet punches and dies during compression, and tablets produced may laminate during decompression [1]. These problems are thought to be due at least in part to the crystal morphology.

Ibuprofen compacts have been observed to undergo strain recovery on storage (expansion of compacts in both radial and axial directions), even at low levels of

humidity [5]. This can eventually lead to capping on storage or splitting of the tablet coating. This may be due to the brittle nature of ibuprofen, forming relatively weak compacts especially in comparison with lactose and other materials which deform plastically [6].

Ibuprofen, in common with other non-steroidal anti-inflammatory drug compounds (NSAIDs), is present as a very high proportion of the tablet bulk, thus its solid-state properties are critical in determining the mechanical behaviour of compacts.

It was found empirically [1] that equant crystals with improved flow and compaction properties can be obtained by changing the solvent of crystallisation from hexane to methanol. The claim of more cost-effective processing due to reduced pharmaceutical production down-time (due to decreased sticking of tablets to punches and dies) is of great importance since the product commands such a large share of the world market. The crystals produced are of relatively larger particle sizes and increased bulk density compared to those recrystallised from hexane, which may also contribute to the change in compactibility. However, the authors did not investigate the possibility that the internal structure and mechanical properties of the crystals also differed, despite noticing changes in other associated properties of the crystals - a decrease in the tendency of the material to sublime, and altered dissolution rates.

Although the crystal structure of ibuprofen is known, no studies characterising growth mechanism or morphology have been carried out, so it is unclear how methanol changes crystal shape. In fact, reference (1) lists twenty other solvents which, used alone or in combination, are claimed to yield the equidimensional or hexagonal morphology. A study of the factors influencing the morphology of ibuprofen is therefore of interest in its own right in addition to possible variation in solid-state properties induced by the changes in crystallisation conditions.

1.1 OBJECTIVES

The objectives of this work were twofold. The first objective was to characterise the effects of solvents on the crystal morphology, by growing larger crystals than those produced commercially, in order that the morphology could be more readily studied. Secondly, the influence of a change in crystallisation solvent on the hardness, reactivity and mechanical properties of ibuprofen crystals, and the mechanisms by which any variation occurred, were also of interest.

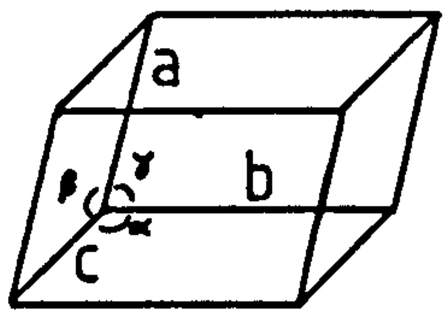

Figure 1.1: A crystal space lattice

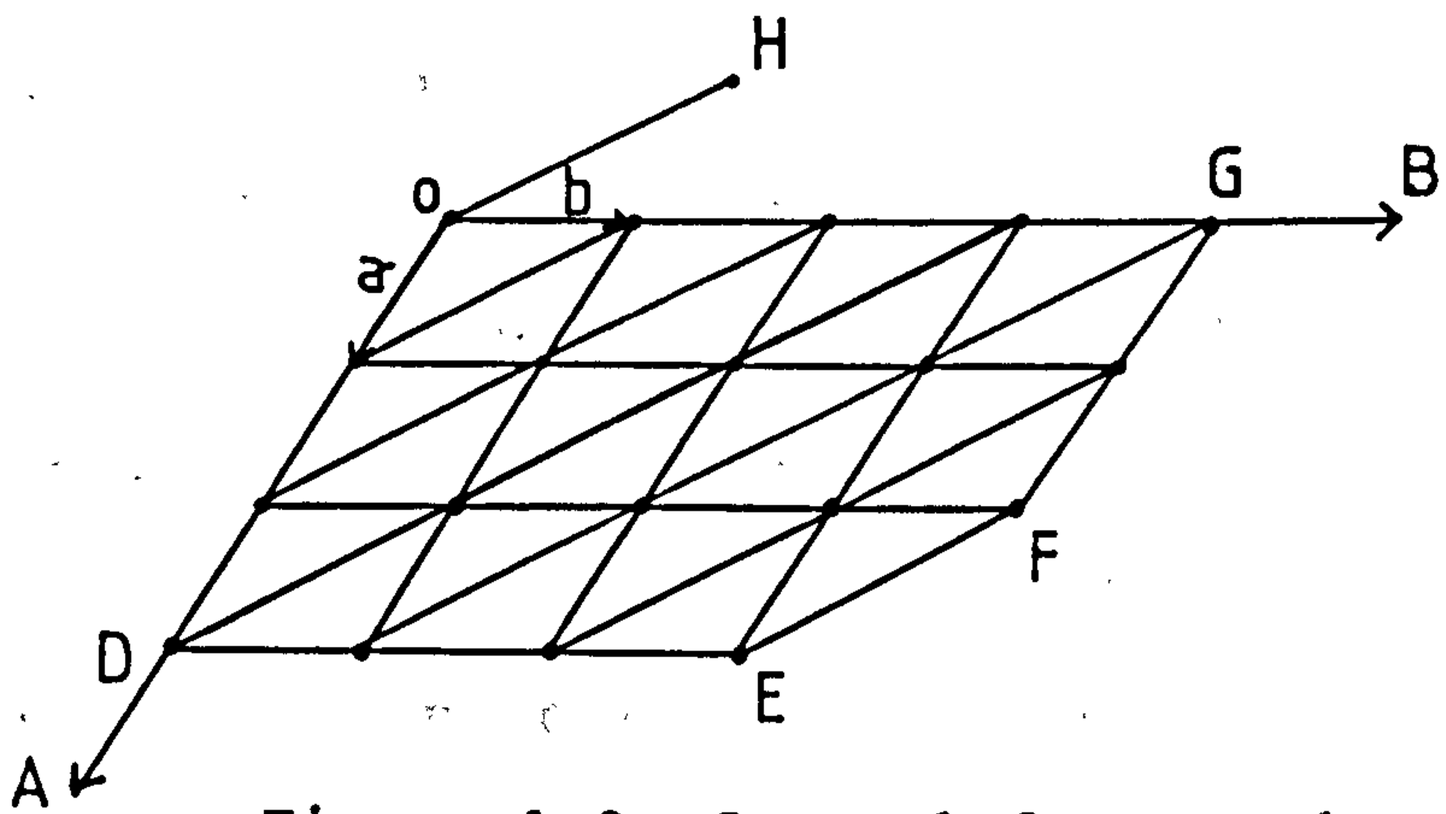

Figure 1.2: Crystal faces and net planes

1.2 CRYSTAL GROWTH AND MORPHOLOGY

Crystal structures consist of regular periodic arrays of lattice points, each having by definition the same local environment. In molecular crystals these lattice points are associated with one or more molecules (which make up the repeating or asymmetric unit) the conformation of which is repeated at equivalent lattice points by the operation of various symmetry operators (reflection, rotation, or translation). The array of translation equivalent points in a three dimensional structure makes a space lattice normally defined by the smallest and least oblique parallelepiped which has the full symmetry of the lattice (the unit cell), defined by the directional vectors a, b and c, and the included angles α, β and γ (figure 1.1).

A crystal lattice can be regarded as infinite in extent, with order that extends in three dimensions. Crystal planes are denoted by Miller indices (hkl). These are illustrated in figure 1.2 which shows a portion of a crystal. The shortest horizontal lattice repeats are a,b and therefore the row lines OA, OB are taken as axes. The third axis OC is vertical. The crystal is bounded by vertical faces DE, EF, and FG. Face DE is parallel to the plane of a net that cuts axis OA at a distance a from O and is parallel to axes OB and OC; it may be denoted by coefficients $1\infty\infty$ of the intercepts 1a, ∞b, ∞c (Weiss coefficients). Similarly

face FG may be denoted by ∞1∞ and EF by 11∞. Integers proportional to the reciprocals of these coefficients (Miller indices) are more convenient to use and these are now universally accepted in geometrical and x-ray crystallography. Table 1.1 contains the Miller indices for the faces described.

Face	Weiss coefficient	Miller indices
OD	∞1∞	(010)
DE	1∞∞	(100)
EF	11∞	(110)
FG	∞1∞	(010)
GO	1∞∞	(100)

TABLE 1.1: WEISS COEFFICIENTS AND MILLER INDICES OF CRYSTAL FACES ILLUSTRATED IN FIGURE 1.2.

Directions within a crystal system are also described in terms of directional vectors a, b and c. For example, row EF in figure 1.2 is parallel to the row line OH joining origin O to lattice point H whose coordinates are -a,b,0. These coordinates are used as indices to designate the row direction, which is [110].

Due to the long-range order present within the crystal, crystal planes will always be at the same interfacial angles to each other provided the internal

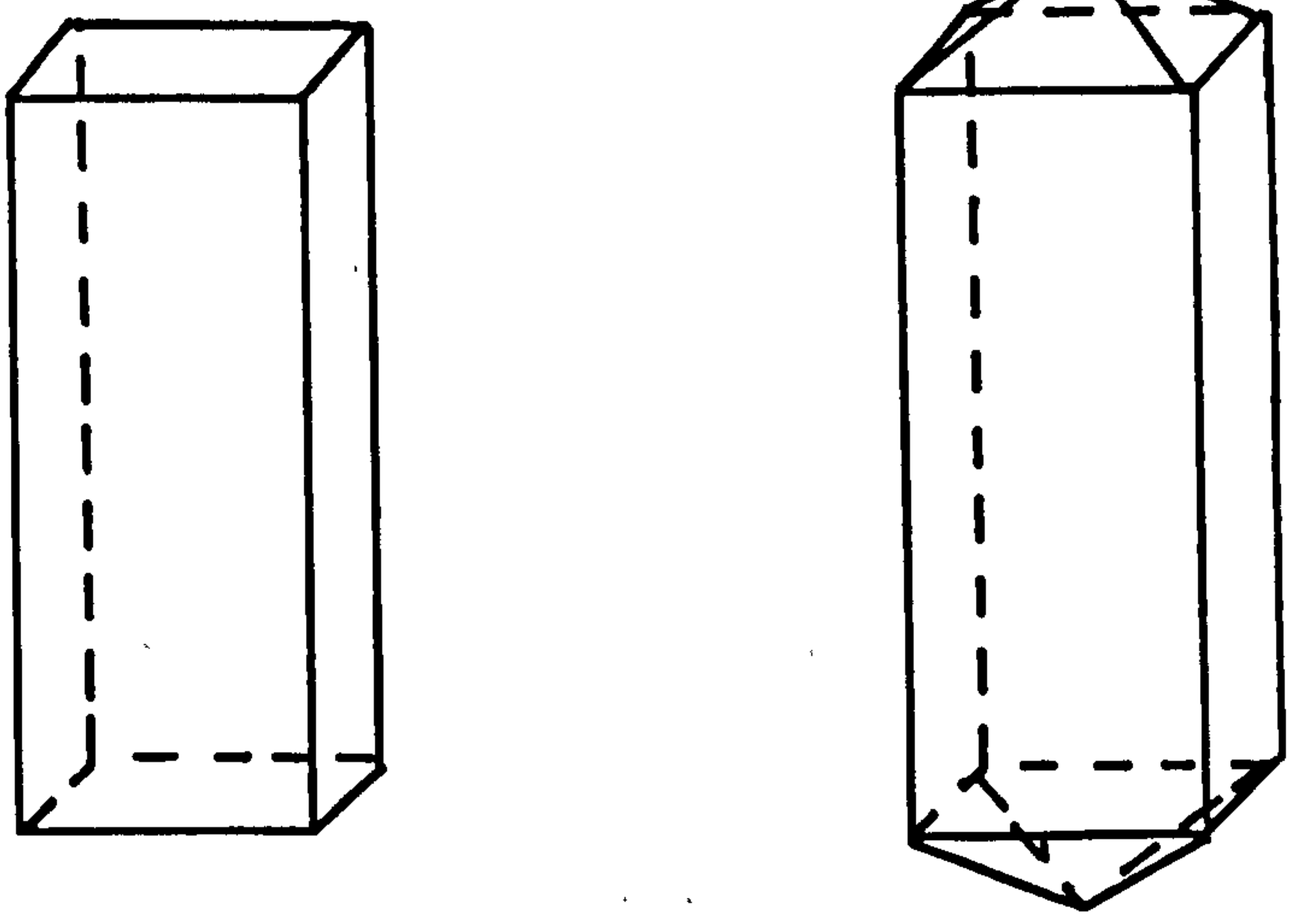

Figure 1.3: Crystals showing the same habit but different combination of forms

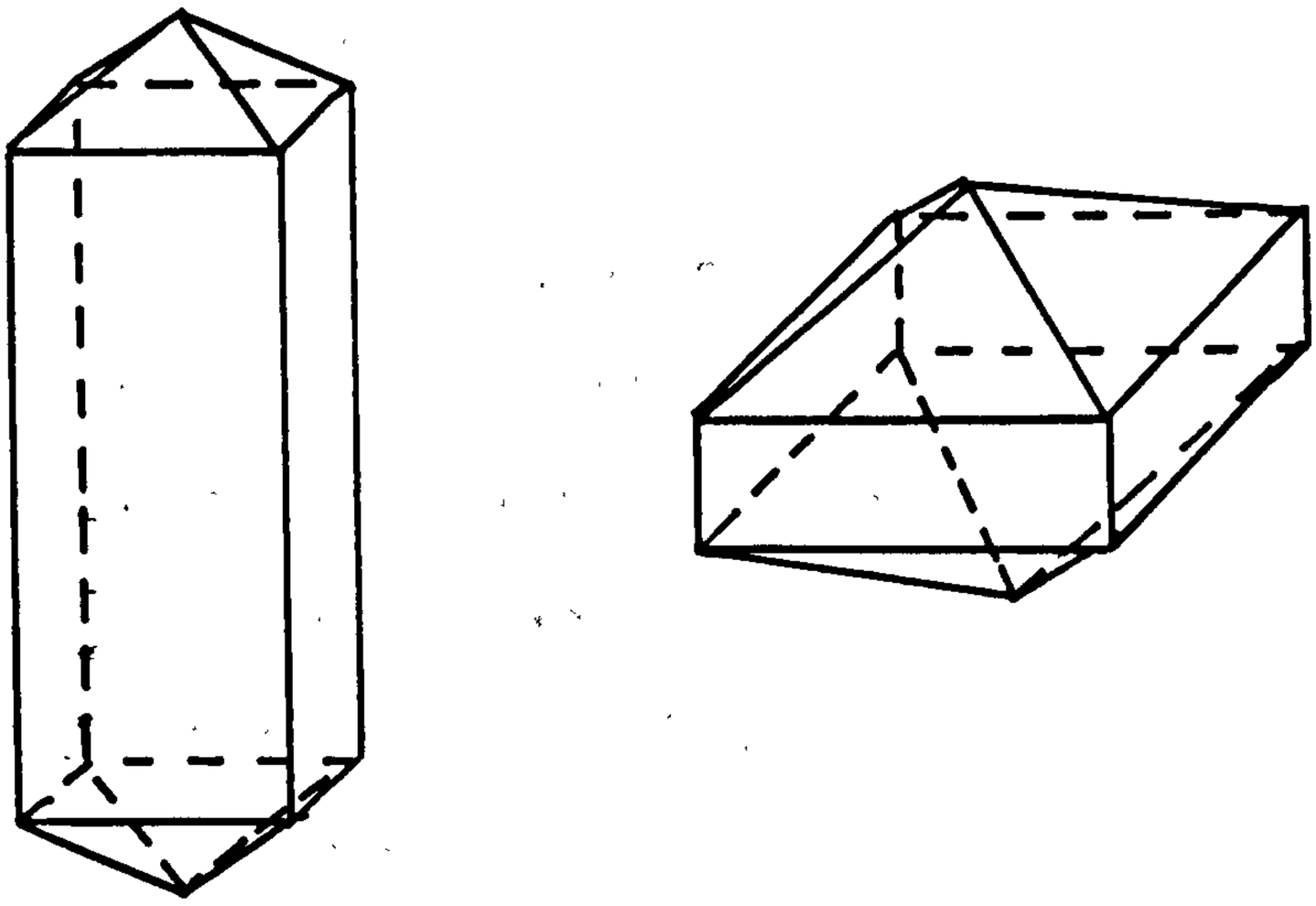

Figure 1.4: Crystals showing the same combination of forms but different habit

structure remains constant. The external appearance of a crystal is described in terms of its overall shape (or habit) and/or the combination of faces (forms) displayed. The difference between these terms is illustrated in figures 1.3 and 1.4.

Stereographic projections are often used to assist in identification of crystal planes or forms. These are representations on a plane of projections of face normals or crystal directions onto the surface of a sphere surrounding the crystal. Further details of the construction of a stereographic projection can be found in reference (7). Figure 1.5 shows the construction of a stereographic projection. C is the centre of the crystal and of a sphere, radius r, with a reference axis SCN vertical. CD is the trace of the horizontal plane through C; this is the plane of the projection. CP denotes a face normal meeting the surface of the sphere at P. The line joining PS cuts plane CD at Q, the stereographic projection point (or pole) of the crystal face. If the face normal makes angle x with the vertical, the stereographic distance CQ = r.tan(x/2). When x=90° the stereographic pole is on the equatorial circle. When x>90° as for CP′, the stereographic pole is outside the projection. Interfacial angles can therefore be calculated from stereographic projections, or more simply by use of a Wulff net such as the one illustrated in figure 1.6, in which the lines are drawn at 2° intervals. The program STEREO [8] on the VAX

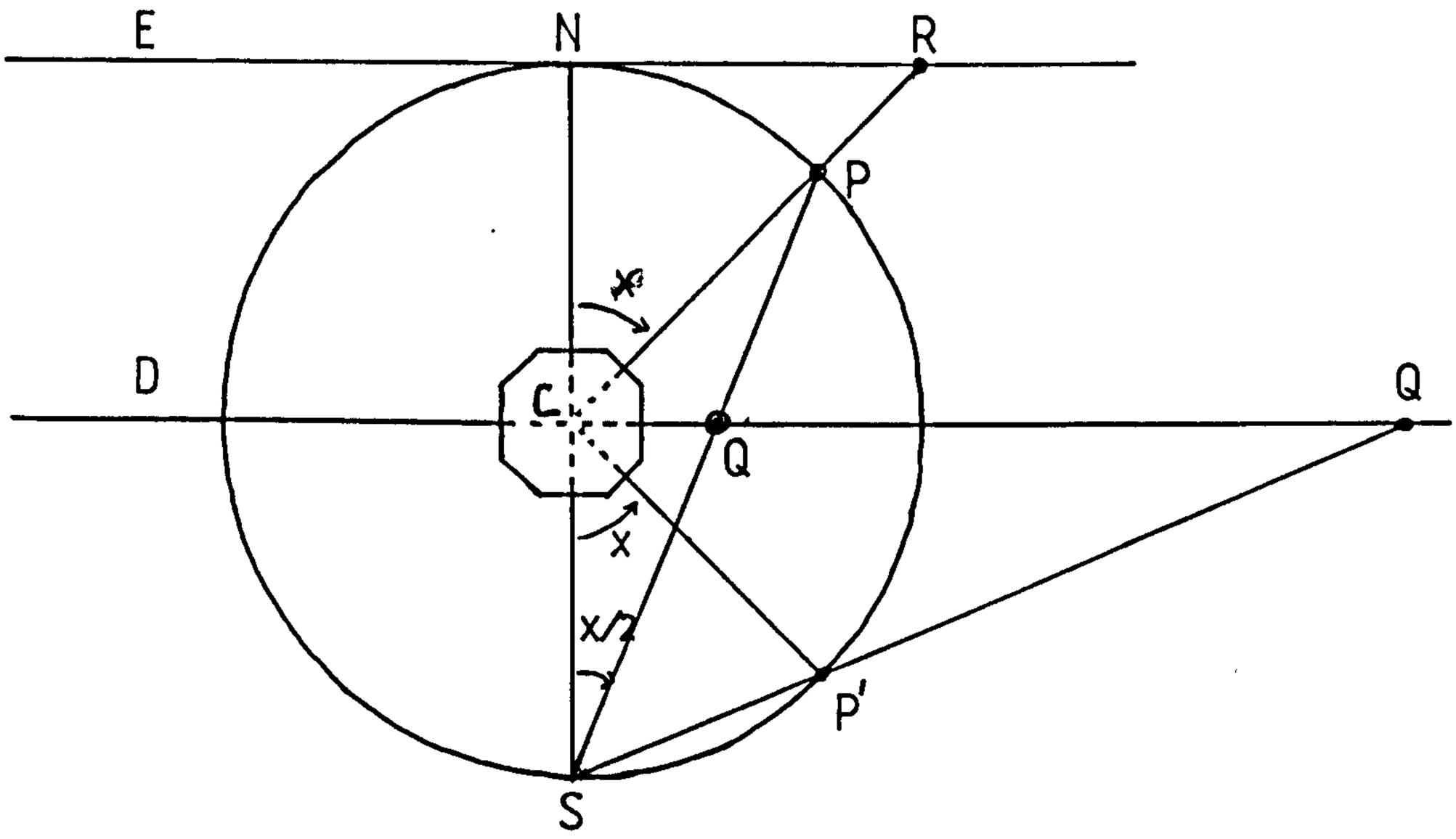

Figure 1.5: Construction of the stereographic projection

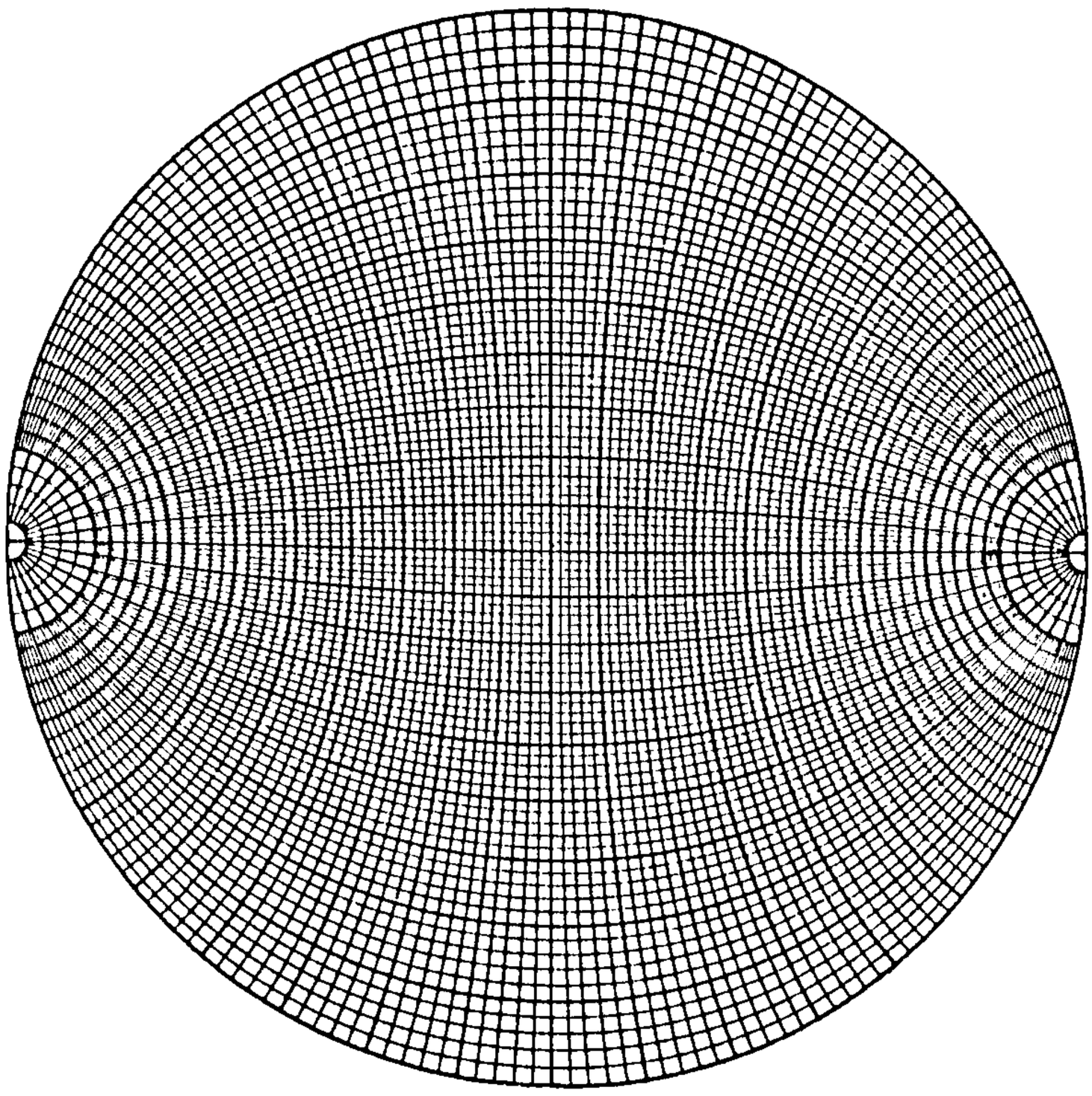

Figure 1.6: A Wulff net

computer at Strathclyde University was used in this work to draw stereographic projections when required (see section 2.4.1).

1.2.1 Crystal Growth

Crystals can be grown by a variety of techniques, the selection of which is dependent on the properties of the material and the end-use of the crystals.

1. Melt growth: Crystals grown by slow cooling of the molten material. Large, good quality crystals can be produced where the melt is stable over the growth period. The morphology of the resulting crystals is generally dependent on the shape of the vessel.

2. Solution growth: Crystal quality is dependent on selection of appropriate growth conditions, but good purity and face development can be obtained as can relatively low dislocation density. The morphology can be affected by the degree of supersaturation, solvent interactions and the rate of cooling or evaporation. Large crystals can in principle be grown by this technique, limited partly by the size of the vessel.

3. Vapour growth: controlled sublimation of the material takes place in a hot zone in the vessel. The vapour diffuses to cooler regions where nucleation can take place. In this case, the morphology is independent of any solvent interactions.

4. Gel growth: Nucleation and growth of small crystals, usually of high purity, occurs by controlled interdiffusion of solutions of two or more materials, either as a controlled reaction or 'salting-out' effect.

A more complete review of crystallisation techniques can be found in B.R.Pamplin (1980) Crystal Growth, 2nd edn., Pergamon Press, Oxford or J.W.Mullin (1961) Crystallisation, Butterworths, London.

Crystallisation of pharmaceuticals on an industrial scale is normally carried out by rapid precipitation of materials from solution as it is usually the most cost-effective technique. Crystals are easily separated from the growth liquor by filtration and drying to evaporate any entrapped solvent. In this work, the influence of solvent on the growth form of ibuprofen is of interest, so only growth of crystals from solution or vapour phase (to determine the morphology in the absence of solvent) will be further considered.

1.2.1.1 Generation of Supersaturation and Formation of Nuclei

The driving force for crystal growth is supersaturation, whether growth is taking place from solution or the vapour phase. Supersaturation can be achieved by addition of a non-solvent (resulting in precipitation of the dissolved material), evaporation of the solvent from a solution or by cooling of a saturated solution or vapour. Supersaturation alone is not sufficient to induce crystal growth - stable nuclei must also be formed before growth can proceed.

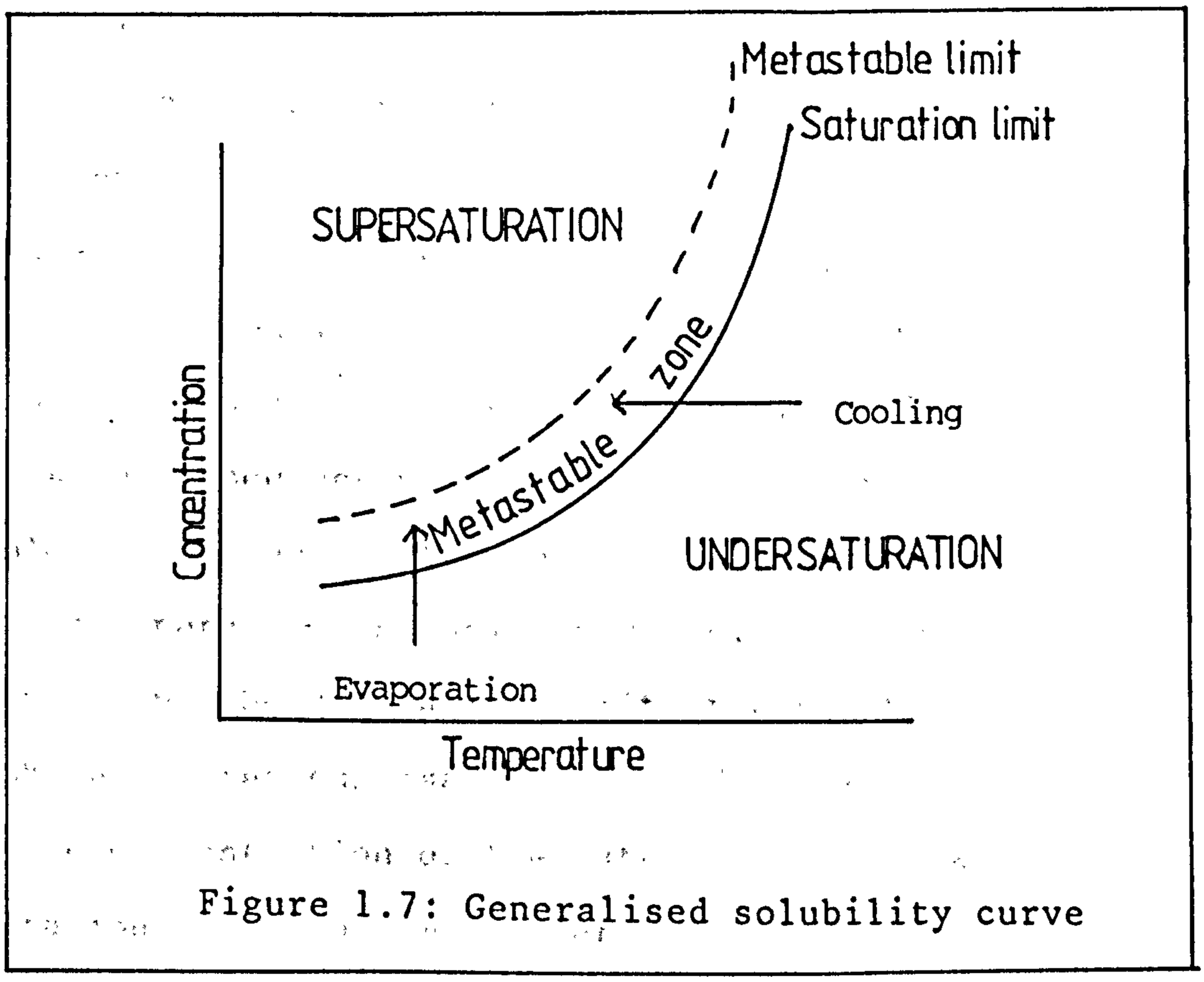

Figure 1.7: Generalised solubility curve

The formation of nuclei takes place randomly, as molecules in solution are attracted to each other by hydrogen-bonding or weak electrostatic interactions. As supersaturation is increased, the probability of molecular collisions will increase. Random association and disassociation of the molecules occurs, but beyond a critical size it becomes more thermodynamically favourable for the nuclei to continue to grow. Figure 1.7 shows a generalised solubility curve. As a solution is cooled beyond the saturation limit, the solution or vapour phase becomes supersaturated. In this metastable region, the concentration of the material remains above the saturation limit, but molecular collisions are not frequent enough to induce nucleation. A seed crystal introduced at this point would, however, immediately start to grow. Once a critical point (the metastable limit) is reached, where it is more thermodynamically favourable for the loose associations of molecules to continue to grow rather than dissociate, nucleation will take place. The size of the molecular aggregates formed is such that their excess free energy is less than that of the molecules in solution, leading to an overall decrease in the free energy of the solution as nucleation takes place. When the solution is cooled too quickly, nuclei do not have time to form and a supercooled liquid phase, may be produced.

Homogeneous nucleation takes place when collisions between molecules are frequent (ie in the situation

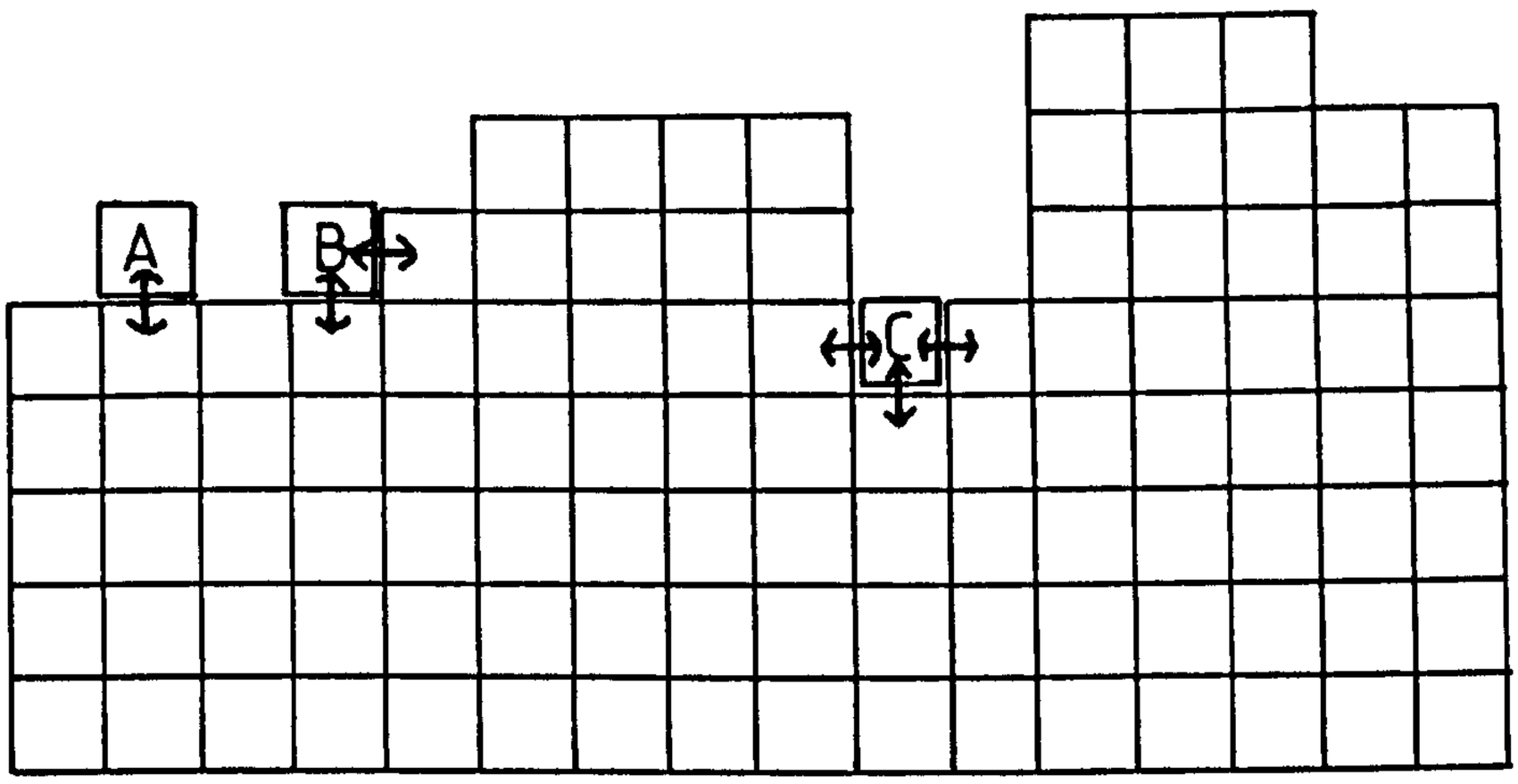

Figure 1.8: Attachment of crystallising units to growing crystal surface

described above). Heterogeneous nucleation takes place at lower levels of supersaturation, when molecules condense onto surfaces (not nuclei of the crystallising material) available in solution eg dust, glass spicules or seed crystals of another substance. In practice it is very difficult to guarantee a solution is free from foreign particles.

Subsequent growth of the nuclei or of seed crystals introduced into the solution or vapour is dependent on transport of new molecular units to the growth interface, and will only occur while the solution or vapour is maintained at or above saturation point.

1.2.1.2 Crystal Growth Mechanisms

The growth of a crystal involves the transport of molecules from the crystallising medium (whether vapour, solution or melt) to the crystal surface, diffusion on the surface to a suitable site, and incorporation into the surface. The probability that a molecule will become attached to the surface is dependent on the amount of energy that will be released during this reaction, and this in turn is dependent on the nature of the surface. Considering a two-dimensional representation of a crystal as shown in figure 1.8, a molecule becoming attached to an atomically smooth surface (position A) can form bonds with only one nearest neighbour. On a

rough surface, bonds may be formed with two (step sites) or three (kink sites) nearest neighbours. B and C respectively represent step sites and kink sites. A rough surface will therefore exhibit faster growth rates. However it is not energetically favourable for crystal surfaces to be rough, as discussed in the following section.

1.2.1.2.1 Equilibrium Forms

In the following theoretical consideration of crystal growth, it is assumed that crystal morphology is only dependent on the internal structure of the crystal, as may be expected in growth of crystals from a slightly supersaturated vapour. In most cases the actual growth form of a crystal may differ significantly from the thermodynamic equilibrium form which is predicted from the above assumption, but nevertheless knowledge of the equilibrium form can be of use when determining the effects of the growth environment on crystal shape.

The equilibrium form is subject to Gibbs' rule [9] which requires that the crystal be bound by a surface having the minimum surface free energy:

$$\Phi = \Sigma \sigma_i A_i = \text{minimum} \qquad (1.1)$$

where σ_i is the specific free energy of the i^{th} face,

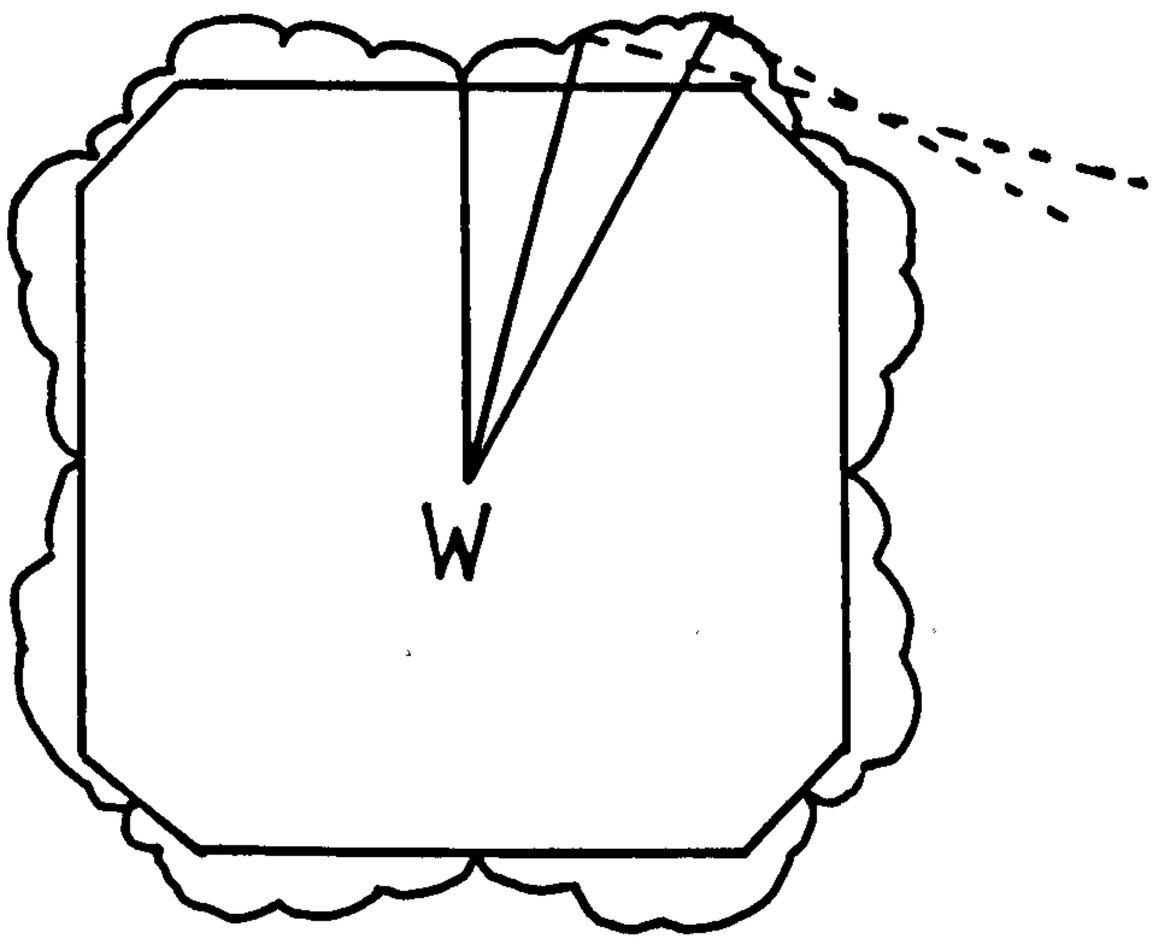

Figure 1.9: Construction of the equilibrium form according to the Gibbs-Wulff relationship, using the Herring construction

and A_i its area. If face normals are drawn from a point inside the crystal, termed the Wulff point (W in figure 1.9), their lengths made proportional to σ_i and the faces drawn as infinite planes through the ends of the normals, then the innermost complete body is the equilibrium form [10]. In the absence of an accessible method for calculating surface free energy, a number of different methods of determining equilibrium morphology have been developed.

We can conclude from the Gibbs-Wulff relationship that the slowest growing faces have a low surface free energy, a condition favoured by close packing of the molecules. This leads to a high interplanar spacing (d_{hkl}) since the unit cell volume remains the same. The geometrical laws of Donnay and Harker [11] are derived using similar reasoning. They concluded that the most important crystallographic faces {hkl} will have the greatest d_{hkl} values taking into account sub-multiples of the interplanar spacing due to space-group symmetry (ie centring, screw axes, glide planes). These rules still provide a good initial guide for identifying the crystal faces likely to dominate the morphology.

Geometric models do not consider the nature of inter-molecular bonding within the crystal structure, which can increase the rate of crystal growth in specific directions. The work of Hartman and Perdok [12,13] attempted to quantify crystal growth theory in

terms of the interaction between crystallising units.

The surface free energy terms were replaced by the surface energies [14], thus only bond energies needed to be taken into account. It was concluded that the morphology of a crystal is governed by chains of strong bonds (periodic bond chains or PBC's) running through the crystal structure.

The attachment energy (E_{att}), defined as the bond energy released when one crystallising unit is attached to the surface of a crystal face, replaces the surface energy term, which is therefore calculated from the strengths of the unfilled bonds left at the crystal surface. Assuming that the time required for a bond to form will decrease with increasing bond energy, the displacement velocity of a face will increase as E_{att} increases. The attachment energy of a crystal face will therefore be representative of its morphological importance [15] and can be used as a measure of growth rate. Flat (F) faces, where the PBC's are parallel to the surface will grow most slowly and so dominate the morphology; Stepped (S) faces will be of lower importance; Kinked (K) faces are very rare or do not occur at all, since the PBC's are protruding from the surface.

It should be noted that for a crystal to grow in the direction of a strong bond, these bonds must form an uninterrupted chain through the structure. If a bond chain contains different types of bonds, the strength of

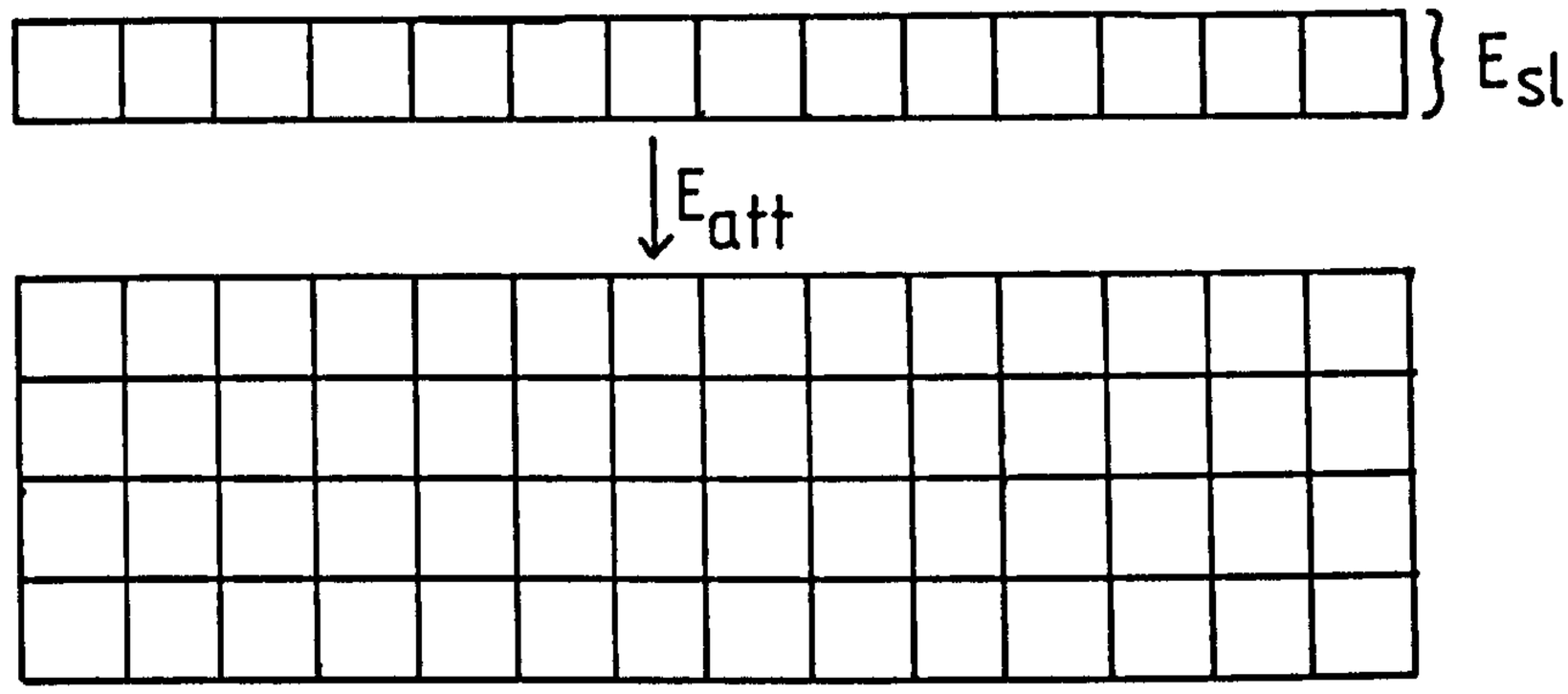

Figure 1.10: Illustration of slice and attachment energies

the weakest bond determines the influence of the PBC.

Another concept resulting from the PBC theory is that of the slice energy (E_{sl}) or layer energy, that is, the energy released on the formation of a layer of molecules of thickness d_{hkl} [15], this is complementary to the E_{att} such that :

$$\Phi_{inter} = E_{att} + E_{sl} \qquad (1.2)$$

where Φ_{inter} is the intermolecular contribution to the crystallisation energy. Both terms are illustrated in figure 1.10.

A variation on the PBC approach was developed [3] to predict morphologies of a number of carboxylic acids. It was assumed that crystal growth could be approximated by a layer mechanism, with the oncoming layer, of thickness d_{hkl}, having the same structure as the bulk crystal. Relaxation of the bulk structures at the crystal surfaces has been shown for naphthalene but the general pattern of the structure was the same as the bulk crystal [16,17].

Atom-atom potential calculations were used to estimate slice and attachment energy terms. E_{sl} was calculated as a pairwise summation of interactions between a central molecule in the slice and all surrounding molecules within the slice; E_{att} was the sum of the interactions between the same molecule and surrounding molecules outwith the slice.

Various authors have derived atom-atom potential parameters to describe intermolecular interactions in different classes of compounds. These can be considered in terms of electrostatic, Van der Waals attractive and repulsive contributions, and, if applicable, a hydrogen-bonding contribution.

The electrostatic contribution is commonly described by a simple coulombic interaction

$$V_{elec} = q_i.q_j / D_{elec}.r \qquad (1.3)$$

where q_i and q_j are the fractional charges on atoms i and j separated by distance, r. D_{elec} is the dielectric constant.

Non-bonded Van der Waals interactions can be described by a number of potential functions, all of which have the same general form, including attractive and repulsive contributions. Two of the most common are:

$$V_{vdw} = -A / r^6 + B / r^{12} \qquad (1.4)$$

a Lennard-Jones 6-12 potential function, and

$$V_{vdw} = -A / r^6 + B \exp(-C.r) \qquad (1.5)$$

a Buckingham 6-exponential function, where r is as defined before. A, B and C are constants, determined by the interacting atoms, and are known as the potential

parameters.

A rough estimate of Φ_{inter} can be obtained from [18] the sublimation enthalpy ΔH_s:

$$\Phi_{inter} \approx -2RT - \Delta H_s \qquad (1.6)$$

and used to check the accuracy of lattice energy calculations performed using potential sets. Atom-atom potential functions such as those described, are generally applicable only to the types of chemical compounds from which they are derived. Accuracy in calculation of Φ_{inter} alone is a poor guide to the usefulness of a potential set to predict the equilibrium morphology, as it is possible to obtain reasonable values for Φ_{inter} with a potential set which produces large discrepancies in the original unit cell parameters when used to determine the minimum energy crystal structure [19]. A potential set should be found such that the minimum in lattice energy occurs at the experimental crystal structure.

If these conditions are fulfilled, then the potential function used may be expected to give reasonable values for E_{att} (these are difficult to verify experimentally due to the difficulty in calculating surface energies).

1.2.1.2.2 BCF Theory

Molecules attaching to a crystal surface are more likely to be incorporated at a rough interface than a smooth one. However, the Gibbs-Wulff and Hartman-Perdok approaches both indicate that the most stable faces are molecularly smooth. Once one molecule attaches to the surface, subsequent molecules may attach themselves more readily to the step formed, being able to form bonds with two nearest neighbours. Growth would then occur relatively rapidly until the surface was once more flat, as illustrated in figure 1.11. A cluster of molecules of critical radius must be formed before a stable nucleus can begin to grow. This two-dimensional nucleation is therefore the rate determining step in the birth-and-spread mechanism, in a manner analogous to the formation of critical nuclei in a supersaturated solution.

The activation energy of formation of a two-dimensional nucleus on a completed surface layer was derived by Burton, Cabrera and Frank [20] (hence BCF theory). It was found that at relatively low supersaturations, no growth should be observed on a perfect crystal since the free energy required was so high that such a process was highly improbable (except under conditions of high supersaturation or low solid/solution interfacial tension). Additionally, observed growth rates were much higher than would be expected if the crystal surfaces were perfect [21]. It was

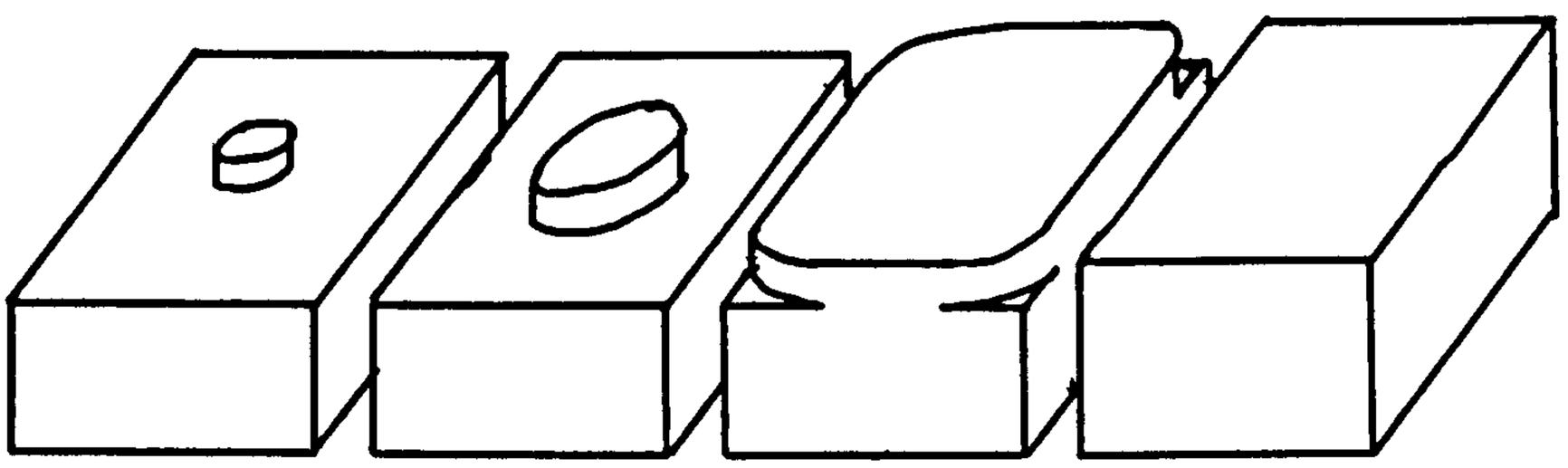

Figure 1.11: Two-dimensional surface nucleation

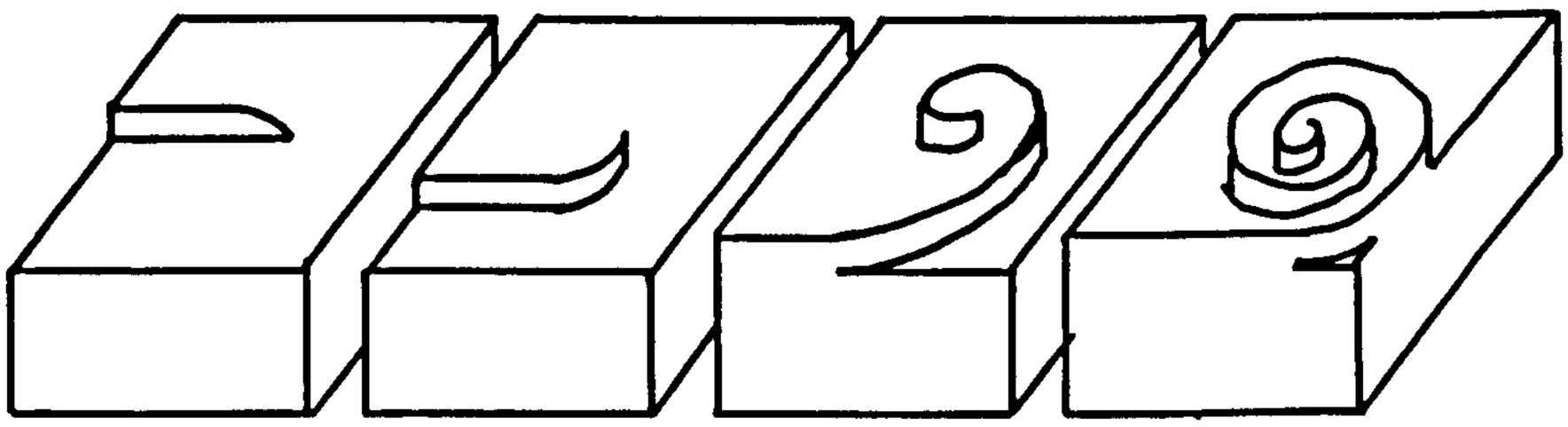

Figure 1.12: Spiral growth due to the presence of a screw dislocation

proposed [20] that dislocations (that is crystal imperfections) having a screw component perpendicular to the surface would provide a continuous source of new surface layers, as shown in figure 1.12, and growth could proceed in a spiral manner. The need for surface nucleation is therefore bypassed.

The physical nature of dislocations and other crystal defects now known to exist will be discussed in section 1.2.3.

1.2.2 Crystal Morphology and its Modification

Crystal growth is a non-equilibrium process, since a crystal in equilibrium with its surroundings will not grow. Because of this, the equilibrium form of a crystal is rarely observed in practice. Crystal morphology is therefore not purely dependent on internal structure, but also on the growth environment. The differing extents to which various growth parameters affect growth rates of individual crystal faces are responsible for morphological changes. These kinetic factors must be superimposed on the underlying thermodynamics in order to predict the most stable form.

Growth parameters which have the most significant effects are supersaturation, temperature, solvent (where applicable), and impurities or additives. None of these factors act independently. For example it may not be possible to distinguish the effects of supersaturation and temperature in early reports of crystal habit modification, since crystal growth experiments were rarely carried out at constant supersaturation [29].

The nature of the crystal surface - its structure and perfection - determines whether two-dimensional nucleation is possible, or whether growth dislocations offer the only source of growth steps. The free energy required to form a closed step around a surface cluster makes such a process unlikely unless supersaturation is very high or solid/solution interfacial tension very

low.

A change in the degree of supersaturation can therefore alter crystal morphology through a change in the mechanism and thereby rate of growth of a particular face. Differences in the surface structure of individual faces mean that growth mechanisms will change at different levels of supersaturation.

Interfacial tension is determined by bonding at the crystal/solution interface, so at a given supersaturation it is the nature of this bonding which is crucial in determining the growth mechanism [22]. The α-factor (or α_J) was introduced by Jackson[22] as a surface-bonding parameter which could be used to determine the growth mechanism of a crystal face.

α_J was initially defined as

$$\alpha_J = \$ \cdot L / kT \qquad (1.7)$$

where L = the change in internal energy on crystallisation; k = Boltzmann constant; T = Absolute temperature; $\$$, the crystallographic anisotropy factor = n_s/n_t where n_s is the number of nearest neighbours in the surface layer and n_t is the total number of nearest neighbours.

Plotting the change in surface free energy $d\Phi$ on crystallisation versus the proportion of filled surface sites, it was found that for low values of α_J (below about 2), $d\Phi$ was a minimum when half the surface sites

were filled, whereas at higher values, a minimum was observed when only a few surface sites were filled.

This was interpreted as meaning that for low values of α_J, surface nucleation would be relatively easy with new layers continuously available. At higher values, growth would be restricted to formation of new layers at a limited number of sites.

Calculation of α_J-values for crystal growth from solution showed that consideration of solvent-solute interactions was also necessary [23]. Strong interactions (high solubility) should lead to a decrease in interfacial tension and hence changes in the value of α_J. Firstly replacing the original definition of S with,

$$S = E_{sl} / \Phi_{inter} \qquad (1.8)$$

allowed the strength of the bonds formed within the new growth layer to be considered [24].

The interaction between solute and solvent was then considered using solid-fluid block models, comparing the relative strength of interaction of solute-solute or solute-solvent, and the influence of solubility could then be taken into account [25]:

$$\alpha_J = S \left[\Delta H_f/R.T - \ln x_{s.eq} \right] \qquad (1.9)$$

where ΔH_f is the heat of fusion; and $x_{s.eq} = N_s/N_c$ = the ratio of solubility to crystal density.

Simulated growth experiments [26] have been used to study the relationship between the value of α_J and the growth mechanism.

Linear growth kinetics were observed at low values of α_J (below about 2.5) that is at high solubilities, since the interface is rough, even at very low supersaturation. The growth rate is directly proportional to the supersaturation. As roughening increases, all growth rate anisotropy is lost and non-facetted growth forms appear. As α_J rises above 2.5, growth is better described by a birth-and-spread model. Eventually as α_J rises above 4.0 (low solubility), the interface becomes so smooth, it poses a high energy barrier to nucleation at low supersaturation. Growth steps produced by emergent screw dislocations offer the only source of step and kink sites. The steps formed in both mechanisms are fed by surface diffusion of adsorbed molecules, so growth rates are still dependent on supersaturation but by a more complex relationship.

From equation 1.9 it can be seen that the α-factor is inversely proportional to temperature. A transition temperature will exist for each crystal face (the roughening temperature, T_R) where the growth mechanism changes.

A change in the crystallisation solvent can therefore lead to a complete change in the growth mechanism of a crystal face due to solubility changes alone. An example of this is the change in growth rate

of {110} faces of hexamethylene tetramine (HMT) crystals [27]. The growth rate from aqueous solution was found to be considerably faster than from ethanolic solution at equivalent supersaturations. Fitting of kinetic data to equations describing different growth mechanisms indicated that in water a surface nucleation mechanism best described the results whereas in ethanol a spiral growth mechanism appeared to operate. This was later confirmed by experimental observation of growth surfaces[28]. Calculation of α-factors in the two solutions found α_J=0.5 in water, and 5.0 in ethanol, where the solubility is an order of magnitude lower [27]. The results are therefore consistent with theory.

As solubility increases (due to temperature or a change of solvent) and α_J increases, dislocations become a more important source of new growth layers, especially at low supersaturations. Temperature, supersaturation and solubility all contribute and cannot be considered in isolation.

1.2.2.1 Solvent Adsorption

The effect of increasing solubility is to roughen the growing crystal surface, increasing the number of kink sites available and thereby increasing the growth rate. However, other factors may interfere with this process, and the influence of different solvents cannot

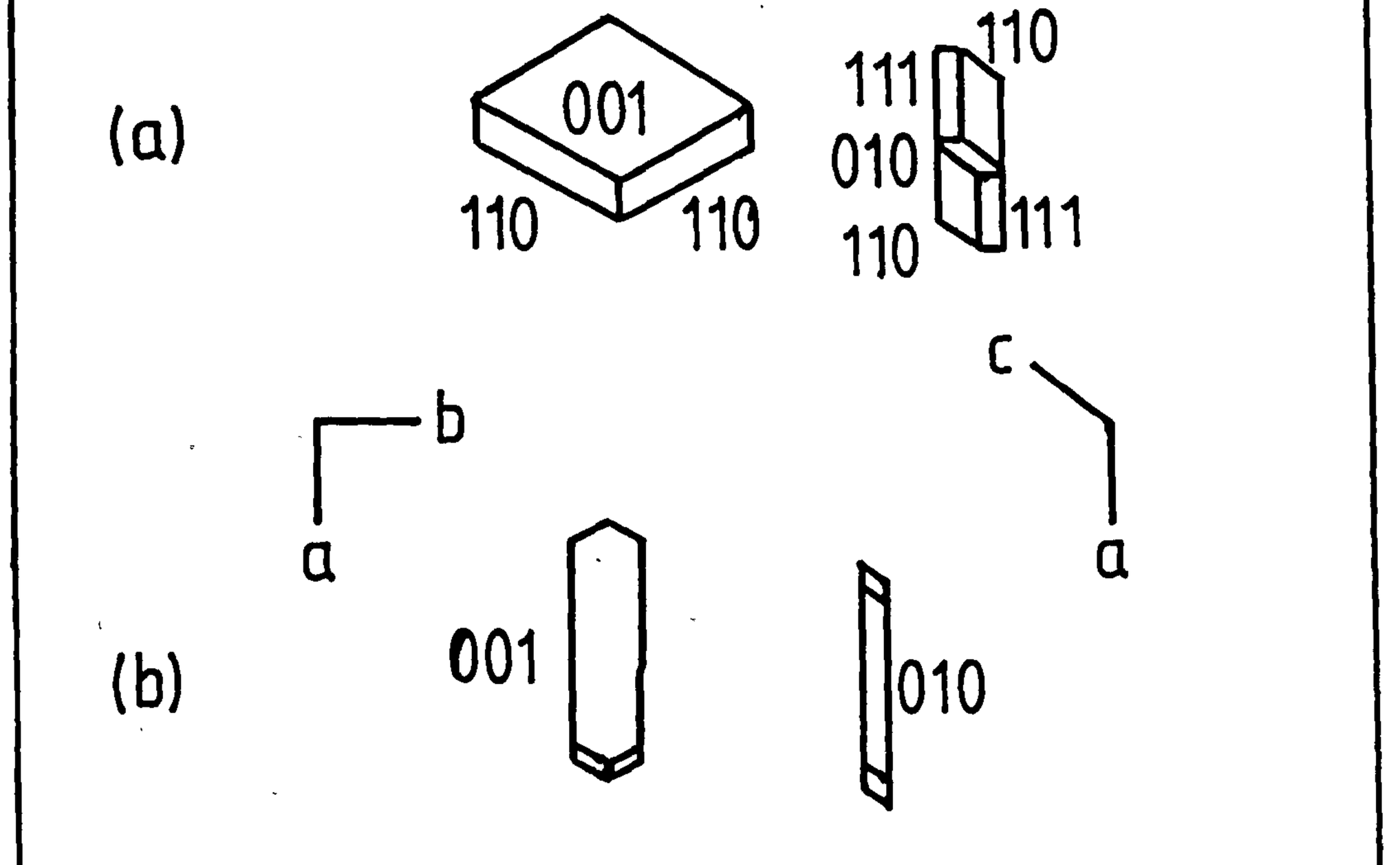

Figure 1.13: The habit of succinic acid crystals grown from
(a) aqueous solution, and
(b) isopropanol solution

always be explained on the basis of solubility changes.

An example of this is seen in the growth of succinic acid crystals from aqueous and isopropanol solutions [29]. The (010) and (001) faces of succinic acid were found to grow faster from water than from isopropanol (figure 1.13), resulting in a change of habit from platelets to needles. Calculation of α-factors indicated that changes in surface roughness were not responsible for the changes in growth rate.

Solubility data showed that isopropanol could interact more strongly with succinic acid (through hydrogen-bonding) than could water, and therefore might be expected to interact more strongly at the crystal-solution interface. The necessity of displacing solvent before growth could take place would result in a slowing of growth compared to that from water. At (001) surfaces, carboxylic acid groups are normal to the surface. Adsorption of solvent would therefore decrease diffusional flux to growth steps. At (010) faces, they are parallel to the surface and kink sites would therefore be blocked by adsorbed solvent. Both are therefore likely to be affected by adsorption of isopropanol.

The morphology of ε-Caprolactam (CAP) is also affected by solvent adsorption. CAP crystals grown from water are elongated flat needles whereas those grown from alkanes form thin plates as illustrated in figure

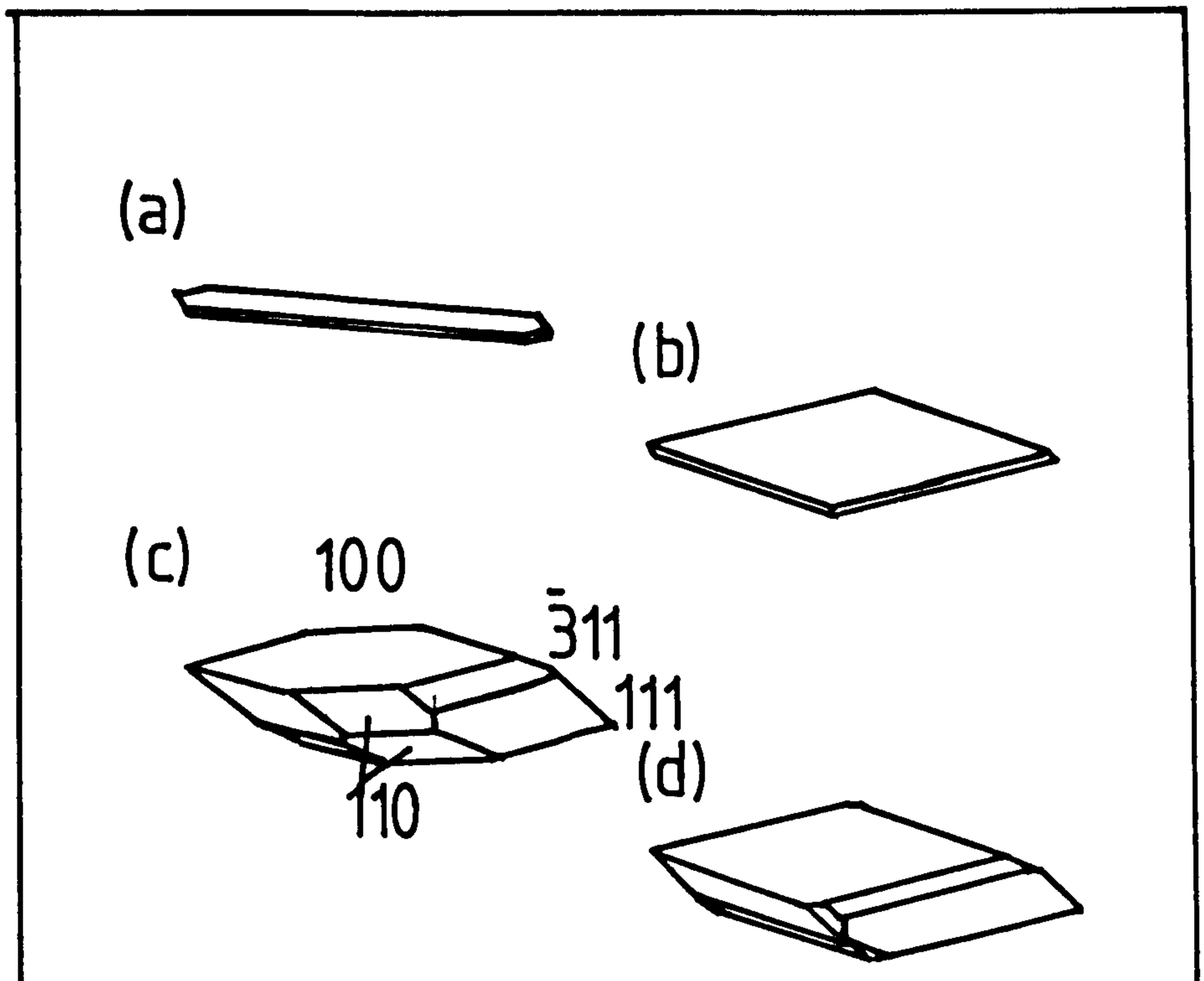

Figure 1.14: Habit of E-Caprolactam grown from
(a) water
(b) alkanes
(c) toluene or ethyl acetate
(d) acetone

(a)

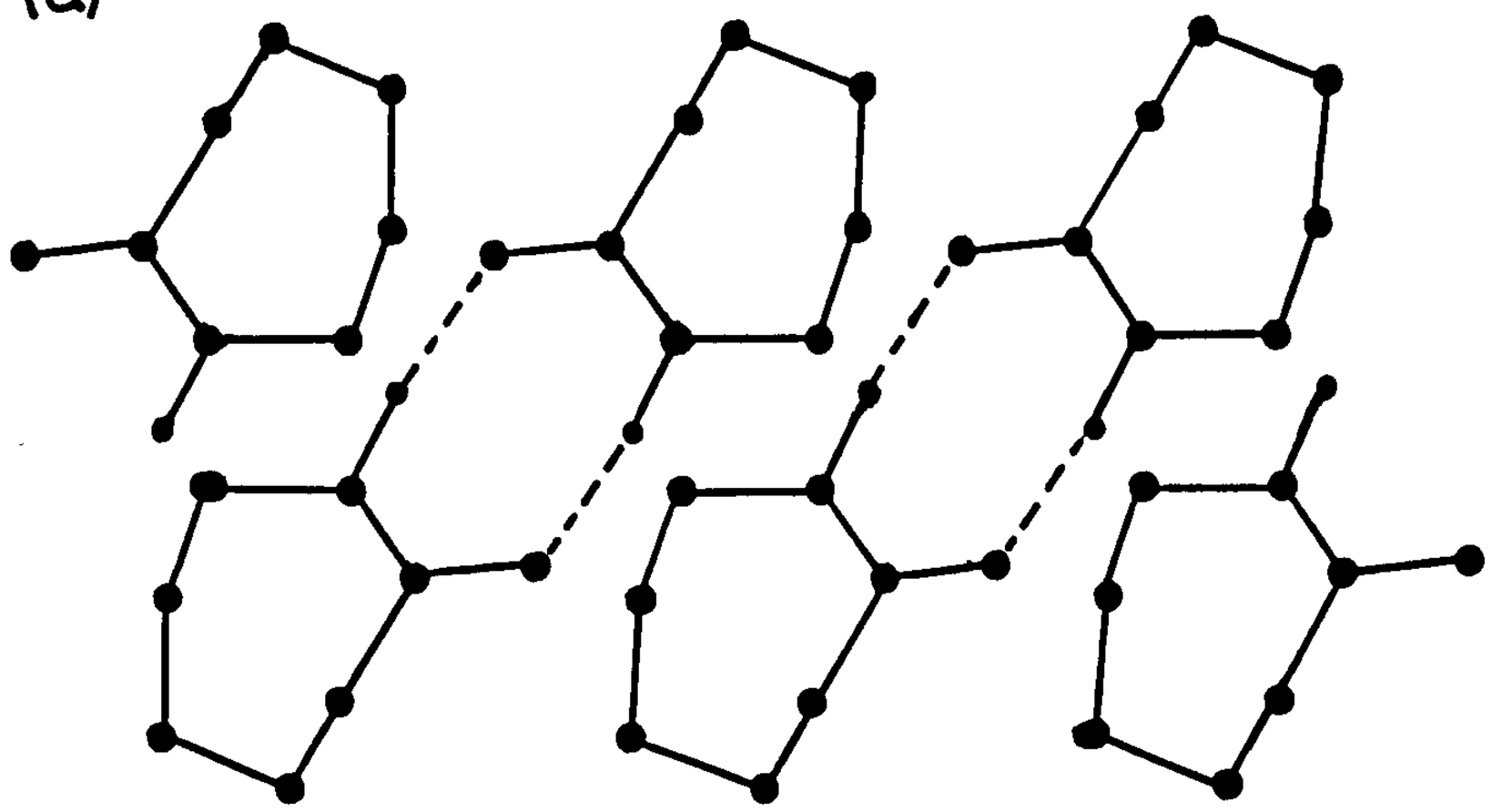

Figure 1.15 (a): Packing arrangement of E-Caprolactam at the (200) face

(b)

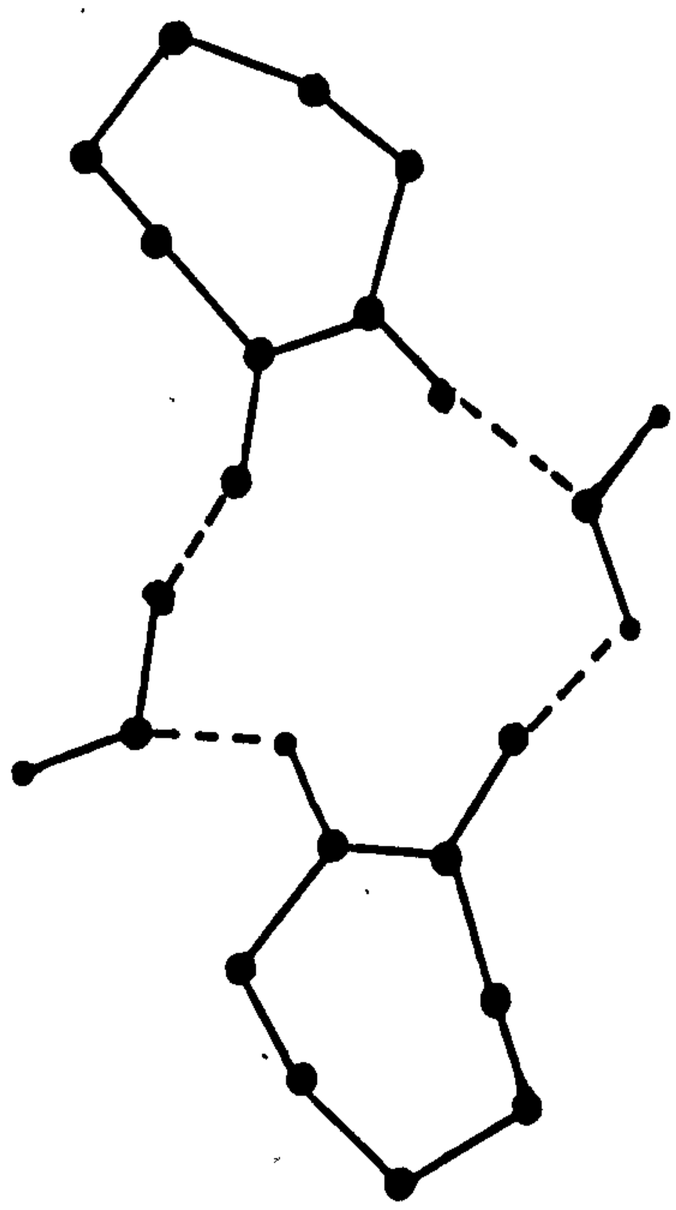

Figure 1.15 (b): Disruption of the E-Caprolactam dimer by water molecules

1.14. Grown from toluene, ethyl acetate or acetone, the crystals become thicker and less elongated than those grown from water.

Observed differences in growth morphology could again be explained on the basis of adsorption of solvent at specific surface sites. The dominant crystal face, {200}, consists of layers of approximately upright dimers as shown in figure 1.15(a). In aqueous solution, the dimer structure is disrupted by interaction with water molecules, illustrated in figure 1.15(b), preventing the direct incorporation of dimer units. Water molecules are also able to block free adsorption sites on the growing surface.

Dimer groups are also aligned along the side {110} faces, and a similar mechanism appears to operate at this face. On the end {111} faces however, the hydrogen bonds zig-zag and obstruction of adsorption sites by water molecules does not appear to be as effective, growth being able to occur by half layers.

Alcohol and other polar molecules form hydrogen bonds much less strongly with CAP than water, hence growth of CAP is less disturbed in these solvents.

A different mechanism was proposed to explain the growth morphology from alkanes, dependent on the change in orientational disorder in the liquid adjacent to the crystal faces. The symmetrical alkane molecules are likely to be regularly packed at the hydrocarbon {200} surfaces (partly due to their shape, partly to the low

solubility of CAP ie there are many more solvent than solute molecules), increasing the free energy required to form new growth steps. In solvents consisting of more asymmetrical molecules, the orientational order at the interface will be decreased, in part due to the increase in the proportion of solute molecules, and a corresponding decrease in the free energy required results in increased growth rates.

The effects of solvent adsorption can also be explained on an attachment energy basis. E_{att} is a measure of the energy released by the formation of new bonds when a crystallising unit becomes attached to a growing crystal surface. If formation of new bonds has to be preceded by the breaking of crystal-solvent bonds then the net amount of energy released will be lessened, resulting in a lower effective E_{att}, and a change in the morphological importance of the affected faces [12].

1.2.2.3 Adsorption of Impurities

The presence of even minute amounts of impurities (mole fractions as low as 10^{-9}) in systems undergoing crystallisation may also cause pronounced changes in growth rate and crystal habit [29]. Their effect can be described in similar terms as solvent adsorption on specific surfaces. Growth from solution has itself been described as growth from an impure melt, with the

solvent acting as the major impurity 31.

The first observations of this phenomenon were made by Buckley [32,33] who reported changes in habit of a number of inorganic chemicals due to the presence of dissolved dyes in solution. The most dramatic effects were observed with dyes such as Brilliant Azurine B(511), Tryptan Red (438), Naphthol Black (315), Brilliant Congo R(456) and Sky Blue FF (518) which were found to alter the morphology of crystals of $KClO_3$, K_2SO_4, K_2CrO_4 and NH_4ClO_4.

Presence of trace amounts of impurities led to adsorption only on the most receptive faces, leading to habit modification. Higher concentrations of impurity however could lead to adsorption on all faces, not necessarily to the same degree, and could produce yet another habit modification or completely prevent crystal growth.

Some of these habit modifiers were very strongly adsorbed and were observed as "hour-glass" patterns or striations in the grown crystals. Modifiers which interacted less strongly with the growing surface were adsorbed and desorbed rapidly by a competitive mechanism, resulting in a modified crystal relatively free from contamination.

Significant changes in morphology can be produced in this way, and can be of use in improving product performance[34]. It is however only recently that work on organic systems by the Weizmann Institute has led to an

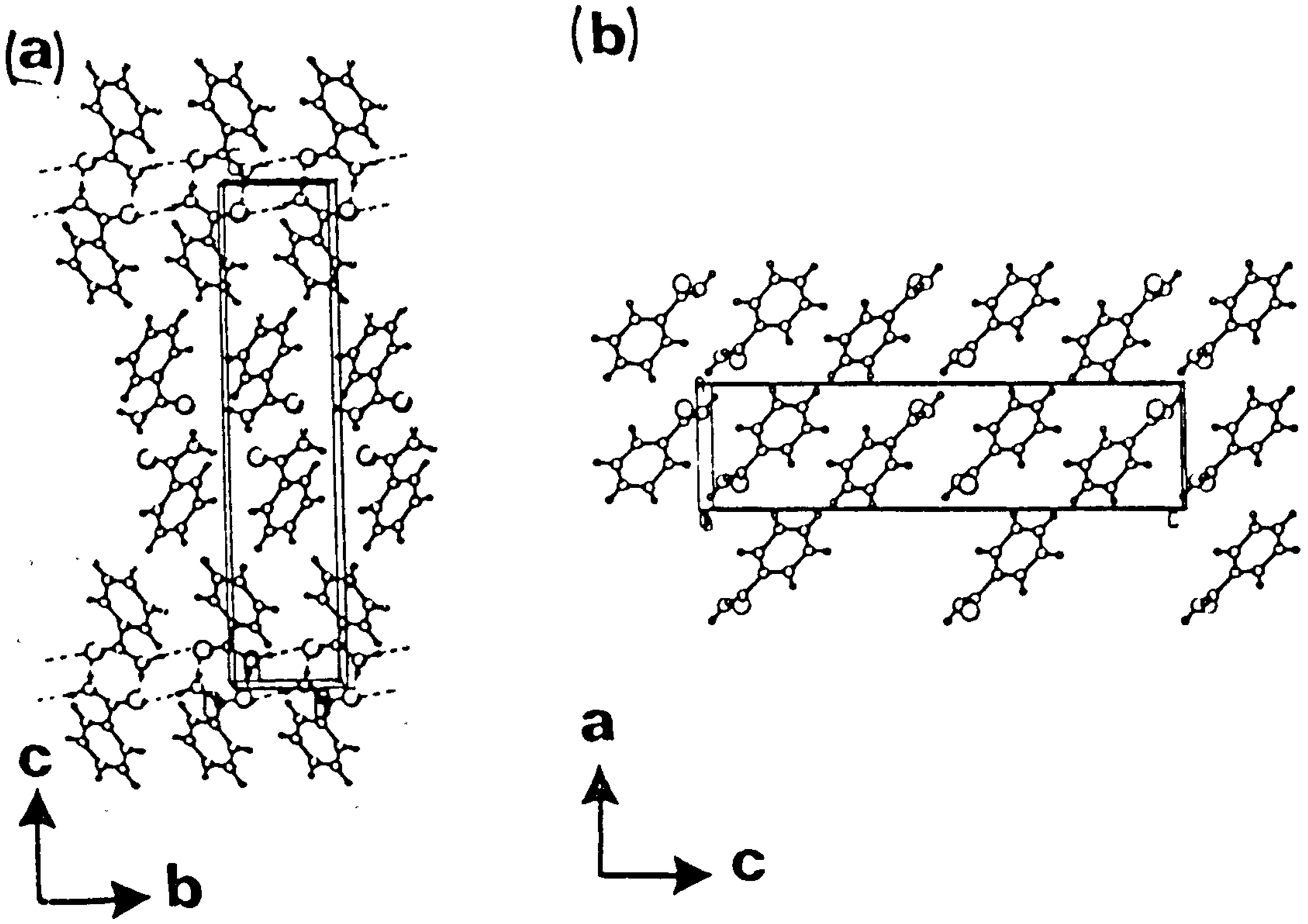

Figure 1.16: Packing arrangement of benzamide viewed
(a) along the a axis
(b) along the b axis

understanding of the ways in which additives can be designed to alter crystal morphology in a predictable way [2,35,36].

A simple correlation can be made between the structure of the "tailor-made" additive and the directions of growth affected. Habit-modifying additives have been designed by slightly modifying substrate molecules. The additive molecules can only be adsorbed on those faces at which the modified moiety emerges from the surface. The modified side-chain then perturbs the regular deposition of oncoming layers, decreasing growth rates normal to these layers, relative to rates normal to unaffected faces. With an understanding of the solid-state system of interest, it is therefore possible to design surface-specific molecules.

This approach is illustrated by the modification of the habit of benzamide crystals [37]. Benzamide grown from ethanol forms plate-like crystals elongated along the b-axis, due to the NH...O bonds interlinking cyclic dimers (see figure 1.16(a)) to form ribbon structures. These are stacked along the a-axis and stabilised by electrostatic interactions. The plate-like nature is due to weak Van der Waals contacts between phenyl groups on adjacent {001} planes. Benzoic acid molecules present in solution decrease the growth rate along the b-axis by interrupting the chain of NH...O bonds. Substitution of benzoic acid for a benzamide molecule results in replacement of a favourable N-H bond by the lone pair of

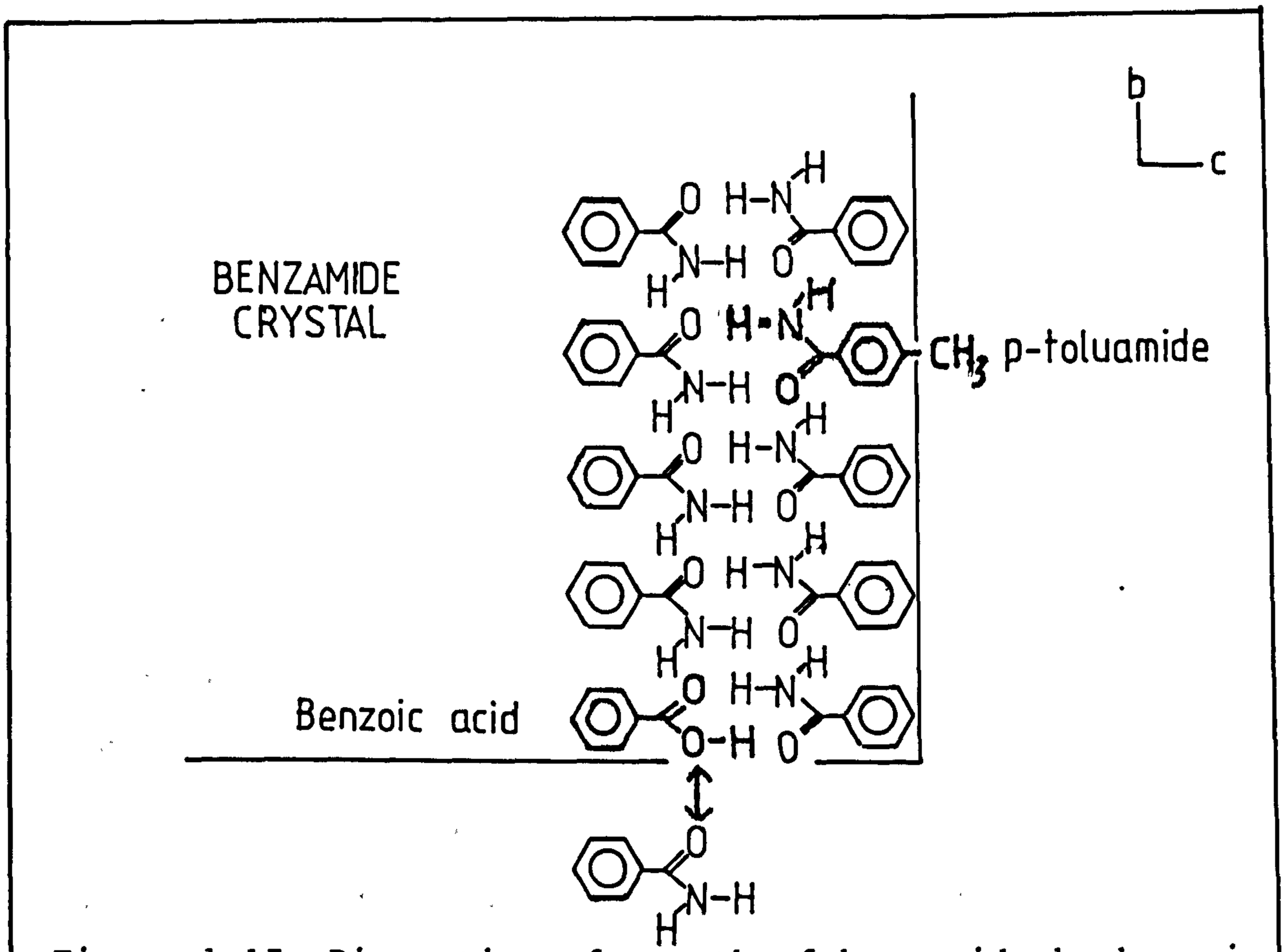

Figure 1.17: Disruption of growth of benzamide by benzoic acid and p-toluamide

electrons of a hydroxyl oxygen atom, thus introducing a repulsive O...O interaction as illustrated in figure 1.17.

Similarly, p-toluamide was found to produce thinner plates by disruption of growth along the c-axis by the methyl substituent on the aromatic ring (see fig 1.17); and o-toluamide (a heavily twisted molecule) decreased growth along the a-axis.

Changes in the crystal habit of amino-acid systems on the addition of small amounts of structurally similar amino-acids have also been closely studied. For instance, modification of the habit of L-asparagine-monohydrate by L-aspartic acid [40] was shown by x-ray diffraction studies to take place by a similar mechanism to that described for modification of benzamide morphology.

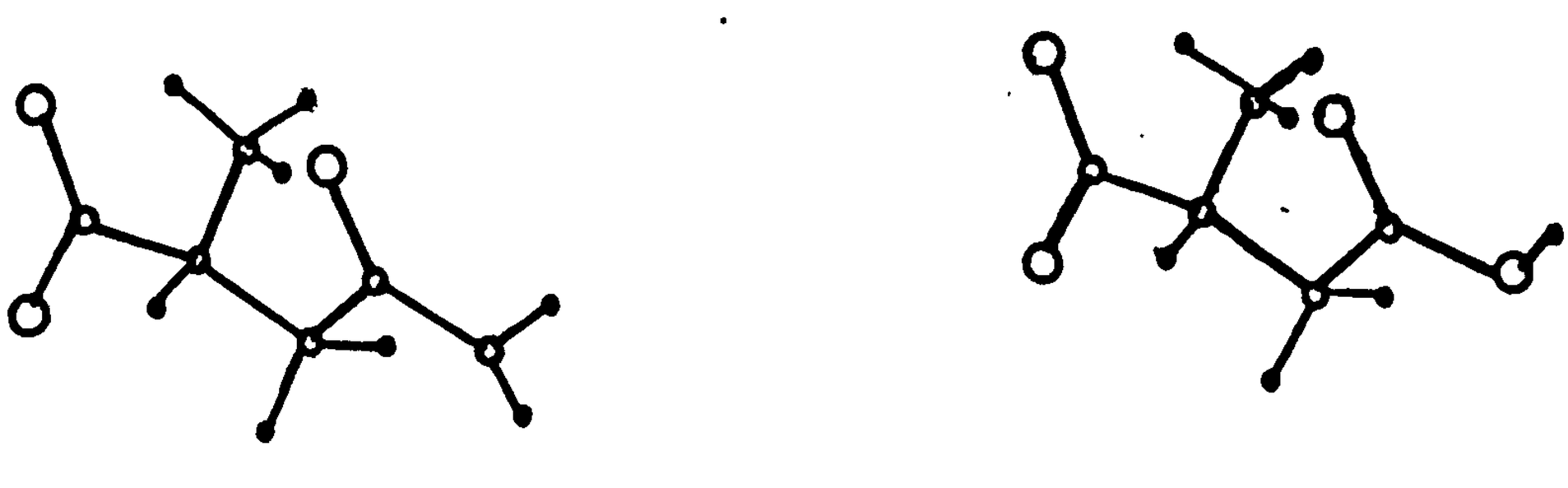

Figure 1.18: The chemical structure of (a) Asparagine
(b) Aspartic acid

Aspartic acid (figure 1.18(b)) is adsorbed in positions where the NH_2-CH-COOH group can substitute for that of Asparagine (figure 1.18(a)), leaving the carboxylic acid

group protruding, and setting up a repulsive O....O interaction with incoming asparagine molecules. This was most effective in reducing the growth rate at {010} faces, where the carboxylic acid groups protruded directly from the surface.

Chiral molecules have been used in a similar fashion to induce morphology changes in achiral crystals (racemic or meso compounds) [38], and also to determine the absolute configuration of polar crystals [36].

1.3 CRYSTAL DEFECTS AND DEFORMATION MECHANISMS

It was shown in section 1.2.1.2.2 that single crystals are not perfect according to Braggs crystal lattice plane model, and indeed that in some circumstances crystal growth can only take place if dislocations are present. A number of different defect types, arising from various sources, have been identified. They can be classified into four main types:

Classification	Defect type	Dimensions
Point defects	Equilibrium	Zero
Line defects	Non-equilibrium	One
Area defects		Two
Volume defects		Three

TABLE 1.2: TYPES OF CRYSTAL DEFECTS

These can in turn affect the reactivity, mechanical properties, optical and electro-optical properties of materials. A comprehensive review can be found in C.Kittel (1986) Introduction to Solid-state Physics, 6th edn., Wiley, New York and J.N.S.Sherwood (1979) The Plastically Crystalline State, Wiley, New York. A summary of the nature, properties and origins of defects follows.

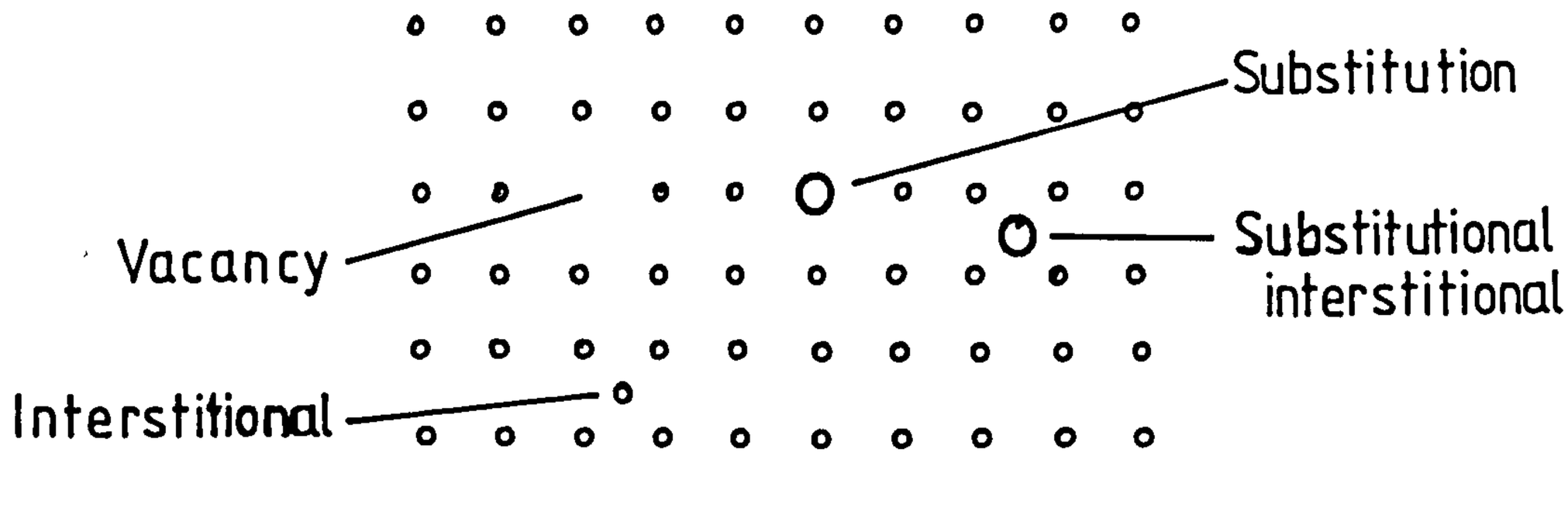

Figure 1.19: Point defects

1.3.1 Crystal defects

Equilibrium defects arise due to atomic or molecular motion. Statistically, some atoms or molecules may have sufficient energy to escape from the forces holding them in position. This produces point defects which can be either vacant atomic/molecular positions or interstitial (between these positions). Point defects can also arise from the incorporation of impurity atoms to give interstitional or substitutional defects. These are illustrated in figure 1.19. Larger aggregations of point defects form small volume defects. Point defects such as grown-in impurities will not necessarily be associated with corresponding vacant positions as are those which arise due to movements as described above.

Non-equilibrium defects involve an assembly of atoms (or molecules) and so the energies involved are too high for thermal vibrations alone to generate and move. They can be generated either during crystal growth or be induced by mechanical stress. Numerous accounts of the geometrical properties and behaviour of line defects are available, for example references 40 or 41. The two simplest cases are edge and screw dislocations, which are described in terms of two principal vectors. The two vectors together define the dislocation type and geometry, its energy, and possible interactions with other defects.

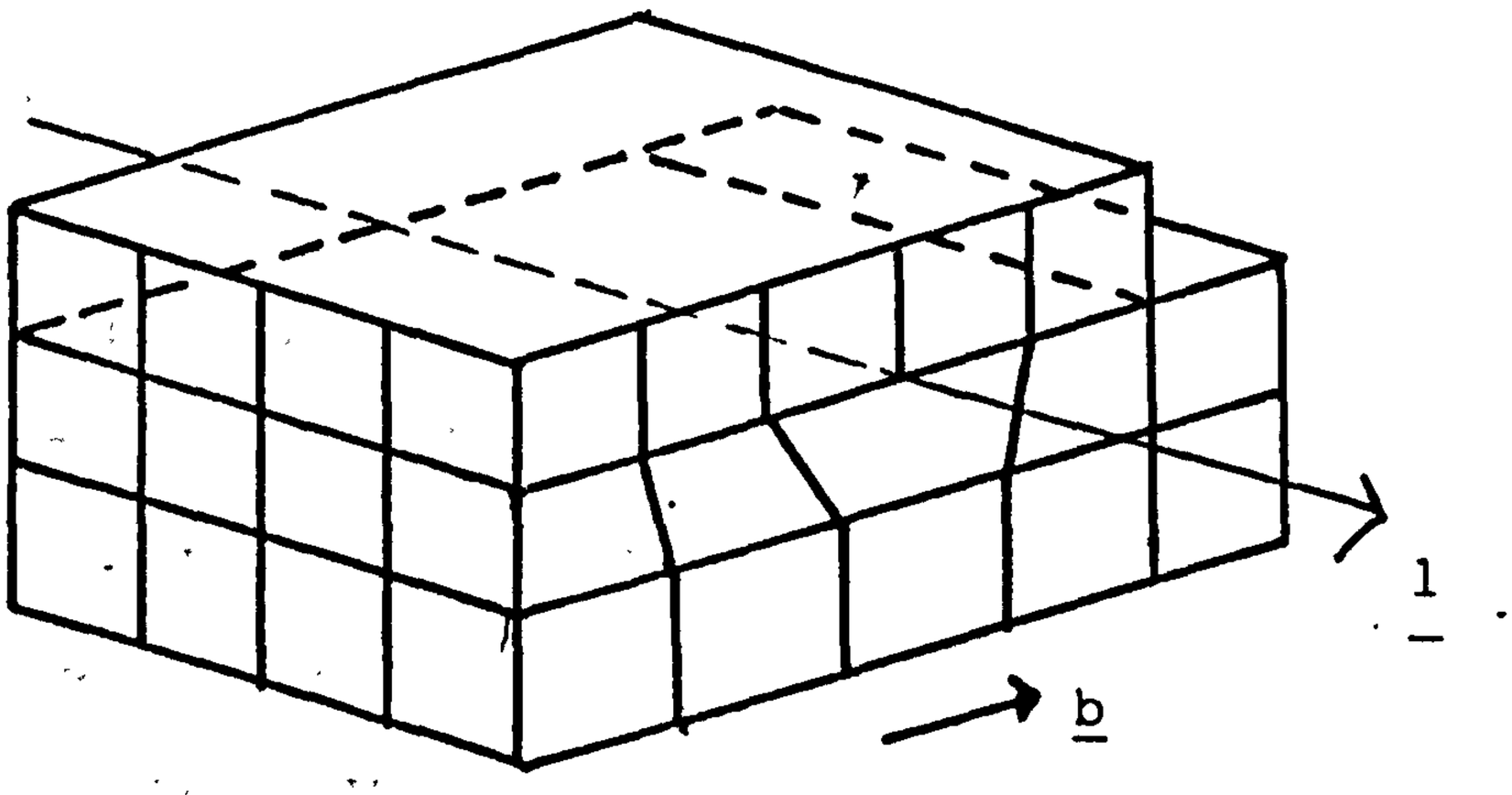

Figure 1.20: Diagrammatic representation of an edge dislocation

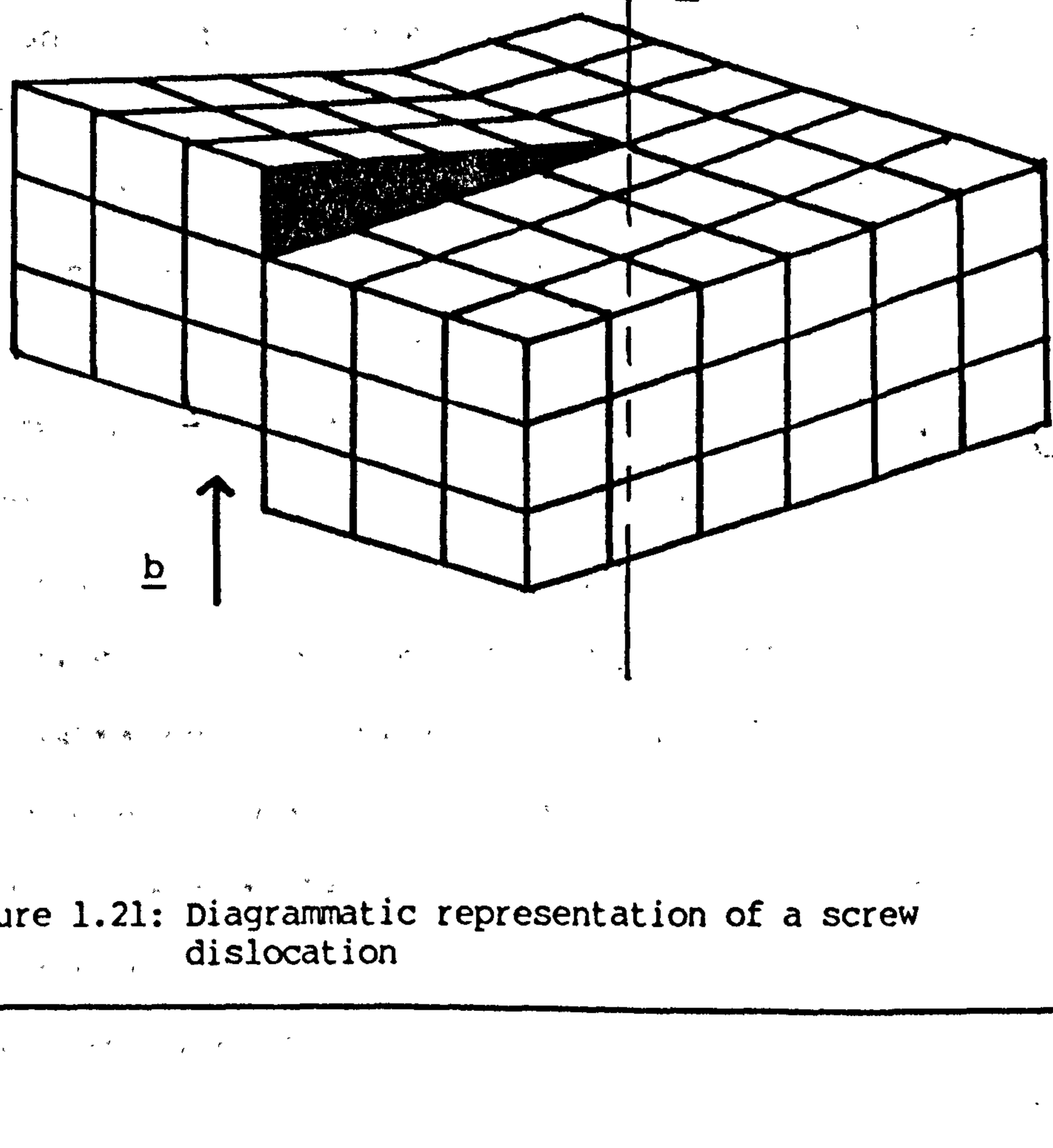

Figure 1.21: Diagrammatic representation of a screw dislocation

An edge dislocation, illustrated in figure 1.20, is equivalent to insertion of an extra half plane of atoms or molecules in the lattice, or where a shear operation has induced displacement of part of the crystal bulk. The line direction $\underline{l}$ of the dislocation, aligned along the termination of the dislocation in an otherwise perfect lattice, is perpendicular to the direction of the Burgers vector $\underline{b}$, which defines the size of the induced distortion. $\underline{b}$ also defines the line energy of the dislocation [42]:

$$\text{Line energy, } E_l = u.\underline{b}^2 \qquad (1.10)$$

Where u = shear modulus. Edge dislocations are usually unit insertions, that is, insertions of a portion of a single crystallographic plane, since an increase in the size of the distortion causes a large increase in the line energy (equation 1.10). The Burgers vector of a dislocation also tends to be one of the short lattice vectors, to minimise the associated strain energy. Despite severe local distortion around the dislocation, the lattice planes match on either side.

In the case of screw dislocations, $\underline{b}$ is parallel to $\underline{l}$, as illustrated in figure 1.21. This is usually a monomolecular displacement in the direction of maximum strain, that is, along the Burgers vector. This results in a spiral mismatch, perpetuating throughout the lattice. This can also be attributed to shear where

movement has been pinned along the line vector. Screw dislocations are often a source of crystal growth.

Mixed dislocations, where $\underline{b}$ is not parallel or perpendicular to $\underline{l}$ are also frequently observed. These are usually in the form of loops, in which the magnitude and direction of $\underline{b}$ are constant, but the line direction changes.

The increase in internal energy associated with dislocations tends to cause a weakening of materials in which they are present. This is partly because they can act as a source of slip when the crystal is stressed. Since very few materials are dislocation free, their presence helps explain why few materials are as strong as theoretical calculations would indicate.

There are three main ways in which dislocations arise in single crystals:

1. due to the growth process;
2. condensation of vacancies to form dislocation loops; and
3. as a result of shear caused by internal or external stress.

Growth dislocations differ from other types in terms of configuration and properties. They are usually straight, and follow well-defined line directions close to the growth direction of the growth sector in which they lie. During growth they may act as sinks for impurities (most commonly the solvent during growth of

crystals from solution). Dislocations present in a seed crystal may propagate into the crystal bulk during growth, or they may be nucleated at the seed-crystal interface. Defects induced by growth accidents such as lattice mismatch as the crystal grows over an impurity inclusion can also act as a source of dislocations.

Lattice mismatch may also occur between crystal growth sectors exhibiting different growth mechanisms, giving rise to area defects known as growth sector boundaries. Stacking faults, where the stacking order of planes within the crystal structure has altered, and the surfaces of volume defects also form area defects. These are one or a few interatomic or intermolecular distances in thickness, but may be macroscopic in extent.

Volume defects are relatively large (of the order of $>100nm^3$) and are analogous to point defects: regions of free space, aggregations of impurities or solvent inclusions. These most frequently form at high growth rates (often along a dislocation). Regions differing from the bulk by their orientation are called grains. Where these are related to the bulk by simple symmetry operations they are termed twins. Twinning can occur during growth or by the action of mechanical stresses.

1.3.1.1 Influence of defects on the physical properties of crystals

The nature and concentration of imperfections influences many of the physical properties of crystals. An increase in defect density leads to an increase in the internal energy, enthalpy and entropy of a crystal system, leading to an increase in its thermodynamic activity [43]. The presence of trace additives within the crystal lattice has been demonstrated to influence the ΔH_f, ΔS_f and ΔS_{soln} of a solid material [44].

The enhanced reactivity around dislocation cores as they reach a crystal surface is used to identify their position and determine their distribution by etching with solvents [45]. Decomposition of a solid may also occur preferentially at the sites of emergent dislocations [46,47] or in general at regions of high dislocation density [48]. Strained regions within the crystal bulk, unassociated with dislocation positions have been shown to be the source of sites where thermal decomposition is initiated,with impurity-doped samples showing enhanced rates of decomposition [49].

Increased defect density tends to lead to increased dissolution rates of crystals for the same reasons - enhanced thermodynamic activity and an increased number of reactive sites on the surface. Differences in the dissolution behaviour of aspirin, initially thought to be due to polymorphism, is now believed to be due at

least in part to differences in defect density caused by differences in the crystallisation technique [50].

Differences in crystal density may be associated with alteration of the degree of crystallinity. Hüttenrauch [51] associated increased perfection with increased density, but this only generally holds with crystalline to amorphous transitions. Although impurities may decrease density by opening up the lattice, interstitial impurities may increase density. The volume change associated with the presence of dislocations is negligible [52] and density changes are therefore unlikely to be detectable if these are the only source of lattice disruption.

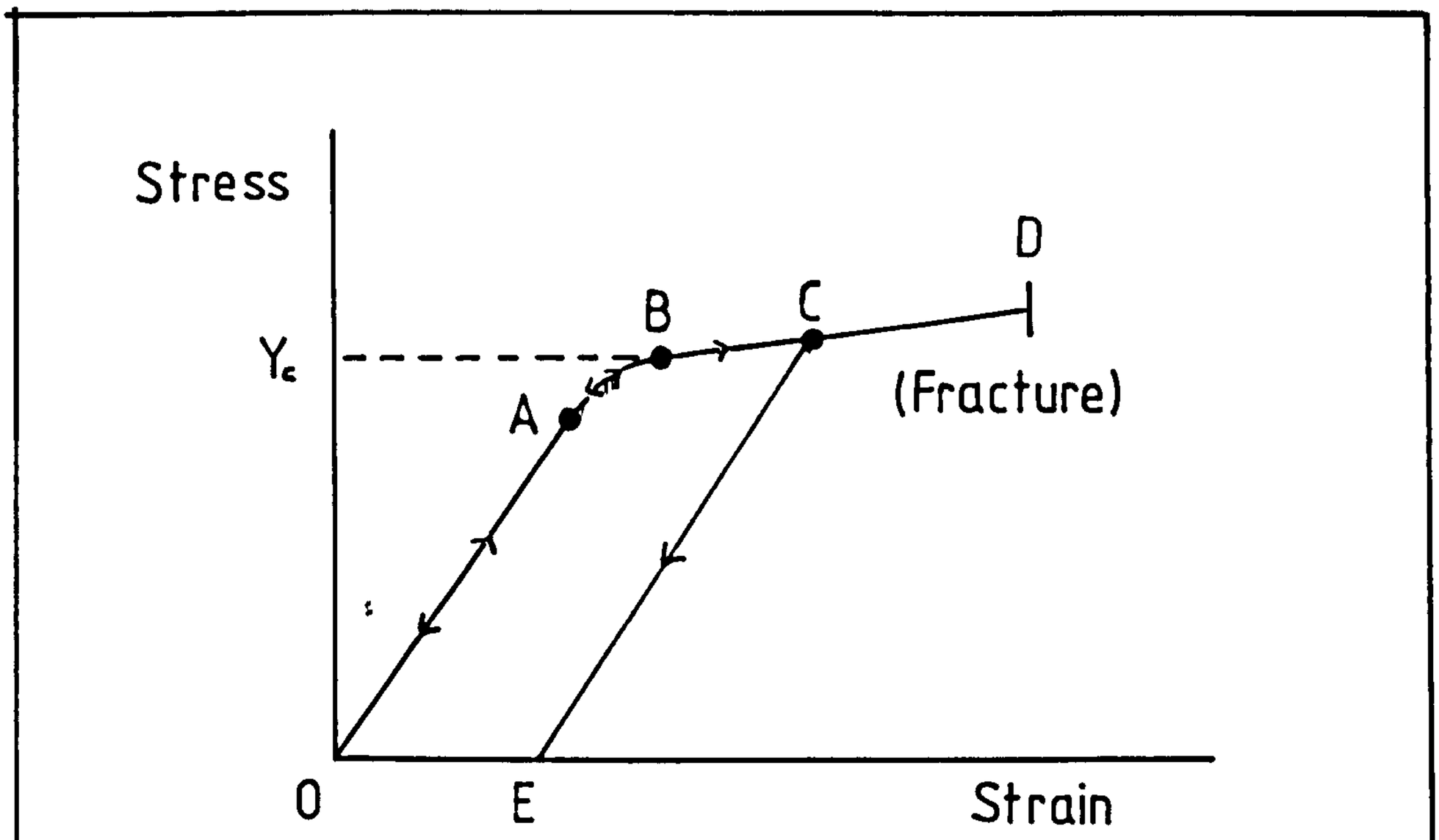

Figure 1.22: Typical stress -strain diagram for a crystal under tensile stress

1.3.2 Crystal Deformation

Application of a load to a crystal causes a strain to develop, measured as the change in the length of the material as a proportion of its original length. A tensile stress, applied to opposite ends of a sample, will tend to pull the material apart. Internal systems of forces between molecules resist this to a greater or lesser extent depending on the material.

Figure 1.22 shows a typical stress-strain diagram. Initial application of stress causes elastic deformation. Strain increases linearly with stress up to point A (Hooke's Law) then at a slower rate to point B. Up to this point, the material will return to its original length when the stress is released. If the material is ductile, beyond this point (the yield stress or elastic limit) strain increases quickly with stress and is not recoverable (BC). The initial elastic strain can still be recovered , but the material will have a permanent "set" (OE) from the plastic deformation which has taken place once the stress is removed. There is generally still an increase in stress with deformation beyond C, known as flow stress, and its increase is due to work hardening. i.e. the build-up of stress-induced dislocations, which pin further slip. Brittle materials resist plastic deformation and tend to fracture readily. beyond their elastic limit, which is generally lower than that for ductile materials.

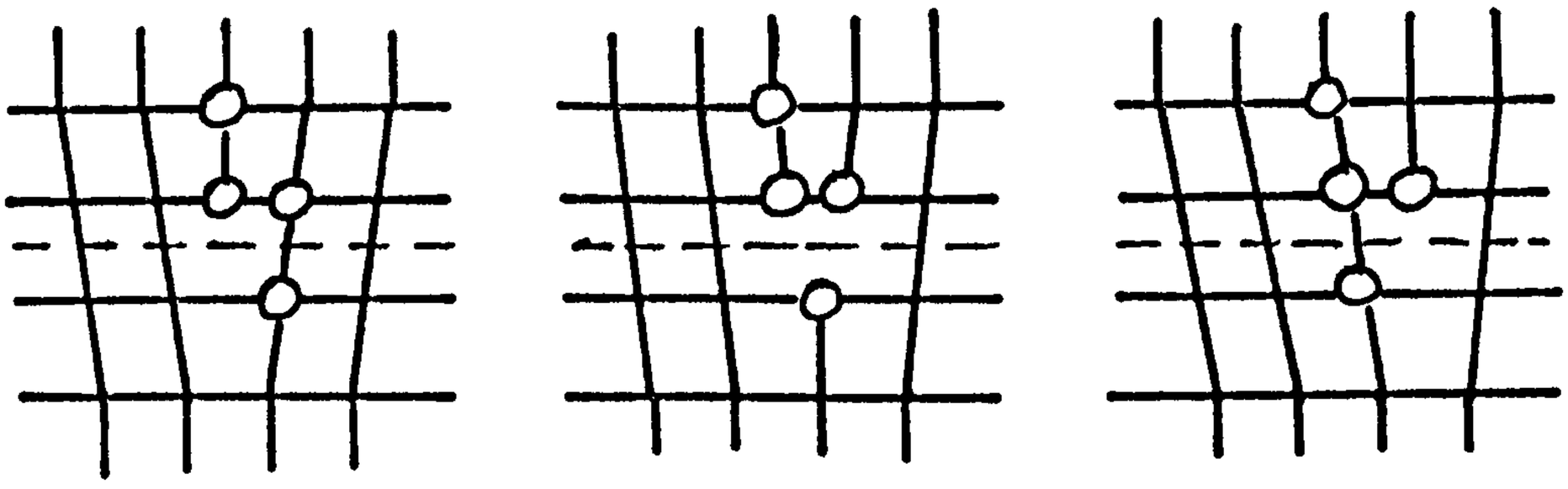

(a) (b) (c)

Figure 1.23: Movement of an edge dislocation by glide

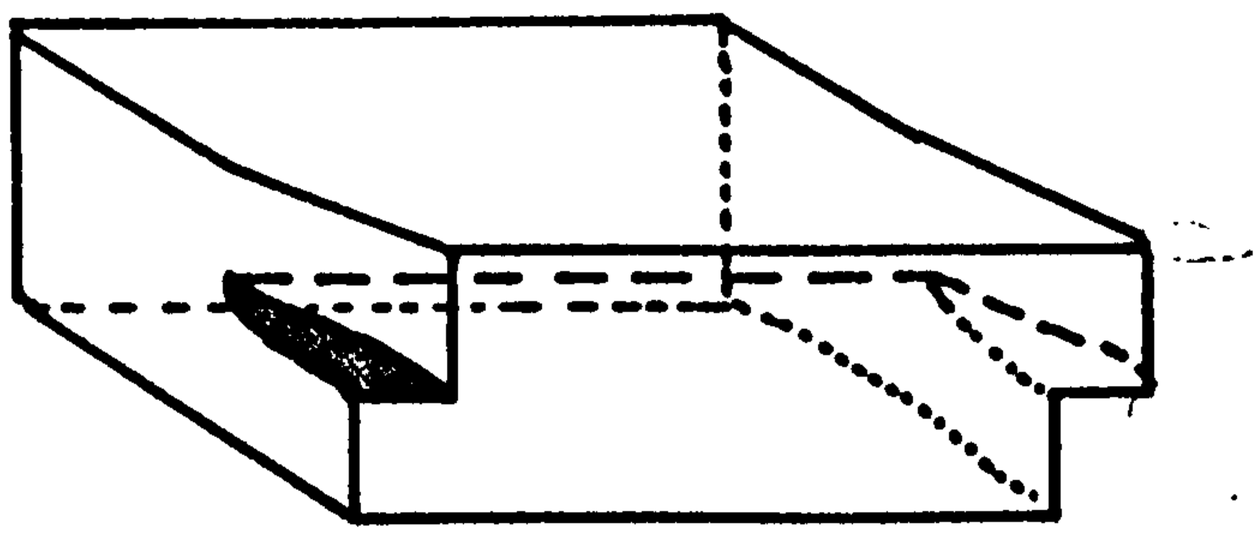

Figure 1.24: Movement of a screw dislocation by glide

Dislocations are often the source of plastic deformation. They are not static, and can move by two different types of mechanism, glide and climb.

During glide, conservative motion occurs along a plane of atoms containing both $\underline{b}$ and $\underline{l}$, termed the slip plane. This can be illustrated by the movement of an edge or a screw dislocation by glide (figures 1.23 and 1.24 respectively). The planes of atoms are in effect moving relative to each other in a direction parallel to $\underline{b}$. The atoms move from stable position (a) in figure 1.23 to stable position (c) via an unstable high energy position (b). This does not occur until the elastic limit is reached, since a threshold amount of energy is required to overcome this energy barrier. The limit varies between different sets of atomic planes due to differences in the intermolecular interactions across the planes, leading to anisotropy in the mechanical properties of crystals. The elastic limit is generally lower on close-packed planes where $\underline{b}$ will be lowest. Intermolecular interactions will also be lower, as discussed in section 1.2.1.2.1.

Glide does not occur simultaneously over a whole slip plane since this would require a very large stress, but by the movement of individual dislocations. Slip begins in a limited region and then spreads through the crystal, by dislocation movement or multiplication.

Screw dislocations, unlike edge dislocations, can move out of one glide plane into another equivalent plane with the same b. This process is known as cross-slip.

Climb is more difficult to generate than glide, and larger stresses are involved. A driving force such as thermal stress is required to allow diffusion of vacancies or interstitials to the half-plane of an edge dislocation enabling it to climb out of its slip plane into one perpendicular to this. Climb does not normally occur in molecular solids, since vacancies and interstitials are uncommon. It will not therefore be discussed further.

The application of stress and subsequent plastic deformation may also lead to formation of new dislocations or multiplication of those originally present. This most commonly occurs at Frank-Read sources or by multiple cross-slip.

If a dislocation is pinned at two points by obstacles such as impurities, then the action of an applied stress may cause the dislocation line to bow out on its slip plane and become semi-circular, generating a shear stress tending to move the dislocation back to its original position. If the applied stress is greater than the shear stress thus generated then the dislocation will continue to move and spiral around the primary

points until the spirals meet and cancel, producing a dislocation loop and regenerating the original dislocation line. If movement of the loop is prevented, then further loops can pile up behind it. This process continues until the back-stress from the piled-up loops equilibrates the applied stress, resulting in a pile-up of dislocations in the slip plane, which may act as a source of strain in brittle fracture.

If a section of a screw dislocation has moved to an equivalent plane by cross-slip, the two points where the dislocation loop crosses planes render the dislocation immobile. These may then act as Frank-Read sources on parallel planes.

Deformation of organic materials has been less thoroughly reported in the available literature than has deformation of inorganic materials. It is not conclusive whether mechanical behaviour in both types of material can be considered according to the same mechanisms. This will be considered in greater detail in section 2.3.9.

1.4 EFFECT OF SOLID-STATE PROPERTIES ON THE COMPACTIBILITY OF MATERIALS.

Small variations in the solid-state properties of the component crystals of a product can lead to manufacturing problems or a product with performance outwith a satisfactory tolerance range [53]. However, very little work has been published on the solid-state properties of the constituent materials. Properties which have been identified as being of particular importance [54] are:

1. Polymorphism;
2. Crystal habit;
3. Crystal hardness; and
4. Defect structure and deformation mechanism.

The influence of the above parameters on the processing characteristics of crystalline materials will be considered, with a brief summary of how they can be affected by the crystallisation process.

1.4.1 Polymorphism

Polymorphs (compounds with the same chemical structure but different crystal structure) are most frequently produced by a change in the temperature, or solvent, of crystallisation. Differences in the

compression properties of different polymorphic forms have been shown for a number of materials, the most stable forms having been shown to produce weaker compacts and vice-versa [55]. This appeared to be due to weaker intermolecular bonding in the less stable forms, enabling compression to take place more readily. (Reversion of the unstable to a more stable polymorph on storage and its effect on the integrity of the compact was not considered).

1.4.2 Crystal habit

Alteration of crystal habit can affect the bulk density, flowability and compaction properties of drugs. Both bulk density and flowability decrease as particle shape becomes less equant[56], potentially resulting in dose variation or tablet weight variability [57].

Differences in the processing behaviour of polymorphs may also be due to habit differences. For example, the platey habit of one polymorph of tolbutamide caused powder bridging in hoppers[58].

Aspirin, recrystallised from various solvents, also shows compressibility differences (originally thought to be due to polymorphism [55]) due to habit changes. In particular, thin plate-like crystals tend to orient preferentially during compaction, with the main face parallel to the upper flat punch face. The resulting layering increases the lamination tendency of the

tablets [59,60,61]. Similar behaviour was observed for talc and ascorbic acid. Due to anisotropy of mechanical properties, compaction may be altered through this dominant face effect. Tablets produced from adipic acid with dominant (001) faces were strongest, due to higher yield strength in the [001] direction[62].

As discussed in section 1.1.2, habit changes can be brought about by alteration of a number of contributing factors. Increased growth rates may however increase defect concentration and habit-modifiers may be incorporated into the crystals. The effects of defect type and density will be further considered in section 1.4.4.

1.4.3 Crystal hardness

As the hardness value of crystals decreases, the pressure on the wall of tablet dies during compaction (radial pressure) increases [63], a factor which has been linked with the ability of materials to form good compacts [64]. Ridgway et al [65] also found that the hardness values of the materials tested were in the same order as their bulk modulus, and so hardness could be used as an indication of the bulk mechanical behaviour of the crystal. Harder materials appear to form compacts with a higher fractional voidage indicating they do not fragment or deform as readily as softer ones [66].

Changes have also been observed in the surface

hardness of a material due to changes in crystallisation conditions [67]. This may be a consequence of alteration in the defect structure, and will be discussed further in the next section.

1.4.4 Mechanical properties and the influence of crystal defects

The defect structure of a crystal is one of the factors responsible for its deformation characteristics. Dislocations are usually the source of plastic deformation (section 1.2.3.3), whereas the presence of defects such as impurities or solvent inclusions which act as points of strain, may increase the propensity for brittle fracture of the crystal under stress.

Materials which can deform plastically are more likely to form strong compacts than those which exhibit elastic behaviour[68]. Compacts produced from brittle materials, or materials which exhibit elastic recovery during decompression, also tend to cap and laminate easily, or form friable tablets [69,70] since energy is used less efficiently for bonding [71].

The type and concentration of defects in crystalline material therefore contributes significantly to its compaction behaviour. Alteration of growth conditions may in turn affect the defect structure. For example, Ridgway & Aulton [67] showed that increased growth rate of potassium bromide resulted in softer

crystals due to decreased crystal perfection. This would seem to have been due to a decrease in crystallinity of the potassium bromide, rather than increased dislocation concentration which may have been expected to cause an increase in the crystal hardness in a manner similar to work hardening, although this would be dependent on the actual numbers of dislocations generated.

Habit modifiers added to growth solutions are generally assumed not to be incorporated into the growing crystal due to bulky side chains or repulsive interactions [62]. However lattice disruption has been observed in some instances and incorporation of impurities must be considered as a possibility [72,73].

1.5 CHOICE OF TECHNIQUES

1.5.1 Assessment of crystal morphology

Characterisation of the crystal habits of materials produced by industrial crystallisation techniques is difficult due to their small size, the inaccessibility of some of the crystal faces when characterising powder samples by microscopy (which also makes measurement of interfacial angles inaccurate) and the damage caused to the crystals by filtration etc.

Slow controlled solvent evaporation from saturated solutions at constant temperature was selected as the most suitable method of producing crystals of sufficient size to enable crystal dimensions and angles to be readily measured. Additionally, the effect of temperature and supersaturation can be kept constant, so that any solvent effects can be detected. Good development of crystal faces can be achieved by this method compared with melt or vapour growth, although it is not directly comparable with the industrial situation due to differences in cooling rates, level of supersaturation etc. However, without accurate assessment of crystal morphology the influence of the crystallisation solvent is difficult to determine.

Small crystals produced in this way could then be

used as seed crystals to produce large crystal samples, grown by controlled cooling, for use in further investigation of chemical and physical properties.

Laue diffraction of x-rays was chosen as a simple, fast, unambiguous method of identifying the main crystal faces, and the orientation of the crystallographic axes. Crystal dimensions could be measured directly with a micrometer; lengths in all three major directions could be measured in this way rather than the two axes accessible to microscopy. Interfacial angles could also be measured directly, or from enlarged optical micrographs for increased accuracy.

1.5.2 Mechanical properties

Crystal hardness is most readily studied using microindentation hardness techniques. Other industrial hardness tests such as scratch or rebounding sphere techniques were not applicable either due to the small size of the samples, or because the nature of the tests would not have provided useful information regarding the deformation mechanisms of the crystals.

For this last reason, the asymmetrical Knoop indenter [74] was used during the microindentation tests. Use of an asymmetrical indenter allows hardness anisotropy, if present, to be investigated [75].

Subsequent etching and microscopical examination of indented surfaces is necessary to identify planes on which slip has been initiated [76,77]. A theoretical treatment of slip induced by the Knoop indenter is possible, and provides further evidence of active slip systems[78].

1.5.3 Investigation of defect structure

Since the presence of defects in crystals tends to increase the reactivity of crystalline materials[79,80,81] techniques utilising this property can be used to assess defect density. Single crystal dissolution testing, as well as being useful for comparing crystal reactivities, also provides information regarding the potential bioavailibilities of crystalline samples (although this may be altered on subsequent compaction).

Lattice strain, due to the presence of defects and hence distortion of the lattice, can be detected using Laue diffraction. This is manifested as asterism (or smearing) of the Laue diffraction spots from which the degree of strain can be estimated[81,82].

Imaging of crystal defects can be carried out by x-ray topography where high quality samples are available [83]. Other techniques such as electron diffraction are also available, but require far thinner

samples, making handling and preparation more problematic, and contain less information regarding the bulk crystal since samples are thinner and of smaller area. Despite the lower resolution of x-ray topographic images, they therefore contain a greater amount of useful information [84]. Characterisation of defect and particularly dislocation types can be of value in determining deformation mechanisms and mechanical properties.

MATERIALS AND METHODS

2 MATERIALS AND METHODS

2.1 MATERIALS

2.1.1 Drugs

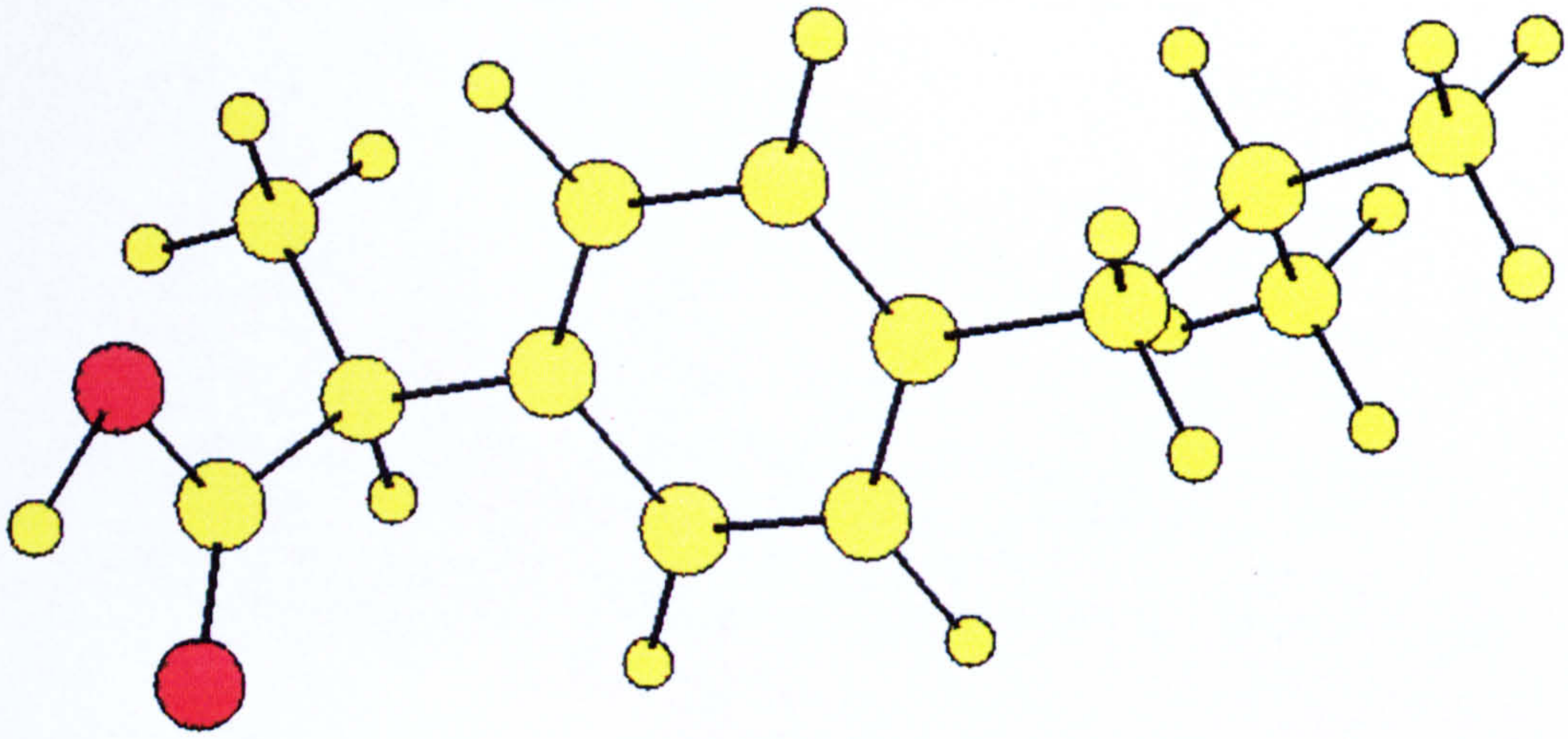

Figure 2.1. IBUPROFEN: 2-(4-isobutylphenyl)propionic acid

Racemic and resolved S(+) ibuprofen were supplied by Boots Company plc, Nottingham, England.

Infra red spectra of samples as received were obtained as described in section 2.3.1. A representative spectrum is shown in figure 2.2, and is in agreement with the published spectrum[85] shown in figure 2.3.

Proton nuclear magnetic resonance spectra were obtained as decribed in section 2.3.2. Samples were dissolved in carbon tetrachloride, without further purification. Spectra were in agreement with the expected structure, as illustrated in figure 2.4.

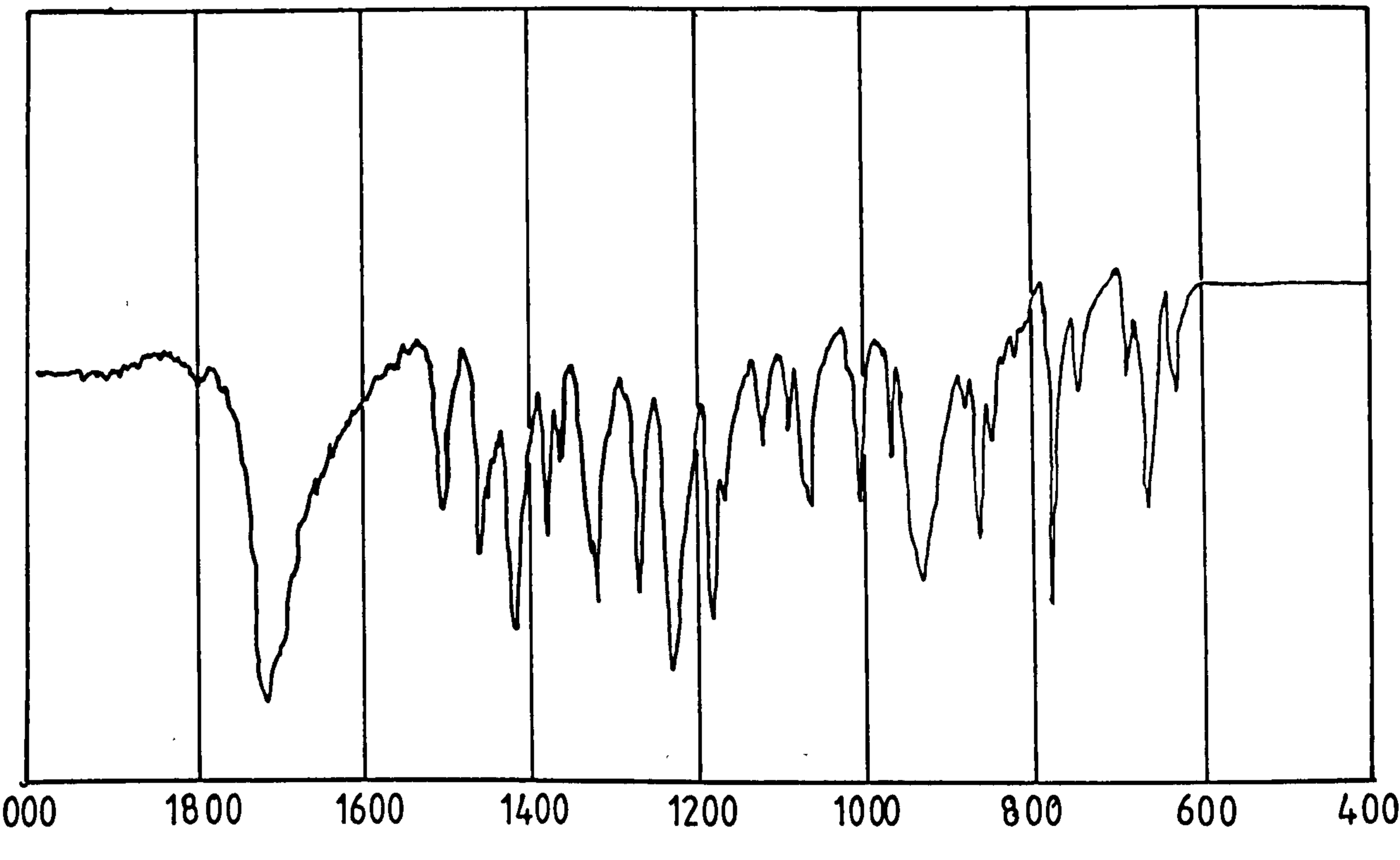

Figure 2.2: Infra red spectrum of ibuprofen

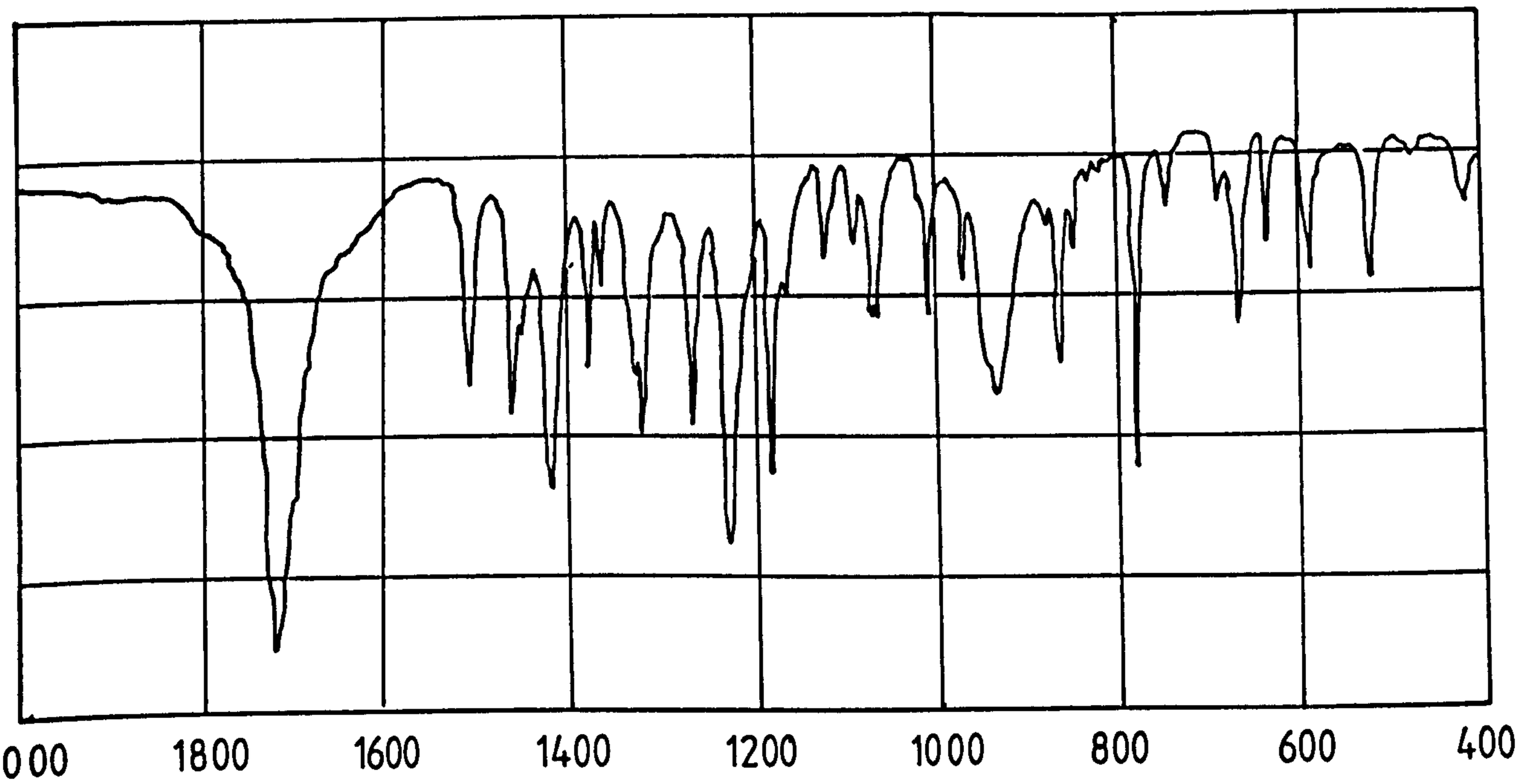

Figure 2.3: Standard infra red spectrum of ibuprofen

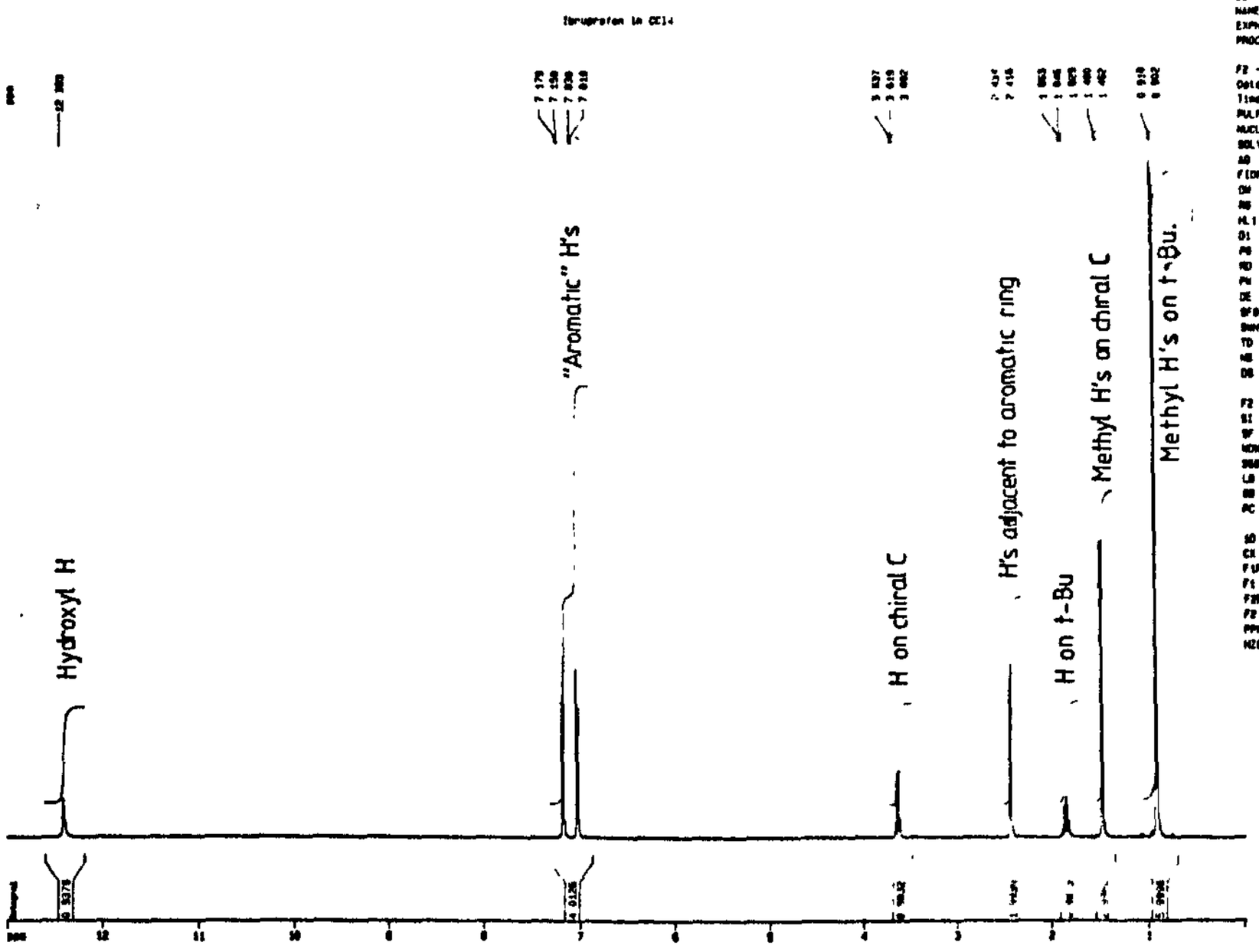

Figure 2.4: Proton nuclear magnetic resonance spectrum of ibuprofen

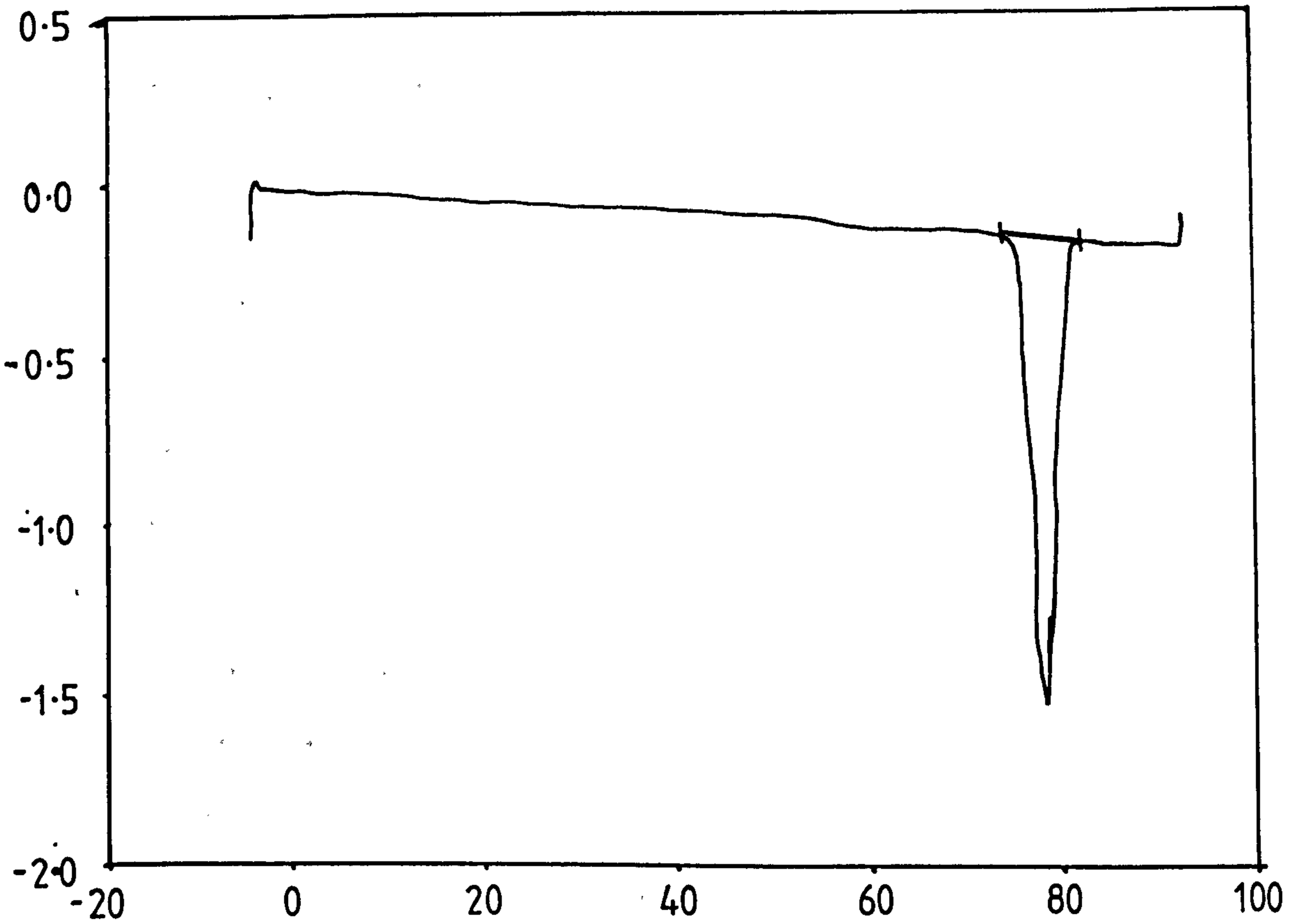

Figure 2.5: Differential scanning calorimetry thermogram for ibuprofen

The melting points of both racemic and S(+)-ibuprofen, obtained as described in section 2.3.3 were 76.5°C to 77.3°C and 51.2°C to 52.1°C respectively. Results were therefore in agreement with published values of 75.0°C to 77.5°C and 50.0°C to 52.0°C respectively [86].

Differential scanning thermograms confirmed the melting point of (±)-ibuprofen. Obtained as described in section 2.3.4, thermograms showed a single melting endotherm at around 76°C as illustrated in figure 2.5. No other endotherms or transitions were observed. Mean values from three determinations of the melting point and dH_f of ibuprofen were 76.25°C (sd 0.386) and 27.91 $kJmol^{-1}$ (sd 0.611) respectively, in good agreement with previously determined values of 76.32°C (sd 0.130) and 28.74 $kJmol^{-1}$ [87].

The purity of the samples as obtained was determined by high pressure liquid chromatography following the method described in section 2.3.5. Sample purities were 99.6% for (±)-ibuprofen and 99.1% for s(+)-ibuprofen.

In the rest of this work, "ibuprofen" refers to the racemic form, unless otherwise indicated.

2.1.2 Solvents and reagents

Acetonitrile, hexane, ethylacetate, toluene, ethanol, methanol and cyclohexane were obtained from Aldrich Chemical Co. Ltd., Gillingham, Dorset, or Rathburn Chemicals, Walkerburn. All were of HPLC grade (at least 99.9% purity) and were used as received. Acetone was obtained from the Department of Pure and Applied Chemistry, Strathclyde University and was twice distilled from glass before use.

Potassium chloride (Analar grade) for infra red spectroscopy was obtained from Aldrich Chemical Co.Ltd., Gillingham, Dorset and was stored in a drying oven.

Carbon tetrachloride for nuclear magnetic resonance spectroscopy (NMR) was HPLC grade as above. It was passed through a sintered glass filter before use.

Deuterated acetonitrile (CD_3CN) for NMR was obtained from Aldrich Chemical Co. Ltd., Milwaukee, USA. The solvent was stated to be 99% deuterated [88].

2.2 PREPARATIVE METHODS

In this section crystal growth techniques will be described, and preparation of samples for further testing considered.

2.2.1 Crystal Growth from Solution

Supersaturation can be generated either by evaporation of solvent from a saturated solution at constant temperature, or cooling of a saturated solution. The solvent evaporation technique is the simpler of the two, requiring less apparatus. However, control of evaporation at a constant rate is important in order to maintain supersaturation at a constant level. Fluctuations in evaporation rate may lead to varying growth rates, which can mask changes due, for example, to differing solvents. Additionally, increased incorporation of impurities, resulting in increased defect density is likely. Low levels of supersaturation allow good face development to take place, and produce better quality crystals. Temperature is more readily controlled than evaporation rate, and so the temperature lowering method is preferred where quality is of prime importance. Growth conditions have a marked effect on the quality of the resulting crystals, but under the correct conditions, growth from solution can yield

crystals of high perfection 89.

Good quality crystals of low defect density were required in this work. Since the effect of solvent on the crystal morphology was of paramount interest, the introduction of defects which may have altered the morphology unpredictably was avoided as far as possible. Very low defect density samples were also required for imaging of individual defects within crystals by x-ray topography, and crystal perfection was kept as high as possible for this reason (although ultimately resolution of individual defects was not possible, for reasons which will be discussed later).

Crystal growth by controlled cooling is generally carried out using a seed crystal suspended in the growth solution, in order to concentrate growth at one point in the solution. The quality of the seed crystal is significant in determining the quality of the resulting large crystal, as it is often a source of growth dislocations as discussed in section 1.3.1.

Seeds are often produced by the solvent evaporation technique. Seeds selected should be of good optical quality, and should be carefully removed from solution and dried quickly, as evaporation of solvent from crystal surfaces tends to cause localised cooling. The resulting stress can cause fracture or introduction of dislocations, termed thermal shock. Drilling of the crystal in order to suspend it in the growth solution can also introduce strain and must be performed with

great care to minimise this. Surface damage such as precipitated material or surface scratches which may also set up localised stresses and generation of imperfections in the growing crystal can be removed by slightly dissolving the crystal surface by a small increase in the temperature of the solution immediately after introducing the seed.

Impurities in the growth system which may promote heterogeneous nucleation on the walls of the solution flask or the surfaces of the growing crystal can be kept to a minimum by fresh distillation of solvent and filtration of the saturated solution directly into the crystallisation vessel. Purification of the solute may also be necessary.

Care must also be taken when placing the seed crystal in the growth solution, and when removing the grown crystal, to avoid thermal shock due to abrupt changes in temperature.

Crystallisation conditions which can markedly affect the resulting crystal quality are; choice of solvent, temperature range and cooling rate. Optimum conditions for crystal growth are often found within the following ranges [89], which may influence the selection of the above conditions:

Solubility, S : 20 - 100g solute per 100g solvent;

Solubility ratio (defined as the ratio of the solubility-temperature gradient to solubility) : 0.01 -

$0.03\ K^{-1}$;

Cooling rate : 0.5 - 1.0 $K.day^{-1}$ (in order to maintain the supersaturation at around 2%).

Accurate solubility-temperature data are therefore necessary to calculate these values. Values outwith these ranges mean the growth apparatus is operating at its functional limits. A small temperature fluctuation under these conditions could lead to a large change in the supersaturation and cause growth to occur in bursts. Control of growth rate is essential to prevent "veiling" of the crystal, bands of inclusions which occur at high growth rates. Even if not optically visible, these act as sources of dislocations, and will also appear on and cause distortion of x-ray topographs.

Lower cooling rates and the consequent decrease in supersaturation generally lead to an improvement in crystal quality, allowing time for the molecules to become properly oriented at growth surfaces, and for good face development. Optimum rates for each system must be established individually.

2.2.1.1 Solution growth by solvent evaporation

Solutions were prepared by adding excess ibuprofen to the solvent, with stirring, at 30°C. Solutions were allowed to equilibrate overnight and any excess removed

by filtration. The resulting solutions were placed in crystallising dishes and covered with several layers of stretch film. Holes were punched in the films to allow controlled evaporation. Head-space between solution and film was minimised. Covered solutions were placed in a controlled temperature oven at 30°C.

Crystals were allowed to grow to several millimetres in length, then removed carefully and quickly dried with tissue paper in order to prevent solvent evaporation from the surfaces. Evaporation may cause localised cooling and hence strain and subsequent dislocations due to thermal shock.

2.2.1.2 Growth of large single crystals by controlled cooling

Choice of solvent system

Gordon and Amin [1] compared the morphologies of ibuprofen crystals grown from hexane (the most commonly used industrial solvent for recrystallisation of ibuprofen) and various more polar solvents. It was decided therefore that one of the crystal growth solvents to be studied should be hexane. A polar solvent system was determined from the initial series of experiments where ibuprofen was recrystallised by slow solvent evaporation from a range of solvents at constant temperature as described in section 2.2.1.2. Good

quality crystals exhibiting the equidimensional morphology described were most readily obtained from acetonitrile (see section 3.1.1), a solvent not included in the original patent. Crystals grown from acetonitrile were therefore selected for special study.

Selection of temperature range and cooling rate

Accurate solubility - temperature curves were determined using the crystal growth apparatus described in the next section.

100g ibuprofen was added to 200ml of solvent in a conical flask and heated with stirring until dissolved. The resulting solution was filtered into the crystallising vessel and allowed to cool slightly until crystallisation had just commenced. Solutions were allowed to equilibrate overnight at this temperature. Subsequently, duplicate 0.5ml samples of supernatant were measured into weighed bottles, evaporated to dryness in an oven and reweighed. A further sample was taken several hours later to confirm the result. Temperature was then dropped by approximately 1°C, the solution allowed to re-equilibrate and the measurements repeated. The solubility curves obtained are shown in figure 2.6.

Solubility-temperature gradients (dS/dT) were determined from the gradients of the solubility curves at specific temperatures where the solubility,S,

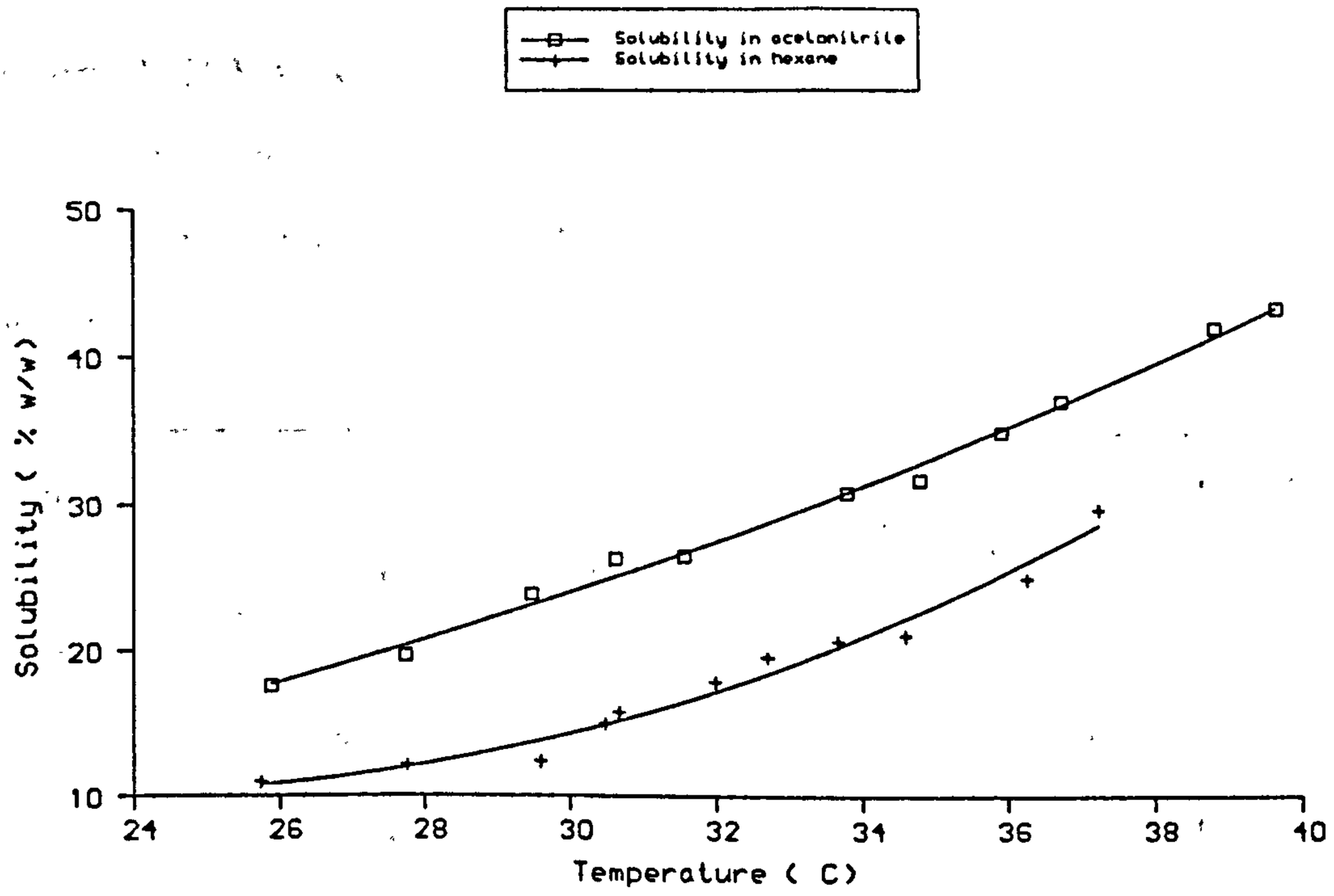

2.6	Solubility of ibuprofen in acetonitrile and hexane

Curve fitting details:

Acetonitrile: $y = 4.1175 - 0.3361x + 0.03324x^2$, $r = 0.997$

Hexane: $y = 65.219 - 4.6403x + 0.09816x^2$, $r = 0.988$

exceeded 20%(w/w) 89. The solubility ratio ((dS/dT)/S) was calculated from this by dividing the solubility-temperature gradient by the solubility at that point. Results are given in table 2.1.

Solvent	Temp (°C)	S (%w/w)	dS/dT ($S.°C^{-1}$)	(dS/dT)/S ($°C^{-1}$)
Hexane	34.0	20.89	2.03	0.097
	37.0	27.88	2.62	0.094
Acetonitrile	29.5	23.13	1.63	0.070
	33.5	30.16	1.89	0.063
	38.0	39.35	2.19	0.058

TABLE 2.1: SOLUBILITY-TEMPERATURE GRADIENTS AND SOLUBILITY RATIOS FOR IBUPROFEN

The cooling rates of 0.5 to 1°C.day^{-1} recommended by Hooper et al[89] apply to materials with solubility gradients of 0.01 to 0.03 K^{-1}. To maintain approximately 2% supersaturation for ibuprofen in the solvents above, cooling rates of 0.1 to 0.15 °C.day^{-1} for growth from hexane, and 0.15 to 0.23 °C.day^{-1} for acetonitrile were more suitable.

Cooling rates are highly dependent on the system under scrutiny. In general, slow cooling allows better quality crystals to develop, but must be fast enough to

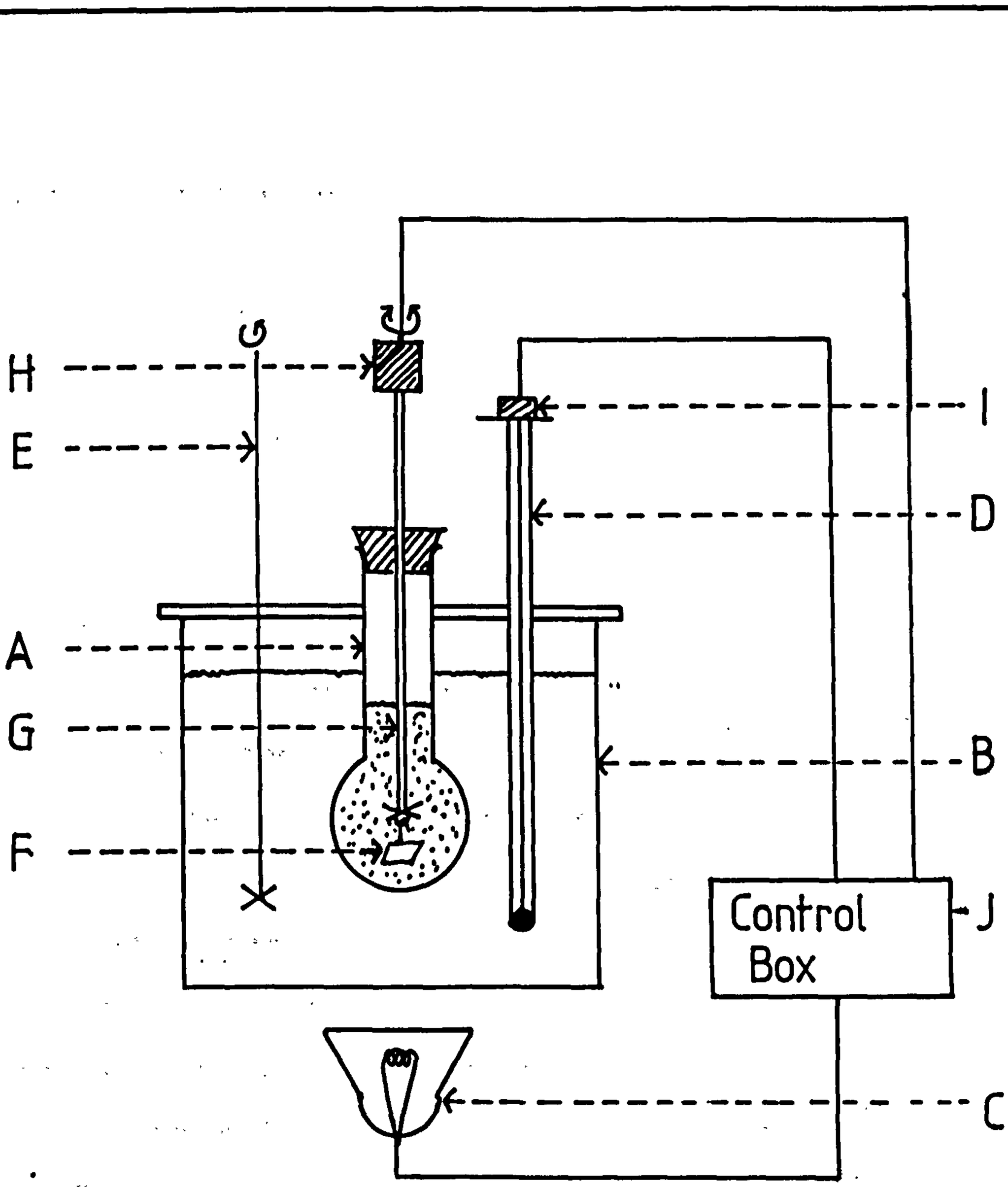

Figure 2.7: Crystal growth apparatus

maintain adequate supersaturation. Initial experiments were conducted with a cooling rate of 0.1 $^{\circ}C.day^{-1}$, as this was suitable for both systems.

Crystal growth apparatus and methodology

Seed crystals of ibuprofen were selected according to the criteria described, and handled in tissue paper. They were drilled by hand using a 0.65mm dental drill lubricated with solvent (acetonitrile or hexane). The drilled seeds were rinsed in the same solvent to dislodge any debris resulting from the drilling process, and were threaded with fine glass filaments to allow suspension in the growth vessel.

Saturated solutions were prepared by dissolving slightly more than the amount of ibuprofen required for the starting temperature in the chosen solvent, to compensate for losses incurred during filtration. The material was dissolved with stirring at around 45°C, and filtered through a paper filter into the growth flask.

The crystal growth apparatus is illustrated in figure 2.7. Letters in brackets refer to this diagram. The prepared flasks (A) were suspended in water baths (B) heated from below by an infra red lamp (C). This was connected to a contact thermometer (D) suspended in the water bath, which was stirred rapidly by a metal paddle stirrer (E) to prevent formation of a temperature gradient. Temperature control within the crystallisation vessel was maintained within $\pm$ 0.001K by this means. The

seed crystal (F) was suspended on a glass stirrer (G) within the growth flask. The action of the stirrer motor (H) was reversed at regular intervals to ensure effective stirring of the solution (to prevent formation of temperature and/or concentration gradients) and to encourage even growth on all faces of the crystal. All ground glass seals were greased to prevent solvent evaporation.

Temperature lowering was controlled by a stepping motor (I), with a speed of one revolution per hour, attached to the contact thermometer, driving down the contact inside. The lowering rate could be altered by a timer inside the control box (J) activating the motor for any required fraction of one minute. 25 complete revolutions of the motor decreased the temperature by 1°C, enabling control of the temperature lowering rate to between 0.015 and 1 $°C.day^{-1}$.

The seed crystal was lowered into the growth solution very slowly to prevent thermal shock. After allowing the system to equilibrate overnight, the temperature was raised by 0.1°C resulting in a slight undersaturation of the solution. This caused dissolution of the strained surfaces of the seed crystal; this is done to prevent propagation of defects into the bulk crystal. After 24 hours the temperature-lowering motor was engaged and crystal growth commenced.

When crystals had reached a suitable size, they were raised up through the solution and the airspace

above it over two to three hours. Slow movement through the temperature gradient prevented thermal shock. Crystals were quickly dried in soft tissue paper.

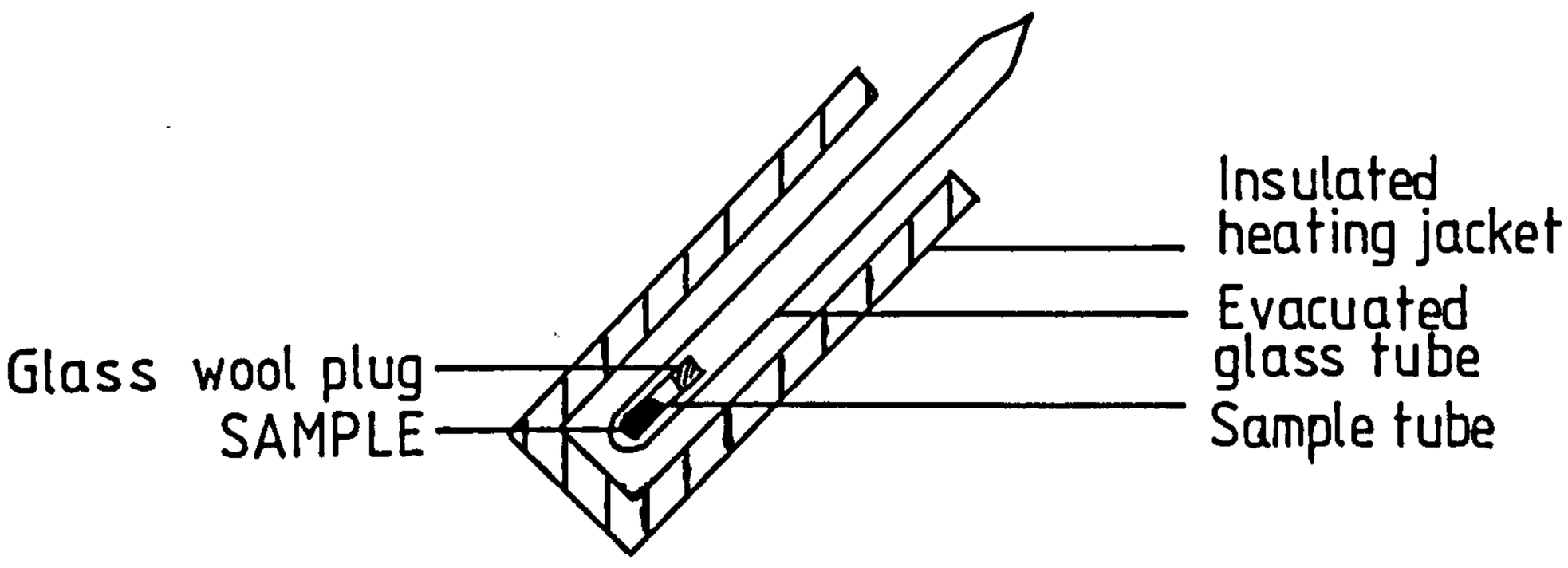

Figure 2.8: Sublimation growth furnace

2.2.2 Growth from the vapour phase

Growth of crystals from the vapour phase is ideal for producing small crystals, particularly when only a small amount of material is available or solubility data have not been determined. The material must have a high vapour pressure for this to be feasible. Separation of impurities will occur simultaneously.

An additional benefit in this instance is that when a compound of known structure crystallises from the vapour, it may be expected that only structural factors exert an influence on morphology [90].

Crystals of enantiomeric and racemic ibuprofen were grown from the vapour phase by sublimation. A small sample of either material was placed in an evacuated glass tube approximately 40cm long. The tube was placed in a furnace with a temperature gradient set up along it. The apparatus is illustrated in figure 2.8. The temperature was initially set about 20°C below the melting point of the sample (at the base of the furnace), and the temperature gradually increased until a few small crystals were formed in the cooler part of the tube, where supersaturation of the vapour induces nucleation. The temperature gradient was maintained, and growth of suitably sized crystals took about 14 days.

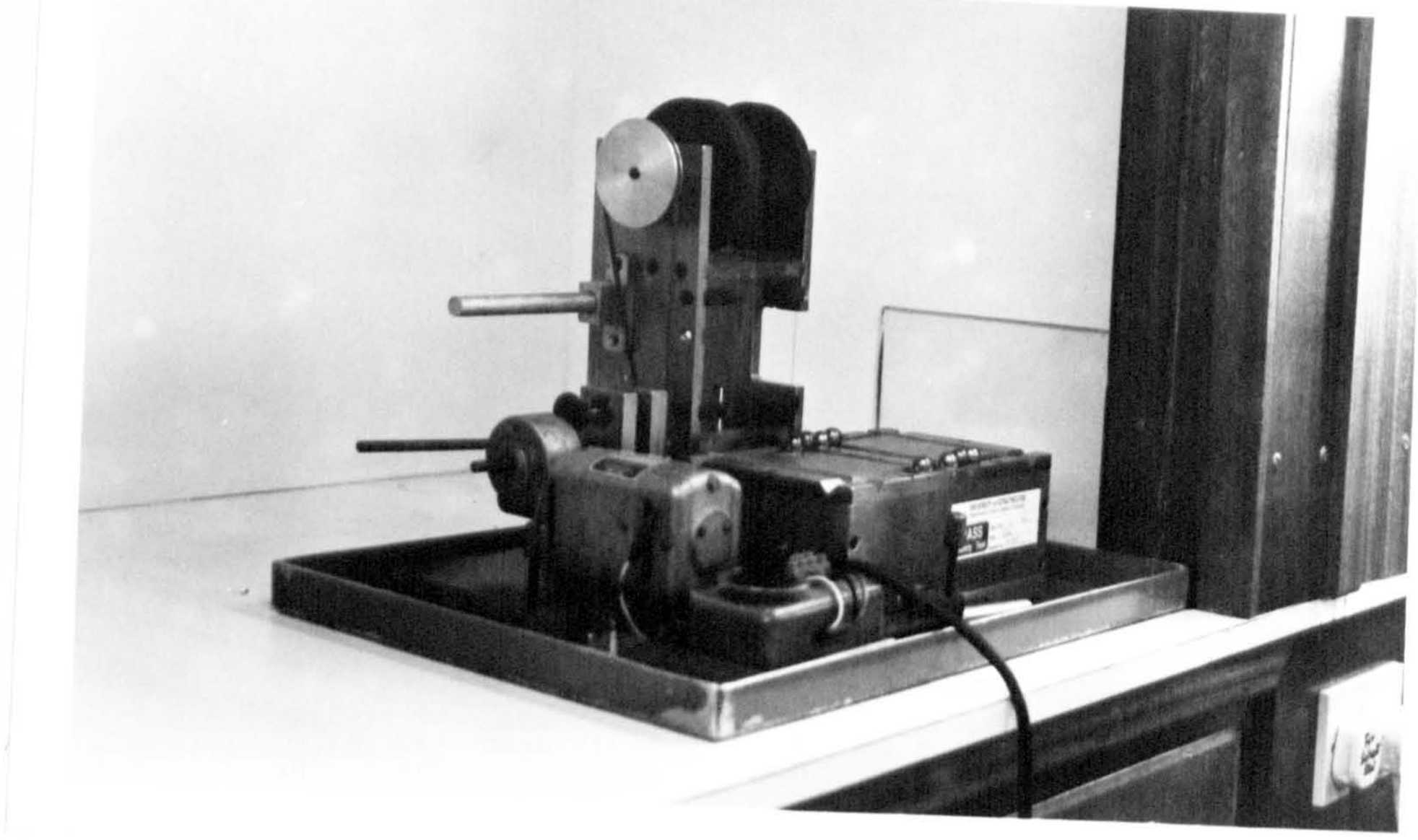

Plate 2.1: The solvent saw

2.2.3 Preparation of crystal slices

Thin flat samples of known crystallographic orientation were required for hardness testing and x-ray topography. These had to be prepared ideally without the addition of defects or strain, which may have masked differences between the samples caused by changes in growth conditions.

Ideally, samples should have been prepared by cleavage of slices from the as-grown crystal. However, ibuprofen has only one cleavage plane (the {100} plane) and samples of other orientations were prepared using a solvent saw (see plate 2.1).

Crystals were mounted on a metal stub using Araldite (Ciba-Geigy Ltd.). The stub was clamped in position on a platform such that the required plane was parallel to the cutting thread. Alignment was confirmed using an adjustable set-square with reference to a known habit face.

The platform was mounted on ball-bearings to allow free play. The whole apparatus could therefore be tilted to maintain the crystal in contact with the cutting thread. This was a continuous loop wound around a pulley and passing through a solvent reservoir. Fresh solvent was continually brought into contact with the crystal and dissolution of the crystal occurred at the point of contact with minimal damage. Excess solvent was removed from the surface with tissue paper to prevent

dissolution of surrounding crystal.

The solvent used was usually acetonitrile, since it dissolves ibuprofen well, and being less volatile than hexane leaves the crystal less susceptible to thermal shock.

Use of the solvent saw occasionally introduced small ridges on the sample surface which could then be removed by gentle polishing on solvent soaked tissue paper lying on a flat glass plate.

2.3 INSTRUMENTAL METHODS

2.3.1 Infra Red Spectroscopy

Infra red (IR) spectra were obtained from samples compressed with potassium chloride into discs using a flat faced punch and dye. A Pye Unicam SP3 spectrophotometer was used to record the spectra.

2.3.2 Nuclear Magnetic Resonance Spectroscopy

Proton Nuclear Magnetic Resonance (NMR) spectra were obtained from dissolved samples using a Bruker AMX400 spectrometer running at 300K and 400MHz.

2.3.3 Melting point determination

Melting points of samples were obtained using a Melting Point Apparatus (Galenkamp). Measurements were made at least in triplicate.

2.3.4 Differential Scanning Calorimetry

Differential Scanning Calorimetry (DSC) thermograms were obtained using a Model 9900 differential scanning calorimeter (Du Pont Instruments Ltd.). Samples of between 5 to 10 mg (accurately weighed) of powdered material were heated at 2 $^{\circ}C.min^{-1}$ in a crimped

aluminium pan. A similar empty pan was used as the reference. The latent heat of fusion (ΔH_f) of the sample was determined by integrating the area under the melting endotherm using the DSC v2.2A program.

2.3.5 High Pressure Liquid Chromatography

Sample purity was determined using a high pressure liquid chromatographic (HPLC) assay. Absorbance was measured using an ultra-violet detector (Spectra-Physics SP 8450 UV/Vis detector) set at 214nm, linked to a column (4.6mm internal diameter, length 10cm) containing 5um spherical octadecylsilane reversed phase packing material (Spherisorb, Queensferry). The mobile phase was acetonitrile, water & orthophosphoric acid (550:450:0.5) filtered and degassed prior to use. An isocratic pump (Spectra-Physics SP 8810) was used to maintain a flow rate of 0.5ml min^{-1}. Samples were dissolved in acetonitrile & water (55:45); 20ul samples were injected onto the column.

2.3.6 X-Ray Methods

The diffraction of x-rays by crystals takes place independently of the nature of the repeating units only at those particular angles of incidence, θ_B, that satisfy Bragg's Law, (equation 2.1).

$$2.d_{hkl}.\sin\theta_B = \lambda. \qquad (2.1)$$

As a result, from knowledge of the angles of reflection of a given incident beam, the orientation and spacing of the various families of crystallographic planes can be found and the cell dimensions determined.

Particular atomic or molecular arrangements can give rise to systematic absences in the diffracted beams, where total destructive interference of the beams occur due to lattice repeats within the unit cell. For example, in a cubic crystal lattice where one of the repeating units is situated at the centre of the unit cell and one at the origin (a body centred cubic lattice) the electron density of the {100} and {200} planes will be equivalent. X-rays diffracted by the {100} planes will be in phase with each other but out of phase by half a wavelength with those diffracted by the {200} planes. No beam will be diffracted by the {100} planes. Diffraction from the {200} planes will however occur, because all the atoms lie on these planes.

Plotting diffracted intensity against the angle of incidence gives rise to a series of lines, from which the cell type and dimensions can be determined.

The intensity of a diffracted beam is proportional to the square of the amplitude diffracted by the repeating unit at the angle of incidence (termed the structure factor, F_{hkl}). F_{hkl} is dependent on the nature of the repeating units, and in particular on the electron density of the diffracting planes.

2.3.6.1 Crystal Structure Determination

Deduction of the positions of atoms within the unit cell is the central problem of x-ray crystallography. Structure determination is based on the principles outlined above but is now highly automated. Measurement of the intensity of the diffracted beam at thousands of incidence angles is carried out, and the electron density distribution within the unit cell mapped out. The positions of atoms are determined from the peak values of the electron density.

Although the crystal structure of (±)-ibuprofen has been reported, there is no structural information available in the literature on the resolved isomers. A structural determination was carried out using small, single crystals of S(+)-ibuprofen, dish-grown from methanol as described in section 2.2.1.1. A colourless,

plate-shaped crystal approximately 0.4mm x 0.4mm x 0.2mm was used for structure analysis on the CAD-4 diffractometer at Glasgow University by Dr.A.A.Freer.

A least-squares technique based on 24 reflections was used to refine lattice parameters h,k and l. Structure solution was performed using MITHRIL [91]. All calculations were performed using the GX package [92].

2.3.6.2 Laue Diffraction Patterns

Diffraction of an x-ray beam incident on a crystal produces a number of diffracted beams since several crystallographic planes will be oriented at suitable angles for Bragg reflection according to equation 2.1. In addition, since the radiation used for Laue diffraction when using laboratory generators is the Bremsstrahlung radiation produced by bombardment of the metal source with electrons, rather than its characteristic monochromatic line, a wide range of x-ray wavelengths are available for diffraction, and a large number of diffraction spots are produced.

The resultant diffraction pattern is dependent on the angle of incidence of the beam (or vice versa, the crystal with respect to the beam), and is unique to the particular crystal structure. Laue patterns can therefore be used, for example, to identify crystal faces, (since the diffraction pattern obtained is dependent on the incident angle), or to check

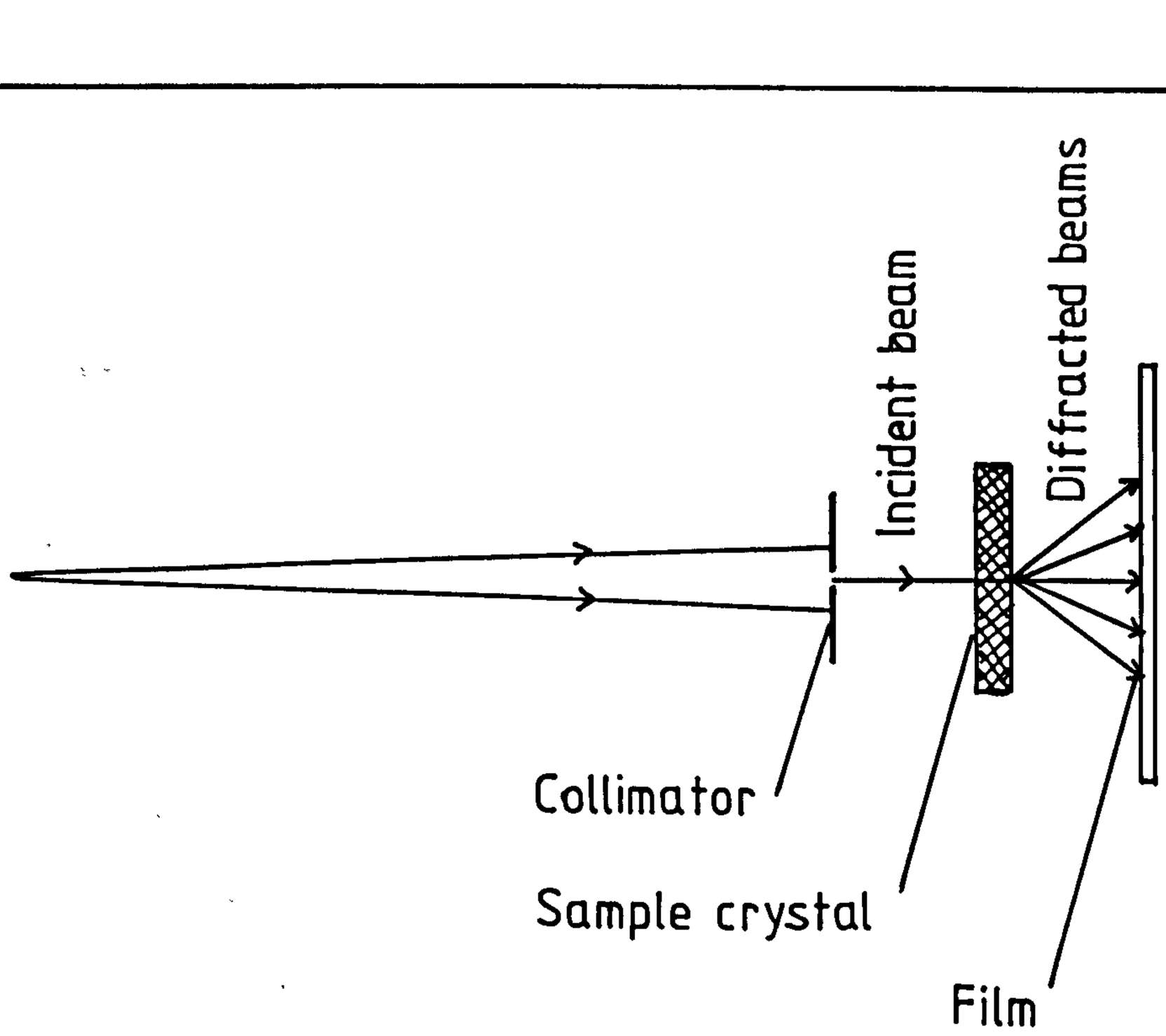

Figure 2.9: The Laue camera

orientation of the crystal for x-ray topography.

Sample crystals were mounted in plasticene on a goniometer head on the Laue camera, shown in figure 2.9 such that the face to be identified was perpendicular to the x-ray beam. Using radiation from a silver source, diffraction patterns were recorded. The sample-to-film distance was 50mm and the exposure time was 30 minutes.

The face was identified by comparison of the recorded pattern with those calculated for the possible low index faces on the LAUE program on the VAX computer at Strathclyde University (see section 2.4 for further details). The direction of other crystallographic axes could be determined from the symmetry of the diffraction patterns.

2.3.6.2.1 Use of Laue diffraction patterns to quantify crystal strain.

A perfect crystal will diffract x-rays at a small angular range around the Bragg angle, typically a few seconds of arc (known as the rocking curve width). Strained crystals, where the crystal planes are bent out of their normal orientation will therefore still be able to diffract x-ray beams, but the diffracted beam will be smeared out, since reflection of additional wavelengths will take place. This will occur whether a conventional or a synchrotron source (section 2.3.6.3) is used. The

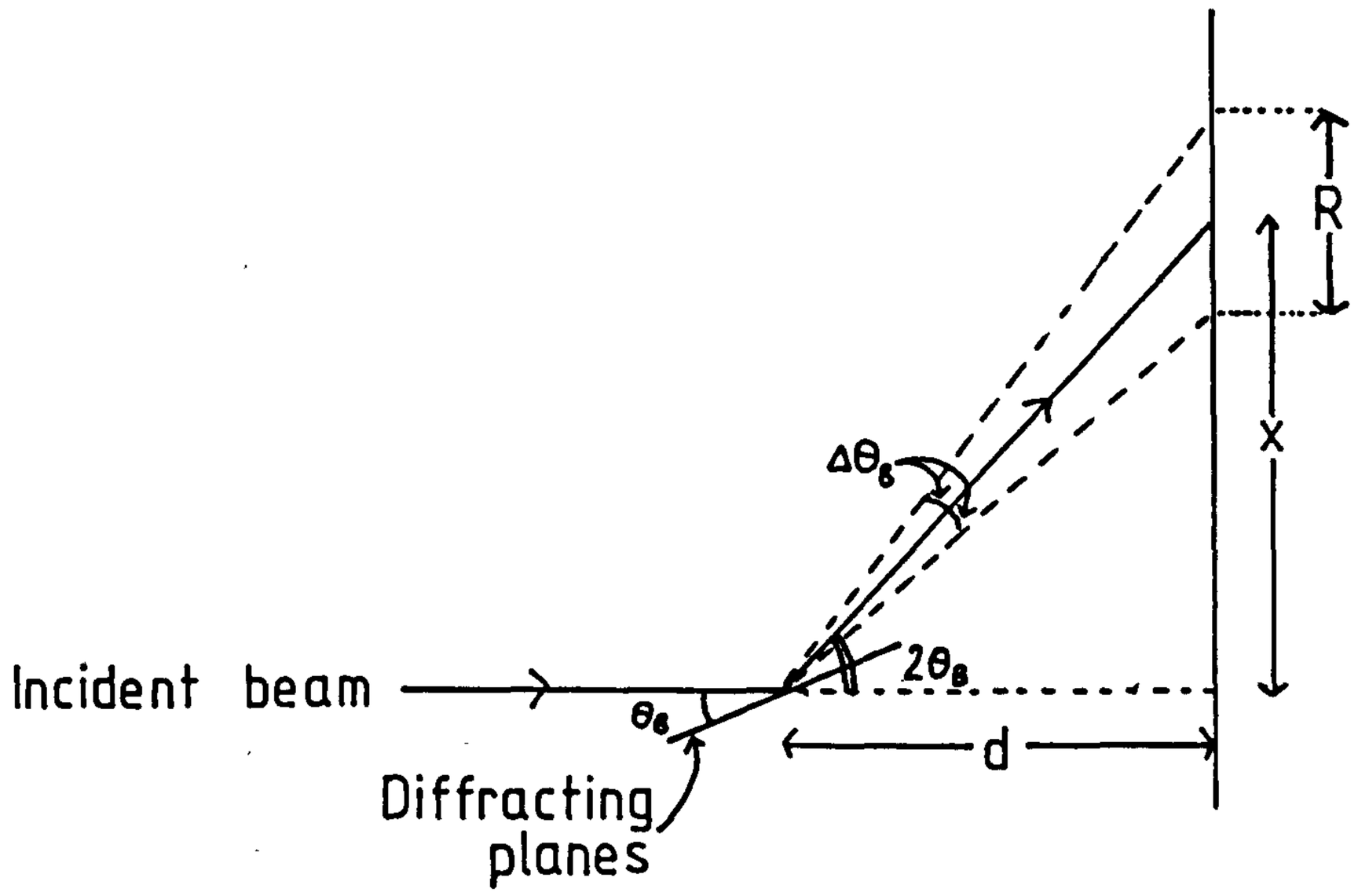

Figure 2.10: Determination of mosaic spread using Laue diffraction patterns

resultant enlargement of the lattice spot is known as asterism.

The mosaic spread (Lattice plane mismatch/ strain/ defect content) of the crystals can be calculated by comparison of the broadened diffraction spot with that from an unstrained crystal of the same size. Use of a pinhole beam and thin crystals of similar size avoids the need for calculation of the size of the unstrained diffraction spot and allows comparison of the mosaic spread between samples to be made directly.

The mosaic spread η, is equivalent to the angular spreading of the diffracted beam $\Delta\theta$ [81], illustrated in figure 2.10. It can be calculated directly from the size of the asterism, R, if the sample-to-film distance, d_{SF} is known [82]:

$$R = 2.\eta.d_{SF} / \cos^2 2\theta_B \qquad (2.2)$$

The radial spread of several reflections at different reflection angles, θ_B, should be measured to gain an indication of the average mosaic spread of a particular crystal. Measurement of the same diffraction spots for each sample is important for accurate comparison.

Laue diffraction patterns were determined as described for crystals grown both from hexane and acetonitrile. Laue diffraction patterns of both the

major face and the cleavage planes were determined. Samples of similar thickness were selected so that Laue patterns could be compared directly between samples.

Nine spots of varying size and position were selected from each Laue pattern and their diameter and distance from the x-ray source measured using a microscope fitted with a graticule. Calculation of the lattice spread was performed according to equation 2.2 and values for crystals grown from the two solvents were compared.

2.3.6.3 X-Ray Diffraction Topography

Dislocations can, in some cases, be the only potential source of crystal growth (see section 1.2.1.2.2) and many mechanical phenomena such as plastic deformation involve dislocation motion (section 1.2.2). Since crystal growth and the mobility of dislocations is strongly dependent on their character, an understanding of growth and mechanical behaviour of solids is aided by knowledge of the concentration and structure of the dislocations present. Any departure from periodicity (perfection) of a crystal lattice will be detected by x-ray diffraction, as outlined briefly in section 2.3.6.2.1, and imaging techniques using x-ray diffraction are therefore of value in dislocation characterisation.

X-ray topographical images are formed when the rays

of the diffracted beams are parallel between the crystal and the recording device. Reviews of diffraction theory can be found in references 83,84,93 & 94. Images are formed of the strain fields around a defect, rather than the defect itself.

The two parameters of paramount importance when designing a topographic experiment are the rocking curve width of a perfect crystal, and the extinction distance of the sample. These will be defined, and their influence on image formation and experimental design discussed.

Rocking curve width ($d\theta^{1/2}$)

The rocking curve width of a symmetrical x-ray reflection is given by:

$$d\theta^{1/2} = 2.d_{hkl}.C_p.\lambda.|F| \;/\; n.V_c.\cos\theta_B \qquad (2.3)$$

where d_{hkl} = interplanar spacing of reflecting planes;

C_p = polarisation factor; c=1 or [cos 2θ]

λ = wavelength

$|F|$ = structure factor in absolute units

n = number of molecules per unit cell

V_c = unit cell volume

A reflection which has a wide $d\theta^{1/2}$ (ie large F_{hkl}, low order reflection) has a high spatial

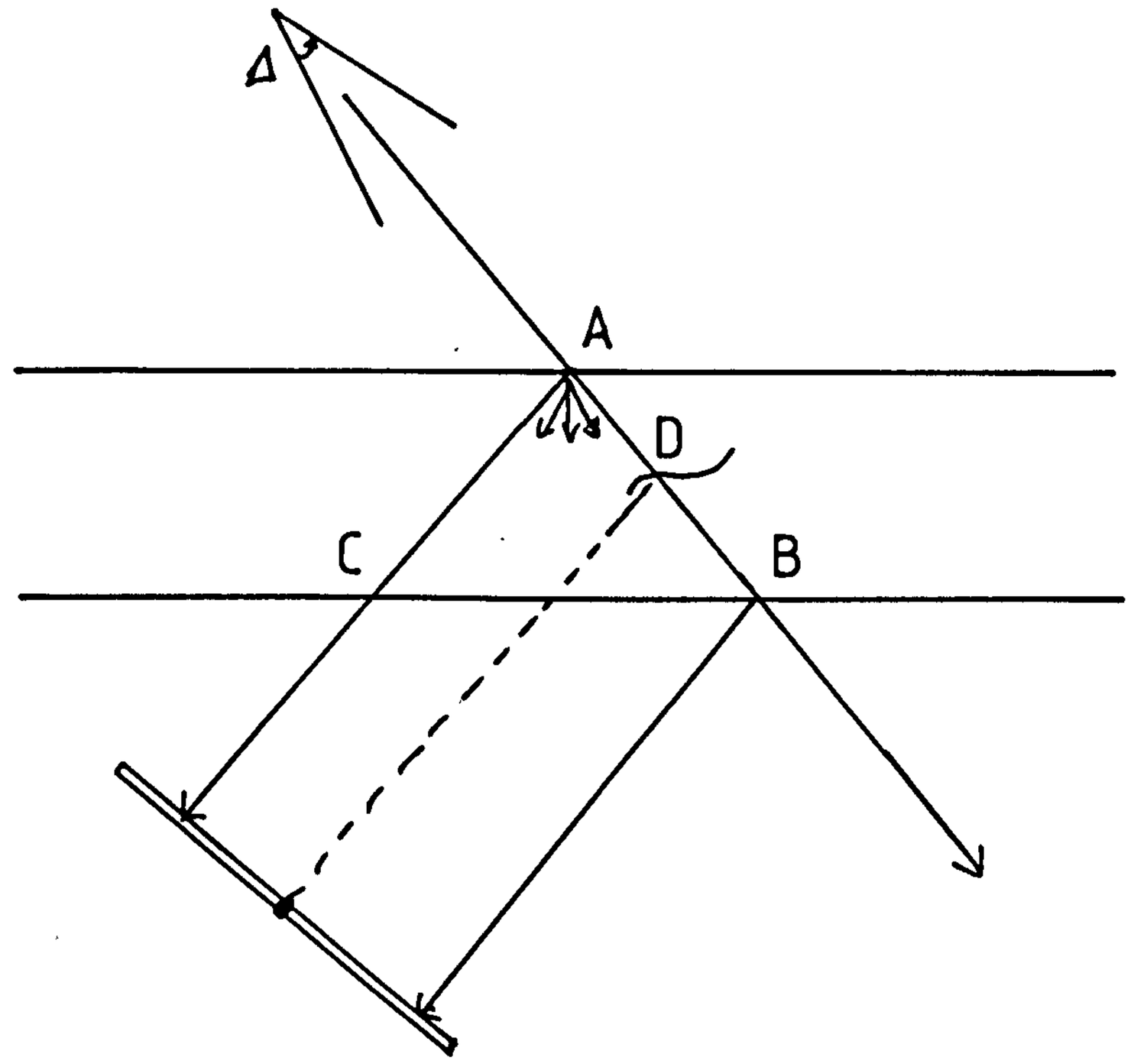

Figure 2.11: Propagation of diffracted and transmitted x-ray beams inside a crystal

resolution and low strain sensitivity. For the purposes of dislocation characterisation, high spatial resolution is desirable, therefore reflections with a wide $d\theta^{1/2}$ are preferable.

Extinction distance, ξ_g

If the incident wave is a plane wave, which can be assumed if synchrotron radiation is used, two beams propagate inside the crystal. These are the transmitted (AB) and diffracted (AC) beams, illustrated in figure 2.11. Since the diffracted and transmitted beams are produced due to Bragg reflection, both are travelling in directions that satisfy Braggs law and so both will continue to be scattered. After penetrating a certain depth ($0.5\xi_g$) all the intensity has been scattered into the diffracted beam; after a further $0.5\xi_g$ it is all scattered back into the transmitted beam, and the diffracted beam is reduced to zero. The proportion of the total transmitted intensity in each component is therefore dependent on the thickness of the crystal relative to the ξ_g for the particular Bragg planes.

$$\xi_g^{-1} = \lambda . |F| \; / \; n . V_c . \cos\theta_B \qquad (2.4)$$

and ξ_g is therefore related to the rocking curve width by:

$$d\theta^{1/2} = 2.d_{hkl}.\xi_g^{-1} \qquad (2.5)$$

Dislocation images cannot be observed in samples less than 0.3ξ thick, but are most strongly contrasted at thicknesses corresponding to 0.8ξ.

Image formation

In all except very thin samples, the repeated transfer of intensity between transmitted and diffracted components must be considered, using the dynamical theory of diffraction [83,94]. The two components are considered to interact to produce two standing wavefields which propagate inside triangle ABC. Type 2 wavefields have their maxima on the crystal planes (& are strongly scattered); maxima of type one wavefields are halfway between the planes (& are weakly scattered). Both wavefields have transmitted and diffracted components which form two beams at the exit surface, forming a fan bounded by the diffracted and transmitted beams within the crystal. The dynamical image of a dislocation is its "shadow" in this fan of wavefields (the Bormann fan), due to the change in the ratio of the diffracted and transmitted components of the wavefields as they pass through the strained area (wavepoint migration). The change in intensity of the diffracted

beam gives rise to the black and white contrast of the dynamical image.

In a perfect crystal, the two wavefields interfere to produce fringes whose spacing is the extinction distance. These are known as PendellÖsung fringes, and, if exhibited when using experimental samples, are an indication of high crystal perfection.

Fringes are also produced when the strain associated with a defect is large. Decoupling of the wavefields into their diffracted and transmitted components occurs. These then recombine to produce two new wavefields which interfere (interbranch scattering).

Absorption of x-rays

The absorption of x-rays by the crystal is of significance when determining the types of image observed in topographs. The linear absorption coefficient, μ, is given by:

$$\mu = n / V_c . \Sigma (\mu_a)_i \qquad (2.6)$$

n = number of molecules in the unit cell,

$(\mu_a)_i$ = atomic absorption coefficient of atomic species i.

In thin crystals, such that $\mu t < 1$ (t = crystal thickness), the direct image is strongly contrasted. No

dynamical images are observed since neither wavefield is appreciably absorbed, and any effects due to wavefield migration are cancelled out (since the change in ratio of diffracted to transmitted components of one wavefield is equal and opposite to that of the other wavefield).

When $1 < \mu t < 10$, the direct image is weakened due to absorption, but still visible. Absorption of type 2 wavefields is greater than for type 1, so the changes in diffracted and transmitted components no longer cancel and wavepoint migration effects produce dynamical images. As ut increases, Pendellösung fringes and interbranch scattering become less pronounced.

In thicker crystal, $\mu t > 10$, both the direct beam and type 2 wavefields are completely absorbed, hence neither direct images or Pendellösung effects are observed. Defects lying close to the exit surface may produce images due to wavepoint migration and interbranch scattering.

Dislocation characterisation

Dislocation characterisation can be carried out utilising the variation in contrast of dislocations in x-ray topographs of different reflections. Since the molecular displacements around the dislocations can be unambiguously defined by the Burgers vector, $\underline{b}$, the strain field will be visible only in reflections from specific planes. A more comprehensive review can be

found in reference 95.

Experimental design

Design of topographic experiments involves selection of four major conditions, which tend to be interdependent, and the final conditions are often a compromise.

1. X-ray reflection: this should have a wide $d\theta^{1/2}$ for good resolution.

2. Slice plane: Growth dislocations are normally revealed in slices cut normal to the growth faces. The chosen slice planes should also allow the maximum number of reflections to be used for dislocation characterisation. Diffracting planes less than ~60° from the slice plane (as $d\theta^{1/2}$ decreases below this due to the reflection geometry) tend to produce distorted images.

3. X-ray wavelength and 4.sample thickness: Use of a longer wavelength radiation will increase spatial resolution (as $d\theta^{1/2}$ increases). Resolution also improves if only direct images are present. This requires a low value of ut, achieved by using lower wavelength radiation or decreasing slice thickness. The lower limit on sample thickness is set by 0.3ξ; the upper limit by the defect density of the sample. When the linear absorption coefficient is low, values of μt = 1 may be achieved at ~5mm, but superimposition of

defects may prevent resolution of individual defects. A compromise of the above factors may therefore be necessary.

Synchrotron radiation

Synchrotron radiation is a polychromatic continuous source of radiation in the range 3 - 25 nm. Its intensity is approximately 100 times greater than that of conventional x-ray sources, allowing topographic images to be obtained in minutes rather than hours. Orientation of the sample at the correct angle for Bragg reflection by the diffracting planes effectively selects out a particular wavelength of radiation. Alternatively, it can be used to obtain topographic images in the same manner as Laue diffraction patterns. The range of wavelengths available allows Laue diffraction from many planes. Increasing the sample-to-film (SF) distance allows separation of any of these images in order to determine which images offer the best resolution and imaging of defects, although resolution of individual images will be decreased. The Bragg angle of the reflection can be calculated from the SF distance and the distance of the image from the centre of the film. A topograph recorded of the selected image using a short sample-to-film distance offers improved resolution.

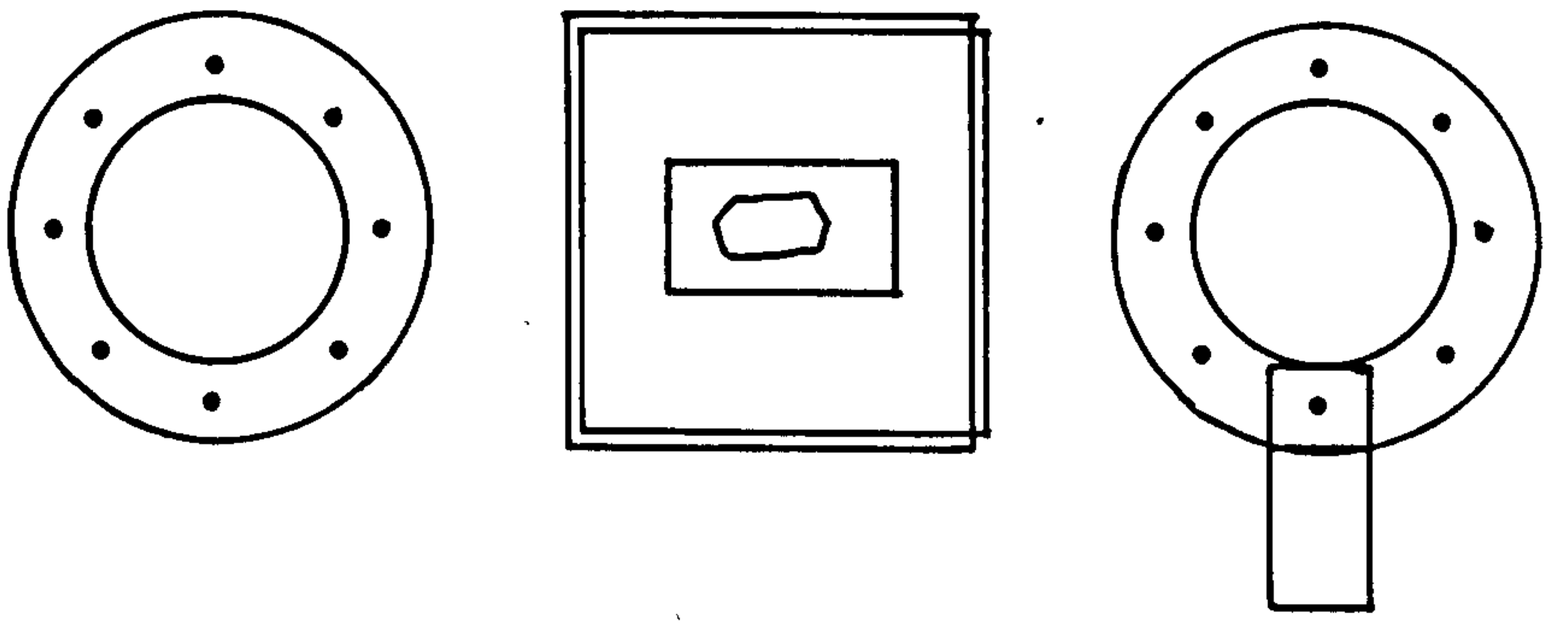

Figure 2.12: Sample holders for x-ray topography

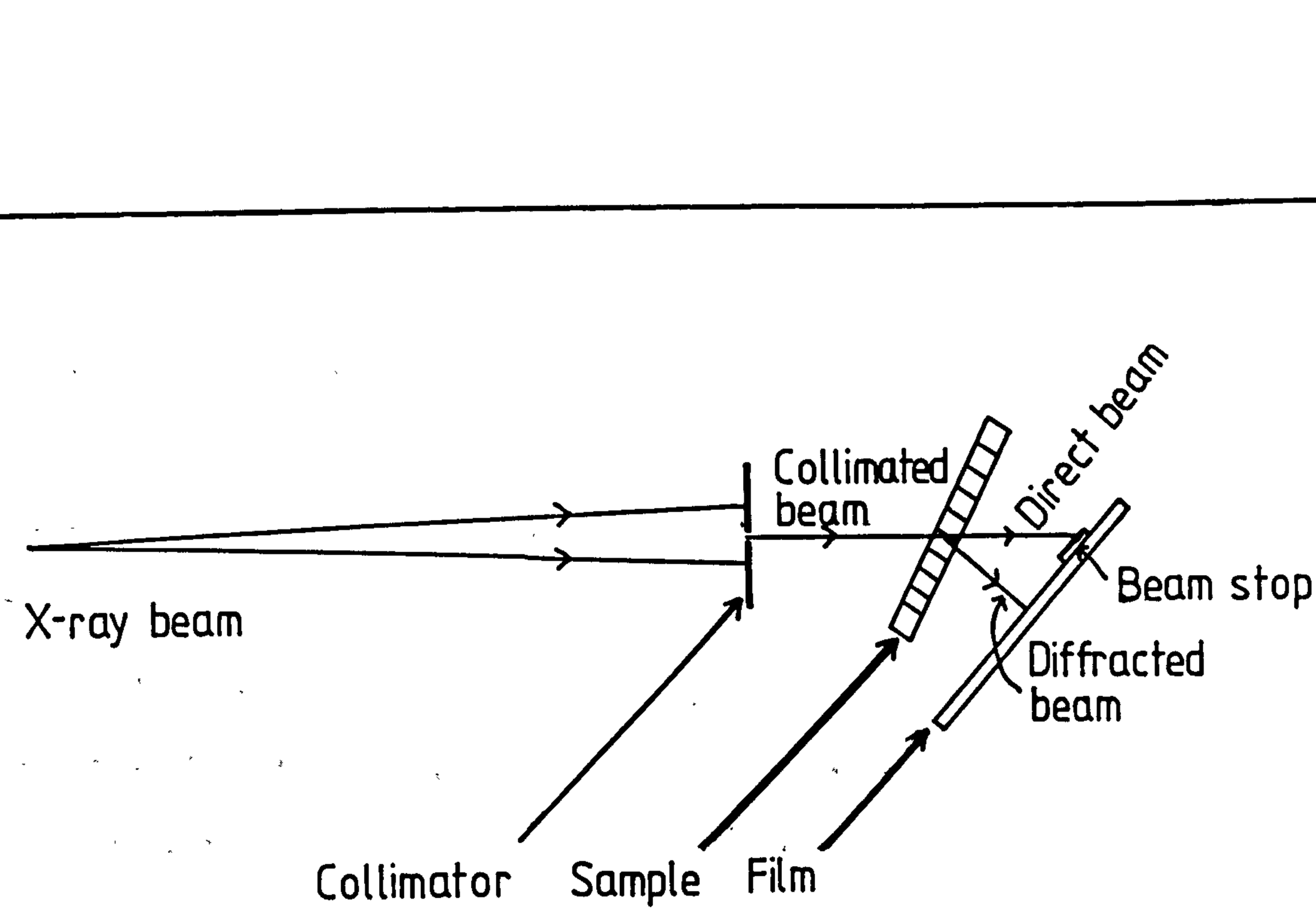

Figure 2.13: Experimental set up for recording x-ray diffraction topographs

Recording of X-ray Diffraction Topographs

The experimental procedures for recording x-ray diffraction topographs have been previously described[83,84]. All experiments in this work were performed on the white radiation camera of the Synchrotron Radiation Source at Daresbury Laboratory.

The sample holders in which crystal slices were mounted for topography are shown in figure 2.12. Crystal slices were held firmly in position between Mylar sheets, which were in turn clamped between aluminium rings. The sample holder was clamped onto the goniometer of the white radiation camera by means of the attached stub. The x-ray beam on this camera is a low divergence, high intensity, polychromatic beam. Good topographs can therefore be obtained in a relatively short time due to the beam intensity; any wavelength required can be selected from the polychromatic beam by orientation of the diffracting planes to the appropriate Bragg angle.

The following method was used on the synchrotron radiation source at SERC Daresbury laboratory using the apparatus illustrated in figure 2.13:

1. The sample was oriented with the slice plane normal to the x-ray beam using spot laues to check orientation.
2. The sample was rotated about the horizontal axis until the diffracting planes were set at the appropriate

Bragg angle, Θ_B, to produce a specific reflection for the selected wavelength.

3. Detector set at an angle of $2\Theta_B$ to the incident beam.

4. A test exposure was recorded using fast film such as Agfa Osray M3 (which requires short exposure times, at the expense of resolution) perpendicular to the diffracted beam, to check sample alignment and allow an estimate of exposure time to be made.

5. If satisfactory, a slower, high resolution film was placed in a lightproof cassette and a topograph recorded.

The recording media used are shown in table 2.2.

Medium	Relative exposure
Ilford L4 plate	5
Agfa Structurix D4 film	4
Agfa Osray M3 film	1

TABLE 2.2: X-RAY RECORDING MEDIA.

Topographs were developed immediately.

Intermediate negatives of the topographic images were recorded on Kodak Technical Pan film, on an Olympus OM-2 camera mounted on an Olympus PMT-35 photomacrography system.

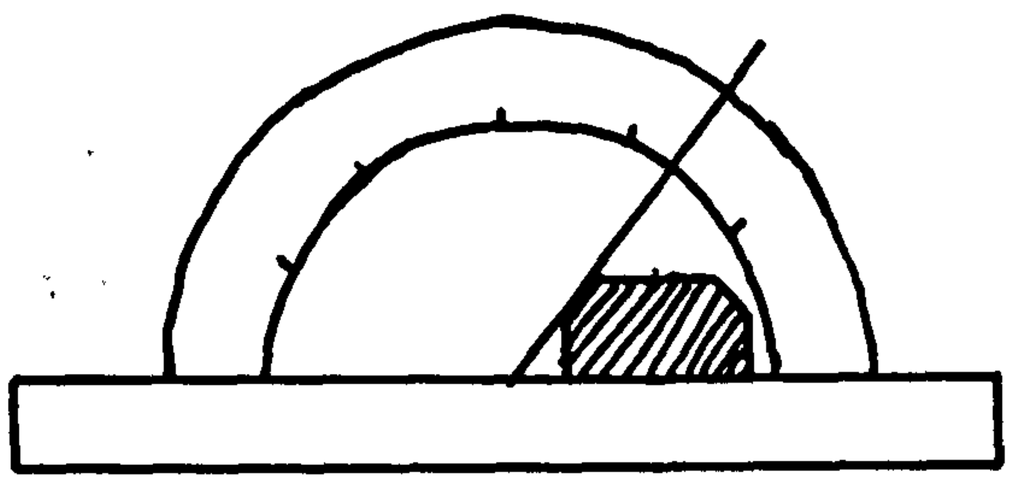

Figure 2.14: Contact goniometer

2.3.7 Characterisation of crystal habit

In order to quantify differences of crystal habit due to crystallisation solvent, the equivalent growth faces present in each crystal must be identified. Laue diffraction patterns were used to identify the major face (as described in section 2.3.6.2), and using this co-reference, the smaller faces could then be identified by measurement of interfacial angles.

Interfacial angles were measured directly, where possible, and faces identified with reference to the major faces using stereographic projections. Where this could not be carried out (on smaller crystals), angles were measured from photographs or from scanning electron micrographs taken perpendicular to one of the major faces. A contact goniometer, illustrated in figure 2.14, could be used either to directly measure some of the interfacial angles, or to measure the angles of intersection of side faces where they met on one of the major faces.

Calculated stereographic projections plotted normal to the major faces were then used to identify the growth forms. An example of this is illustrated in figure 2.15, which illustrates identification of some of the smaller faces with angles measured as they intersected on the {100} face.

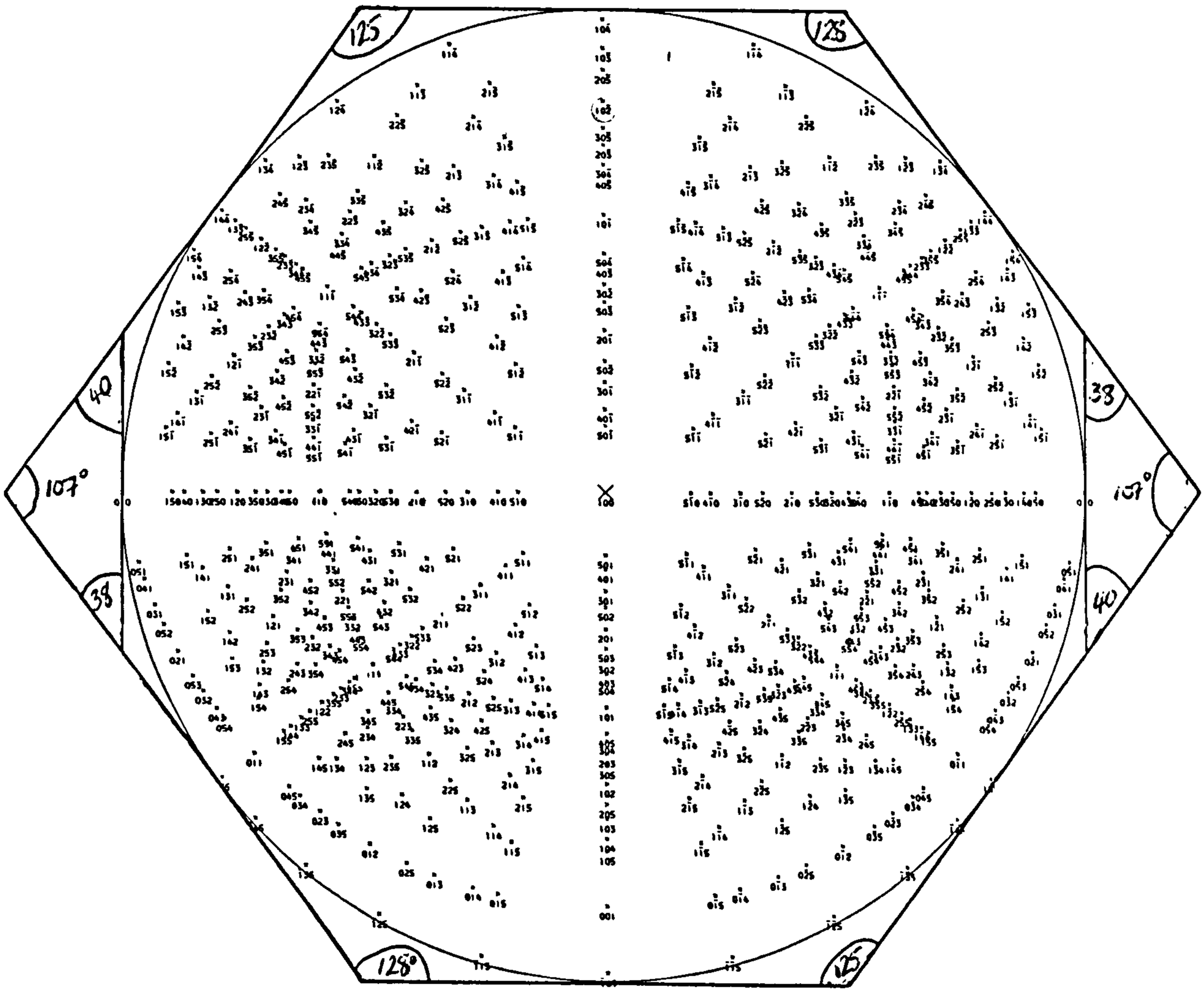

Stereographic Projection of POLES

.OF IBUPROFEN

VIEW ALONG THE NORMAL OF (1 0 0)

A= 14.667 B= 7.886 C= 10.730
ALPHA= 90.00 BETA= 99.36 GAMMA= 90.00

Figure 2.15: Use of stereographic projections to identify crystal faces

For larger crystals, a micrometer was used to measure the crystal dimensions along the three axes. For smaller crystals, the relative lengths along the growth dimensions was measured from optical micrographs or SEM's.

2.3.8 Single crystal dissolution testing

Increasing defect density (dislocations and other imperfections) tends to lead to increases in crystal dissolution rate [43] as outlined in section 1.2.1.1. Bulk dissolution rates are also affected by crystal habit however [96], and so were not suitable for comparison of ibuprofen crystals grown from hexane and acetonitrile. Single crystal dissolution techniques, more commonly used to investigate dissolution anisotropy of crystals[97] allow the rate of dissolution of individual crystal faces to be measured, and so the effect of defect density on dissolution rate can be determined.

When considering dissolution kinetics, the rate-controlling process must be considered. If the rate of removal of molecules at the crystal-solvent interface is very much faster than the rate of transport of dissolved solute away from the surface, the rate of dissolution will be the rate controlling process, and no dissolution anisotropy will be observed. Differences in the dissolution rates of different crystal faces, or due to differing defect density, will only be observed if the rate of surface "reaction" is rate controlling, or if both rates are of the same order of magnitude (mixed transport-surface-controlled dissolution).

Transport-controlled dissolution is generally represented by the Noyes-Nernst equation:

$$\text{Rate} = S.k_t.(C_s - C) \qquad (2.7)$$

where k_t = transport rate constant = D/h; D is the diffusion coefficient of the solute in the stationary layer of thickness h considered to be adhering to the crystal surface;

C_s is the equilibrium concentration in the saturated layer at the solid-solvent interface;

C is the concentration in the bulk solution at time t; and

S is the surface area of the solid.

If it is assumed that the surface interaction and transport processes occur sequentially, equation 2.7 can be extended to include the mixed control situation, becoming:

$$\text{Rate} = S.k_{obs}.(C_s - C) \qquad (2.8)$$

$$k_{obs} = k_r.k_t \;/\; (k_r + k_t) \qquad (2.9)$$

where k_r is the rate constant for the surface reaction.

When $k_r >> k_t$, equation 2.8 becomes the Noyes-Nernst equation. When $k_r << k_t$ dissolution becomes surface-controlled, in which the equilibrium concentration in the interfacial layer C_i is less than the equilibrium solubility.

The rate controlling process can be determined by measurement of dissolution rates at several flow rates. Values of the rate constants can be calculated by repeating the experiment at various temperatures [97].

The single crystal dissolution apparatus (shown in Figure 2.16) consisted of a cylindrical flow cell with glass windows. Deionised water at the desired temperature was pumped through at the required flow rate from a thermostatted reservoir controlled with a contact thermometer and infra red heating lamp.

The temperature was monitored using a thermocouple inside the flow cell, and the flow rate by a flowmeter on the return of water to the reservoir.

The sample crystal was mounted on an aluminium stub with Araldite and was inserted into the flow cell; air bubbles were removed, and the system allowed to equilibrate for one hour.

The retraction of any individual crystal face could be measured using an adjustable micrometer mounted in the eyepiece lens of the microscope on which the flow cell was mounted. For consistency between samples, the movement of the same face, mounted perpendicular to the flow of water, was always measured.

Three samples each of small crystals grown from acetonitrile and from hexane were studied at three different temperatures (30, 35 and 40°C) and at two different flow rates.

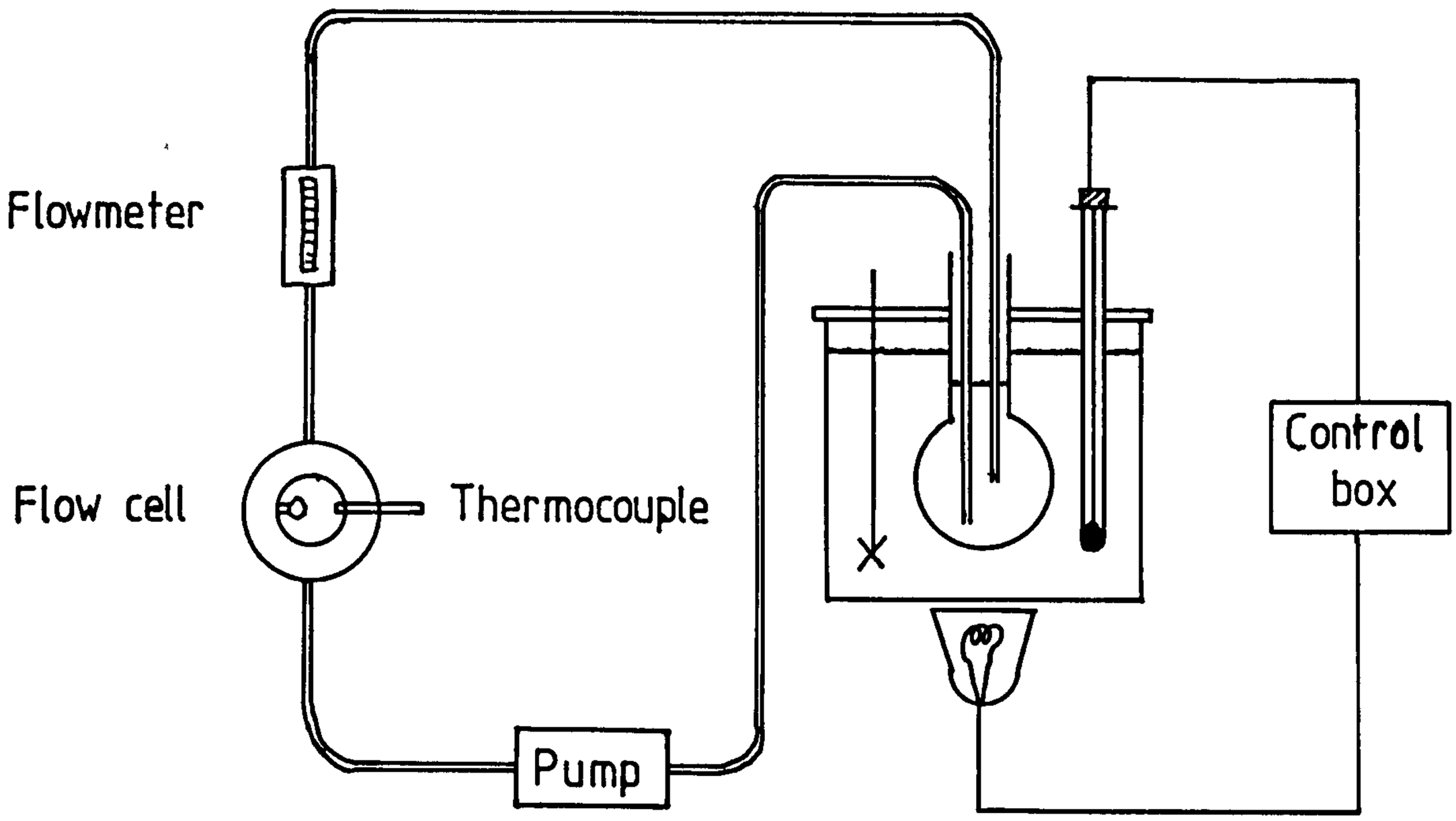

Figure 2.16: Single crystal dissolution apparatus

The volume of water used was 2.0 litres, sufficient to ensure sink conditions were maintained, and dissolved ibuprofen was not sufficient to alter the pH of the solution, which may have suppressed further dissolution.

2.3.9 The Knoop Microindentation Hardness Test

Hardness is defined as the resistance of a solid to local deformation. Since permanent deformation is due to the plastic behaviour of the material, measurement of hardness can provide information concerning the processes involved during plastic deformation. Hardness testing techniques involve pressing a hard indenter into the sample surface and measuring the size of the permanent indentation formed. These techniques have been employed industrially using spherical [98], conical [99] and pyramidal indenters [100], amongst others [101]. General reviews can also be found in references 75 and 102. For small crystals, microindentation techniques at very low loads can be used, enabling many measurements to be made on one sample.

Very few studies have been made on hardness anisotropy of organic materials. It is not clear whether the deformation processes which operate in inorganic materials will still function, or whether the molecularly rough surfaces will change the nature of the slip process. Organic materials tend for example to be more brittle [70], as slip occurs less readily. The following discussion primarily considers deformation of inorganic materials, but includes discussion of any additional factors which must be considered.

An increase in crystal hardness has been shown to

be associated with an increase in the bulk modulus 65 of the material, and provided indents are deep enough, microindentation hardness measurements can be used to compare bulk properties.

In microindentation hardness tests, a diamond indenter is pressed normally on to the surface under examination, being lowered at a controlled rate. Loads of 15g to 1kg can be employed as necessary. The indenter stresses the sample for a standard length of time, generally of the order of 30 seconds to 1 minute. During this period, plastic flow occurs, producing a permanent indentation of the same shape as the indenter. The indenter pressure will be proportional to the uniaxial flow stress of the material, the proportionality factor being dependent on the elasticity of the material.

As the indenter is removed, there is some elastic recovery, depending not only on the elasticity of the material, but also on the shape of the indenter. The magnitude of the projected area of the indentation is a measure of the hardness number of the material, which has units of stress.

As described in section 1.2.2, plastic flow or slip occurs more or less readily on different sets of crystal planes. The hardness number will therefore vary with the orientation of an indenter on the specimen surface, being dependent on the stresses applied in the slip direction. The Knoop indenter [74] is the only indenter which is useful in the study of the effect of crystal

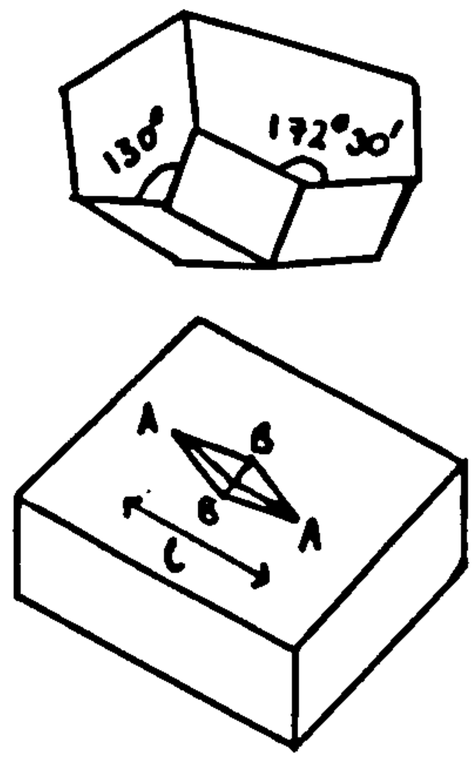

Figure 2.17: The Knoop indenter and the indentation produced

orientation on hardness, due to its asymmetrical shape. This means both that the stresses applied along the two diagonals will be unequal, and orientation of the indenter with respect to the various crystal planes can therefore be more easily determined. Its shape is such that it produces elongated pyramidal impressions as illustrated in figure 2.17. The length to breadth ratio is approximately 7:1. A specimen under load will therefore be greatly strained across the breadth BB, and relatively unstrained beyond AA. The major part of the elastic recovery of the indentation upon removal of the indenter will therefore take place across the breadth, and the length will remain that of the unrecovered indentation. Thus both plastic and elastic properties of the material can be determined if required. As the size of the unrecovered indentation is more useful in this study (since this will include both elastic and plastic portions of the deformation [103]) the Knoop hardness number, KHN, may be calculated from the length, l of the long diagonal.

$$KHN = \text{Load} / \text{Projected Area}$$
$$= 14.23 \times \text{load} / l^2 \ (kgmm^{-2}) \qquad (2.10)$$

A small amount of cracking around an indentation does not affect the validity of the hardness measurements [104], although it may lead to difficulty in determining the end of the indentation if the crack lies

along the long axis of the indenter. The Knoop indenter was developed to allow determination of hardness values from relatively brittle materials minimising fracture, since its blunt nature causes development of a high hydrostatic pressure.

The principle of geometric similarity states that two indentations of the same shape have geometrically equivalent stress patterns associated with them, implying that hardness is independent of load. This is only valid for large indentations (>100μm). At low loads, hardness may apparently increase with decreasing load since fewer dislocations may become available for slip in the small volumes of crystal involved [105]. It is also more difficult to resolve the ends of smaller indentations [74]. If more than one slip system can be activated, increasing the load may increase the number of active systems and so decrease the apparent hardness by this means also. The load must therefore remain constant during testing.

Hardness is also time-dependent, especially for ductile materials. Application of a stress over a long period of time may cause creep processes to operate. Contact times must also remain constant from one indentation to another to avoid complications arising from this effect.

Crystal slices were prepared as described in section 2.3.3, by cleaving, or cutting crystals with the

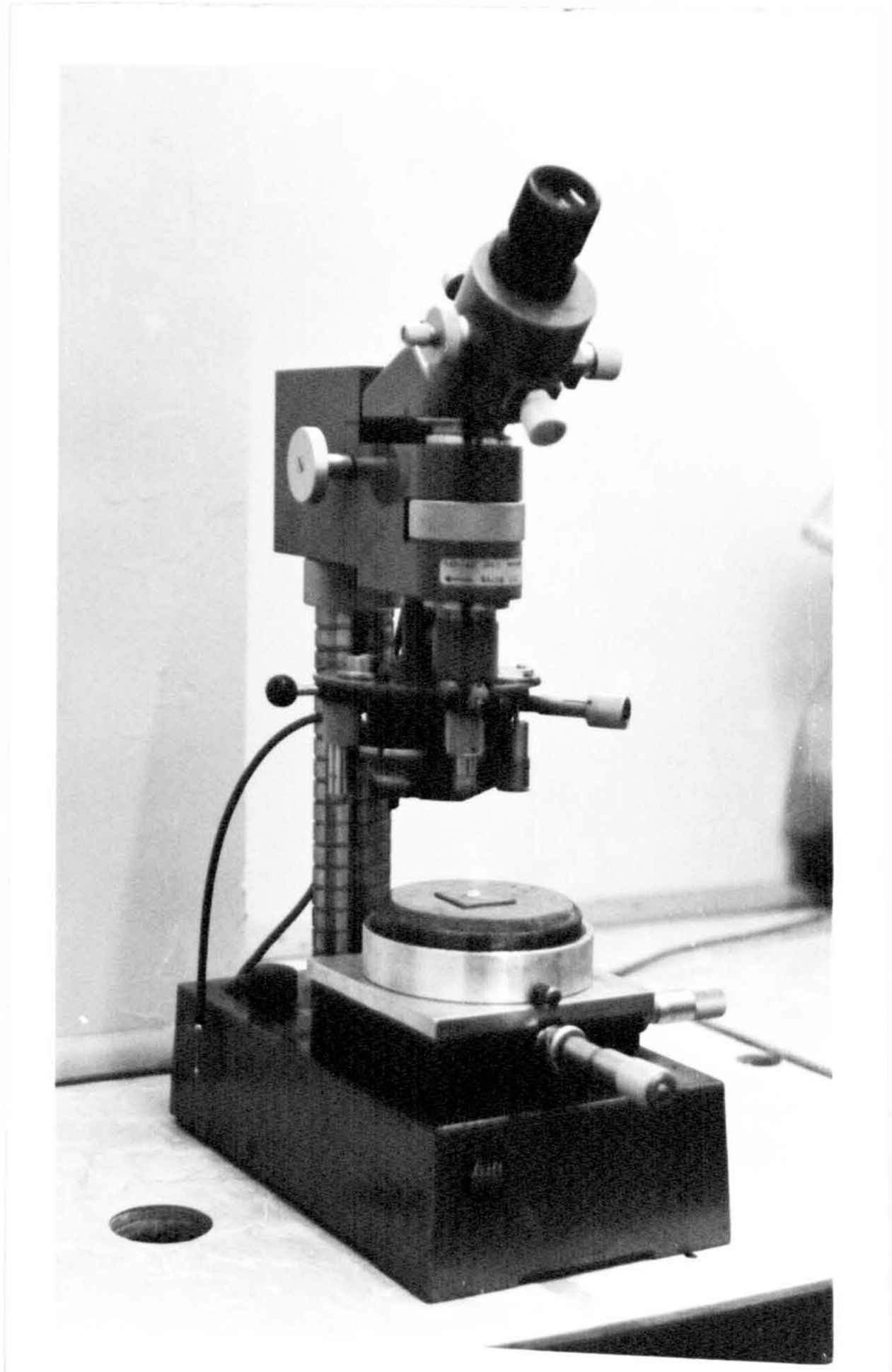

Plate 2.2: The Leitz microindenter

solvent saw as necessary. Habit or cleavage faces were preferred due to their flatness. The samples were at least ten times the depth of the indentations, to prevent the underlying mount affecting the hardness number. 1mm thick samples were found to be suitable for this. Crystal slices were fixed on 1mm thick brass plates with Araldite, and allowed to set for at least 24 hours prior to testing.

Hardness measurements were determined using the Leitz miniload hardness tester (shown in plate 2.2) fitted with a Knoop indenter. The prepared samples were mounted on the measuring stage of the miniload tester and the surface to be indented adjusted to the level (horizontal) position using the adjustable legs of the stage. This was done initially by eye, then refined by focusing across the sample surface using a 40 x microscopic objective. Trial indents were checked for symmetry to ensure that the surface was level.

The instrument has a number of interchangeable loading weights in the range 15g to 1000g so an appropriate weight could be chosen. A suitable weight was found to be 15g - giving reproducible indents of reasonable size without cracking the samples.

The travelling stage of the indenter could be moved to allow selection of a suitable indentation site, away from obviously strained areas (such as inclusions below the surface) and the edge of the sample, since this would not give indentations representative of the bulk

crystal. The measuring objective was focussed on the sample surface to ensure the indenter was always dropped from a constant height. The indenter was then moved into position and lowered on to the sample surface. This was carried out at a constant rate to ensure testing conditions were identical between indentations, and between different samples. A 15 second lowering time, 30 second indentation time and then 15 seconds to raise the indenter were found to give adequately sized indentations. Measurement of the length of the main diagonal was made using an adjustable scale in the eyepiece graticule. This process was repeated six to ten times at various positions over the sample surface for the same indenter orientation. The stage was then rotated through ten degrees to a new position using a turntable and the process repeated. Distorted indentations were discarded as measurement errors were unavoidable.

2.3.9.1 Analysis of plastic flow around the indenter

Hardness anisotropy arises on a particular surface due to plastic flow being possible on only a limited number of slip planes. The active slip systems are generally those on which the highest resolved shear stresses can be generated. This is dependent on the crystal structure and hardness anisotropy may be

correlated with effective resolved shear stress (ERSS) in order to identify the active slip systems in a particular material.

The relationship between hardness anisotropy and crystal orientation was derived by Daniels and Dunn [106], on the basis of calculated ERSS. A large indentation (ie low hardness) indicates high shear on the slip planes, and hardness may be considered as an inverse function of shear stress (ie ease of slip). The primary slip system may be identified by this relationship. Calculation of ERSS firstly involves analysis of the deformation process and identification of potential slip systems.

As a general rule, when considering inorganic materials, slip takes place only in the direction and on the plane of densest atomic packing. Whilst this is useful in making an initial forecast of potential slip planes and Burgers vectors in organic molecular solids, consideration must also be given to the conformation of the surfaces of the proposed slip planes in order to ensure there are no molecular barriers to slip.

It has been shown that hardness anisotropy can generally be better correlated with tensile stresses (generated parallel to the indenter facets) than with compressive stresses (normal to the indenter facets) [78]. Since tensile stresses generated during Knoop indentation are highest along the long axis of the indenter, slip systems will be most easily activated when the long axis is parallel to the relevant slip

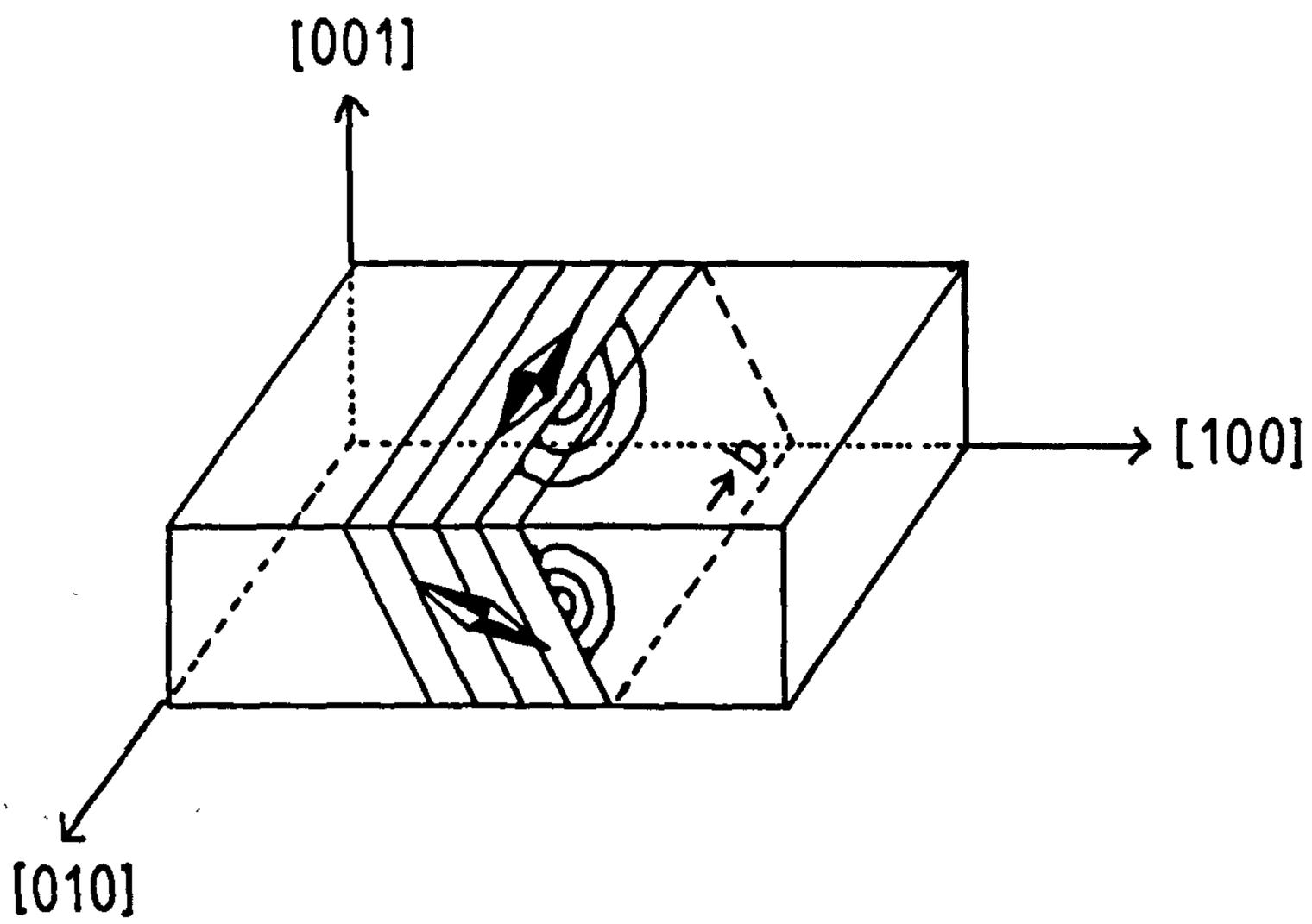

Figure 2.18: Formation of dislocation loops under an indentation

planes, resulting in a minimum in the KHN at this orientation.

The movement of dislocations during indentation results in the formation of dislocation loops as illustrated in figure 2.18. These may be circular as illustrated, but are more likely to consist of segments of straight edge and screw dislocations with the same Burgers vector. Alignments of the emergent dislocations on the crystal surfaces follow the intersection of the slip plane with the indented surface.

Examination of the movement of dislocations in samples under stress was first carried out using chemical etching techniques[108]. Etching is a technique based on the enhanced reactivity of a material at emergent dislocations. The strain associated with the dislocation core [109], or surface steps produced by a screw dislocation for example [20], results in preferential dissolution by solutions (chemical etching)[76] or enhanced sublimation rates (thermal etching) [77] due to a decrease in the relevant activation energy.

Since dislocations tend to glide along certain planes within a crystal, etch pits are often aligned in specific directions. Examination of these alignments on various crystallographic planes may disclose the active slip planes within a crystal. Used in conjunction with hardness tests, the etch pit alignment may provide an indication of the slip systems activated by shear

stresses.

Potential slip systems can therefore be identified on the basis of:

1. high d_{hkl} - usually associated with the weakest interactions between planes;

2. small $\underline{b}$ - to minimise the line energy of associated dislocations (eqn.1.10). $\underline{b}$ must lie in the slip plane;

3. lack of molecular impediments to slip in organic materials must be considered - e.g. hydrogen-bonding or molecularly rough surfaces. Some conformational changes are possible, to allow slip to occur, and will be dependent on the molecular structure of the individual system.

1. and 2. above can be determined from unit cell parameters. 3. requires closer investigation of the molecular structure of the proposed slip planes, which can be most simply undertaken with the aid of crystal drawing programs such as ORTEP [111] or INTERCHEM [112] which can be used to generate drawings of the crystal planes of interest.

Daniels and Dunn [106] suggested that the process of indentation could be considered in terms of the deformation of cylindrical elements of the material, subject to tensile forces parallel to the line of steepest slope on the individual facets of the indenter.

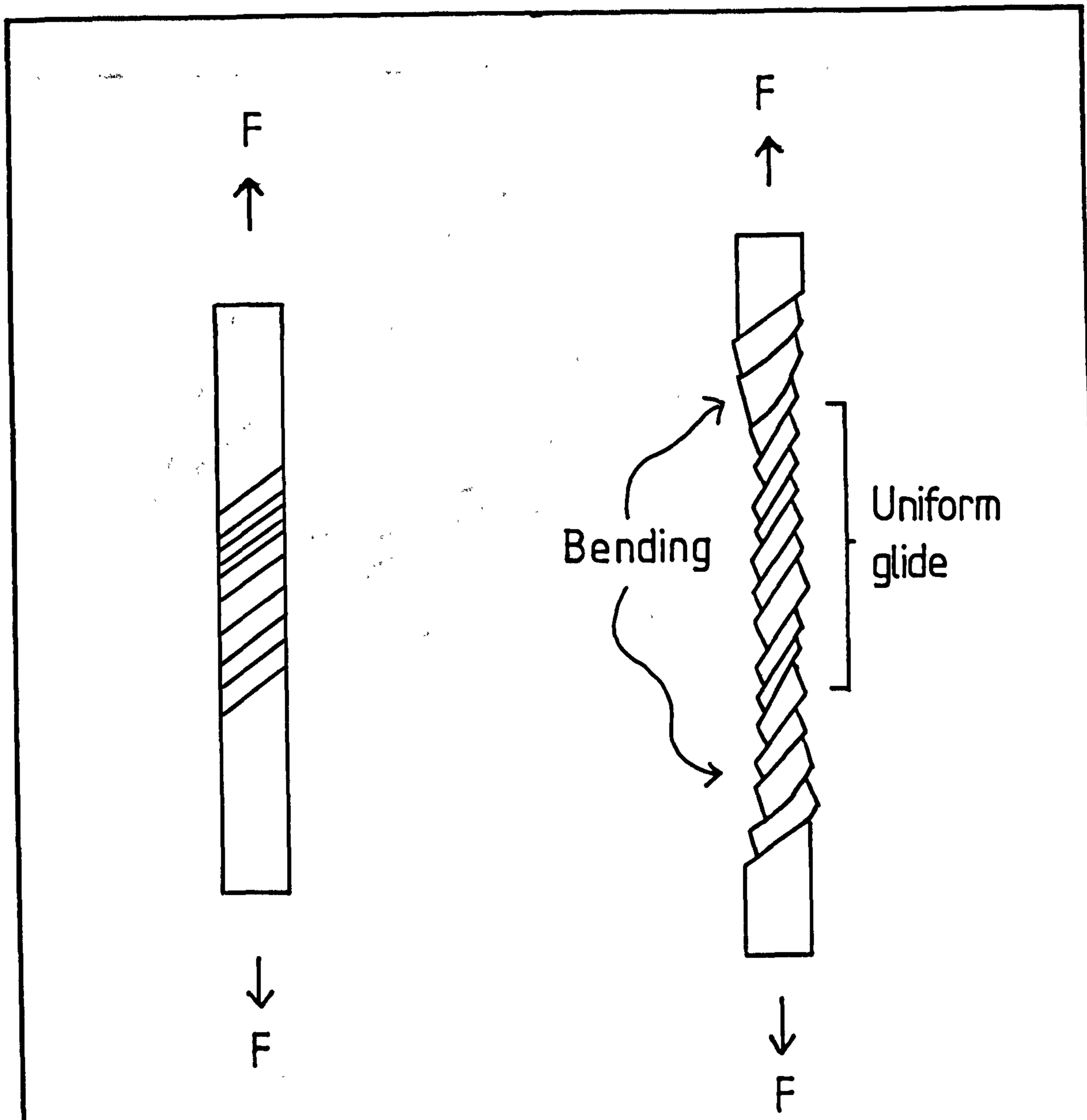

Figure 2.19: Deformation of a crystal under tensile stress

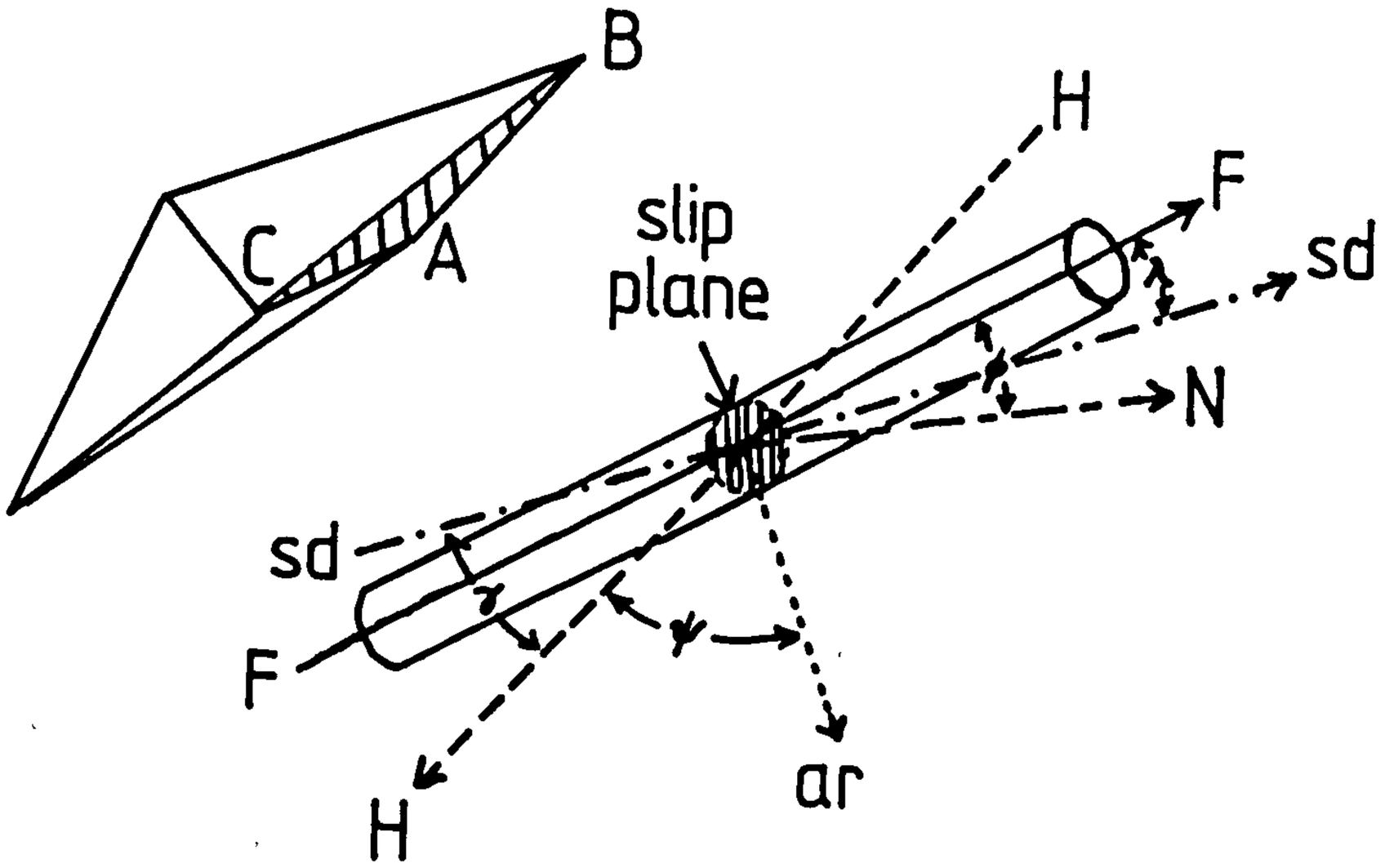

Figure 2.20: Schematic illustration of angles used in equation 2.11

The cylinder tends to become elliptical in cross-section as shown in figure 2.19, due to the rotation of slip planes about an axis lying in these planes (axis of rotation, ar) normal to the slip direction, sd.

The constraint opposing this rotation is governed both by the angle between the face of the adjacent facet and the axis of rotation (ψ), and the angle between the facet and the slip direction (γ) ^{110} illustrated in figure 2.20. The latter is only of importance when $\psi = 90°$, since slip can still take place provided $\gamma > 0$.

The complete form of the resolved shear stress equation for each individual facet is:

$$\tau_e = (F/A).\cos\lambda.\cos\phi.(\cos\psi + \sin\gamma)/2 \qquad (2.11)$$

where F = applied tensile force

A = area supporting F

λ = angle between axis of F (tensile axis FF) & sd

ϕ = angle between FF & the slip plane normal, N

ψ = angle between each facet (HH) & the ar of the slip system

γ = angle between HH & sd.

τ_e must be calculated for each facet of the indenter, since the directions FF and HH will differ. The effective resolved shear stress τ_e' is considered to be the mean of the four values for τ_e.

Values of F and A cannot be unambiguously defined, and are ignored, since the product of the cosine factors

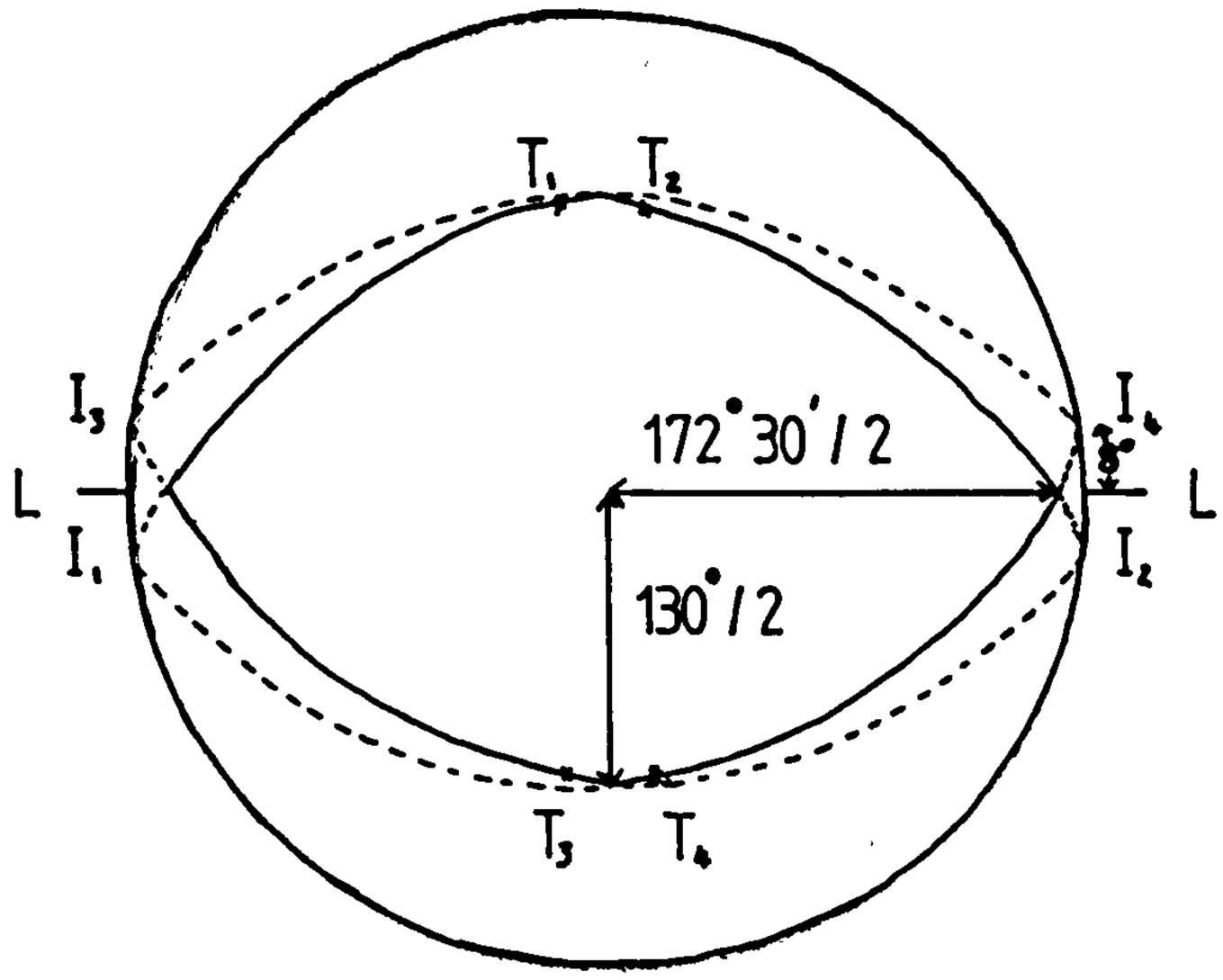

LL : long diagonal of indenter

T_n : direction of tensile axis (FF) for facet n of indenter

I_n : direction of axis (HH) parallel to indenter facet n

Figure 2.21: Stereographic projection of the Knoop indenter

alone in equation 2.11 can nevertheless be used to demonstrate the relative magnitude of τ_e for indentations in various crystallographic directions on a given crystal plane. Directions showing the lowest ERSS should be the hardest. The slip system which tends to act will be the one which has higher ERSS values than others of the same type, and crossover between systems at different indenter angles is possible. Slip traces produced during etching studies can be used to determine whether crossover has occurred. When comparing slip systems with a different family of Burgers vectors, the relative ease of activation (due to differences in intermolecular interactions and molecular obstruction) must also be considered, in addition to consideration of d_{hkl} and $\underline{b}$. ERSS values alone will not necessarily give the definitive answer.

Values of λ, ϕ, ψ and δ can be read from a stereographic projection normal to the indented plane, overlaid with a stereographic projection of the indenter constructed as shown in figure 2.21. The above angles can therefore be determined for any orientation of the indenter on the crystal surface.

Diagrams of the structure of proposed slip planes were used to determine whether slip could occur, and if so, in which direction. The lengths of Burgers vectors were calculated from unit cell dimensions. Samples were photographed immediately after indentation and 30 days

later in order to allow etching by sublimation, and any longer term relaxation effects to take place. This was carried out in order to identify planes on which slip had occurred. Samples were not solvent etched as this was found difficult to control, even at low temperatures, and tended to dissolve the indentations, making their position and orientation difficult to detect. The angles required for ERSS calculation were measured from stereographic projections plotted normal to the indented face as described for every orientation of the indenter on the sample crystals.

The resolved shear stress (RSS) for each facet of the indenter was calculated according to equation 2.11. The ERSS was determined from the mean of the four RSS values at each orientation of the indenter, and was also plotted as a function of the indenter angle.

ERSS calculations could only be performed on the (100) and (001) faces, due to difficulties obtaining stereographic projections of directions on the $(1\ \bar{1}0)$ and $(1\ \bar{1}1)$ faces.

2.4 COMPUTATIONAL METHODS

2.4.1 STEREO

STEREO [8] is a FORTRAN program used to construct stereographic projections of a given crystal structure for any given orientation. The program is based on equations derived by Stokes et al [113]. Projections of face normals (poles) can be constructed for any crystal system, but projections of crystal directions can only be accurately produced for highly symmetrical systems.

2.4.2 LAUE

LAUE is a FORTRAN program designed to produce simulated Laue diffraction patterns for a given crystal structure, at a given orientation and sample-to-film distance. This can be used to identify crystal faces or check crystal orientation.

2.4.3 MORANG

MORANG [114] is an interactive package used as an aid in identification of crystal morphology. Three main functions are available:

(1) Identification of the most important morphological forms on the basis of highest interplanar spacings according to the rules of Donnay and Harker [11].

(2) Calculation of angles between crystal planes and/or crystal directions.

(3) Identification of likely crystal planes given an observed angle and associated experimental error.

2.4.4 SHAPE

SHAPE [115] is a crystal drawing program. Using information including unit cell dimensions, space group symmetry and centre-to-face distances, the smallest polyhedron enclosed by the inputted faces is computed (using classical Wulff plot technique as described in section 1.2.1.2.1) to produce a drawing of the crystal.

A drawing of the observed morphology can be produced if observed centre-to-face distances are inputted. Using the reciprocal of the interplanar spacings produces a Donnay-Harker model, and substituting attachment energy for the centre-to-face distance results in construction of the attachment energy model.

2.4.5 HABIT

HABIT [116] can be used to calculate lattice, slice and attachment energies (see section 1.2.1.2:1) and predict the morphology of molecular crystals. Fractional coordinates of one asymmetric unit and the symmetry operators of the appropriate space group are used to

construct the unit cell, which is then repeated along the three crystallographic axes to create a three dimensional model of the crystal structure.

The intermolecular interactions are considered to consist of the sum of all the non-bonded atom-atom interactions, which are each assumed to have a Van der Waals and an electrostatic component (section 1.2.1.2.1).

In this work, the most probable growth forms were identified using the program MORANG to search through all possible low index planes and select those with the highest interplanar spacings (d_{khl}) based on the principles of Donnay and Harker. In some instances this resulted in selection of planes which consisted only of R or S molecules; although crystallographically identical, these were not chemically identical and therefore did not contain a complete repeat of the crystal structure. In these cases, the interplanar spacing had to be doubled (in practical terms this affected only the {002} faces, which become {001}).

It was necessary to minimise the position of hydrogen atoms in the crystal structure before calculation of attachment energies (E_{att}) for these faces. X-ray diffraction data does not always provide an accurate representation of hydrogen positions, tending to underestimate bond lengths to hydrogen atoms, since their scattering power is too small to contribute

materially to diffraction intensity [117]. However, their position may significantly affect intermolecular energy calculations[118], and inaccuracy may therefore lead to erroneous results of energy calculations. Hydrogen atom positions tend to be estimated and refined along with diffraction data for heavy atom positions. They were therefore optimised by fitting to data for bond lengths and angles from neutron diffraction studies (which can pinpoint hydrogen positions more accurately), and their positions minimised [119]. The methodology is reported in fuller detail elsewhere [120]. The heavy atoms and unit cell dimensions remained fixed during the calculation.

The modified structure coordinates were then used to calculate E_{att} values for the selected growth forms, and the crystal energy (Φ_{inter}) using the force field developed by Lifson et al [121] for carboxylic acids, which uses a Lennard-Jones 6-12 potential to calculate Van der Waals interactions. No special function for hydrogen-bonding was found to be necessary.

2.4.6 INTERCHEM

INTERCHEM [112] is an interactive package which can be used, amongst other things, to produce molecular drawings or drawings of portions of crystal structures. The diagrams can be readily manipulated until the desired orientation is obtained.

RESULTS AND DISCUSSION

3 RESULTS AND DISCUSSION

3.1 CRYSTAL GROWTH AND CHARACTERISATION

The solvent evaporation technique was used to study the effect of solvent on the morphology of ibuprofen, to grow crystals of S(+)-ibuprofen for structure determination, and to produce seed crystals for growth of large single crystals by controlled cooling. Vapour growth techniques were used to determine crystal morphology in the absence of potentially interacting solvents. Differential scanning calorimetry, single crystal dissolution and x-ray techniques were used to characterise the quality of the resulting crystals.

3.1.1 Crystal Growth Experiments

3.1.1.1 Growth of small crystals by solvent evaporation

Ibuprofen was recrystallised from hexane, acetonitrile, acetone, ethylacetate, toluene, ethanol, methanol and propan-2-ol. The resulting morphologies are illustrated in figure 3.1. All crystals are drawn in the same orientation, and are average morphologies derived from measurement of at least six crystals representative of each type. The identification of the crystallographic axes and face assignments illustrated will be described in detail in section 3.1.2.1.

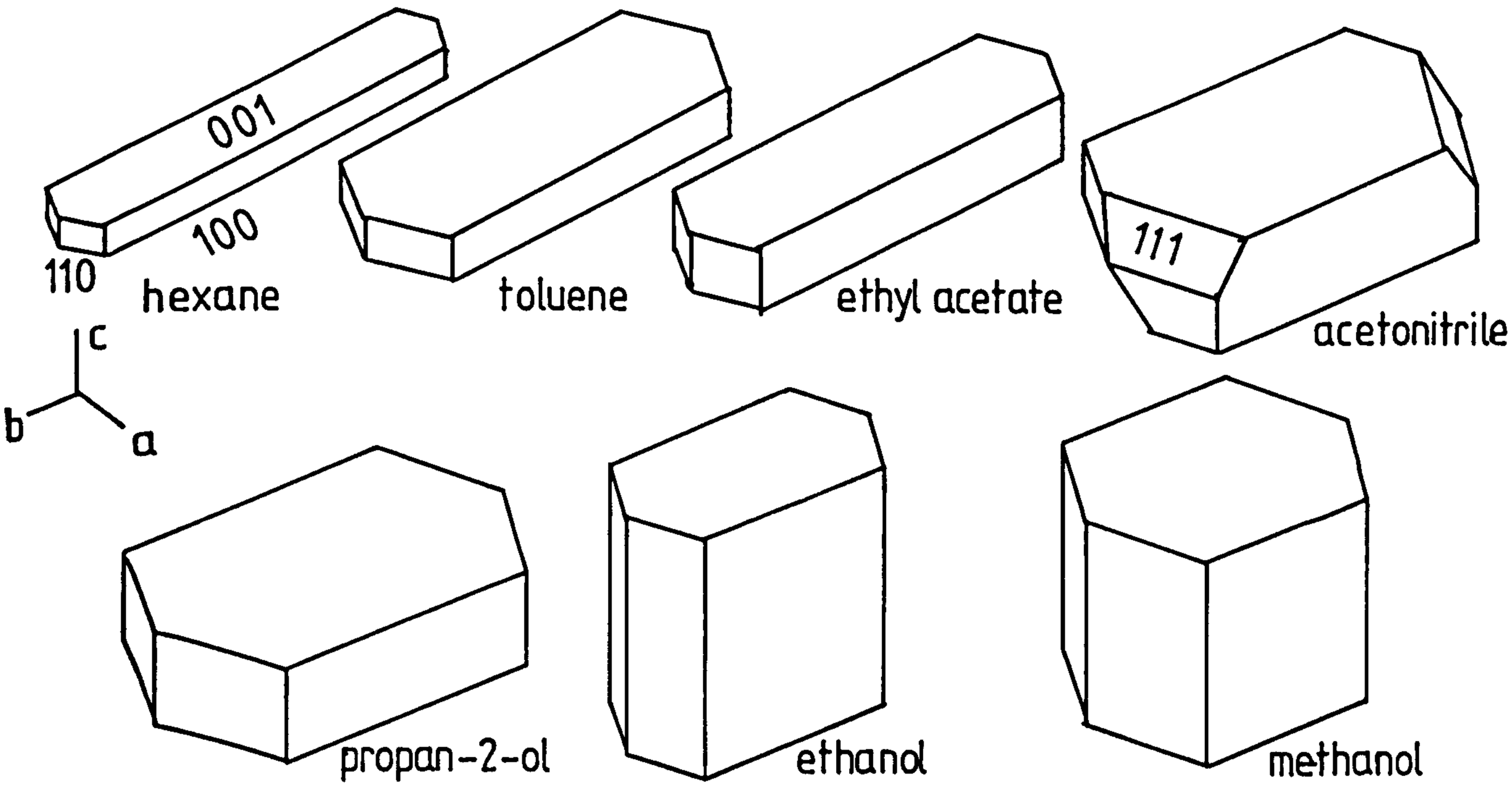

figure 3.1: Morphologies of ibuprofen crystals grown from different solvents

DSC thermograms of powdered samples of recrystallised material, obtained as described in section 2.3.4, were identical with those of the starting material, and confirmed that the observed morphologies were different habits of the same crystal structure and not different polymorphic forms.

S(+)-ibuprofen was recrystallised from methanol. No crystal growth was observed after slow evaporation of the methanol from a saturated solution for 14 days at room temperature. The solution was cooled to 5°C to further increase supersaturation. Small crystals were formed in 24 hours. The high supersaturation required to nucleate S(+)-ibuprofen crystals (when compared with the racemate) indicates that the free energy change on nucleation is lower, i.e. that the S(+)-ibuprofen nuclei are less thermodynamically stable than racemic nuclei, which may be a contributing factor to the absence of spontaneous resolution of ibuprofen.

The resulting crystals had poorly developed habits, but were single crystals when examined under crossed polarisers. They were used for x-ray structure determination, but insufficient starting material was available for growth of larger crystals.

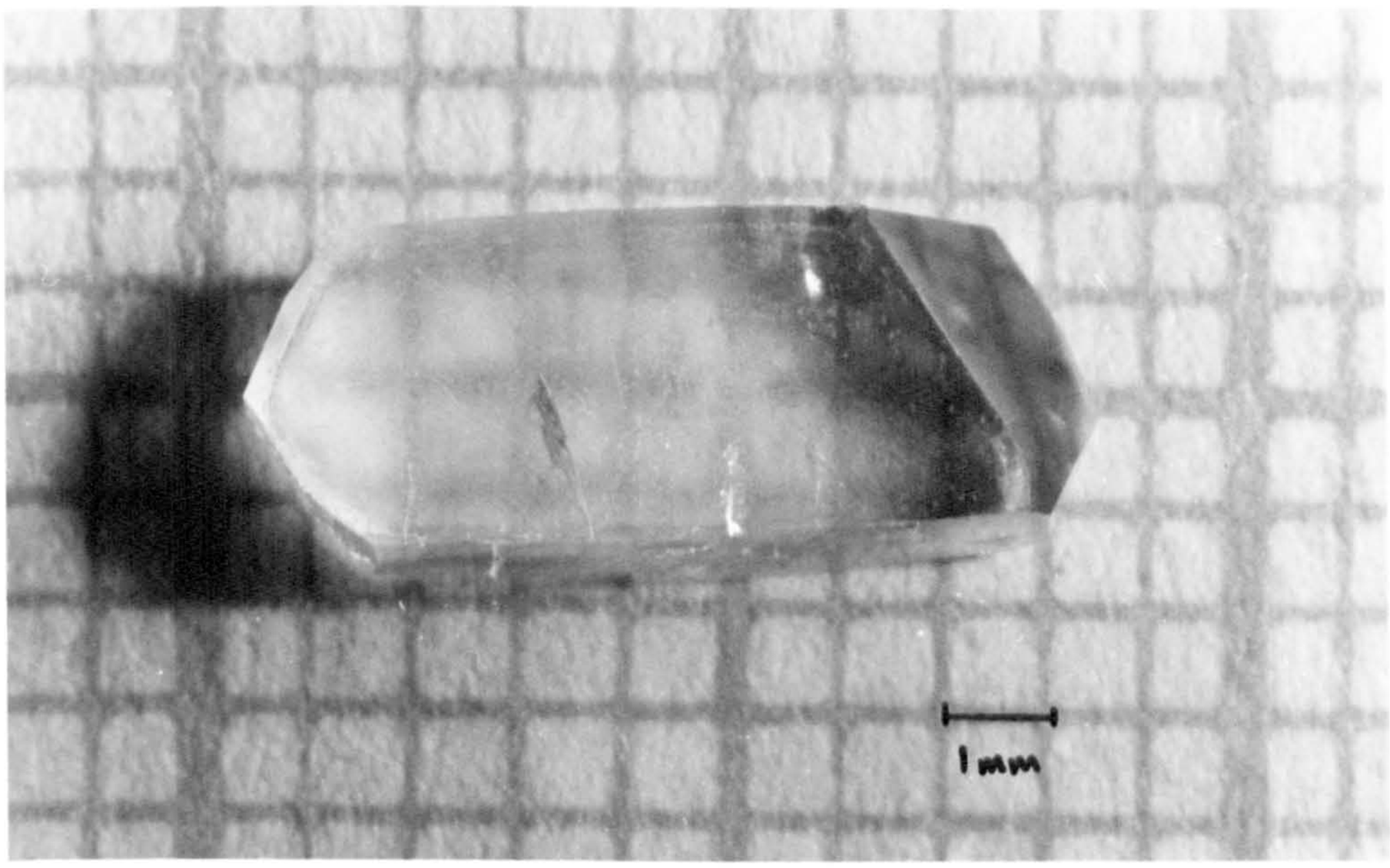

Plate 3.1: Ibuprofen crystal grown from acetonitrile by controlled cooling

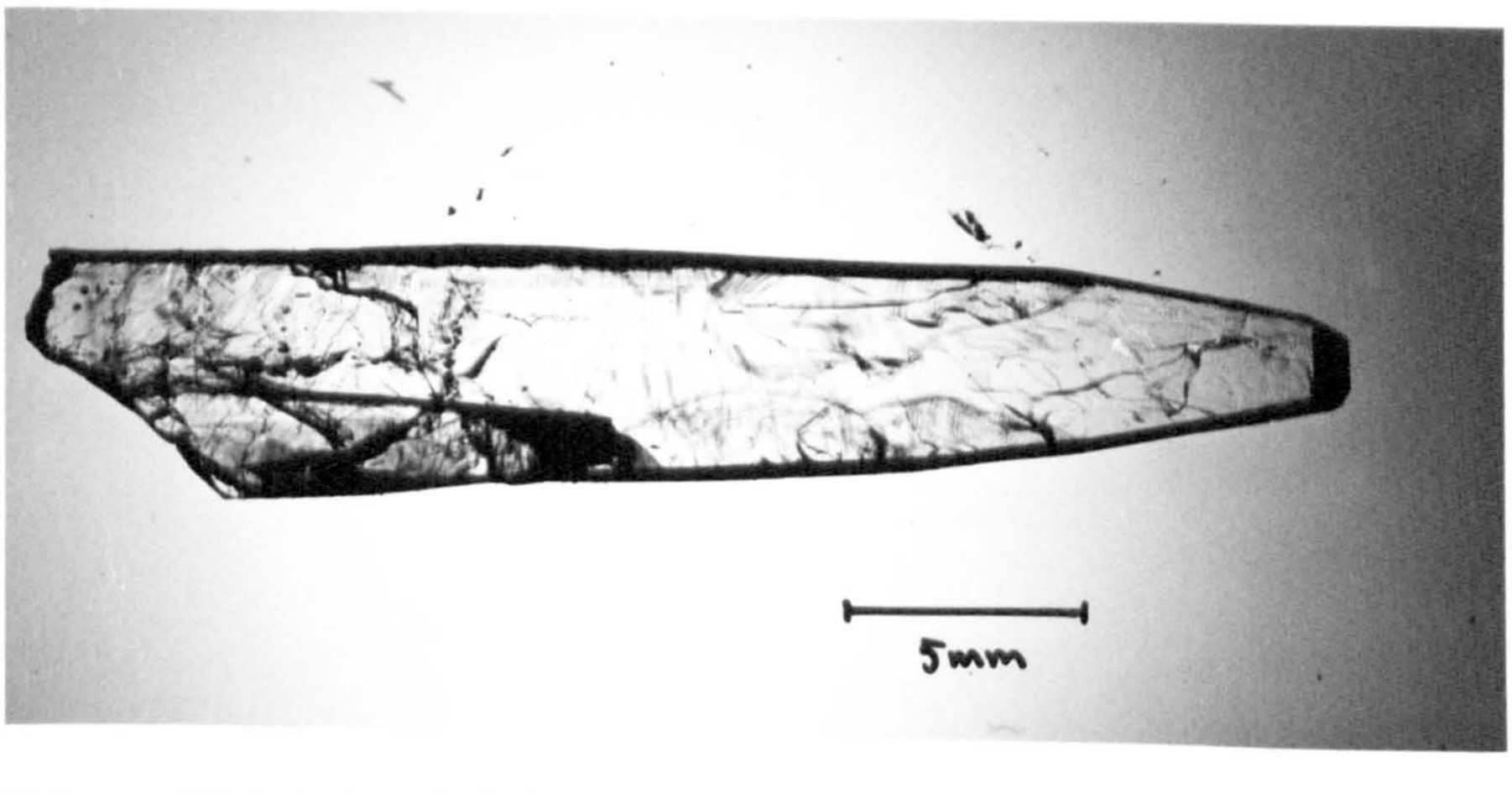

Plate 3.2: Ibuprofen crystal (Cleaved) grown from hexane by controlled cooling

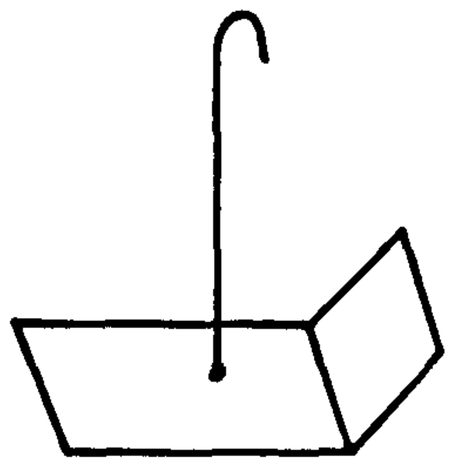

Figure 3.2: Diagram of the orientation of growth twins in hexane-grown crystals

3.1.1.2 Growth of large single crystals by controlled cooling

Well-formed crystals of ibuprofen, 20 to 30mm long, were grown from acetonitrile solution over a temperature range of 31 to 38°C. Cooling rates from 0.05 to 0.1°C.day^{-1} produced the crystals of best optical quality. Morphology closely matched that observed in the initial solvent evaporation experiments; occasionally additional small side faces were present. A typical seed-grown crystal is shown in plate 3.1.

Growth of good quality crystals from hexane solution was more difficult. Twinning parallel to the side face occasionally occurred, as illustrated in figure 3.2. More commonly, crystals were of poor optical quality, with curvature on the major face indicating strained growth. An example of this is shown in plate 3.2. The best quality crystals were produced between 34 and 37°C, and at very slow cooling rates (0.015 to 0.033°C.day^{-1}). This was much lower than the cooling rate necessary to maintain 2% supersaturation, indicating that despite all precautions some evaporation from the system may have taken place.

It should also be noted that crystal growth from systems exhibiting steep solubility gradients (such as in these systems), involves working at the operational limits of the growth apparatus [89], small temperature fluctuations producing relatively large changes in the

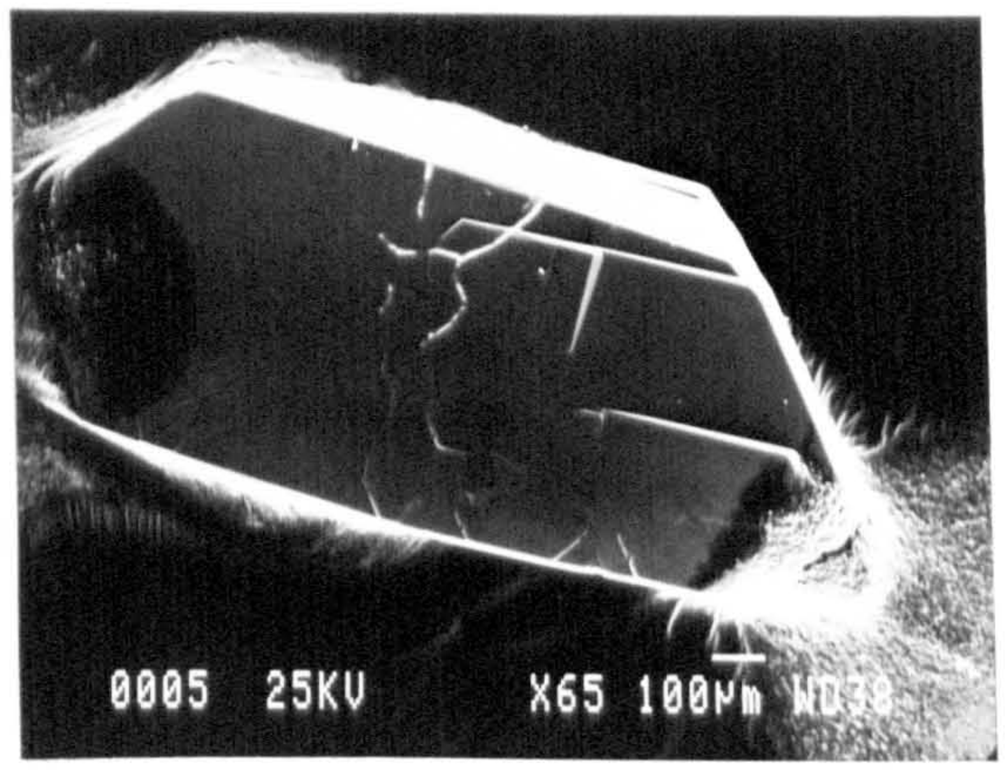

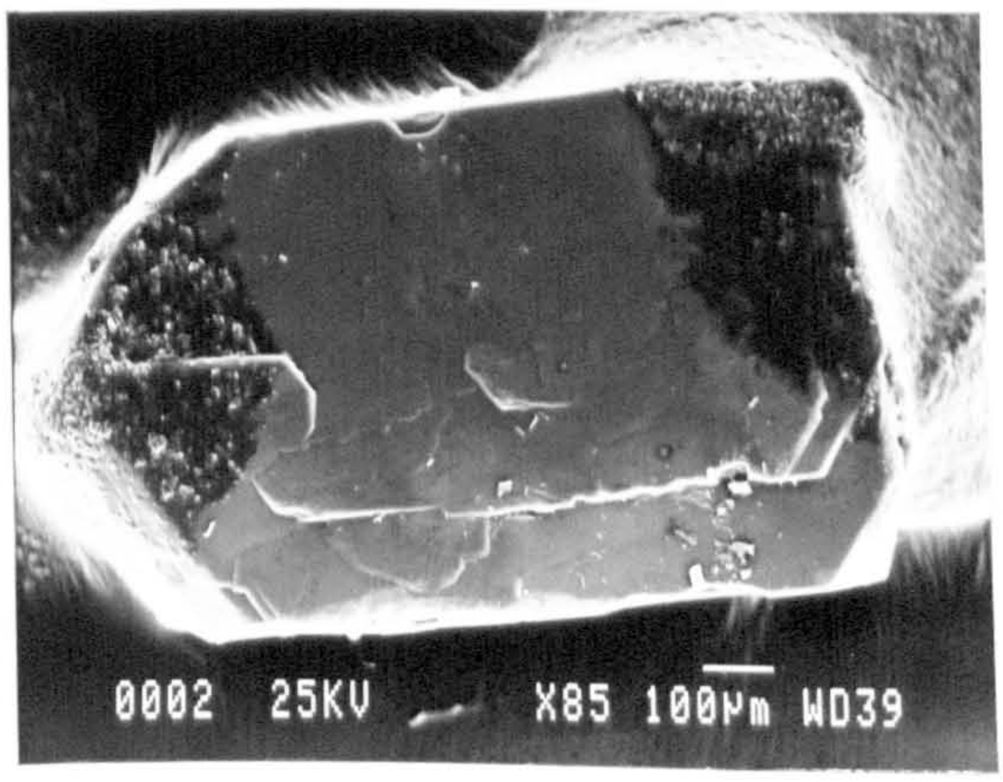

Plate 3.3: Ibuprofen crystals grown from the vapour phase

supersaturation ratio. Growth therefore occurs spasmodically, rather than at a slow constant rate, which may induce strain in the form of defects such as solvent inclusions.

3.1.1.3 Crystals grown from the vapour phase

Ibuprofen crystals were grown from the vapour phase as described in section 2.2.1.3. Crystals began to form when the temperature reached 56.1°C at the base and 41.4°C at the open end. Single crystals of good optical quality were obtained in the region of the glass tube where the temperature ranged between 49.6°C and 47.7°C. These are shown in plate 3.3.

No crystallisation of S(+)-ibuprofen was observed until the furnace temperature gradient was the same as for growth of the racemate, by which point the powder had completely melted. Small crystallites had formed after 14 days, but again nucleation seemed to be a problem; none of the crystallites were single crystals, but were polycrystalline aggregates or amorphous.

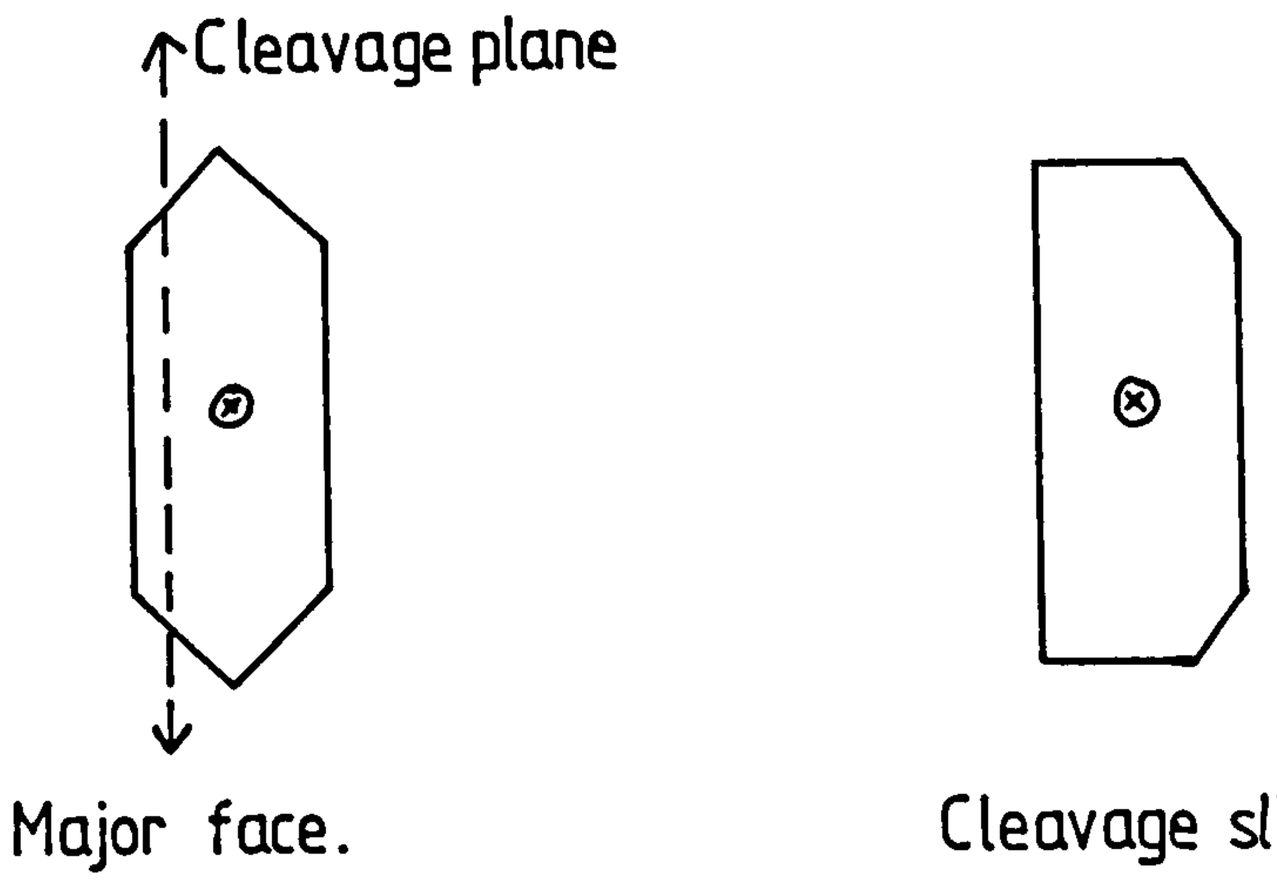

Figure 3.3: Sample orientations from which Laue diffraction patterns were obtained

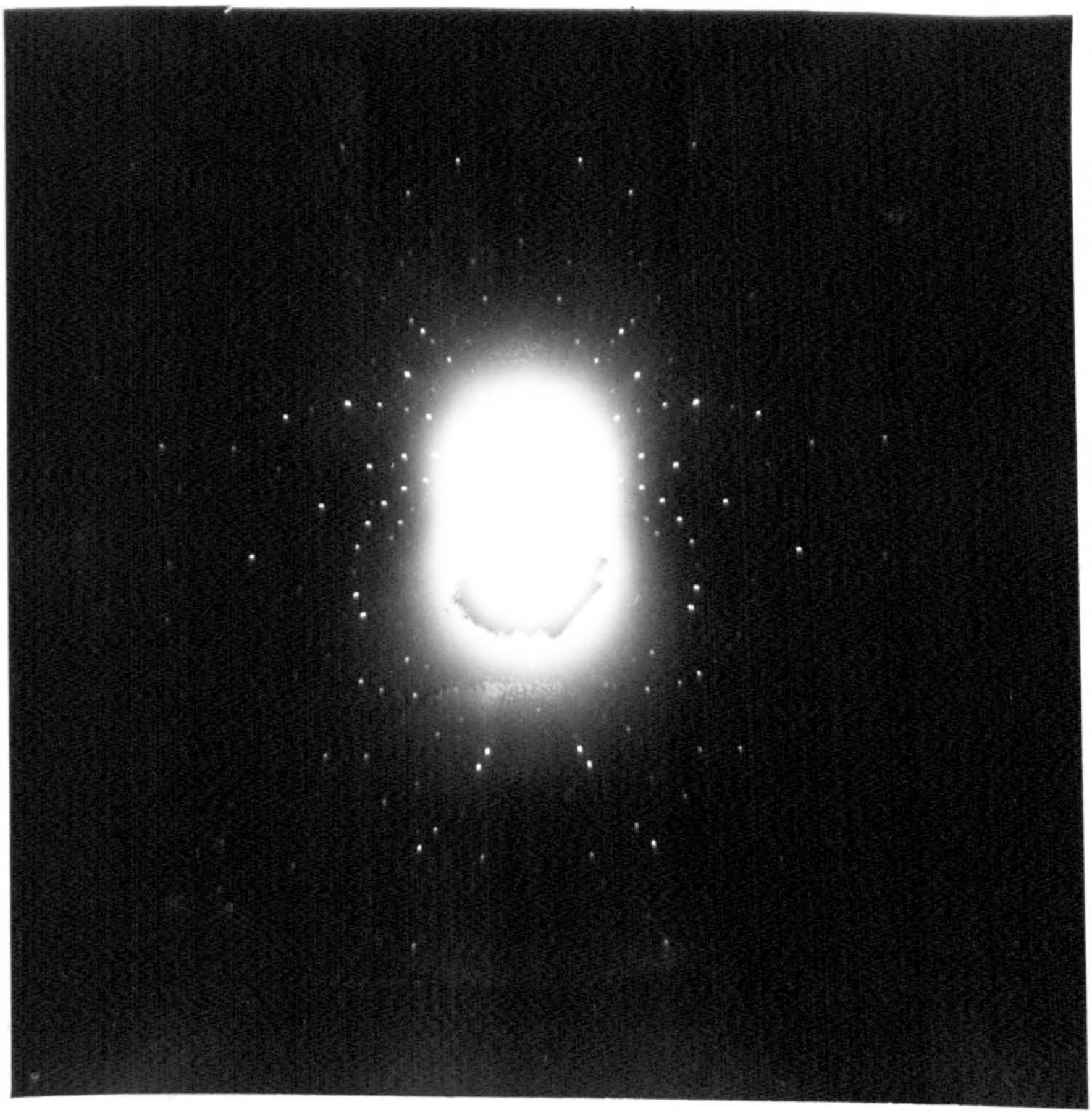

Plate 3.4: Laue diffraction pattern from the major face of ibuprofen

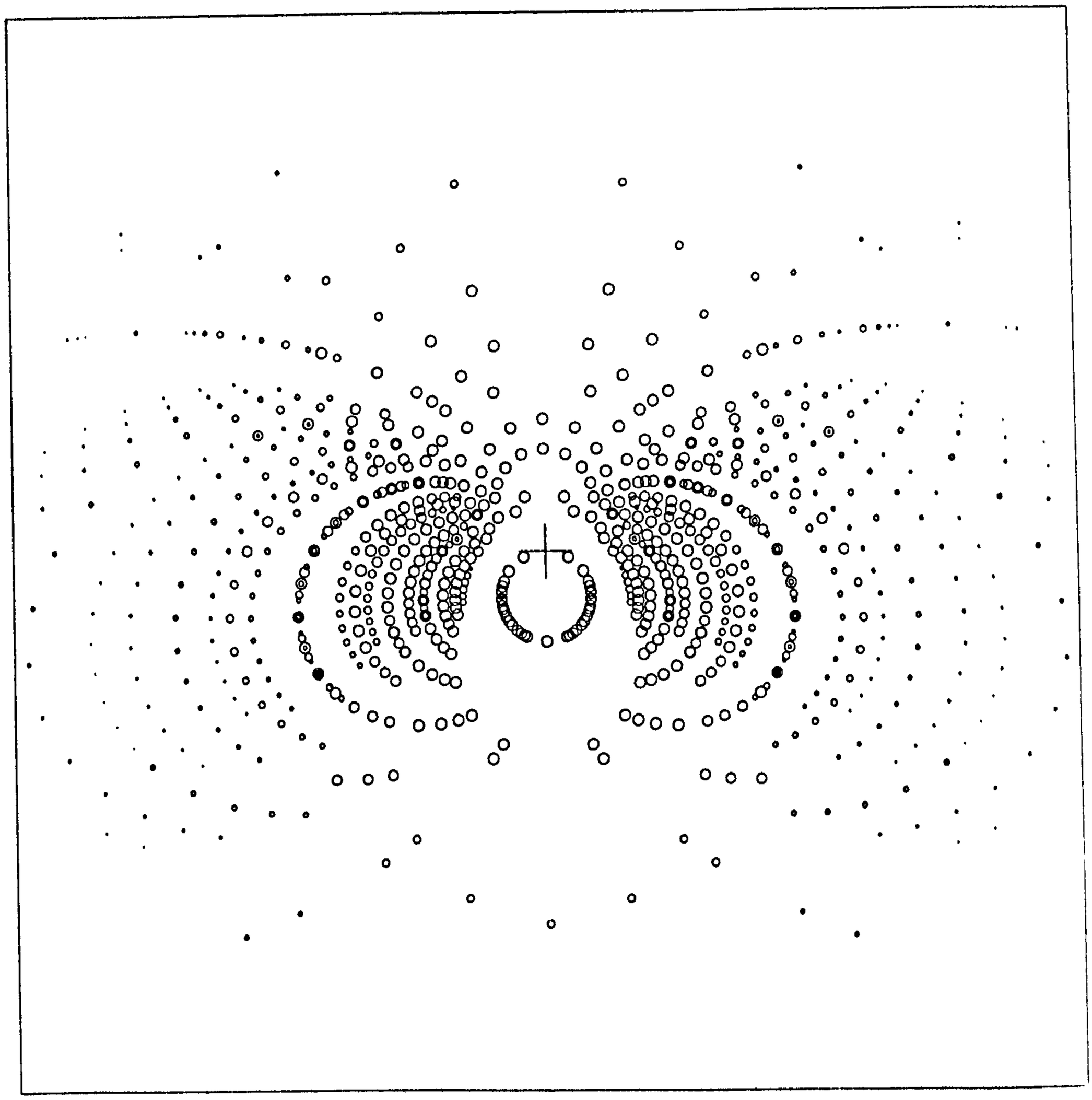

Figure 3.4: Calculated Laue diffraction pattern for (001) crystal face of ibuprofen

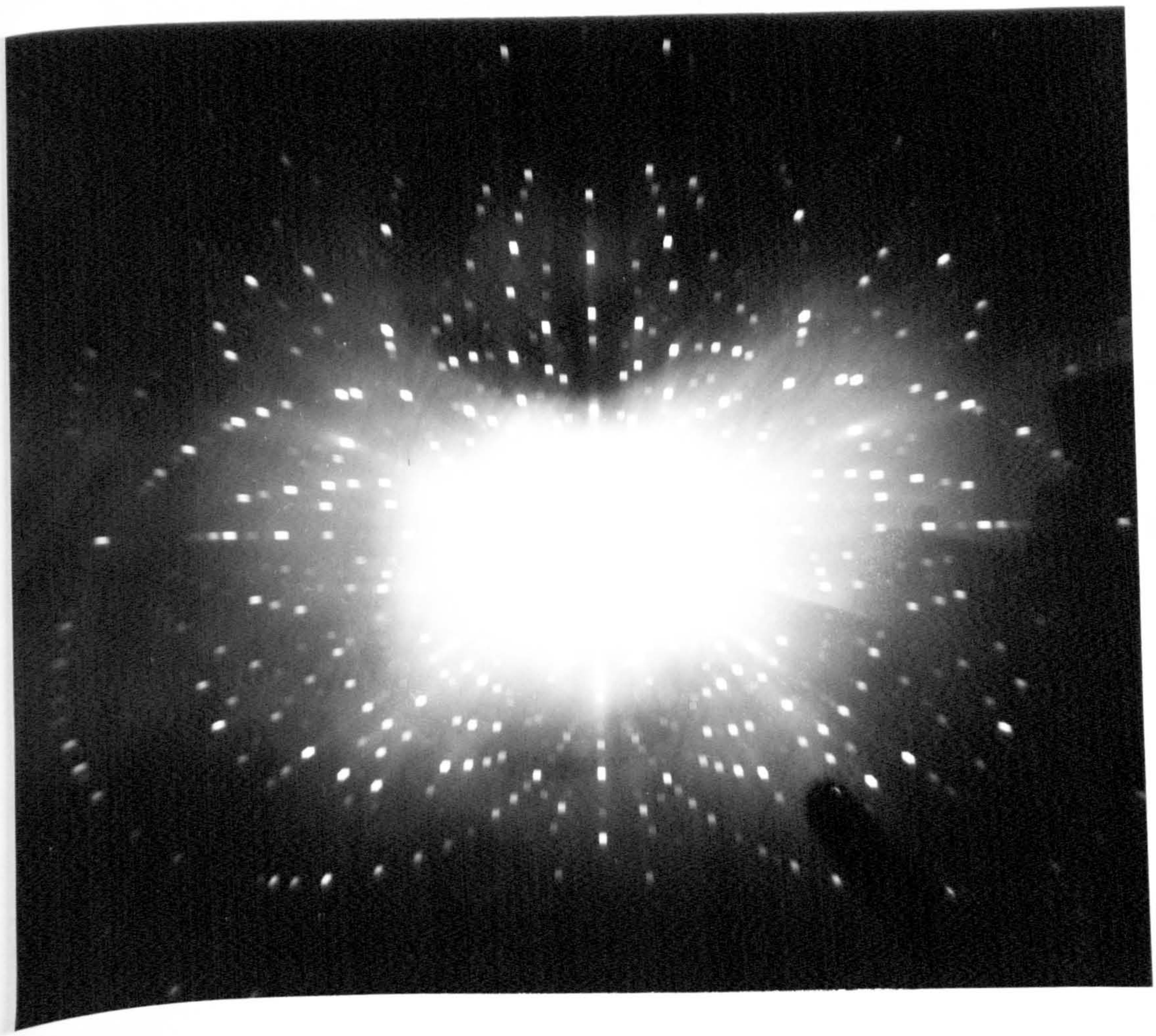

Plate 3.5: Laue diffraction pattern from the cleavage plane of ibuprofen

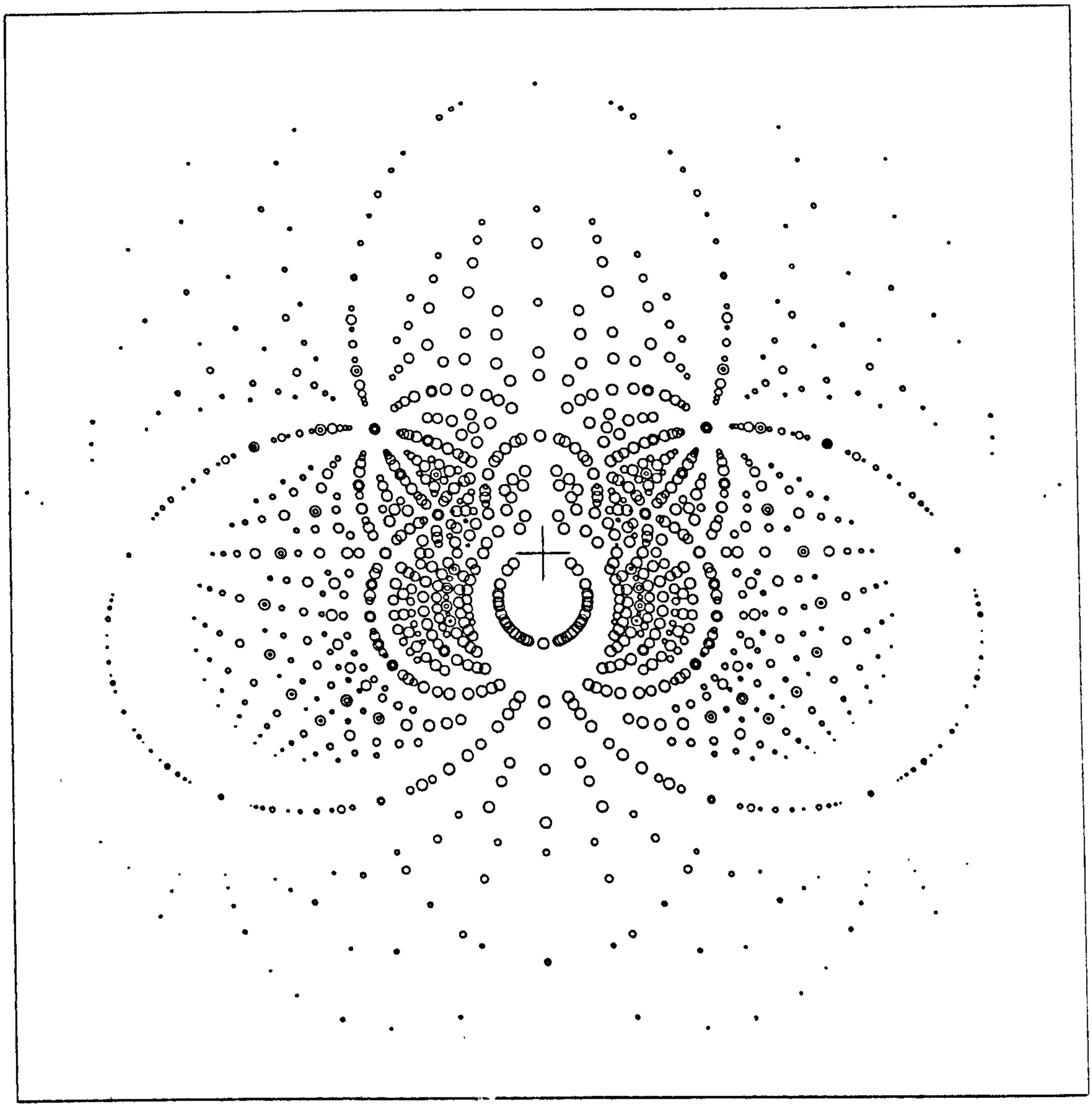

Figure 3.5: Calculated Laue diffraction pattern for (100) crystal face of ibuprofen

3.1.2 Characterisation and Comparison of Crystal Morphologies

3.1.2.1 Laue Diffraction Patterns and Identification of Crystal Faces.

Figure 3.3 illustrates the orientations of crystal slices from which Laue diffraction patterns were obtained. Laue diffraction patterns of the major (usually six-sided) growth form, shown in plate 3.4, in all cases identified it as the {001} face with the long edges of the crystals being parallel to the b-axis. Calculated Laue patterns are illustrated in figure 3.4 for comparison. Laue diffraction patterns were also determined from cleavage planes to further confirm that they were {100} planes (also the case for aspirin, which crystallises in the same space-group [122]): this was found to be correct, as illustrated by comparison of plate 3.5 and figure 3.5.

Figure 3.6 shows typical interfacial angles measured on a crystal grown from acetonitrile. Crystals grown from other solvents exhibited the same growth forms, although relative surface areas differed. The identity of the most common growth forms exhibited on ibuprofen crystals grown from solution are illustrated in figure 3.7. Additional side faces occasionally observed on acetonitrile-grown crystals were identified

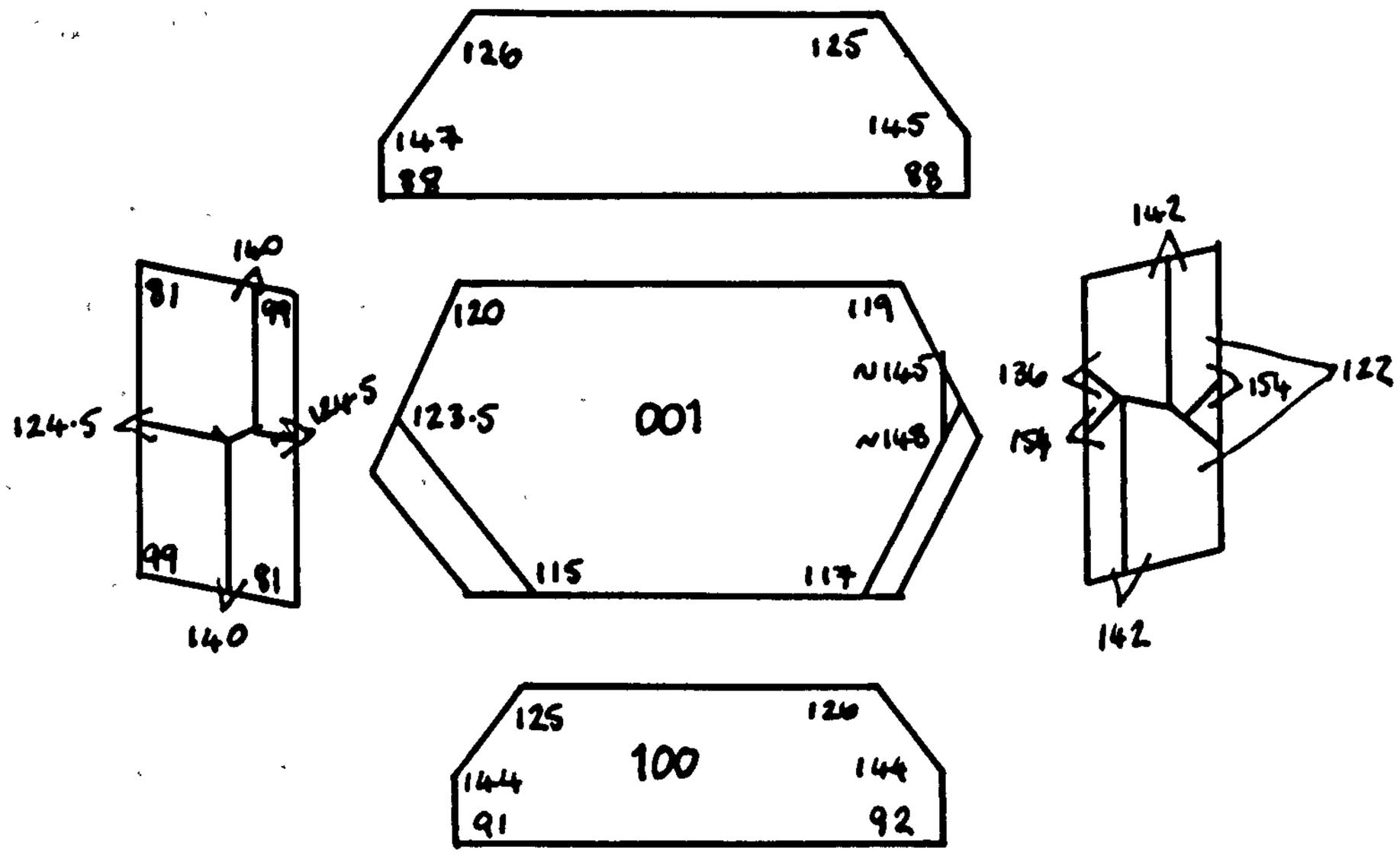

Figure 3.6: Interfacial angles measured from typical ibuprofen crystals

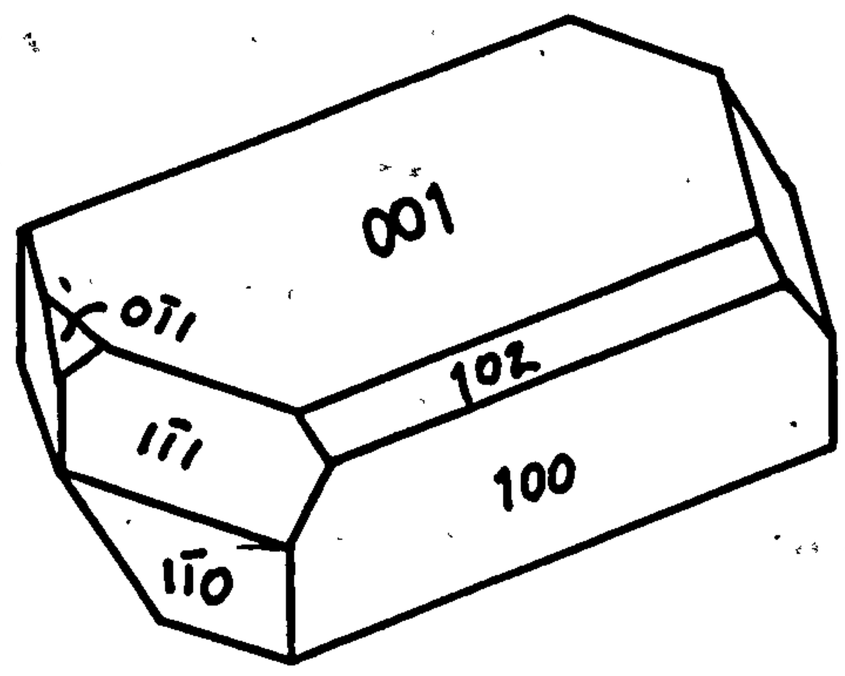

Figure 3.7: Ibuprofen growth forms

as {102}. The twin plane observed in large seed-grown crystals using hexane corresponded with the {100} cleavage plane.

Crystals grown from vapour were too small for the Laue method to be used to identify the major face. Interfacial angles were measured from scanning electron micrographs and enlarged optical micrographs to allow characterisation. Interfacial angles are shown in figure 3.8.

Interfacial angles on the major face of vapour grown ibuprofen matched those calculated for the {100} face. The {001} face was not dominant, unlike all solution grown crystals, but was very much smaller. This is partly due to restricted growth, since the {100} face tended to be aligned with the sides of the growth tube, allowing growth to occur on only one face. Figure 3.9 shows a SHAPE drawing of the general morphology of vapour grown crystals. $\{0\bar{1}1\}$ faces were apparently observed, which rarely occurred on solution grown crystals. However, the vapour grown crystals were too thin for absolute identification to be made, and these faces may have been the more commonly observed $\{1\bar{1}1\}$ faces.

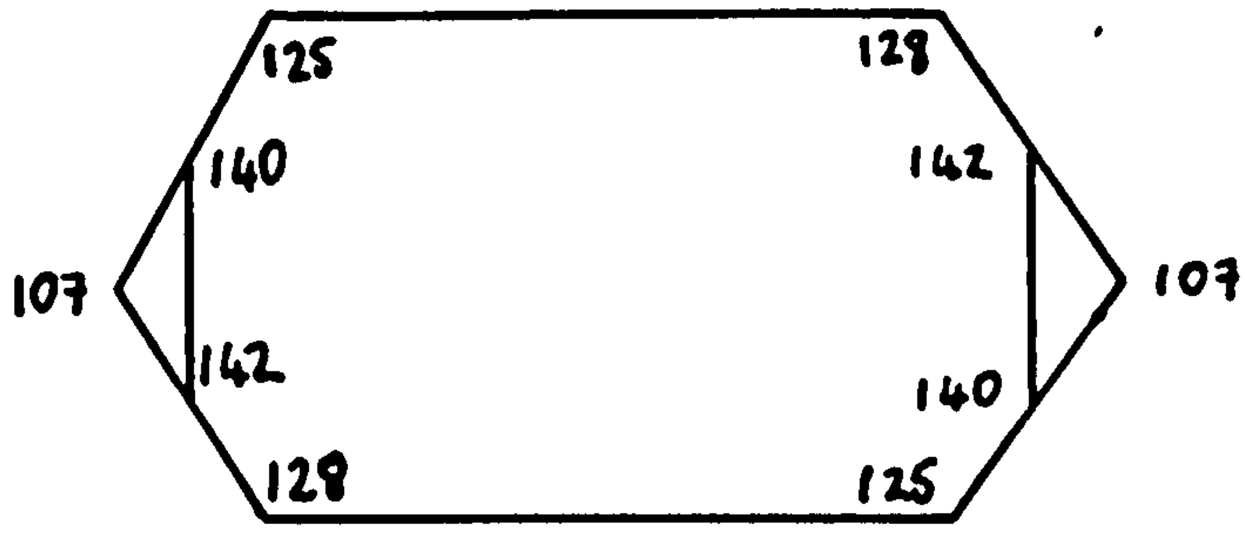

Figure 3.8: Interfacial angles measured from typical vapour grown crystals of ibuprofen

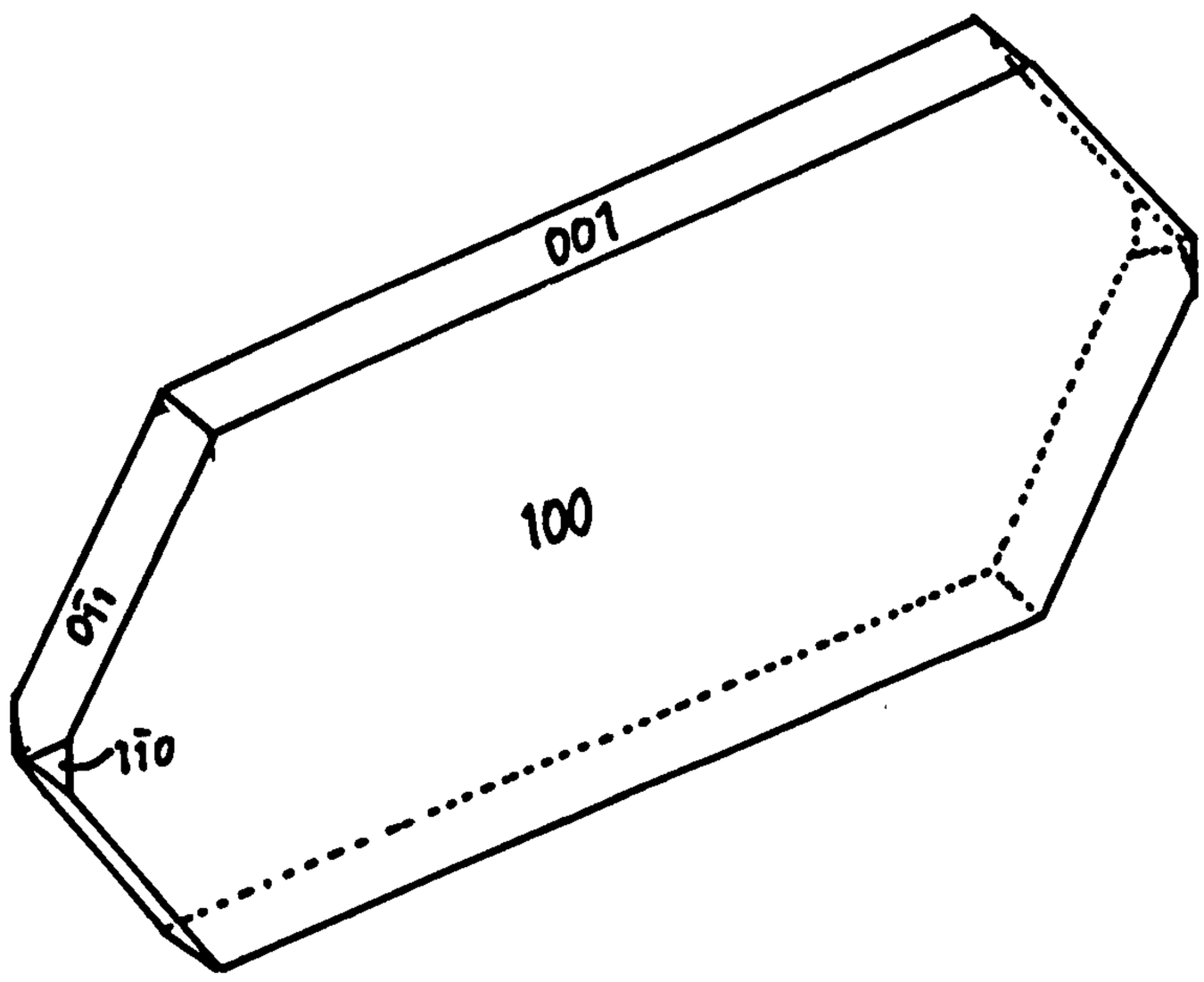

Figure 3.9: Growth forms of vapour grown crystals of ibuprofen

3.1.2.2 Comparison of crystal habits from different solvent systems

It can be seen from the crystal drawings in figure 3.1 that, in general, as the polarity of the solvent increased, the crystals exhibited slower growth along the b axis, and increased growth along the c axis, thus becoming more equant compared with the thin plates grown from hexane.

Gordon and Amin [1] attempted to quantify this effect by plotting the ratios of the lengths of the two longest crystal axes (the aspect ratio) of the crystals against the hydrogen-bonding parameter of the solvent. This is a semi-empirical concept developed to allow some quantification of physical interactions between solvents and a substrate material. It is assumed that the cohesive energy of a solvent, ΔE (equivalent to the energy of vapourisation) [123,124] arises from contributions from hydrogen-bonding (ΔE_H), permanent dipole-permanent dipole interactions (ΔE_P) and nonpolar interactions (ΔE_D), such that:

$$\Delta E = \Delta E_H + \Delta E_P + \Delta E_D \qquad (3.1)$$

The hydrogen-bonding parameter is calculated from

$$\delta_H = (\Delta E_H / V)^{1/2}, \qquad (3.2)$$

where V is the molar volume of the solvent and ΔE_V is calculated from ΔH_V measurements of 4650 cal for each OH group. δ_H also includes contributions from other association bonds, pi-bonds etc. [125]. The dipole and non-polar terms were found to be relatively unimportant in altering the morphology of ibuprofen. No mechanisms were proposed to explain these results.

Following the example of Gordon and Amin [1], the b/a aspect ratios of the crystals were plotted against the hydrogen-bonding parameter of the solvent of crystallisation. The results, shown in figure 3.10, show a similar trend to the published results. b/a was also plotted against δ_D or δ_P (shown in figures 3.11 and 3.12 respectively) but does not produce any obvious trend, again in agreement with published results.

Gordon and Amin [1] were unable to estimate the thickness of the crystals by their measurement technique and so the effects of solvents on the {001} crystal face were not determined. Growth of larger crystals in this work allowed measurement of crystals along the c axis to be made. Figure 3.13 shows a plot of the c/a aspect ratio versus δ_H. No obvious trend in the results is apparent, except that only in the cases of methanol- and ethanol-grown crystals is c/a > 1, i.e. the relative morphological importance of the {100} and {001} growth faces was the same as for vapour grown crystals, whereas for all other solvents c/a < 1 suggesting disruption of growth at the {001} faces.

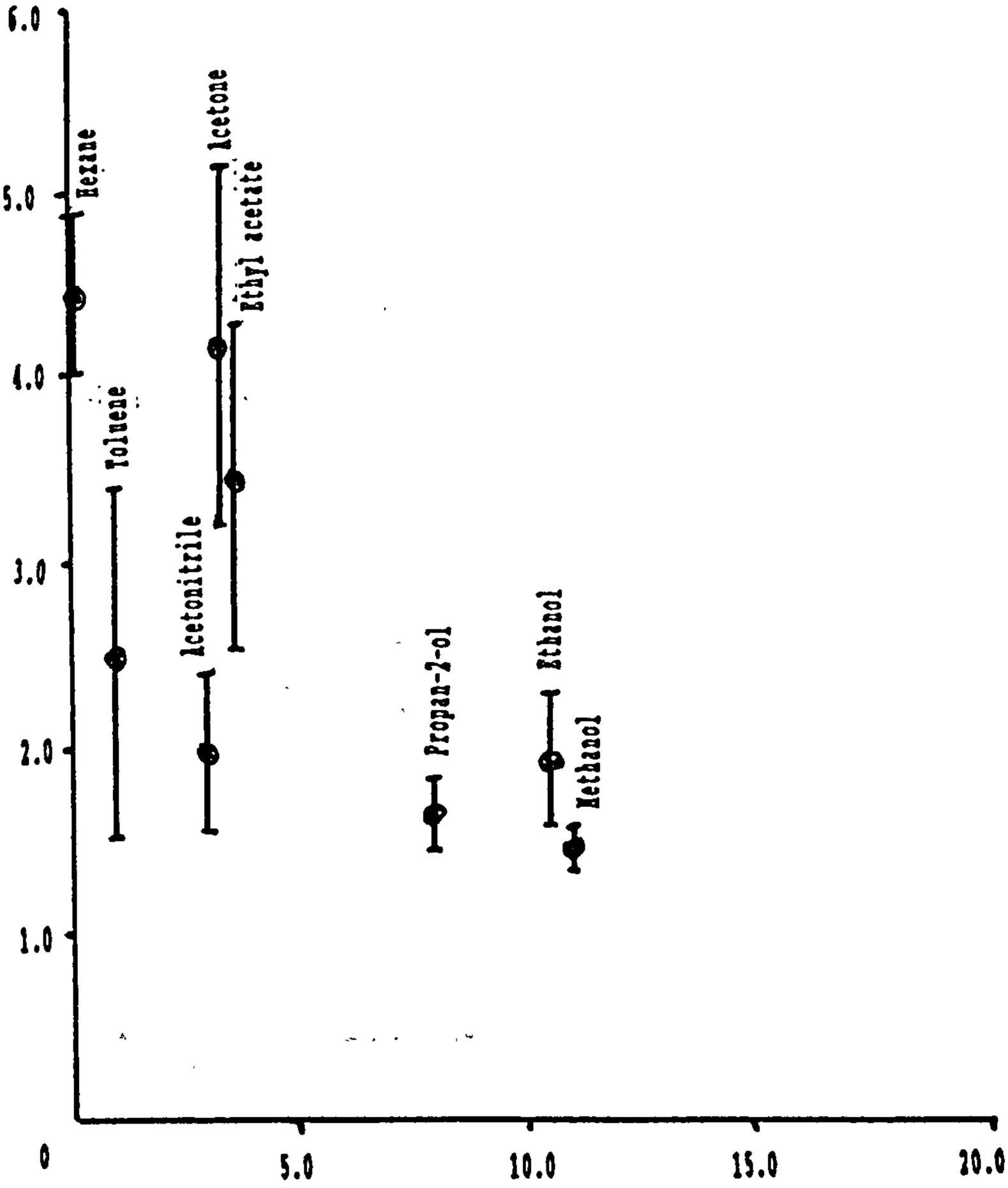

Figure 3.10: Graph of aspect ratio b/a versus hydrogen bonding parameter of solvent

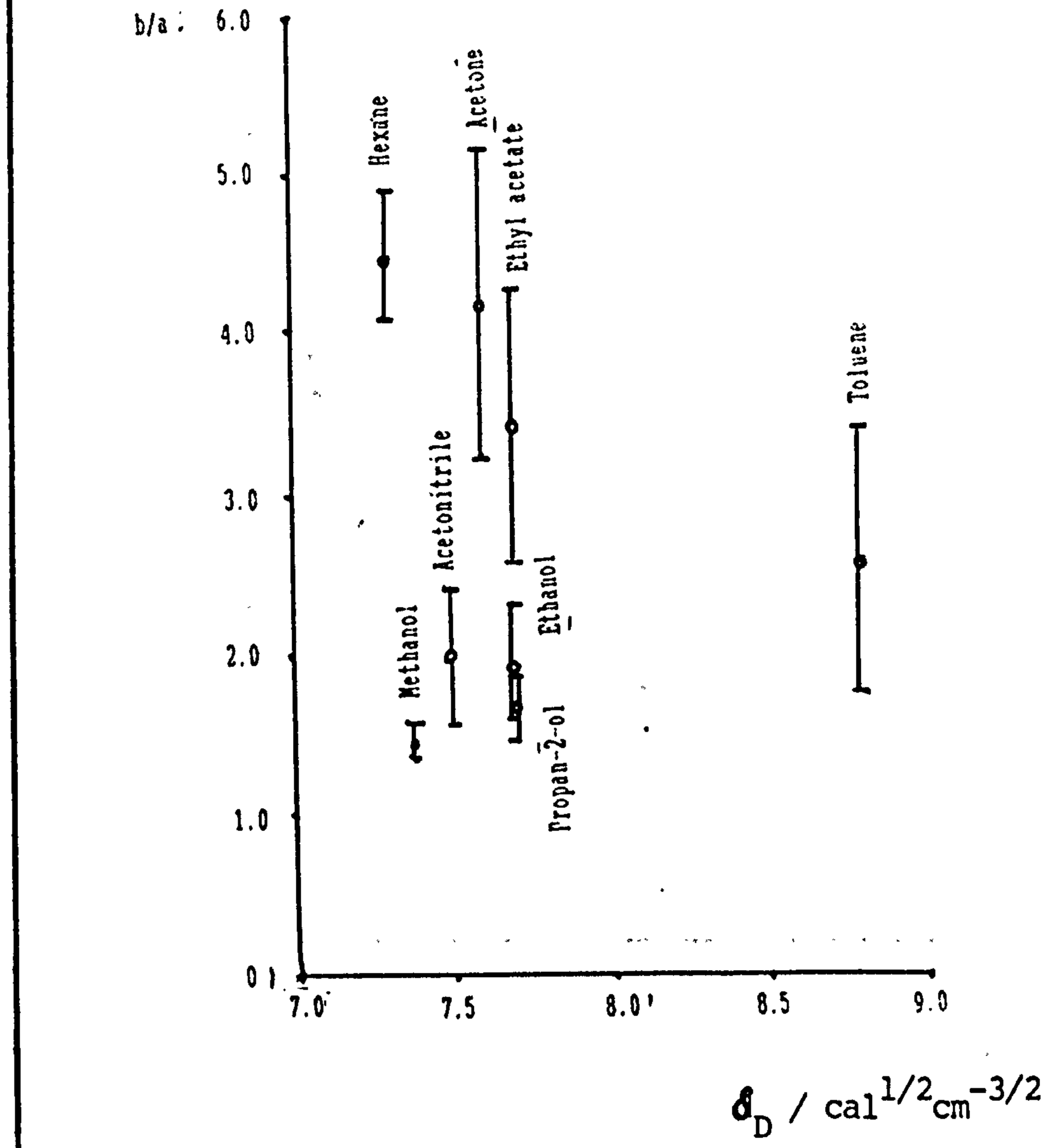

Figure 3.11: Graph of aspect ratio b/a versus dipole interaction parameter of solvent

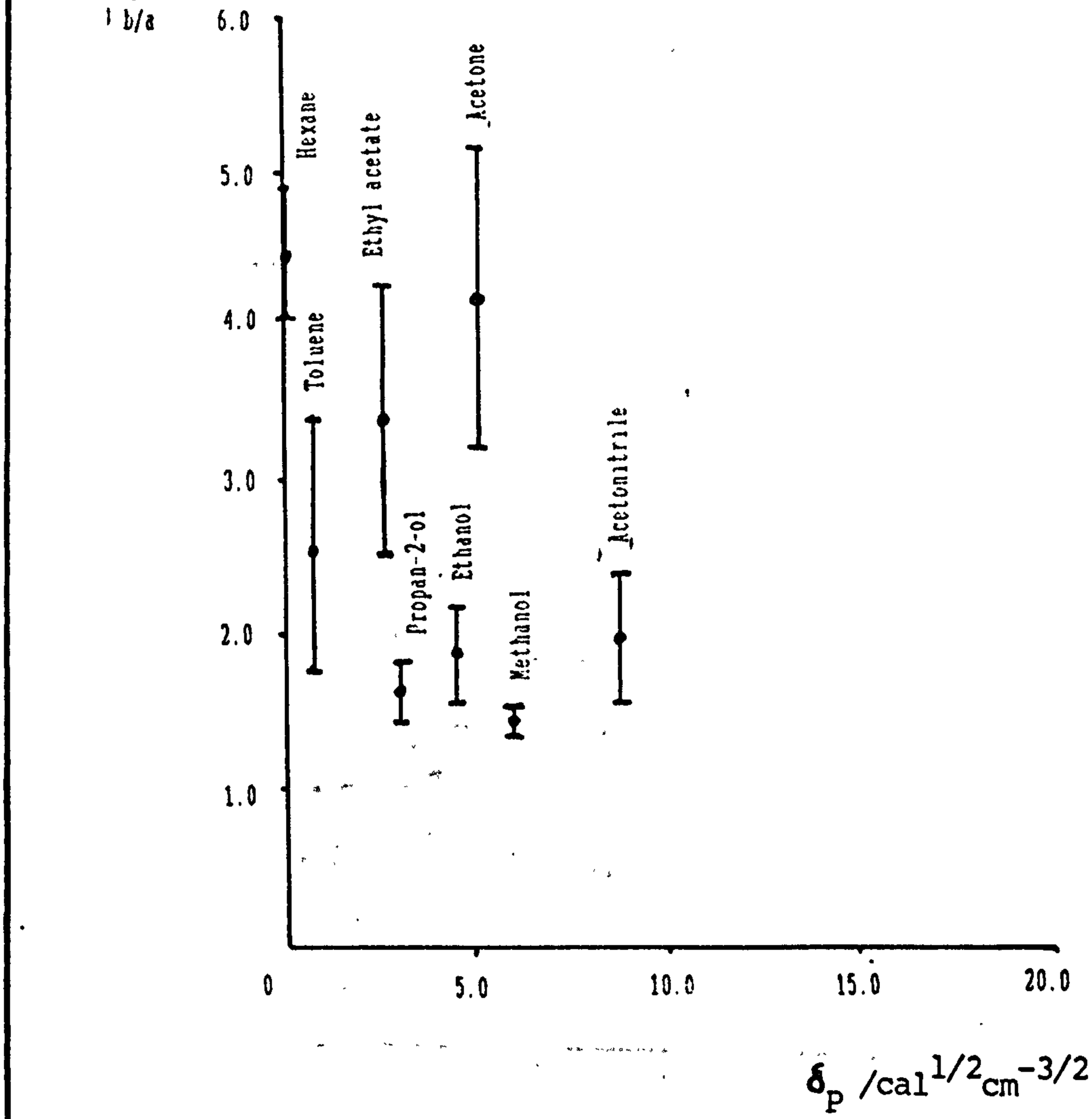

Figure 3.12: Graph of aspect ratio b/a versus non-polar interaction parameter of solvent

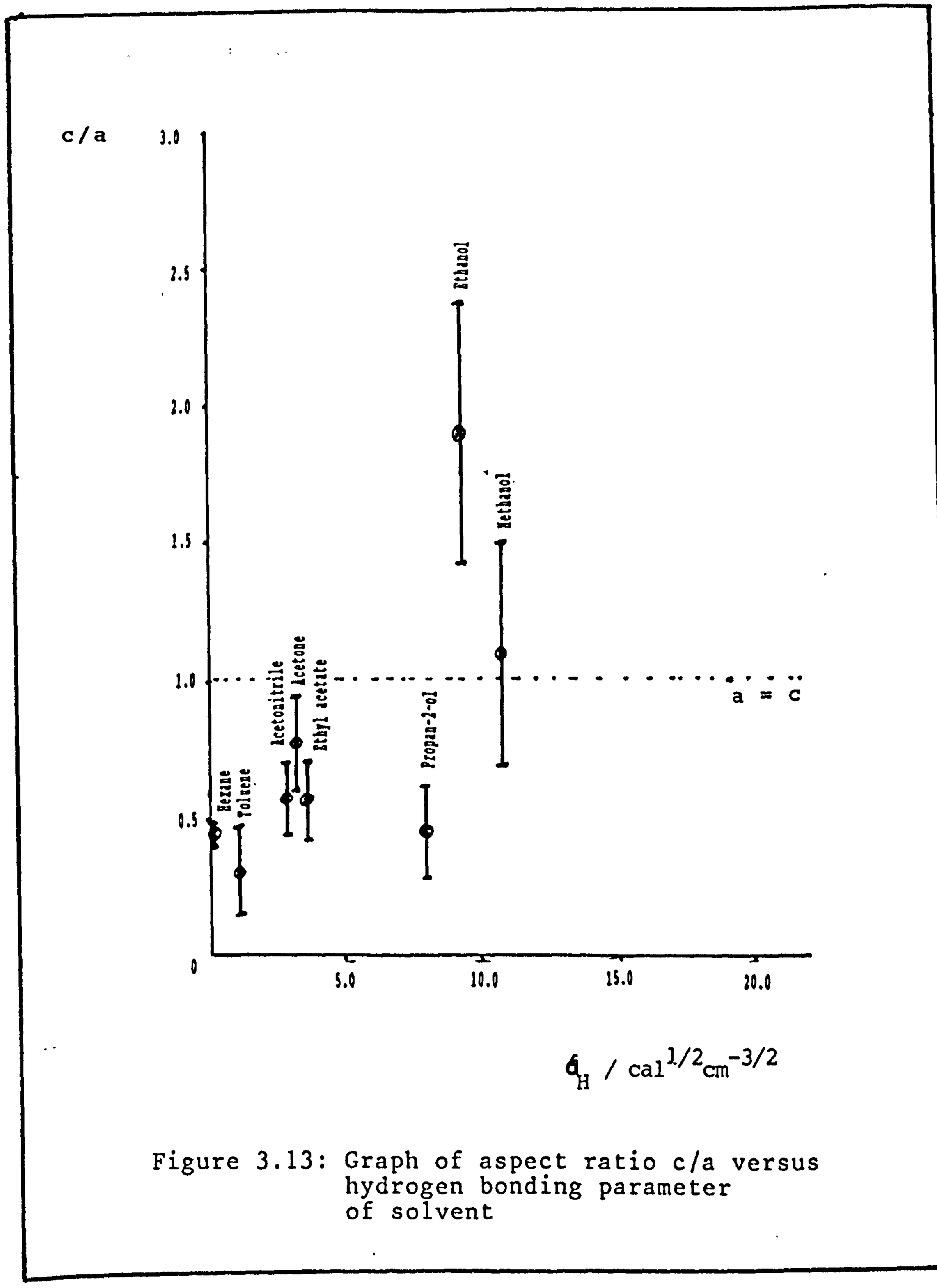

Figure 3.13: Graph of aspect ratio c/a versus hydrogen bonding parameter of solvent

Factors affecting the morphology of ibuprofen will be considered in section 3.2.

3.1.3 Comparison of lattice strain induced by crystallisation solvent

In section 3.1.1.2 it was noted that ibuprofen crystals grown from hexane appeared to show increased lattice strain compared with those grown from acetonitrile. In the following section, the results of a series of experiments to determine the nature of the lattice disruption and quantify the crystalline disorder are reported.

The presence of crystal defects may be expected to increase the internal energy, enthalpy and entropy of a crystal system [80]. Parameters such as ΔH_f and melting point (T_m) can therefore be used as a measure of crystal imperfection. DSC thermograms were therefore obtained from samples of small crystals grown from each solvent investigated.

Single crystal dissolution tests were used to compare the surface reactivity of ibuprofen crystals grown from hexane and acetonitrile, which may also increase at the site of emergent dislocations or other strained regions.

The degree of lattice disruption was quantified by measurement of the mosaic spread of crystal samples using Laue diffraction patterns. X-ray topography allowed further characterisation of strained regions.

3.1.3.1 Differential scanning calorimetry of crystals grown from different solvents

DSC thermograms were obtained as described in section 2.3.4. Small as-grown crystals were used instead of the powdered form, since comminution would have introduced further changes in the degree of crystallinity.

Melting points and heats of fusion are presented in table 3.1. All samples were run in duplicate and mean values are presented.

Solvent	Melting point (°C)	ΔH_f (kJ.mol^{-1})
Acetonitrile	78.62	25.62
Hexane	78.52	25.80
Toluene	78.48	26.02
Acetone	79.08	26.03
Ethylacetate	78.71	25.82
Propan-2-ol	78.89	25.76
Ethanol	78.48	25.96

TABLE 3.1: MELTING POINTS AND HEATS OF FUSION FOR IBUPROFEN CRYSTALS GROWN FROM VARIOUS SOLVENTS

A sharp melting endotherm at around 79°C was the only feature observed on all thermograms, which show a consistently higher melting point and lower heat of fusion than the powder samples examined. This was considered to be due to less efficient heat transmission in the crystals.

Florence et al [126] observed changes in the melting point of digoxin due to differences in the degree of crystallinity. Changes in the latent heat of fusion and internal energy of crystals grown in the presence of habit-modifying impurities, have also been detected by DSC [72,73,127]. Differences in the melting point and heats of fusion of the samples studied here, however, appear to be insignificant, and are not detectable within the errors of measurement of the apparatus.

3.1.3.2 Single crystal dissolution

The retraction of the {100} face of ibuprofen was measured as a function of time, temperature, flow rate and solvent of crystallisation. From equation 2.8, when C_s >> C, the overall dissolution rate is proportional to the observed rate constant, k_{obs}. In this work, the slope ($cm.s^{-1}$) of a plot of movement of the crystal face with time is itself an observed apparent rate constant (K'_{obs}), and can be used as an indication of k_{obs}.

Figure 3.14 shows a typical plot of the retraction of the crystal face as a function of time at different

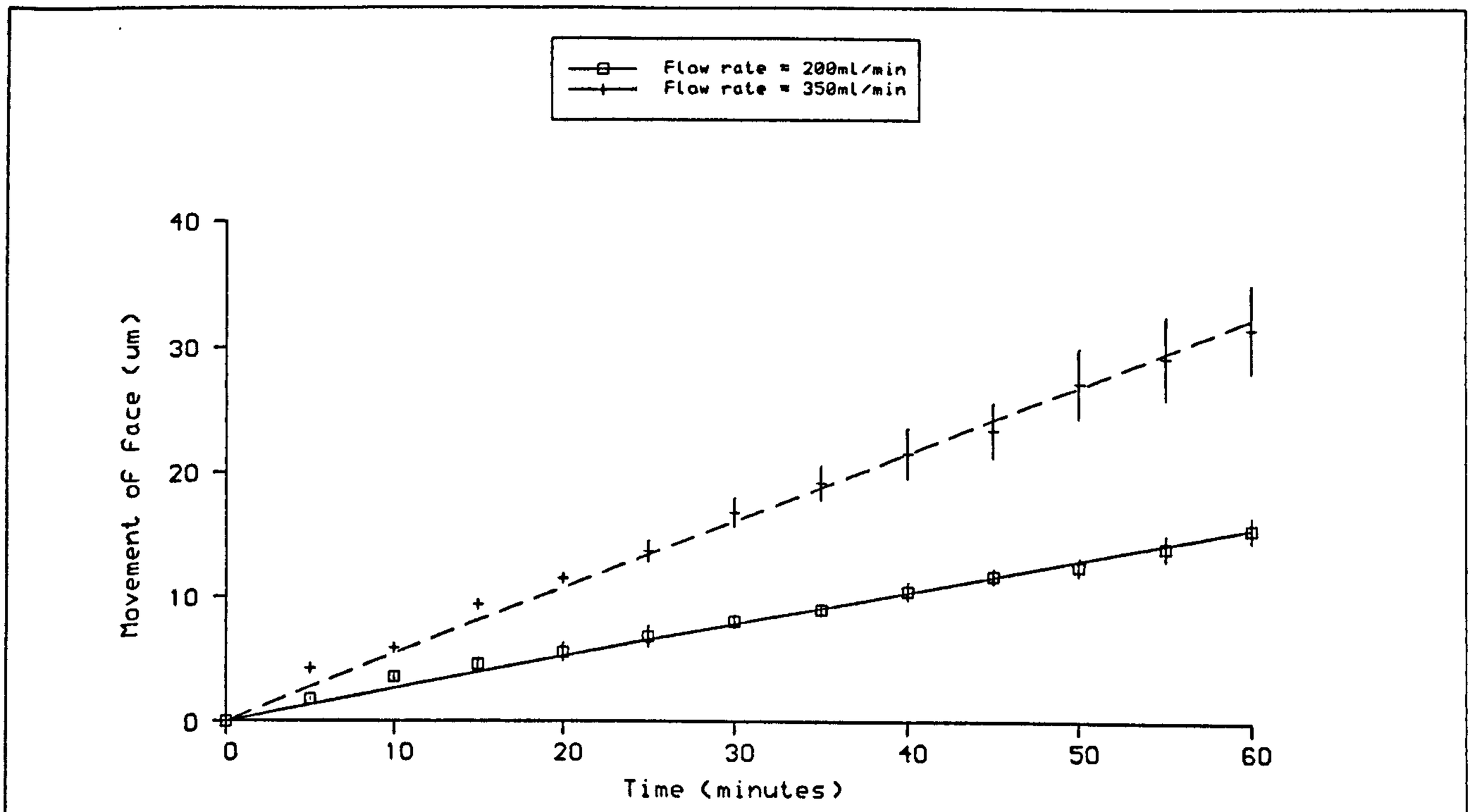

Figure 3.14: Dissolution of acetonitrile grown ibuprofen crystals at 40 C

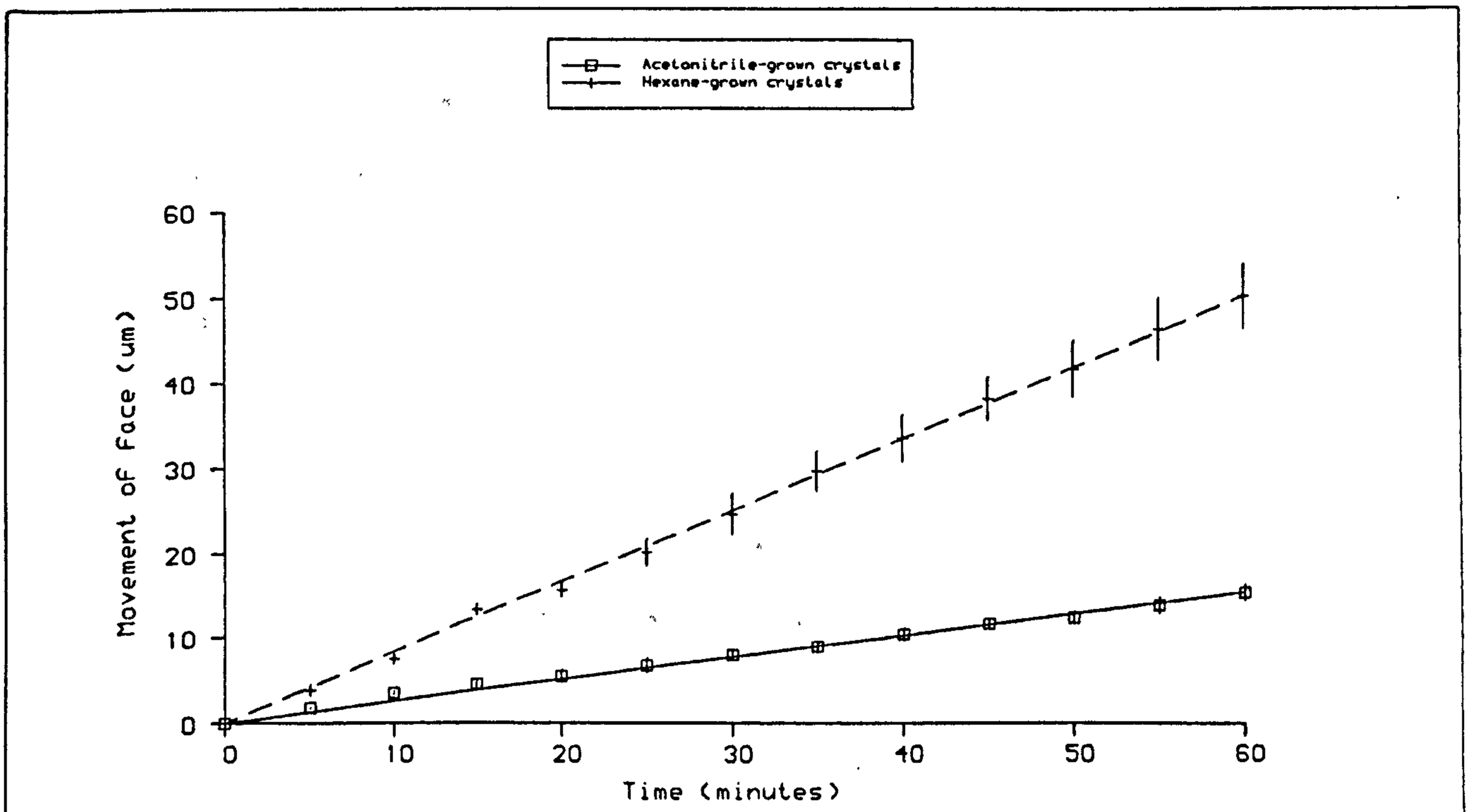

Figure 3.15: Dissolution of ibuprofen crystals at 40C and Flow rate 200ml/min

flow rates, all other parameters being kept constant. The increased movement of the face at the higher flow rate indicates that dissolution is transport dependent.

Figure 3.15 shows typical plots of distance moved as a function of time at constant flow rate and temperature for crystals grown from hexane and acetonitrile. K_{obs} is higher for hexane-grown crystals, and is always higher than that for acetonitrile-grown crystals, allowing equivalent transport conditions. The rate of the surface "reaction" is therefore also a contributing factor to dissolution (ie a mixed transport- surface-controlled process) with the rate of dissolution from the {100} surface of hexane-grown crystals being faster. Since data were obtained for dissolution at only two flow rates, it was not possible to determine actual values for the rate constants of the two processes.

The increased reactivity of the hexane-grown crystals suggested that they were more strained than those grown from acetonitrile i.e. they showed a higher degrée of molecular mismatch or misalignment, leading to an increase in the internal energy and entropy of the hexane-grown crystals, although no significant differences in the heats of fusion of ibuprofen crystals grown from the two solvents were observed in the DSC results, as discussed earlier.

Gordon and Amin [1] found that recrystallisation of

ibuprofen from polar solvents caused an increase in the dissolution rate of crystalline material. The method by which they obtained their results. which are in direct contradiction with those above, was not stated, but appeared to be conducted on compressed powder samples. Their results cannot therefore be directly compared with those above, due to differences in particle sizes and the influence of the compaction process itself.

Sublimation of ibuprofen is reported to be greatly reduced when polar solvents are used in the crystallisation process [1]. This is in agreement with the results presented here, since it is proposed that crystals grown from a polar solvent will be less reactive due to the lower defect content.

3.1.3.3 Determination of mosaic spread using Laue diffraction patterns

Laue diffraction patterns were produced from the {001} habit face for four ibuprofen crystals grown from hexane and four from acetonitrile. Two Laue diffraction patterns for {100} cleavage slices of crystals grown from each solvent were also produced. Diffraction patterns from two of the samples are shown in plates 3.6 and 3.7. The first is from a good quality crystal grown from acetonitrile and shows low strain ($\eta = 7.358 \times 10^{-3}$). The second is from a crystal grown from hexane and shows considerably greater radial elongation of the spots due to increased lattice strain ($\eta = 10.730 \times 10^{-3}$).

Results are given in table 3.3. Comparing all samples from each solvent, the t_{data} are outwith 95% probability that the samples are the same, hence samples are statistically different. Those grown from hexane showed more lattice strain than those grown from acetonitrile, suggesting differences in the crystal growth process due to these solvents.

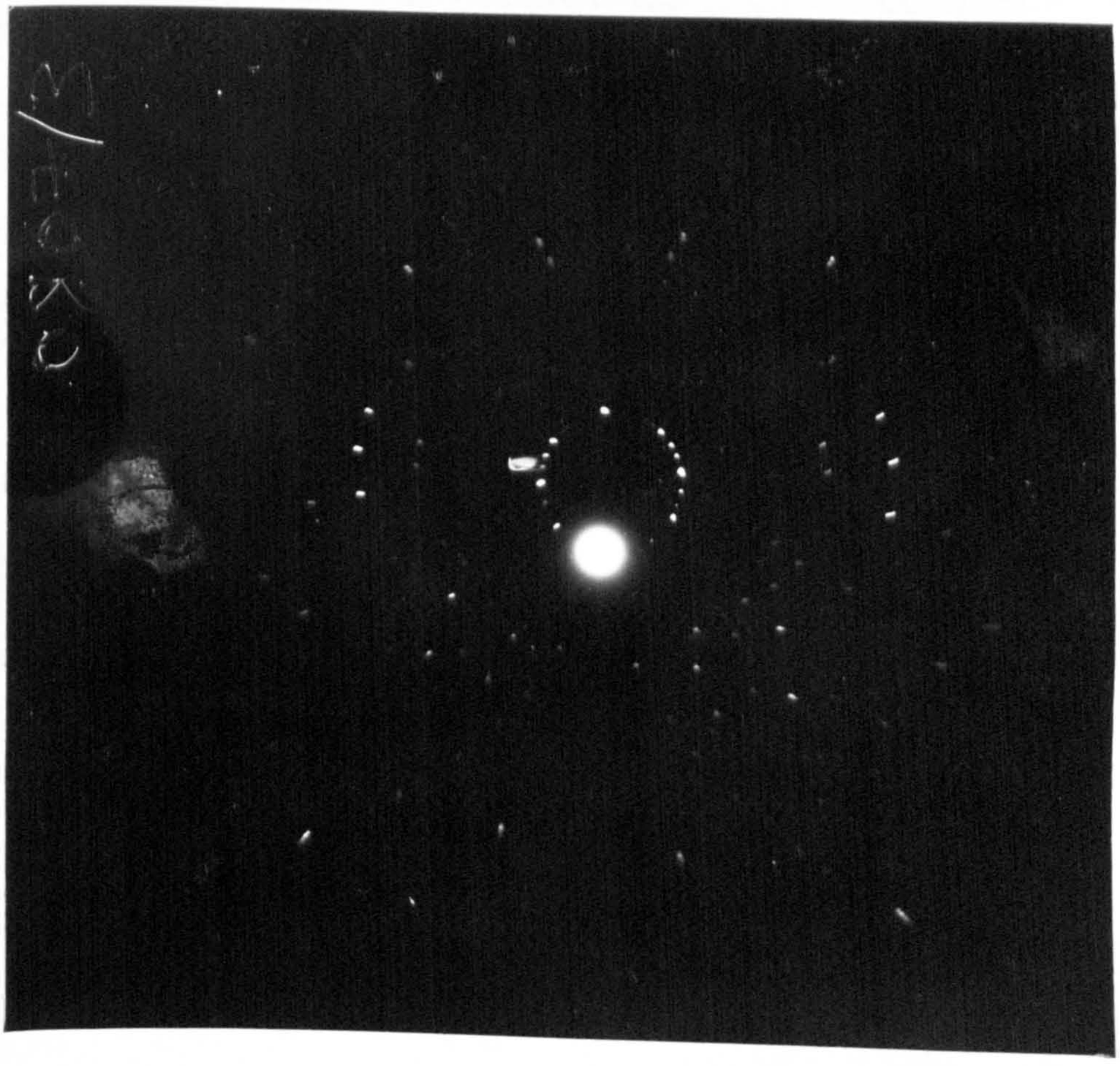

Plate 3.6: Laue diffraction pattern from a good quality ibuprofen crystal (001) face

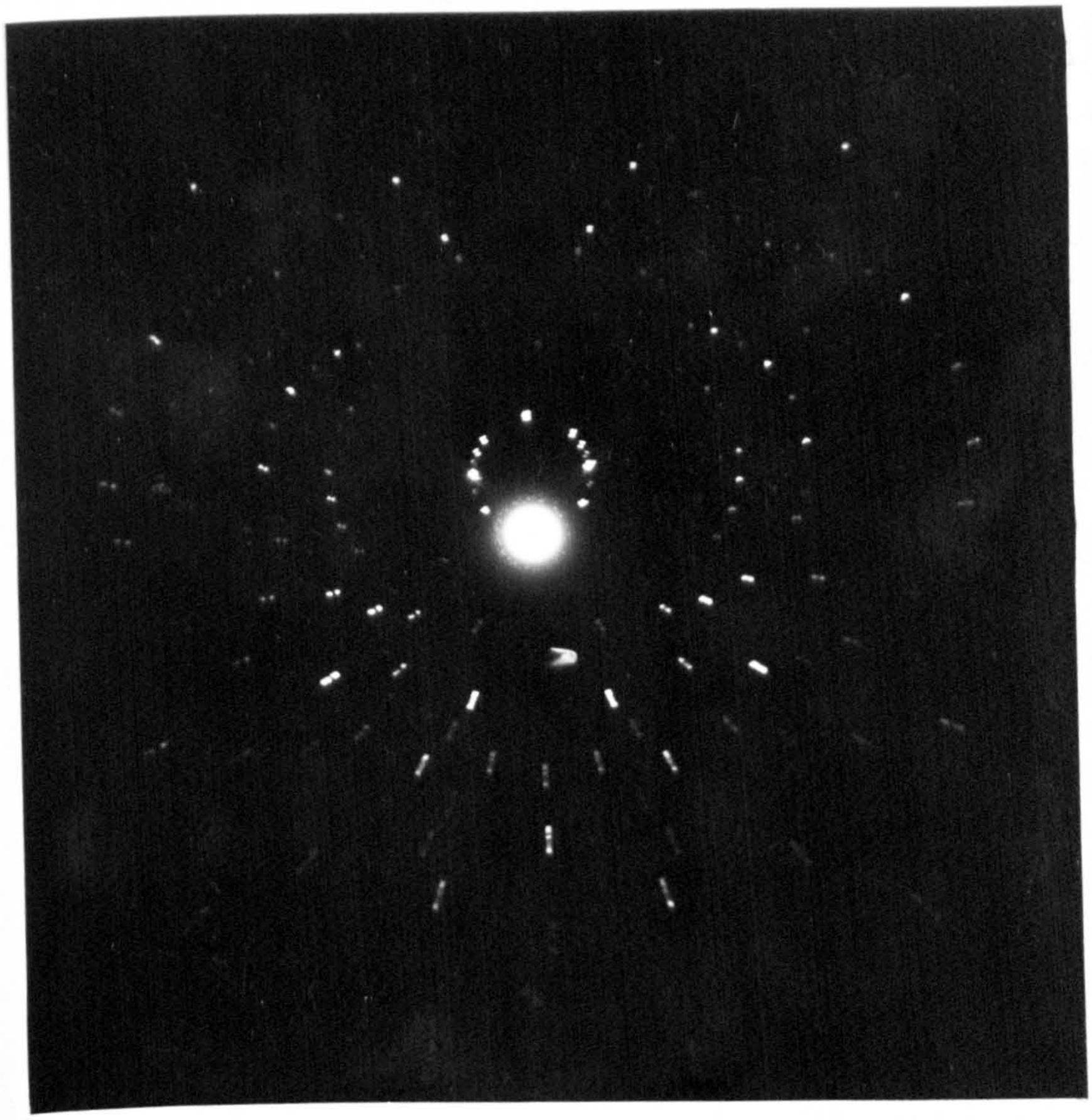

Plate 3.7: Laue diffraction pattern from a poorer quality ibuprofen crystal (001) face

Solvent	Sample	Face	Mosaic spread (degrees$\times 10^{3}$)
Acetonitrile	0507/3	{100}	11.113
	0807/2		8.658
	JC3	{001}	5.485
	JC1		7.661
	JC2		5.357
	0807/3		7.358
	mean		7.605, sd=2.146
Hexane	JH1	{100}	17.97
	1806/1		13.73
	0306/1	{001}	14.626
	1706/1		13.002
	2706/1		8.320
	2806/2		10.730
	mean		13.063, sd = 3.314

TABLE 3.2: COMPARISON OF MOSAIC SPREAD BETWEEN CRYSTAL SAMPLES

3.1.3.4 X-ray Topographs

X-ray topographs were obtained from slices of crystals grown from hexane and acetonitrile, in order to compare the internal structures of the crystals (in particular the number and types of crystal imperfections).

Initial comparison of topographs from the two types of crystal confirmed the results of the mosaic spread experiments. The hexane-grown samples showed more strain and lattice disruption than acetone- or acetonitrile-grown samples, whether dish-grown or grown by controlled cooling. The topographic images were therefore correspondingly more distorted. Images were obtained from {100} slices, cleaved from seed-grown crystals, from both hexane (plate 3.8) and acetonitrile (plate 3.9), where the {001} growth sector is dominant. Much greater distortion can be observed in the hexane-grown sample. Additionally, plate 3.9 shows greater distortion in the {001} growth sectors than in the {100} or faster growing (110), (111) or $(11\bar{1})$ growth sectors. Similarly, {001} reflections in samples of {100} orientation showed greater distortion than other images (using Laue type topographs), implying that {001} planes are more highly strained. Dish-grown crystals produced by spontaneous nucleation and slow solvent evaporation proved to be of better topographic quality than those grown from seed crystals under more controlled

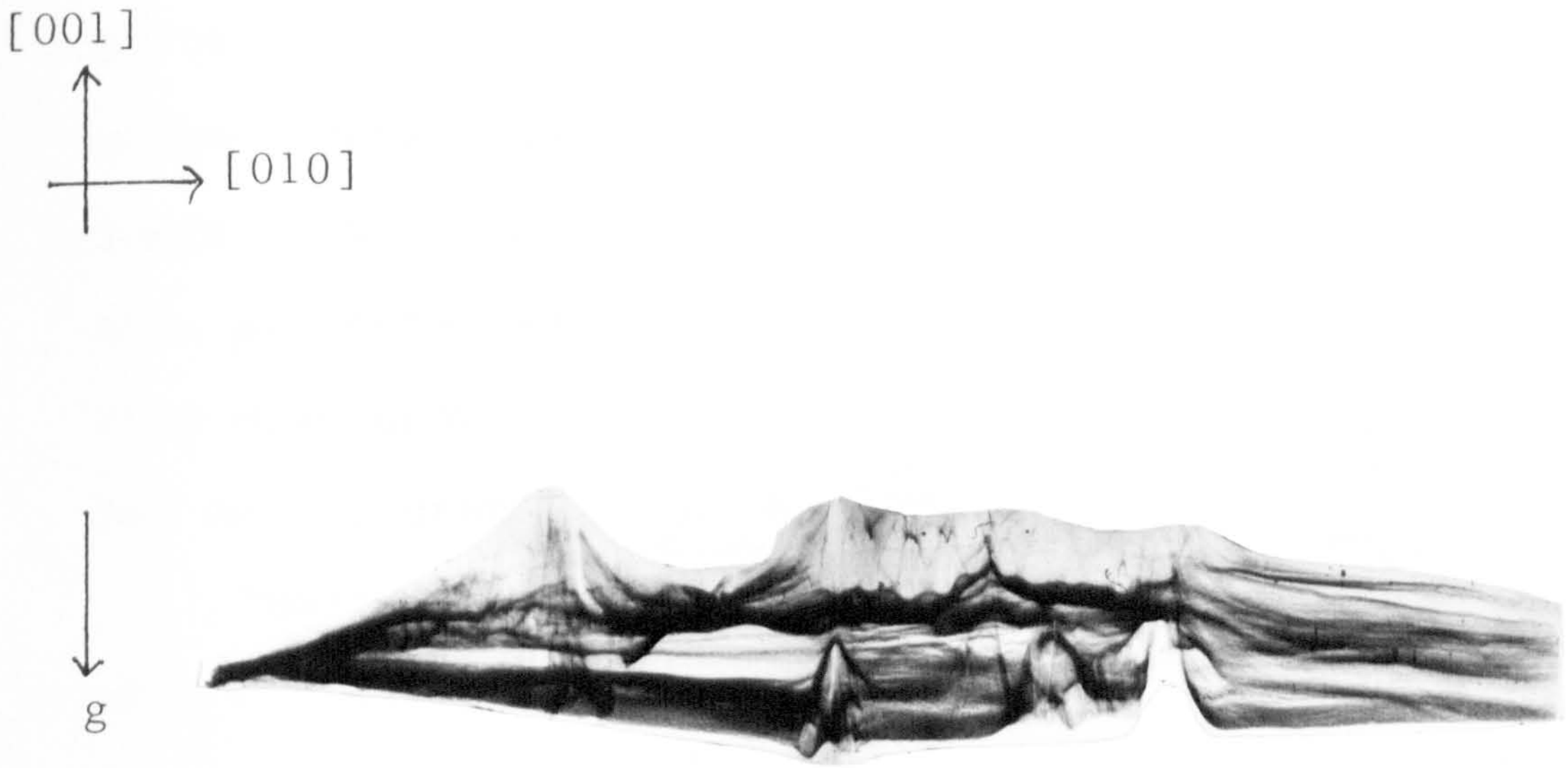

Plate 3.8: (002) reflection of (100) slice of a seed-grown crystal from hexane solution

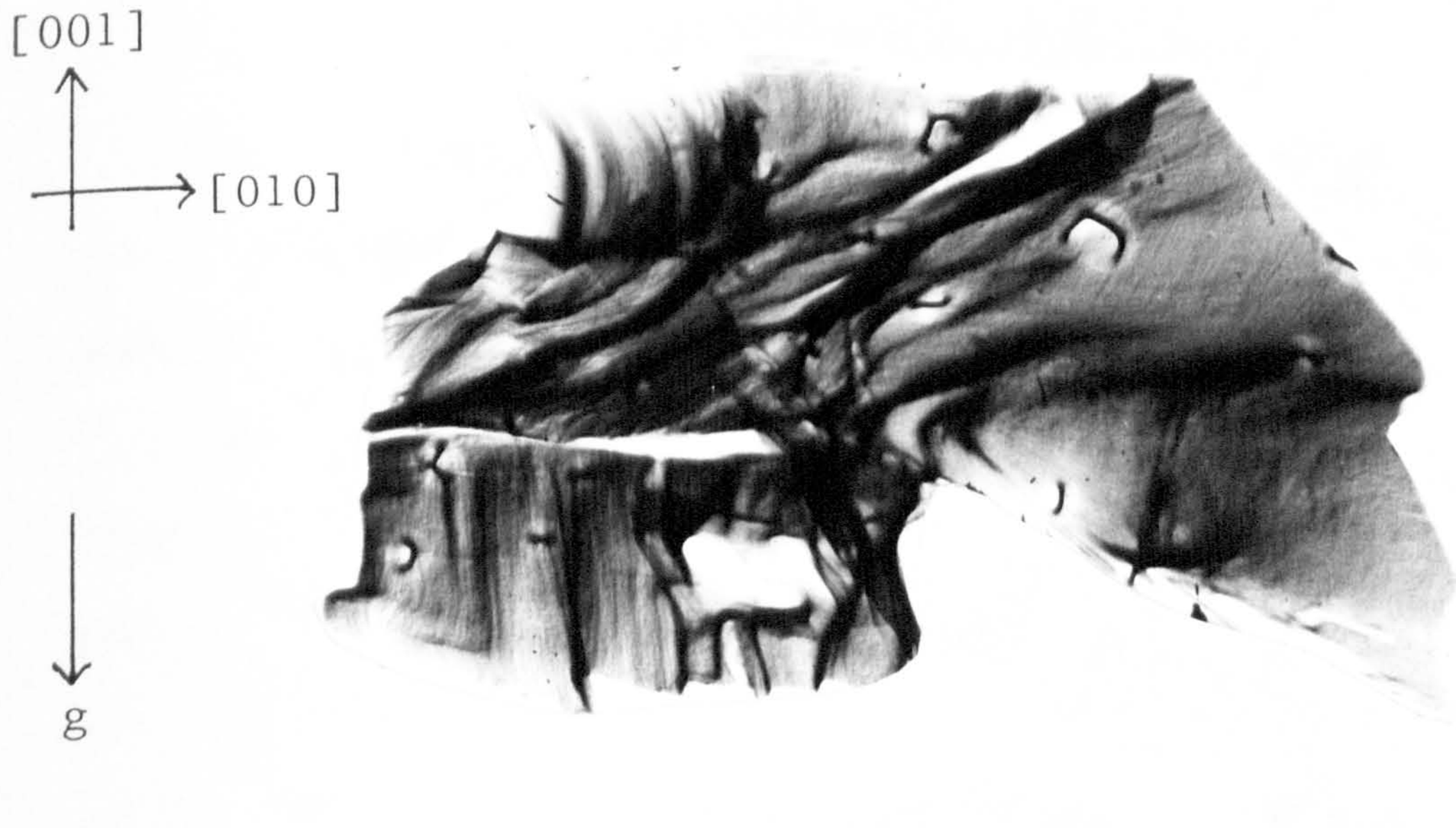

Plate 3.9: (002) reflection of (100) slice of a seed-grown crystal from acetonitrile solution

conditions. Plate 3.10 shows the same reflection as plate 3.9, but obtained from a {100} slice of a dish-grown crystal, using acetonitrile as a solvent. The image is much less distorted, and shows greater detail than any obtained from seed-grown crystals. {100} slices from dish-grown crystals using hexane as a solvent could not be topographed due to their thinness.

Images obtained from samples of {001} orientation were not distorted to the same extent. Plate 3.11 and 3.12 show, respectively, the same reflections from {001} slices from dish-grown crystals using hexane and acetonitrile. Images from the hexane-grown crystal are more distorted, with separation of sections of the image, possibly due either to partial cleavage of the {100} planes, or simply due to the increased distortion (bending of the lattice).

In general, crystal strain was too great to allow the individual dislocations observed in some growth sectors to be identified and characterised. Interesting features were noted consistently in topographs of crystals grown from acetone or acetonitrile (shown in plates 3.10 and 3.12) which were in the form of fringes, the orientation of which was dependent on the growth sector in which they were observed, being normal to the growth direction. They were observed in all reflections and all growth sectors.

Fringes arise in topographic images either due to

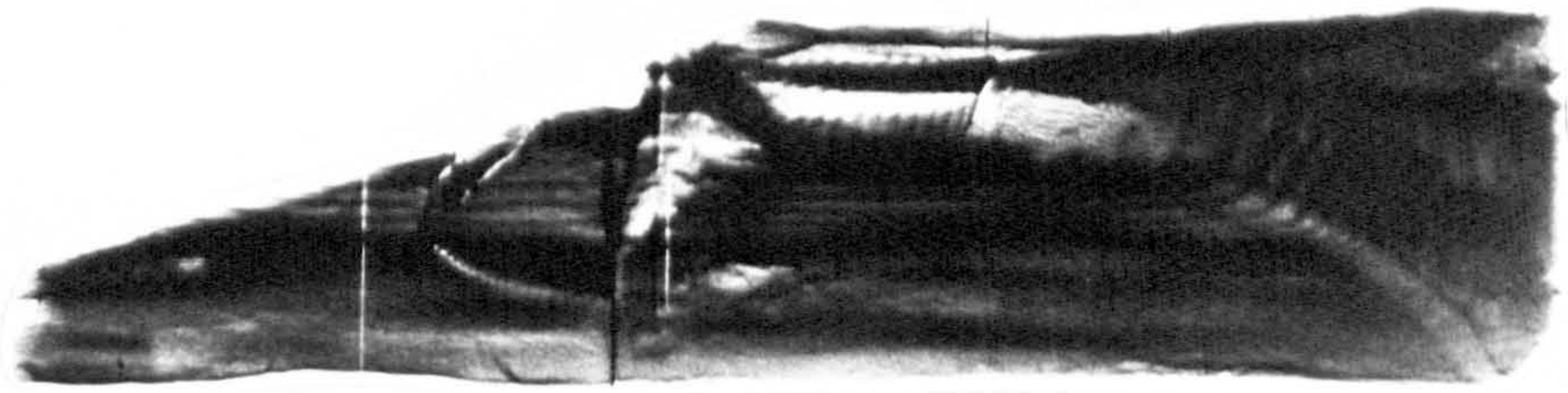

Plate 3.10: (002) reflection of (100) slice from a dish-grown crystal using acetonitrile

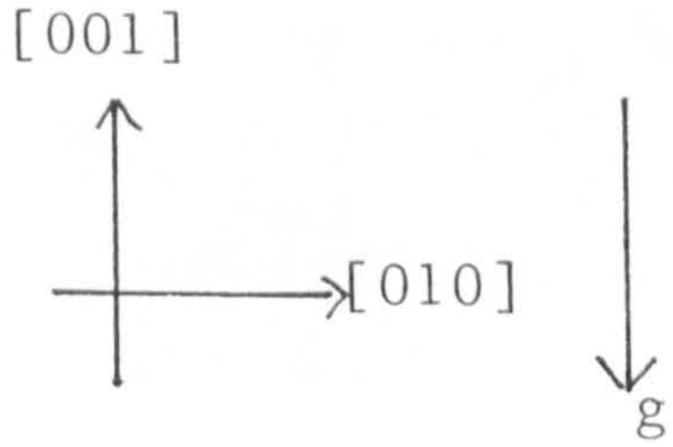

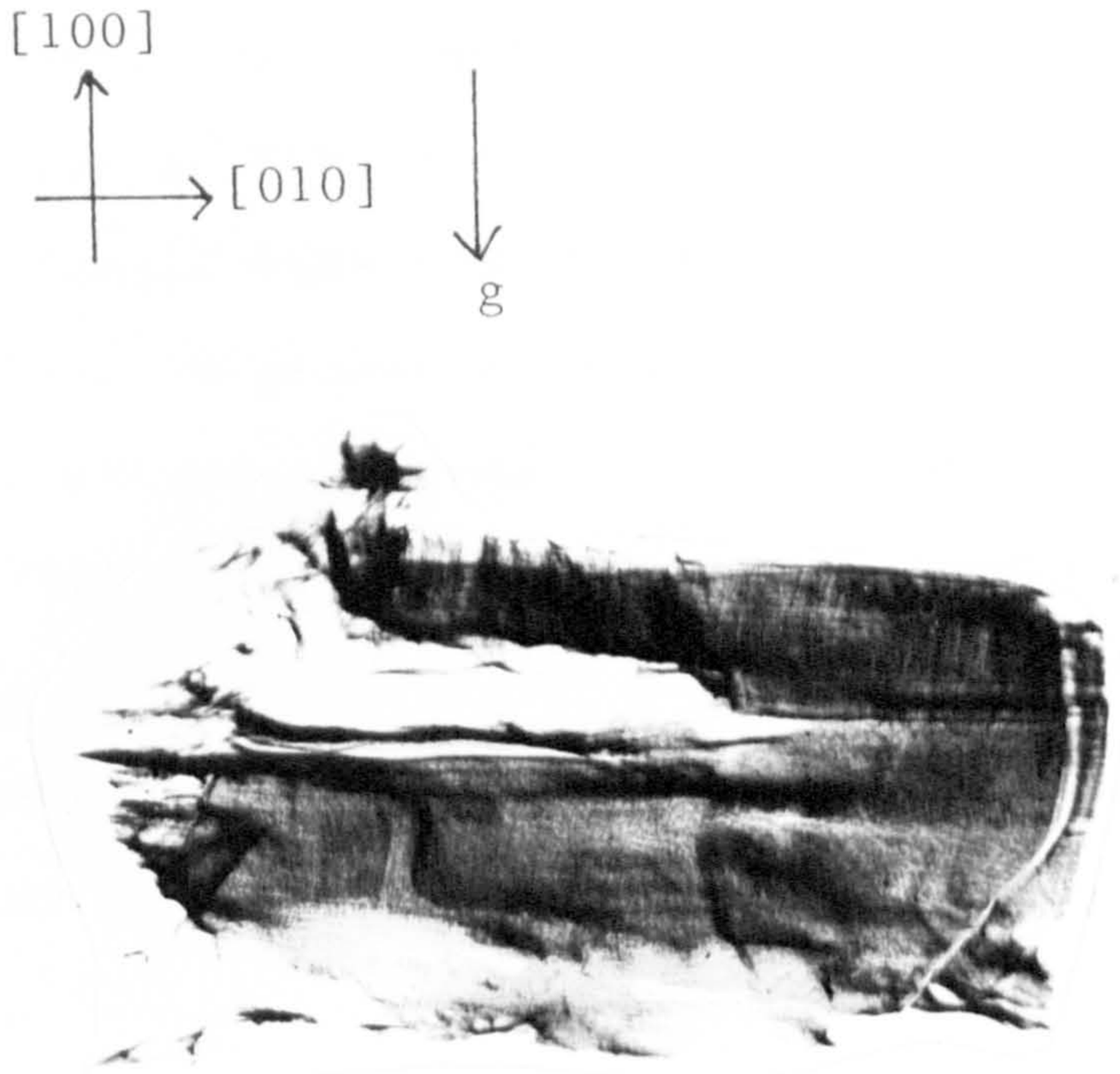

Plate 3.11: (100) reflection of (001) slice of a dish-grown crystal from hexane solution

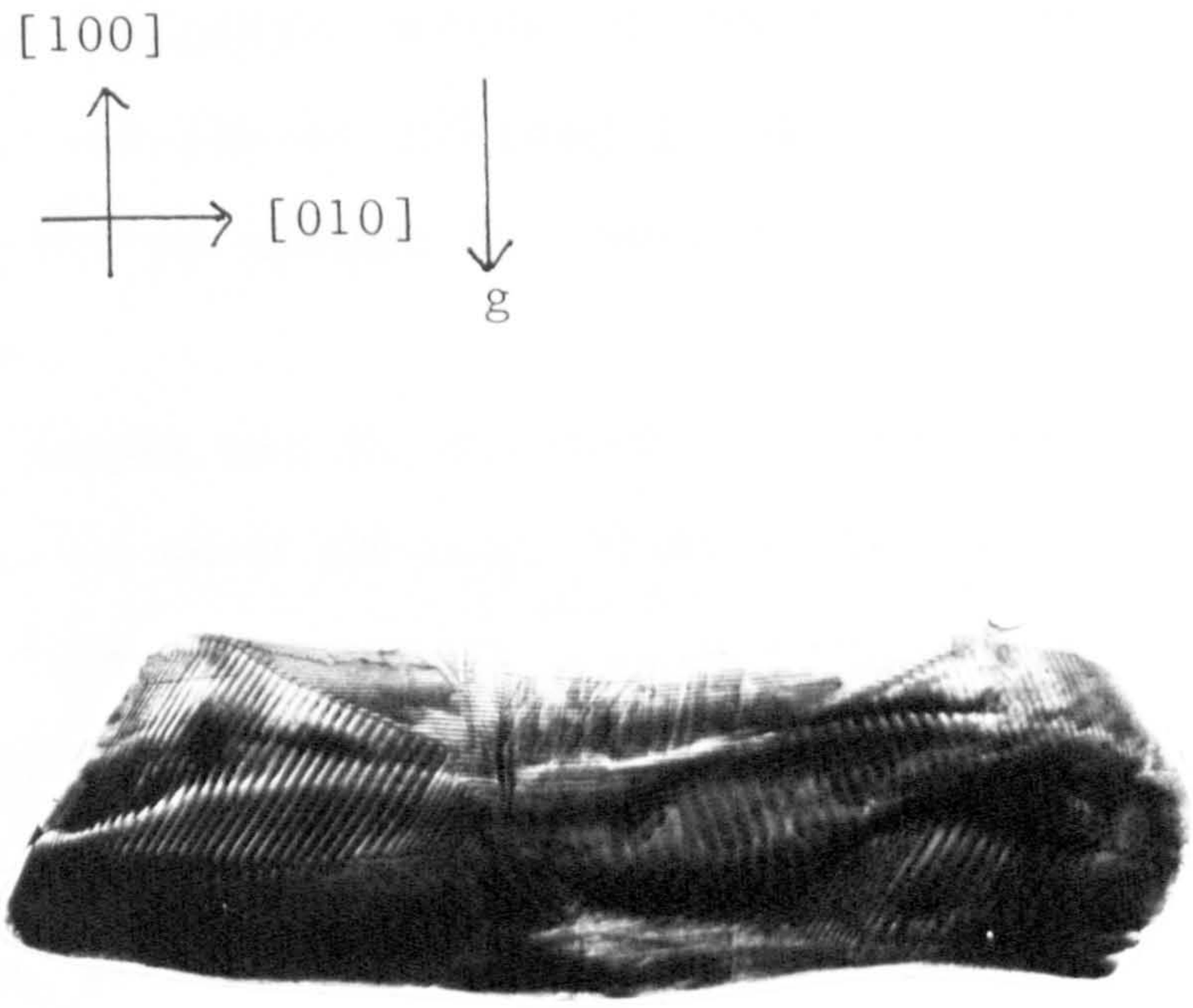

Plate 3.12: (100) reflection of (001) slice of a dish-grown crystal from acetonitrile solution

growth-related or dynamical effects. Since the spacing of the fringes alters as the relative growth rates in adjacent sectors changes (see regions marked A in plate 3.12) they appear to be growth-related. They are unlikely to be due to growth bands (accumulations of impurities and solvent inclusions caused by a sudden increase in the growth rate) due to their regularity. Growth sector boundaries also often appear fringed in topographs, the contrast arising due to differences in lattice parameters due to variation in the growth rate in different sectors. A similar effect seems to be observed here, although it is unusual for growth sector boundaries to extend over the whole image, usually being restricted to the area around a seed crystal or to the intersection of two growth sectors [95] where these are at an angle to the diffraction vector. In this instance the fringes appear to overlap at sloping growth sector boundaries (see regions marked B), rather than to arise at the boundaries.

Dynamical fringes can be divided into two types, those which arise in very perfect crystal due to the interference of direct and diffracted beams (Pendellösung fringes), and those which arise due to interbranch scattering, where the decoupling of wavefields occurs around a very strained defect. Interference of the two new wavefields produces fringes similar to Pendellösung fringes. Neither of the above are very likely in this instance, since the samples are

not of high quality, and the fringes extend over the whole image, not just around individual defects. Fringes produced by dynamical scattering also tend to be less regular and curve as the crystal thickness changes.

The fringes observed in topographs of {100} and {001} slices of acetonitrile grown crystals, appear to be growth-related, although their exact source is not clear.

3.2 INVESTIGATION OF POSSIBLE FACTORS AFFECTING THE MORPHOLOGY OF IBUPROFEN

The equilibrium morphology of ibuprofen was calculated using HABIT. This was then compared with the as-grown morphologies and used to determine the effect of different solvents on the crystal morphology. Calculation of Jackson α-factors allowed determination of the possible growth mechanisms in different solvents. Possible differences of molecular association in solution were also investigated and the molecular structure of the growth interfaces studied to identify potential interaction sites for solvent molecules.

3.2.1 Determination of Theoretical Morphology

The growth forms with the largest interplanar spacings (d_{hkl}) were calculated using the program MORANG. They are presented in table 3.4 with their d_{hkl} values and attachment energies (E_{att}) calculated from HABIT.

Growth form {hkl}	d_{hkl} (A)	E_{att} (kcal.mol^{-1})
100	14.472	-4.73
001	10.587	-8.05
$1\bar{1}0$	6.925	-17.85
$01\bar{1}$	6.324	-18.04
$11\bar{1}$	5.599	-17.40
$1\bar{1}1$	5.601	-16.70
$2\bar{1}0$	5.330	-18.76
$10\bar{2}$	5.567	-17.20
102	4.731	-15.86
E_{latt} = -28.94 kcal.mol^{-1}		

TABLE 3.3: INTERPLANAR SPACINGS AND ATTACHMENT ENERGIES FOR IBUPROFEN

The lattice energy calculated using HABIT, as described in section 2.4.5, compares well with that derived from experimental values for the sublimation

energy (using a value for ΔH_s obtained from reference 128) using equation 1.6. This gave a value for the experimental lattice energy of -30.10 kcal.mol^{-1}. Given an experimental error in measuring ΔH_s of $\pm$ 1 to 3 kcal.mol^{-1} [18,129] the atom-atom potential calculations give a reasonable result.

Inputting the E_{att} values into the SHAPE program, which assumes growth rate is proportional to E_{att}, an equilibrium morphology was constructed based on the assumption that only intermolecular forces within the crystal affected its morphology. This is illustrated in figure 3.16.

The calculated morphology is in better agreement with that of vapour grown crystals than any of those grown from solution. In particular, the dominant face in the calculated morphology was {100} (rather than {001} as observed in the solution grown crystals) since intermolecular interactions on this plane were weakest. This is in agreement with the identification of {100} as a cleavage plane; similar calculations performed on the aspirin crystal structure also identified the cleavage plane as having the weakest intermolecular interactions [122]. As in this case, it was not the dominant face in the solution grown crystals, and a solvent interaction was implicated but not proved.

It is useful to compare the experimental crystal dimensions with those of the calculated morphology in order to determine the effects of the solvent of

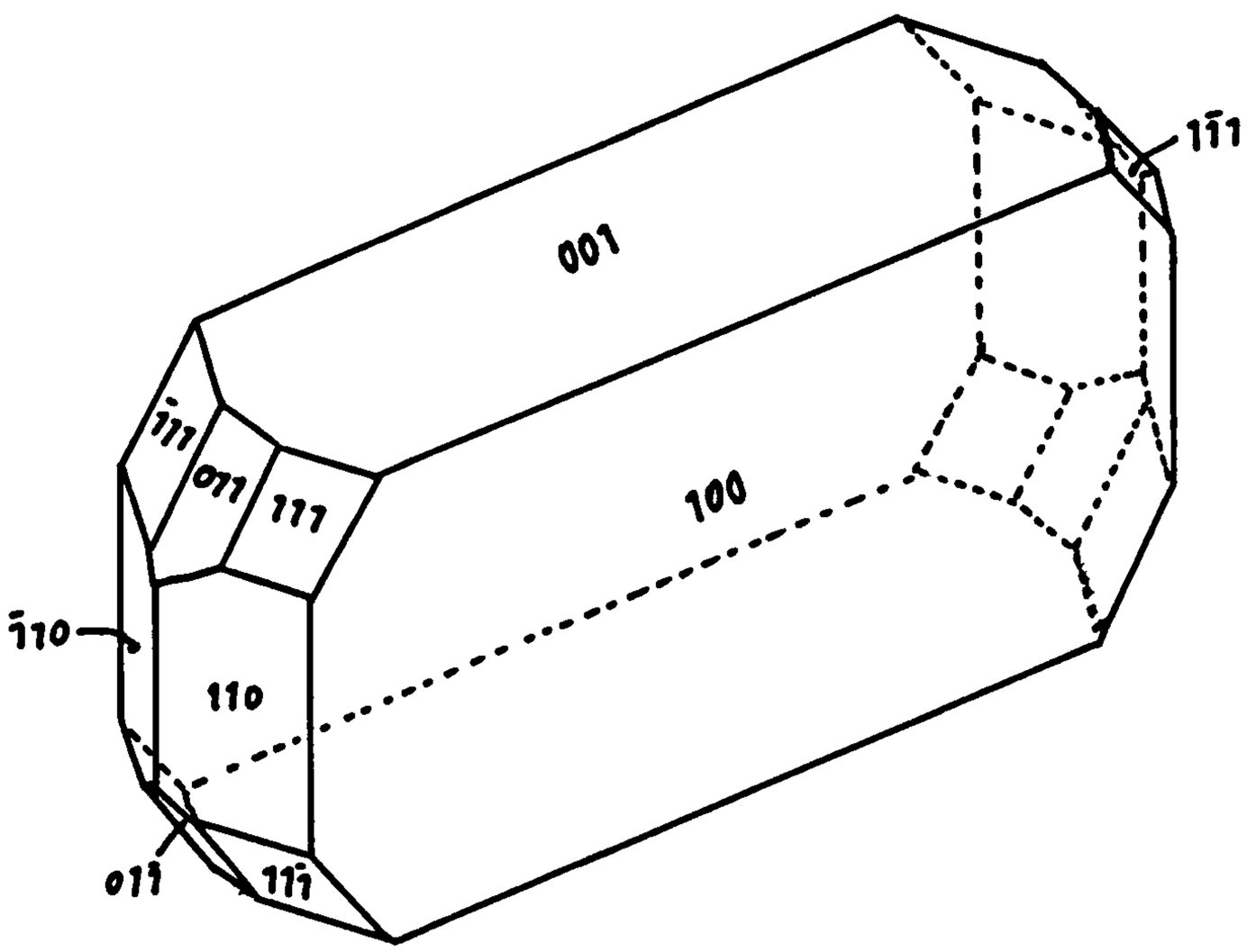

Figure 3.16: Equilibrium morphology calculated using attachment energy model

crystallisation on the crystal morphology. Table 3.4 lists these values.

Solvent	Relative rate of growth along axis: a	b	c
Theoretical model	1	3.88	1.74
Hexane	1	4.47	0.37
Toluene	1	2.56	0.31
Ethylacetate	1	3.39	0.56
Acetone	1	4.17	0.77
Acetonitrile	1	1.98	0.57
Propan-2-ol	1	1.64	0.45
Ethanol	1	1.88	1.89

TABLE 3.4: RATIO OF CRYSTAL DIMENSIONS ALONG a, b AND c AXES

All solvents (with the exception of hexane and acetone) appeared to reduce the growth rate along the a axis to some extent, the effect generally increasing with polarity. Growth along the c axis also appeared to be decreased by all solvents investigated, excepting ethanol, resulting in {001} becoming the dominant face. It was only when ibuprofen was grown from ethanol (or methanol) that {100} became dominant in the morphology

as predicted by theory.

Polar solvents did not therefore only promote relatively slower growth along the b axis as initially proposed in section 3.1.1.4.; growth was also altered along the c axis by both non-polar solvents and all polar solvents apart from those with the highest hydrogen-bonding capacity.

3.2.2 Calculation of Jackson α-factors

None of the previously published studies on ibuprofen morphology [1,87] considered possible changes in growth mechanism due to the change in solvent as a source of the morphology changes. Solvent interactions with specific faces were suspected, but adsorption sites were not proposed [87].

Since supersaturation levels were kept constant during the controlled cooling experiments, Jackson α-factors could be determined for the growth faces of ibuprofen in both hexane and acetonitrile solutions. Calculations were carried out using equation 1.9. E_{sl} and Φ_{inter} were obtained from theoretical calculations; ΔH_f from DSC results; $x_{s.eq}$ was calculated by dividing the saturation solubility (from solubility curves) by density (from crystallographic data).

α-factors were calculated at 35°C, in the middle of the growth range for both acetonitrile and hexane solutions. Results are presented in table 3.5.

	α-factor	
Face {hkl}	Hexane	Acetonitrile
100	6.90	6.59
001	5.95	5.69
$1\bar{1}1$	3.49	3.33
$1\bar{1}0$	3.16	3.02
Est.error	±2.56%	±2.80%

TABLE 3.5: CALCULATED α-FACTORS FOR IBUPROFEN CRYSTAL FACES

From these results, it would appear that the two end-faces of ibuprofen can grow by a "birth-and-spread" (two-dimensional nucleation) mechanism, but that the main {100} and {001} faces can only grow by a spiral dislocation mechanism. More importantly, no changes in growth mechanism are seen between the two different solvent systems.

It is likely therefore, that solvent adsorption is the source of relative changes in the growth rate.

3.2.3 Proton NMR to investigate association of ibuprofen molecules in solution

Since ibuprofen is a polar molecule, its state of molecular association in polar and non-polar solvents is likely to be different; in polar or hydrogen-bonding solvents the carboxylic acid group can be stabilised by hydrogen-bonding with the solvent, whereas in non-polar solvents it can only be stabilised by hydrogen-bonding to another ibuprofen molecule. Vapour pressure osmometry data indicated that ibuprofen existed predominantly as monomers in acetonitrile solution as expected, but that in hexane, dimer structures were predominant [130].

Nuclear magnetic resonance (NMR) spectra were obtained from saturated solutions of ibuprofen in both deuterated acetonitrile and carbon tetrachloride and are illustrated in figures 3.17 and 3.18 respectively. The major difference between the two spectra was in the position of the peak associated with the hydroxyl hydrogen. In carbon tetrachloride a sharp peak was observed at 12.45ppm. In acetonitrile a broadened peak was observed, superimposed on the quadruplet of aromatic hydrogens at approximately 7ppm.

The shift in position of the peak in CD_3CN indicated that different interactions were taking place than in CCl_4 solution; the peak broadening indicated that the interactions replacing hydrogen-bonding were transient, and that a number of different association

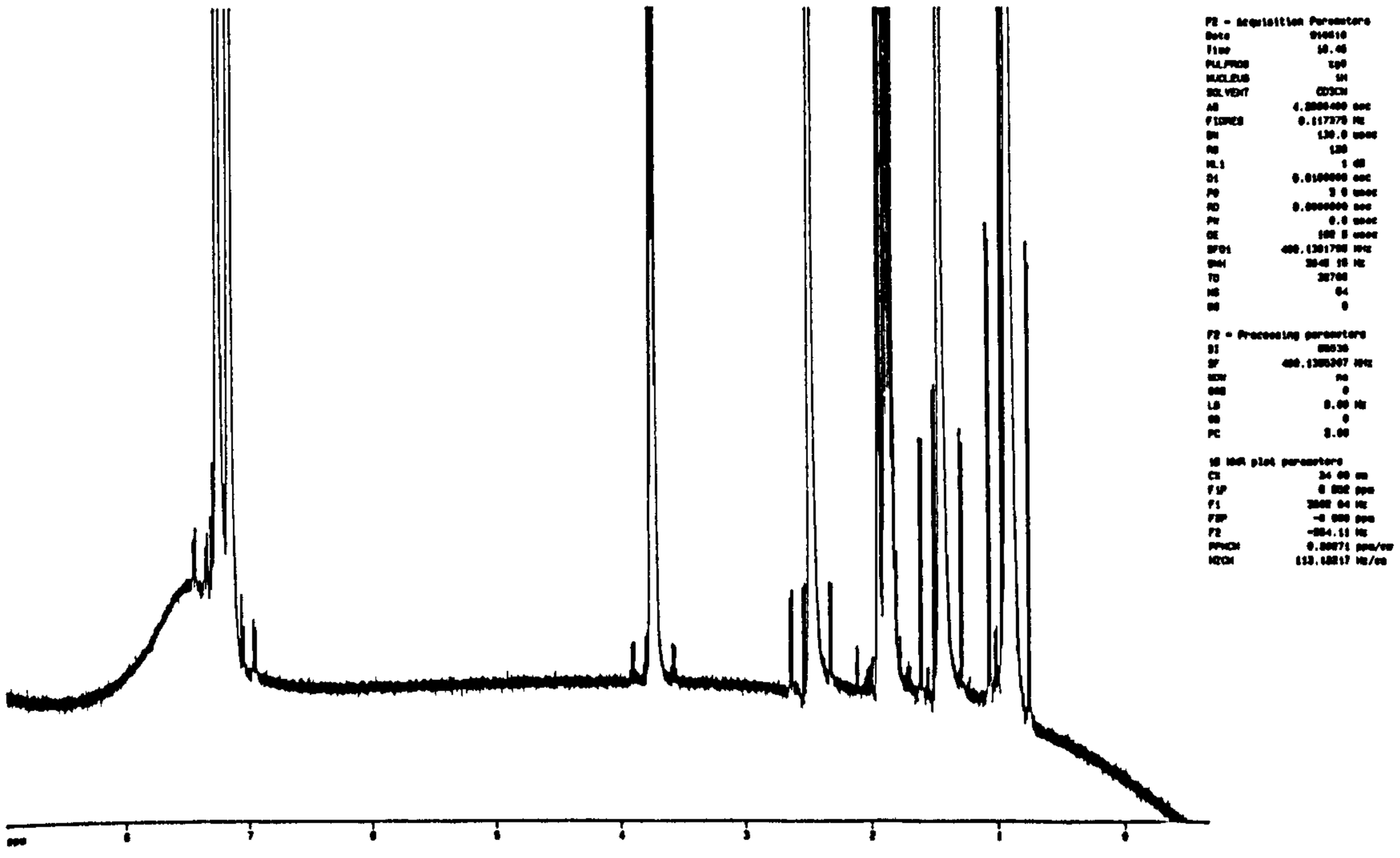

Figure 3.17: Proton NMR spectrum of ibuprofen in deuterated acetonitrile

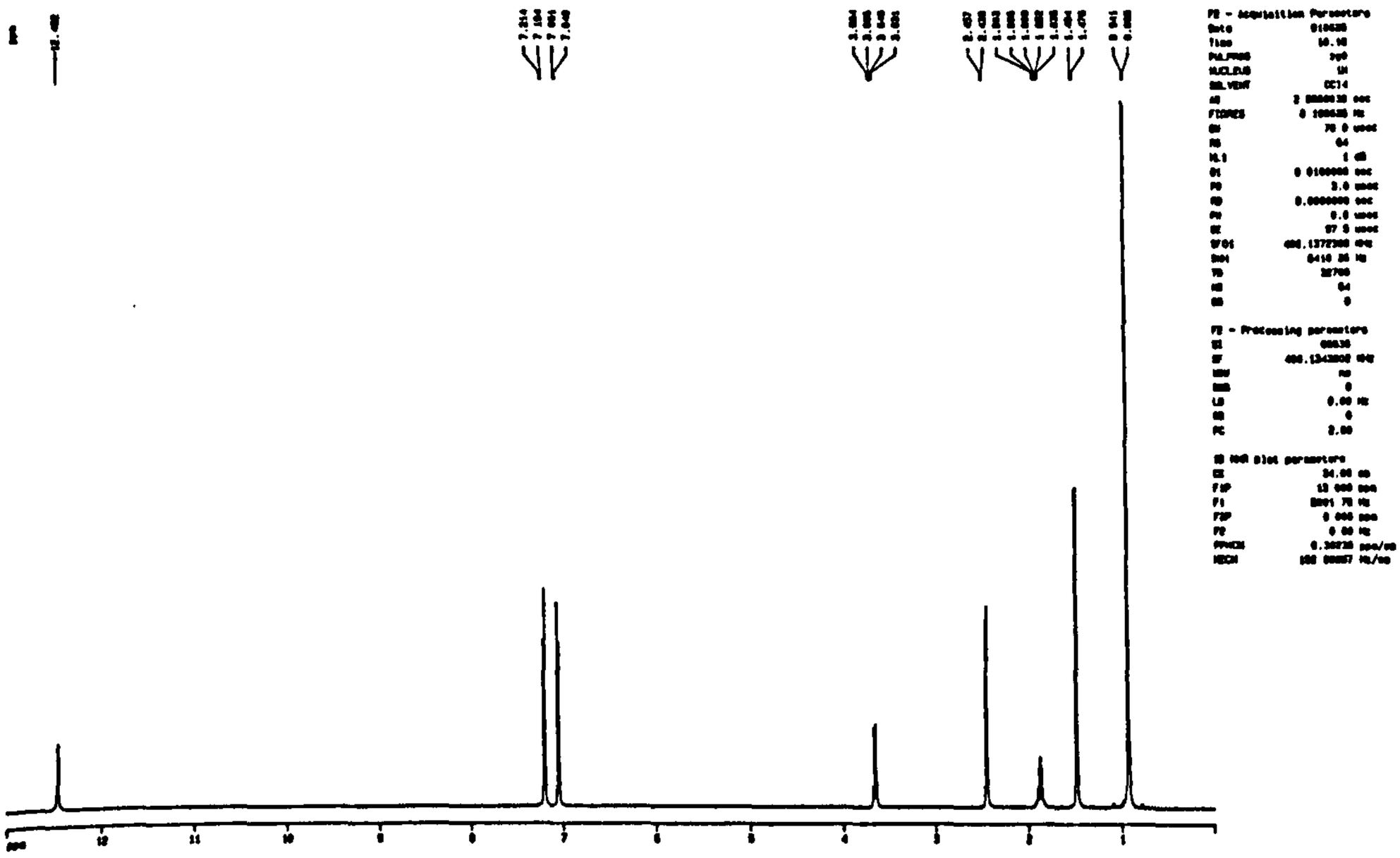

Figure 3.18: Proton NMR spectrum of ibuprofen in carbon tetrachloride

states were possible. The hydroxyl hydrogens were likely to be exchanging with the solvent [131].

Spectra of 50% and 25% dilutions of the original solutions were obtained to determine whether any changes to the molecular association occurred. Little change was observed in the spectra of diluted carbon tetrachloride solution, with the peak at 12.45ppm remaining sharp. In acetonitrile solution however, the band associated with the hydroxyl hydrogen broadened and moved further down the spectrum as shown in figure 3.19. This indicated more frequent exchange with the solvent, and dissociation of remaining carboxylic acid dimers.

Deposition of ibuprofen on the surface of a growing crystal is therefore unlikely to occur by the same mechanism from polar and non-polar solvents. In the latter case, it is more likely that the growth units being deposited at the growth interface from solution will be a dimer rather than monomers, since individual ibuprofen molecules will be energetically unstable in a non-polar solvent. Being a larger growth unit, it is likely that reorientation of the dimer units at the growth surface will be more difficult than for the corresponding monomers, with possible effects on both the growth rate and defect structure of the material which will be discussed later.

Ibuprofen dimers in non-polar solutions will not necessarily be racemic - dimers of both enantiomers will

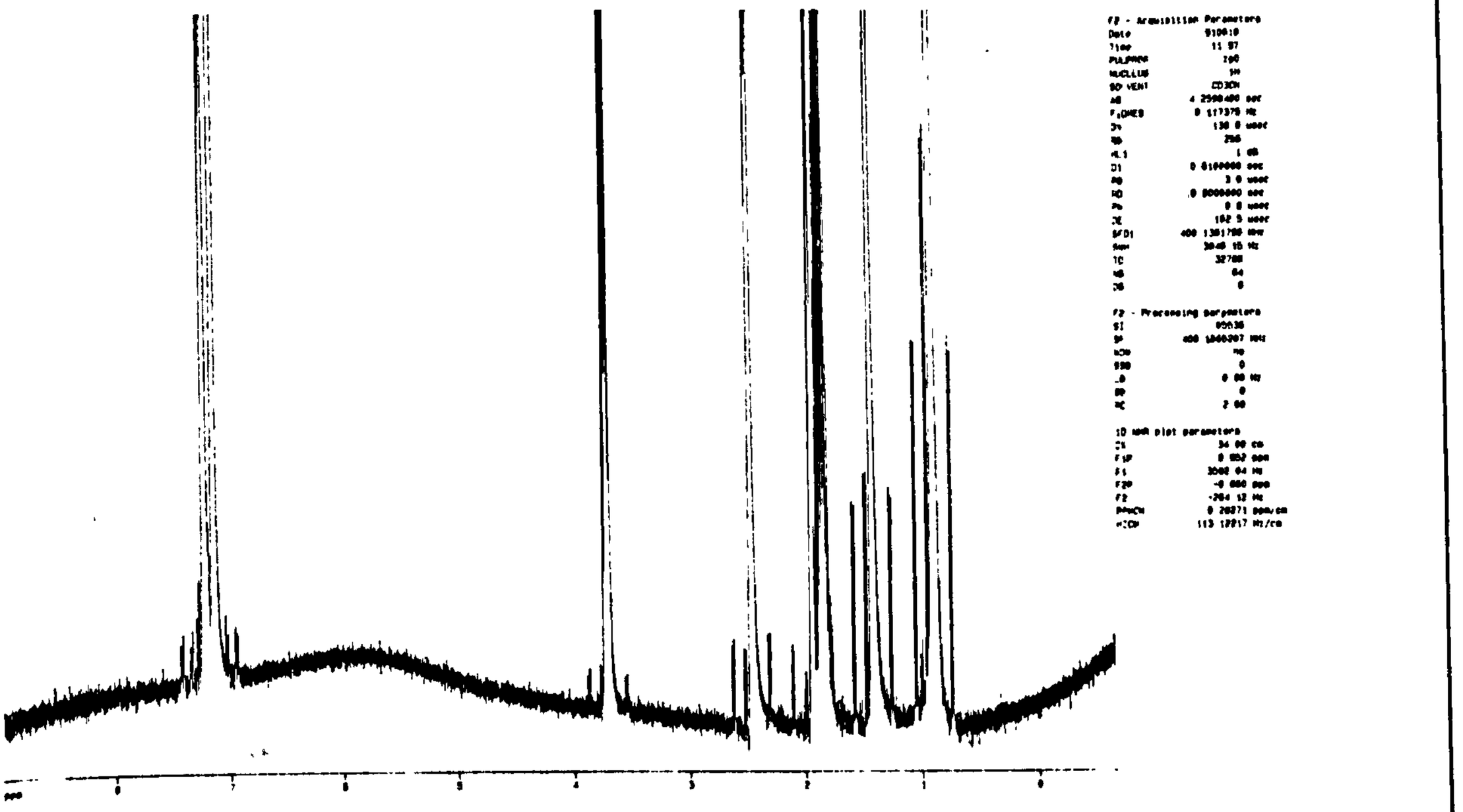

Figure 3.19: Proton NMR spectrum of 50% dilution of the acetonitrile solution

also be present. These could both act in the manner of tailor-made additives as discussed in section 1.1.2.2; if one half of the dimer is incorporated at the growth surface, the protruding part will be different from that normally encountered by oncoming growth units and may be sufficiently different to slow crystal growth until the molecule is replaced with the "correct" one. Alternatively, if the enantiomeric dimers are incorporated into the crystal bulk, this is likely to be a source of strain within the crystal.

Growth from polar solvents probably occurs by deposition of monomers. Growth rates are more likely to be altered at specific faces by adsorption of polar solvents at specific sites, for example where carboxylic acid groups protrude, slowing growth by competition with oncoming ibuprofen molecules.

A study of the molecular structure at the growth interface was undertaken to determine:

1. whether it was possible that enantiomeric dimers could become incorporated in the crystal bulk, or only at the growth interface, and if so why growth was affected to different extents at the various crystal faces in non-polar solvents; and
2. potential sites for adsorption of polar solvents.

3.2.4 X-ray structure of S(+)-ibuprofen

Atomic coordinates and unit cell parameters of S(+)-ibuprofen were determined by Dr.A.A.Freer at the department of Chemistry, Glasgow University, and are listed in the appendix.

Systematic absences indicated the crystals were monoclinic, space group $P2_1$, with two ibuprofen molecules in the asymmetric unit forming an acid dimer. Full matrix least squares refinement of the data including calculated hydrogen atom positions gave final R and wR of 0.063 and 0.080. Unlike the racemic form, where the two halves of the dimer are related by inversion through a centre of symmetry, the two halves of the enantiomeric dimer have different conformations as shown in figure 3.20.

The structures of enantiomeric and racemic ibuprofen are compared in table 3.6.

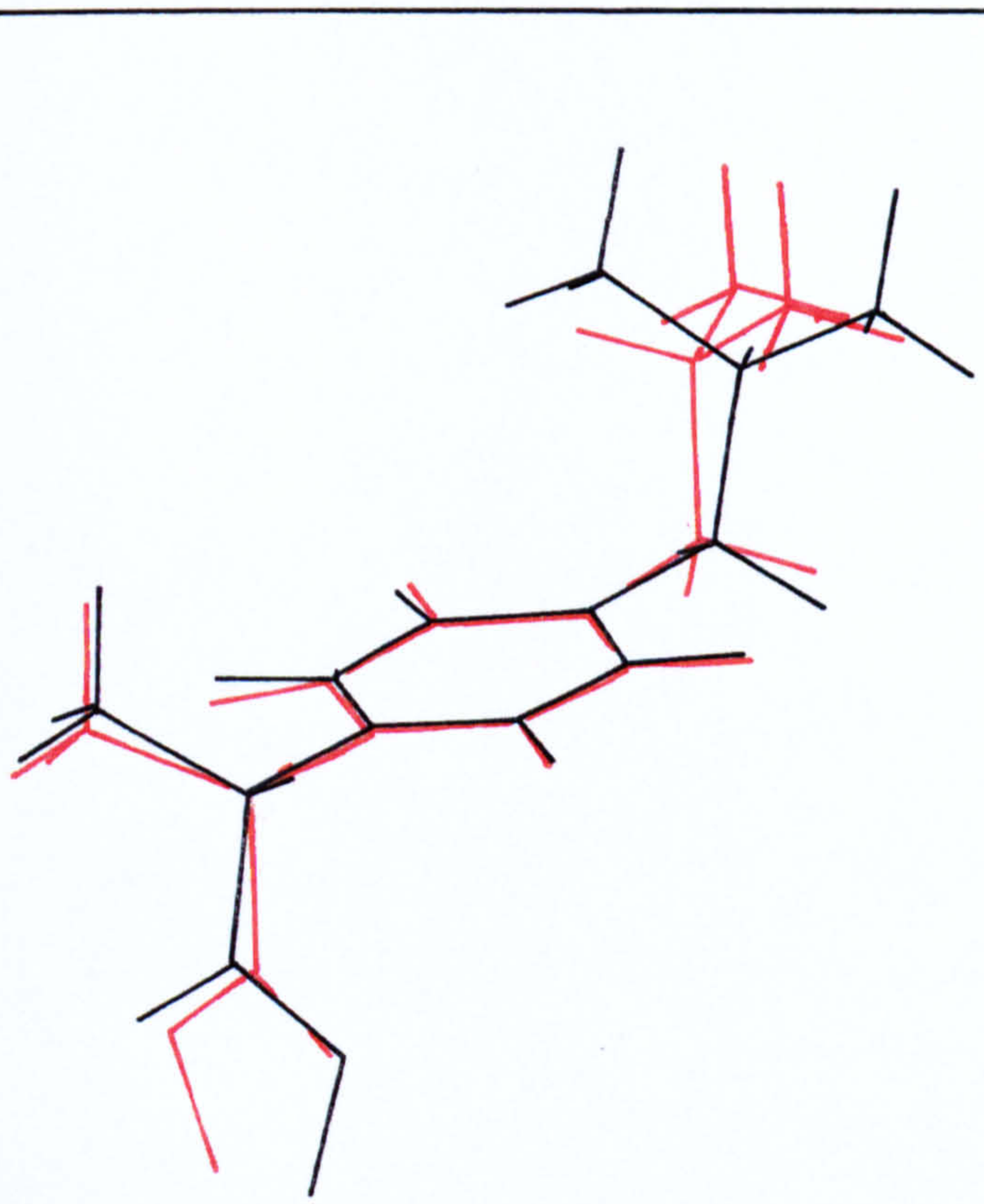

Figure 3.20: Conformations of the two parts of the asymmetric unit in the S(+)-dimer

	(±)-ibuprofen	S(+)-ibuprofen
Space group	$P2_1/c$	$P2_1$
a	14.667A	12.462A
b	7.886A	8.035A
c	10.730A	13.539A
ß	99.362°	112.890°
z	4	2(dimers)
Cell volume	1224.54	1248.80

TABLE 3.6: COMPARISON OF UNIT CELL PARAMETERS IN ENANTIOMERIC AND RACEMIC IBUPROFEN

Space groups $P2_1/c$ and $P2_1$ are amongst those most commonly seen for racemates and their enantiomers respectively [132]; 60 - 80% of racemates crystallise as $P2_1/c$, C2/c or $P\bar{1}$, with 70-90% of the corresponding optically active compounds crystallising as $P2_12_12_1$ or $P2_1$. These space groups offer the most favourable combination of compactness and symmetry. The stability of molecular crystals is directly related to both these factors, and a decrease in either leads to a decrease in stability. The optically active form of ibuprofen has both a higher unit cell volume and decreased symmetry compared to the racemic form (due to loss of a centre of

inversion between the two halves of the dimer), and so is likely to be less thermodynamically stable. This decrease in stability will combine with the nucleation difficulties observed for the enantiomeric crystals to prevent spontaneous resolution of the racemate.

The conformation of one of the molecules in the enantiomeric dimer in the solid state is identical to that of the corresponding moiety in the racemate unit as shown in figure 3.21. It should therefore be possible for this half of the enantiomeric dimer to be adsorbed onto the surface of the growing racemate crystal, leaving the other half, which has a different conformation, protruding. It therefore has the potential to act as a tailor-made additive as outlined in section 1.1.2.2, and in the following section it will be determined which crystal faces if any, could be affected by this.

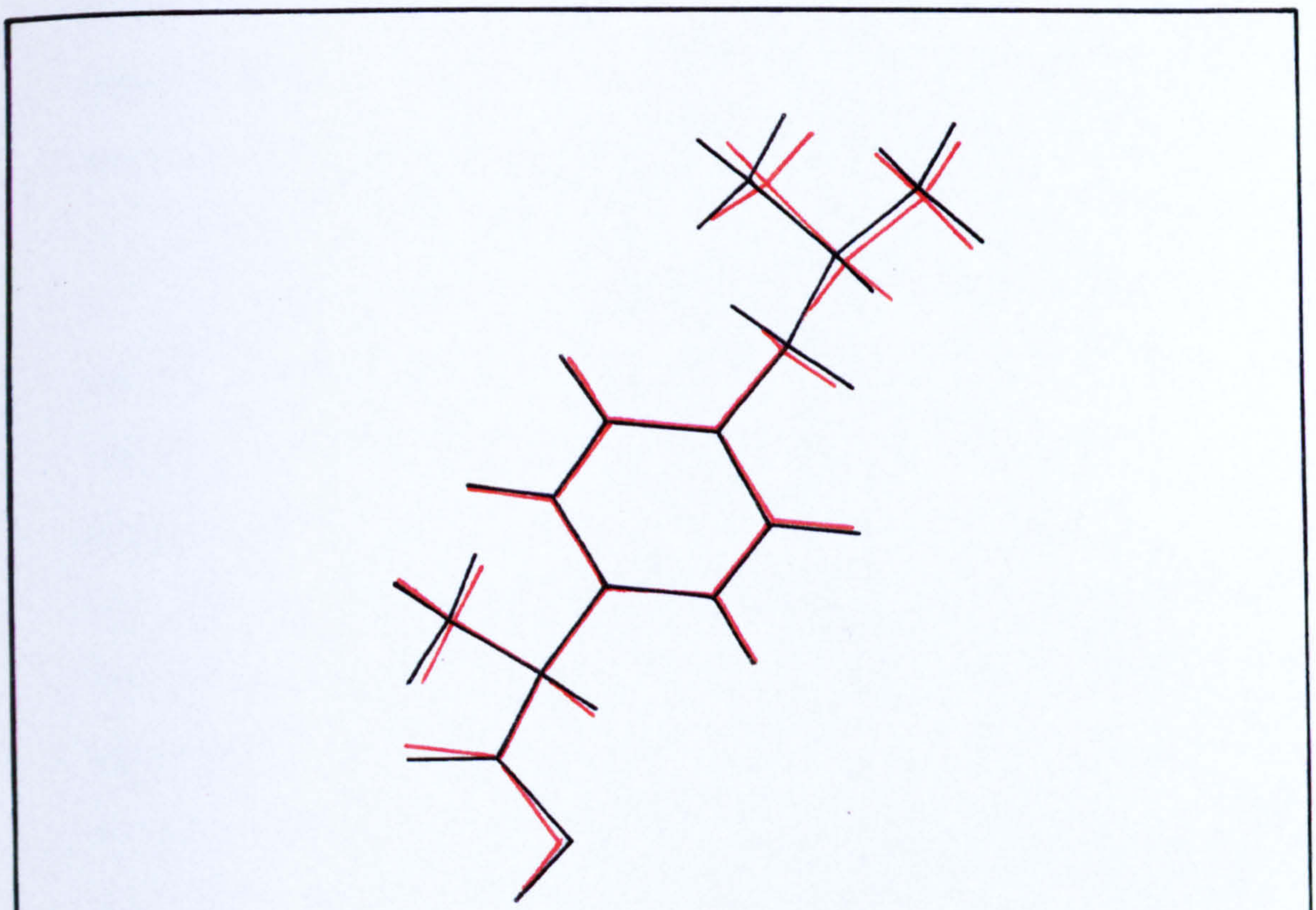

Figure 3.21: Comparison of the conformations of S(+)- and (±)-ibuprofen

3.2.5 Identification of potential adsorption sites

Molecular structures at each growth face of ibuprofen were studied in order to determine potential sites of interaction for hydrogen-bonding solvents or enantiomeric dimers. Diagrams of the surface structures were all constructed using the INTERCHEM [112] package.

The aims of this study were to determine

1. why the dominant face was {001} rather than {100} as calculated when ibuprofen was grown from non-polar solvent, or solvents with low hydrogen-bonding potential;
2. why solvents of higher hydrogen-bonding potential did not interact at the {001} surface, or whether they were able to bind more strongly to {100} than other solvents such that it remained the dominant face; and,
3. the nature of the solvent interactions causing a decrease in the growth rate in the [010] direction in solvents as hydrogen-bonding potential increased.

The actions of hydrogen-bonding solvents will be discussed first, followed by a study of the crystal growth mechanism in non-polar solvents.

3.2.5.1 Solvent interactions at the {100} face

The {100} face of ibuprofen can be either polar or non-polar as successive molecular layers are laid down. Figure 3.22 shows a cross section through the surface in which this is clearly illustrated. The surface alternates between a polar form, with carboxylic acid groups projecting directly from the surface, and a non-polar form consisting of the hydrocarbon portions of the ibuprofen molecules. Interactions between the hydrocarbon groups of adjacent layers are very weak (as confirmed by the low value of the attachment energy calculated in section 3.2.1), and there are no periodic bond chains (PBC's) promoting crystal growth in this direction.

Hydrogen bonding solvent molecules can interact with the carboxylic acid groups protruding from the polar surfaces, with no geometrical restrictions apparent. The growth surfaces are in fact relatively flat. Since adsorption of solvent is not interrupting a PBC it is not likely to have a major effect on growth rate: growth rate, however, is probably dependent on the interaction at the non-polar surface, which could be described as a rate limiting step.

Solvent interaction at the {100} surface should only cause a significant change in growth rate if the solvent can hydrogen bond very strongly to the polar surface (when difficult displacement of solvent could

switch the rate determining step to the polar surface variant). Of the solvents investigated, this is only likely to occur with methanol and ethanol which have the highest hydrogen bonding capacities.

3.2.5.2 Solvent interactions at the {001} face

In comparison with the almost flat {100} faces, the {001} faces consist of ridged layers of ibuprofen dimers lying parallel to the surface. The polar carboxylic acid groups in this case lie in the bottom of a shallow concavity.

Interactions between {001} layers are relatively low (see section 3.2.1). The major contributing factor appears to be electrostatic interactions between carboxylic acid dimers in adjacent layers. The most likely site for solvents to adsorb is therefore as a substitute for an ibuprofen molecule, that is, bound to the carboxylic acid group, and held in place by electrostatic interactions with the layer below.

Steric factors must also be considered at the {001} face due to the shape of the binding site. Figure 3.22 shows a side view of this, and figure 3.23 a view looking directly down onto the binding site. Consider molecule B being incorporated into the new growth layer: it will first have to displace any polar solvent which has solvated molecule A. As this is at the bottom of the hollow, surrounded by other molecules, steric restrictions will make displacement of the solvent difficult.

Ibuprofen dimers lie parallel to the surface on the {001} growth faces, so lateral growth of the surface layers is likely to be suppressed, since the presence of

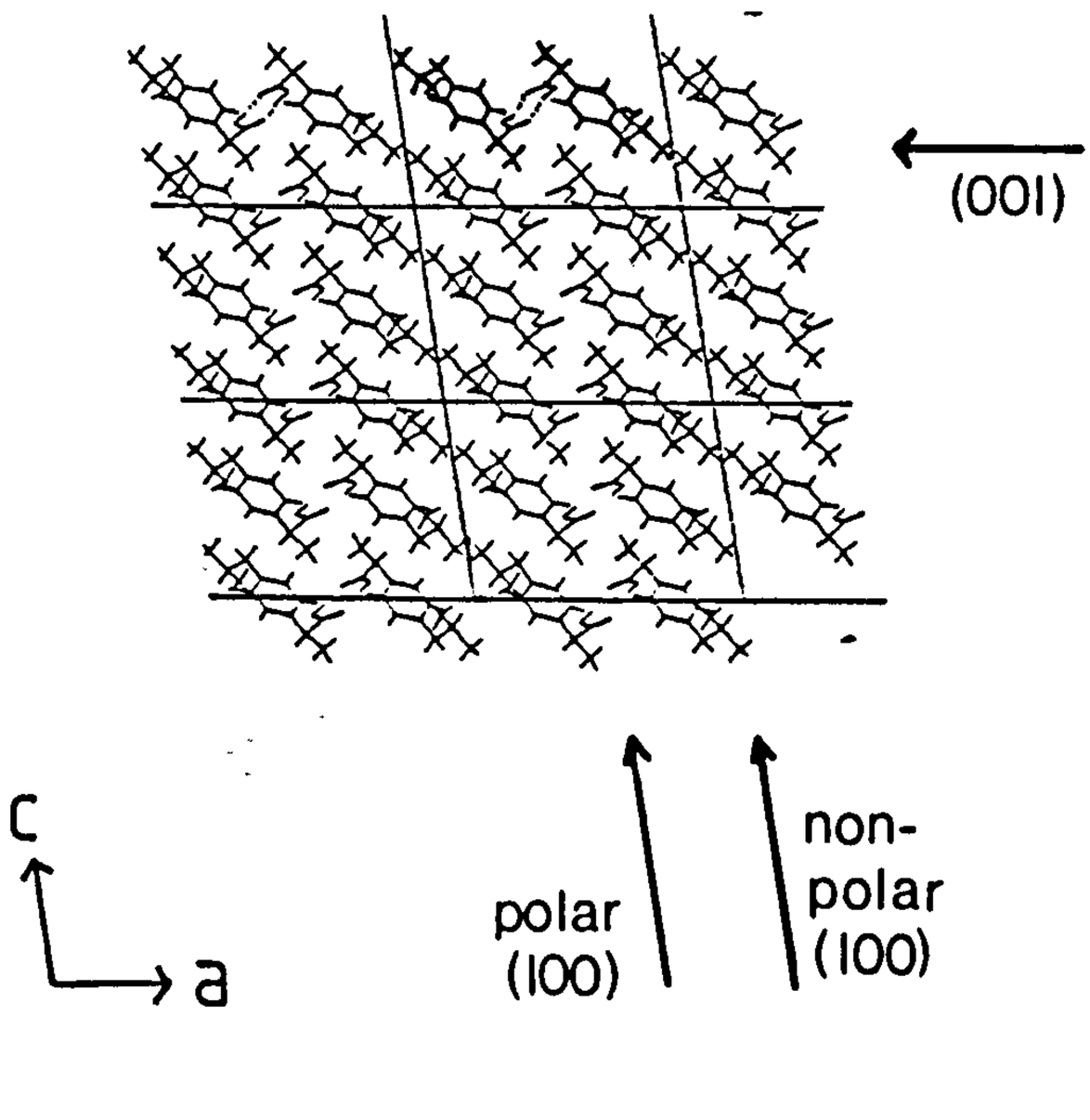

Figure 3.22: Cross section through ibuprofen crystal structure along (010) plane showing surface structures of (100) and (001) growth forms

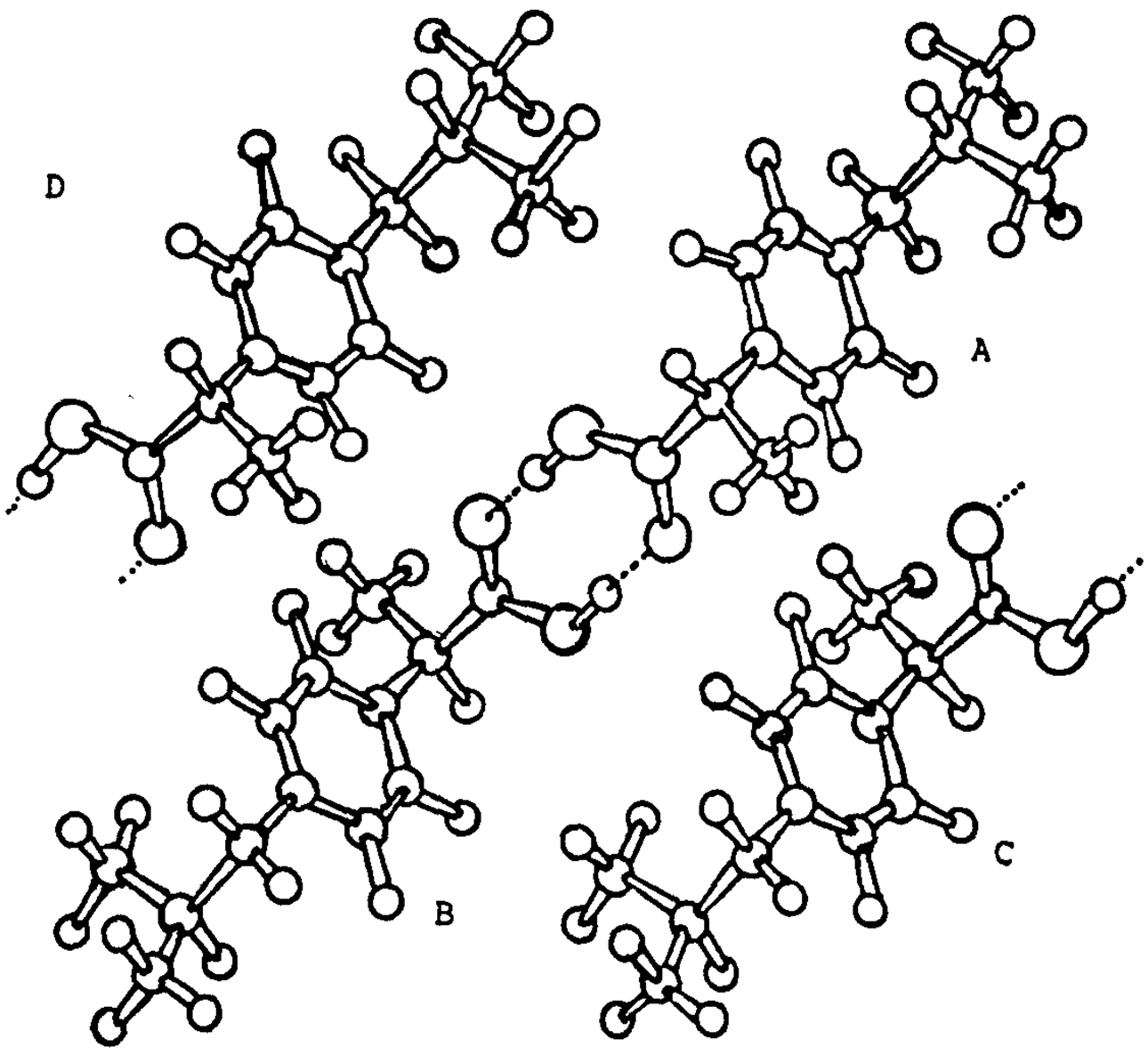

Figure 3.23: Binding site for ibuprofen dimer on (001) face

adsorbed solvent in the binding site will also disrupt the weak lateral interactions between dimers. The appearance of small, additional {102} faces in crystals grown carefully from polar solvents may be explained by this mechanism. The presence of adsorbed solvent molecules would also block electrostatic interactions between layers, which would also act to decrease growth, particularly if any bulky side groups were left protruding from the surface. Solvents which are too bulky will however be prevented by steric restrictions from gaining access to the binding site.

3.2.5.3 Growth in the [010] direction

Theoretical models predict rate of growth in the [010] direction to be fastest (see section 3.2.1): {010} faces have not been observed due to their fast growth rate. Strong PBC's associated with the carboxylic acid groupings along the [010] direction contribute to the high growth rate, but make it more vulnerable to the effects of solvent interaction. Both $\{1\bar{1}0\}$ and $\{1\bar{1}1\}$ growth forms at the ends of the b axis have carboxylic acid groupings protruding from their surfaces. The structure of the $\{1\bar{1}0\}$ face is illustrated in figure 3.24 (that of $\{1\bar{1}1\}$ is similar but lies at a slightly different angle to the plane of the paper).

Interaction of solvent with the carboxylic acid groups is therefore not sterically restricted, and solvent molecules will be able to exchange with surface groupings in the same way as the monomers in solution. Disruption of the PBC's leads to growth rates for this face being more significantly affected than for the {100} face where the growth rate determining step was not altered by the interaction.

Solvents which can bind most strongly to carboxylic acid groups will therefore have the greatest effect at this surface - resulting in the greatest decrease in growth along the b axis.

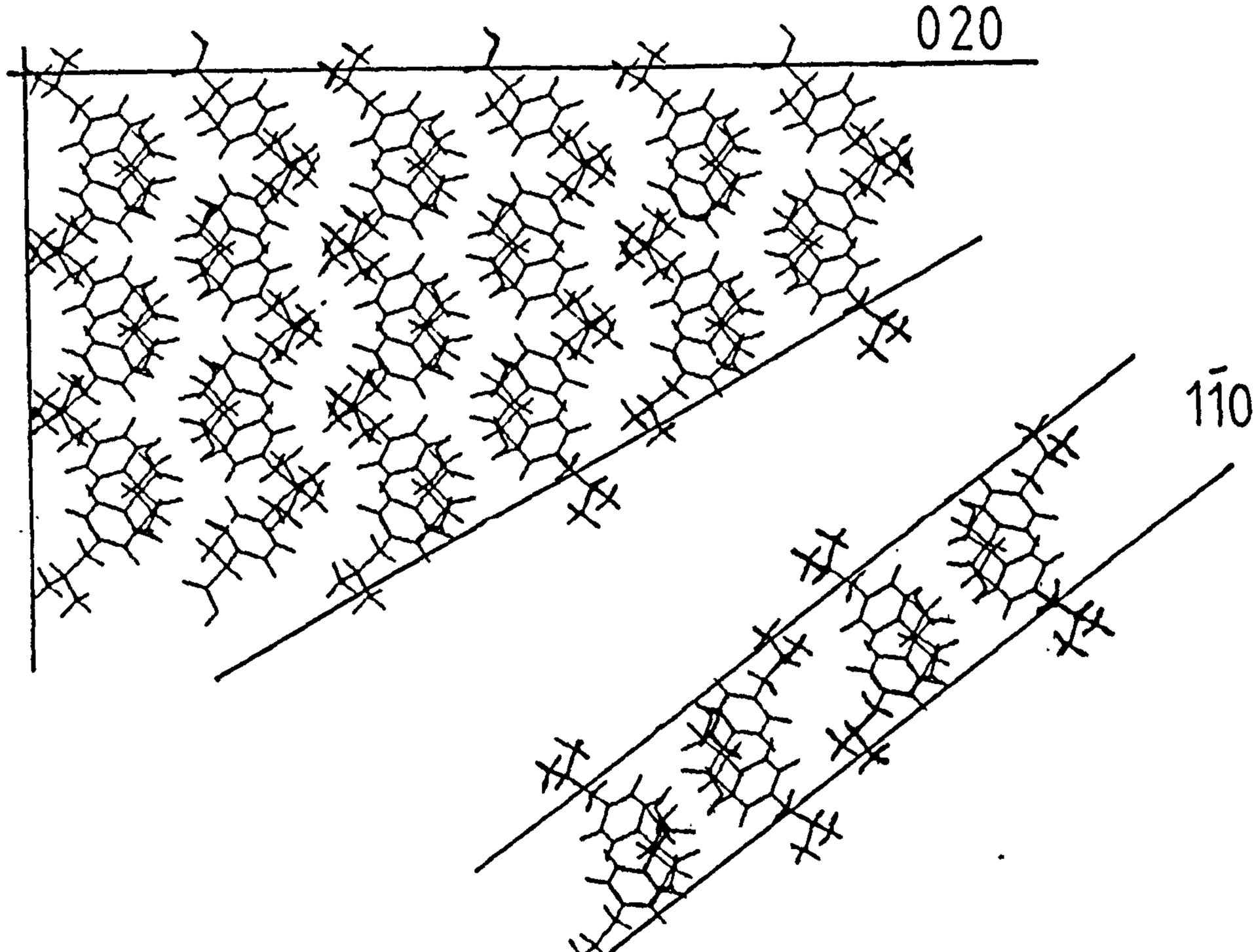

Figure 3.24: Surface structure of the (1$\bar{1}$0) face of ibuprofen

3.2.5.4 General assessment of growth in hydrogen bonding solvents

Plots of relative growth rates in the [010] and [100] directions against the hydrogen bonding capacity of the solvent (see figures 3.10 and 3.13 respectively) indicate that the proposed mechanism for solvent-induced growth inhibition along the b axis is possible. Hydrogen-bonding also appears to be a factor in the decreased growth rates observed at the {001} habit face. Steric factors may enhance the solvent effect by making bound solvent more difficult to displace than at the ends of the b axis.

Methanol and ethanol would also be expected to bind at the {001} surface, being small molecules of high polarity. However ibuprofen crystals grown from these solvents had dominant {100} faces as predicted by the theoretical calculations. This apparent anomaly can also be explained by their hydrogen bonding capacity; they appear to be capable of binding to the polar variant of the {100} faces strongly enough that the rate determining step was changed. {100} faces have carboxylic acid groups projecting directly from the surface, and a greater number are therefore available as binding sites when compared with the $\{1\bar{1}0\}$ and $\{\bar{1}\bar{1}1\}$ faces.

PAGE NUMBERING AS ORIGINAL

3.2.5.5 General assessment of growth in non-polar solvents

Hexane and toluene have negligible hydrogen bonding potential and are therefore unlikely to affect crystal growth rates by any of the preceding proposed mechanisms. An alternative mechanism must be found to explain their ability to reduce the rate of growth selectively at the {001} crystal faces.

Proton NMR confirmed that ibuprofen exists as hydrogen-bonded acid dimers in solution in non-polar solvents; these are likely to be the growth units when ibuprofen is crystallised from non-polar solvents since it is energetically unstable for ibuprofen to exist as monomers (no change was seen in the position and shape of the peak associated with the hydroxyl hydrogen even at 25% of saturation concentration, indicating lability of the dimers to be low). Since the crystallisation rate is also dependent on the time taken for molecules to attain the correct orientation for incorporation into the growth layer [20], growth of faces where a large surface area of the dimer has to be orientated correctly will be slowed, particularly in comparison with the equivalent face on crystals grown from polar solvents. In particular this is likely to affect {001} faces to the greatest extent, where the dimer lies parallel to the surface.

{001} faces are indeed the only faces affected to any extent in non-polar solvents, which are unlikely to adsorb onto polar surfaces. However, as suggested in section 3.2.3, enantiomeric dimers present in non-polar solutions may act as growth inhibitors at faces where they can be adsorbed.

It was demonstrated that one half of the enantiomeric dimer takes up the same conformation in the crystal structure as the racemic form. It could therefore become incorporated at the growing crystal surface. Reversal of conformation at the chiral carbon of the other half of the enantiomeric dimer, compared to that of the racemate, would cause significant distortion if incorporated into the surface of the growing racemic crystal. Replacement for example of molecule B in figure 3.23 with one of the opposite conformation would cause increased repulsive interactions with surrounding molecules.

Figure 3.25 shows a new growth layer approaching the {001} crystal face. One of the molecules has been replaced by a molecule of the opposite chiral conformation; it can be seen how it can be relatively easily incorporated into the layer, but that the altered part of the molecule would cause steric interactions with an oncoming layer. The dimer is held in place by electrostatic interactions with the layer below and so would be difficult for solvents or a racemic dimer to displace.

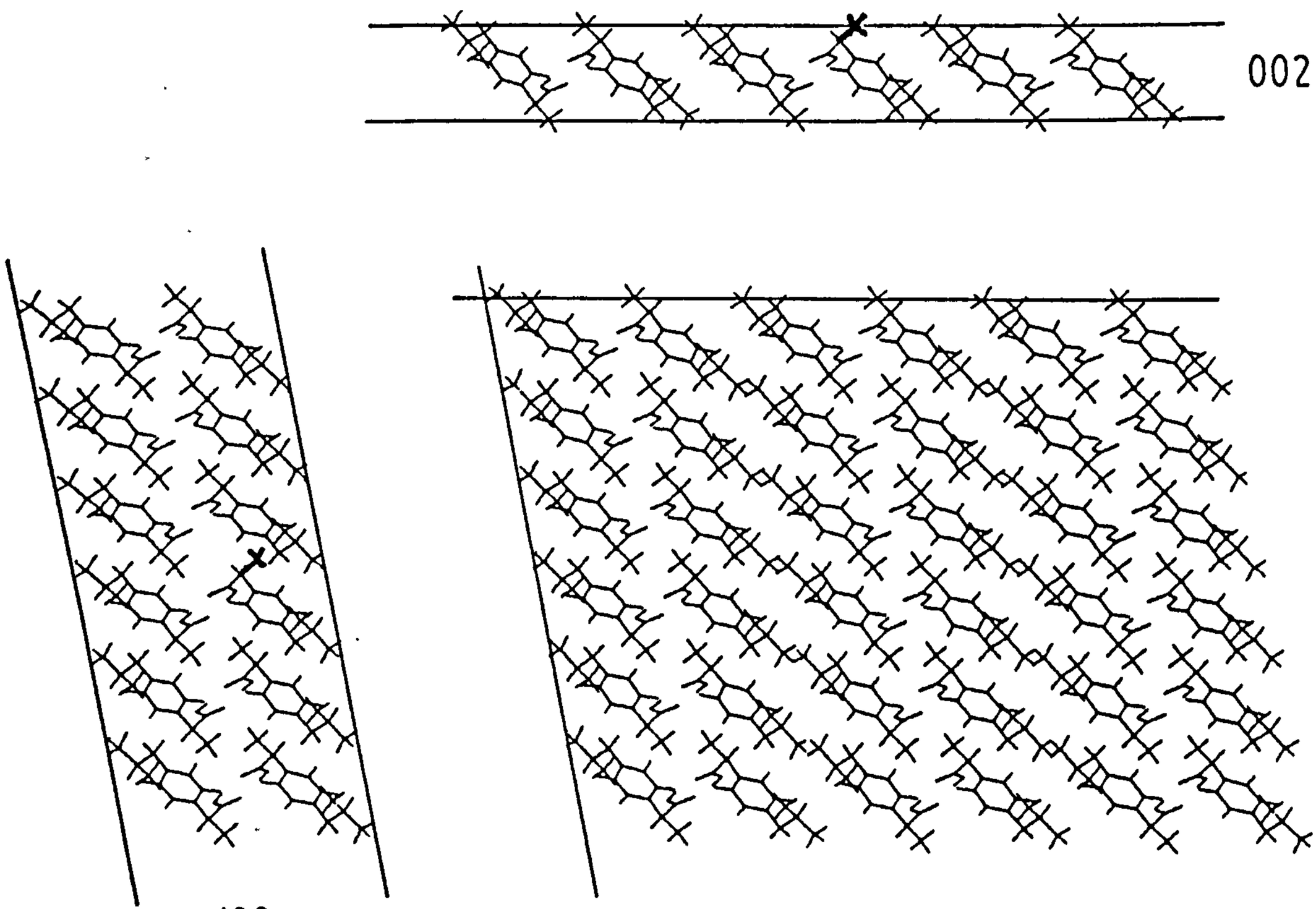

Figure 3.25: Surface structures of the (100) and (001) faces with S(+)-ibuprofen dimer incorporated

Some incorporation of the enantiomeric dimer into the bulk crystal may occur. Comparison of the crystal structures of the racemic and enantiomeric forms in section 3.2.4 showed an increased unit cell volume for the enantiomeric form. Incorporation of enantiomeric dimers into the racemic crystal would therefore cause some distortion of the crystal lattice. Lattice strain has been shown to inhibit growth in some inorganic materials [30,133], and the same effect may reinforce the "additive" effect in this system, since it is likely that ordered growth would be more difficult at a strained surface compared to an unstrained one. Topographs of solvent-grown crystals showed greatest strain in {001} growth sectors, thus it seems likely that some incorporation of enantiomeric dimers may be taking place. {001} growth sectors in acetonitrile grown crystals were less strained, suggesting adsorption of enantiomeric dimers may still be taking place, but that increased lability of the ibuprofen monomers in polar solvents makes incorporation less likely.

Other growing crystal faces are not affected to the same extent by adsorption of the enantiomeric dimers (and those growth sectors therefore showed less distortion in x-ray topographs) since generally a smaller area of the dimer is in contact with the crystal surface, and the dimer units will therefore be more labile. Binding at the {001} surface is also stronger than at most others, and it is more difficult for the

"incorrect" dimers to be displaced from the {001} surface due to their position in a trough as described previously. Steric factors may also prevent incorporation of the enantiomeric dimers into other growth layers. The surface structure of each growth form was studied in order to determine why they were less affected by the proposed "additive" mechanism.

<u>{100}</u>

The altered chiral part of the molecule (shown in red in figure 3.25 is oriented towards the interior of the growth slice. This sets up additional steric repulsive interactions making incorporation unlikely. Since interactions between {100} planes are weak hydrocarbon interactions, adsorbed additive molecules are more labile than at {001} and would readily desorb.

<u>{0$\bar{1}$1}</u>

Steric repulsive interactions due to the presence of the modified portion of the dimer inside the growth slice again would prevent incorporation of the enantiomeric dimer into the growth slice as illustrated in figure 3.26.

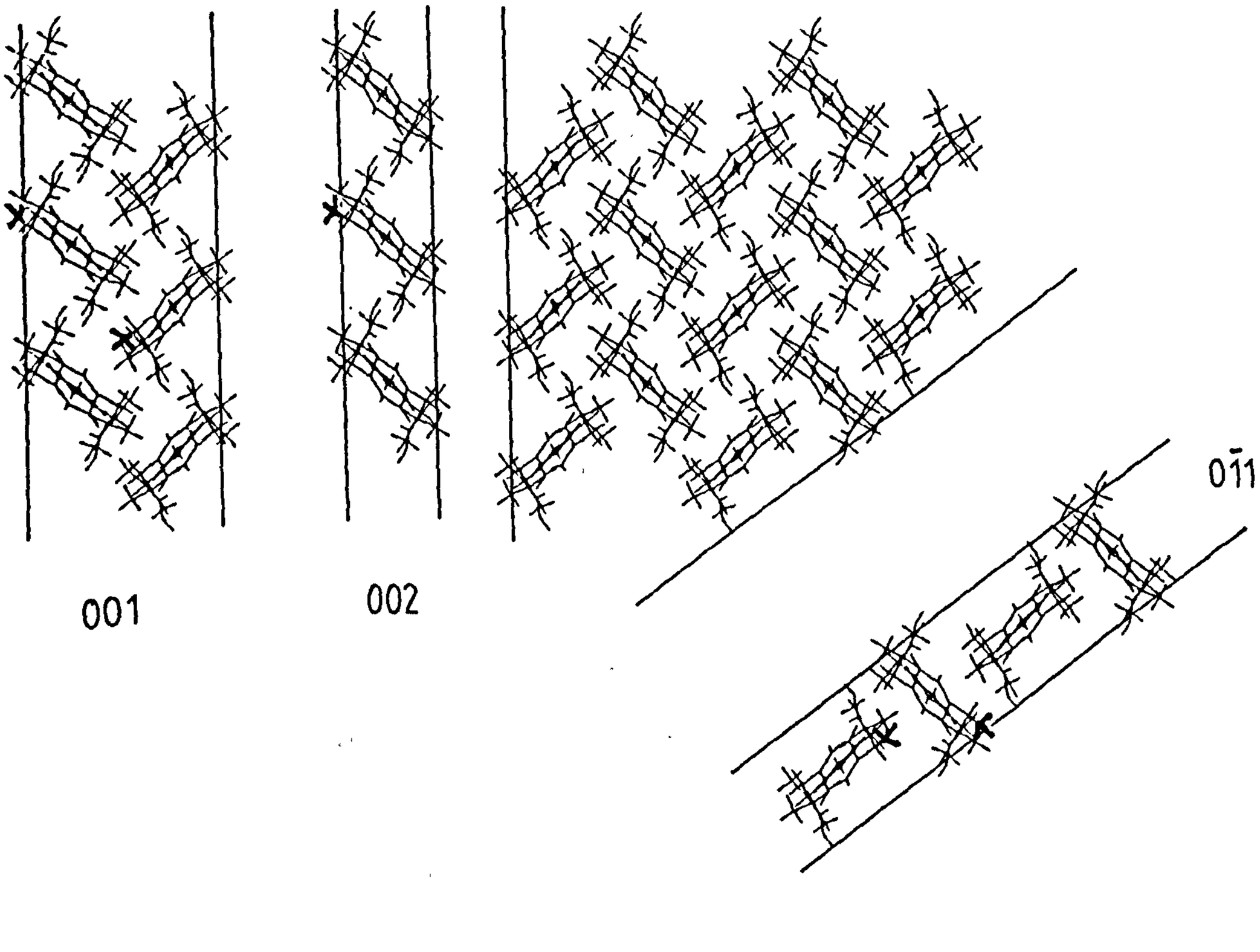

Figure 3.26: Surface structure of the $(0\bar{1}1)$ face with S(+)-ibuprofen dimer incorporated

{1$\bar{1}$0}

Similar steric interactions are set up by the additive as in the {0$\bar{1}$1) growth slice (see figure 3.27).

{102}

The altered part of the molecule is in this instance pointing directly out of the growth slice, as illustrated in figure 3.28, allowing it to be incorporated at the growth interface, but would block oncoming layers. {102} faces occurred more frequently in crystals grown from hexane by solvent evaporation than from other more polar solvents.

{10$\bar{2}$}

Similar to {102}, but the chiral methyl group is oriented more into the slice, therefore the dimer is less likely to be adsorbed at this face (figure 3.28).

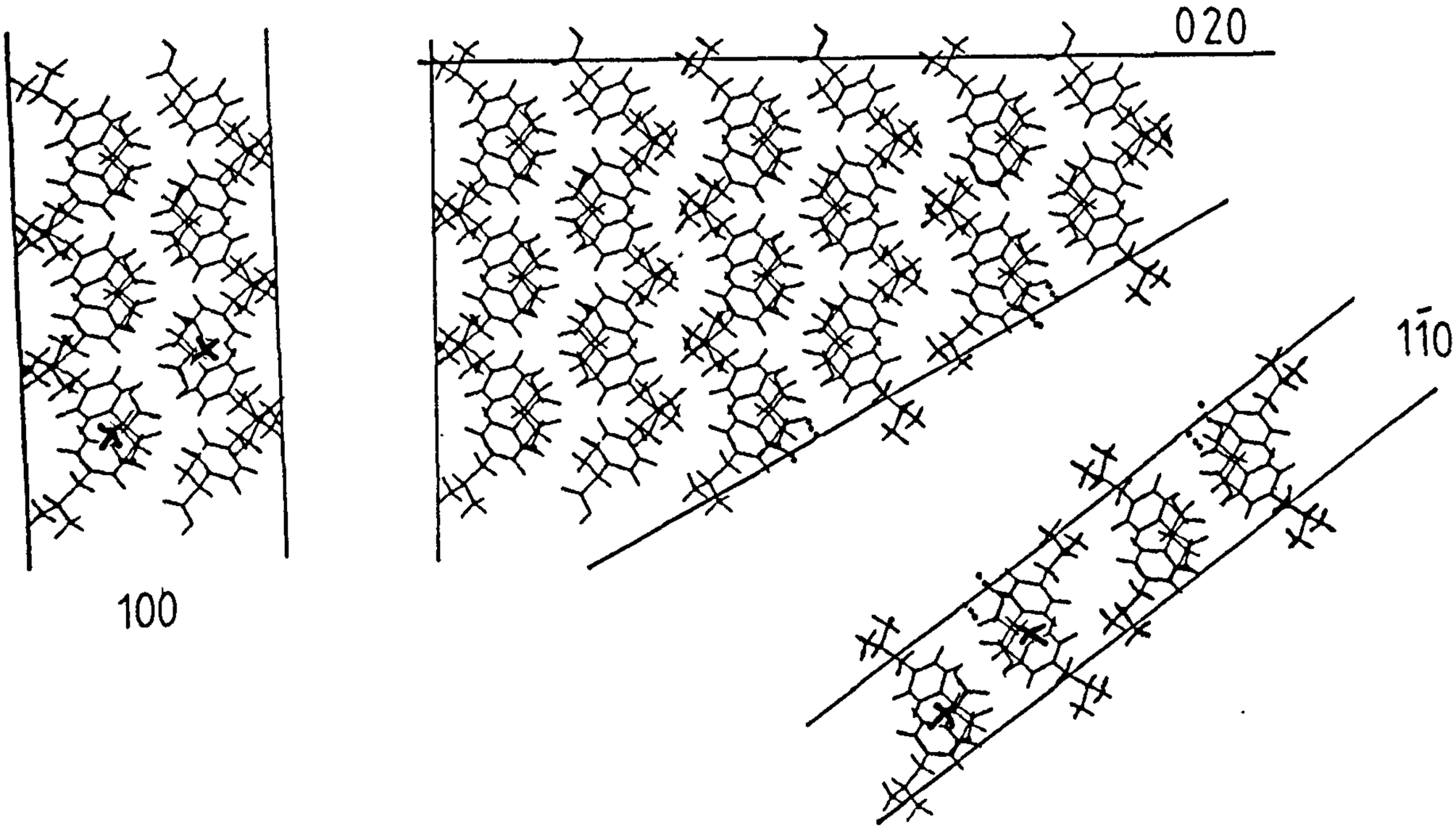

Figure 3.27: Surface structure of the (1$\bar{1}$0) face with S(+)-ibuprofen dimer incorporated

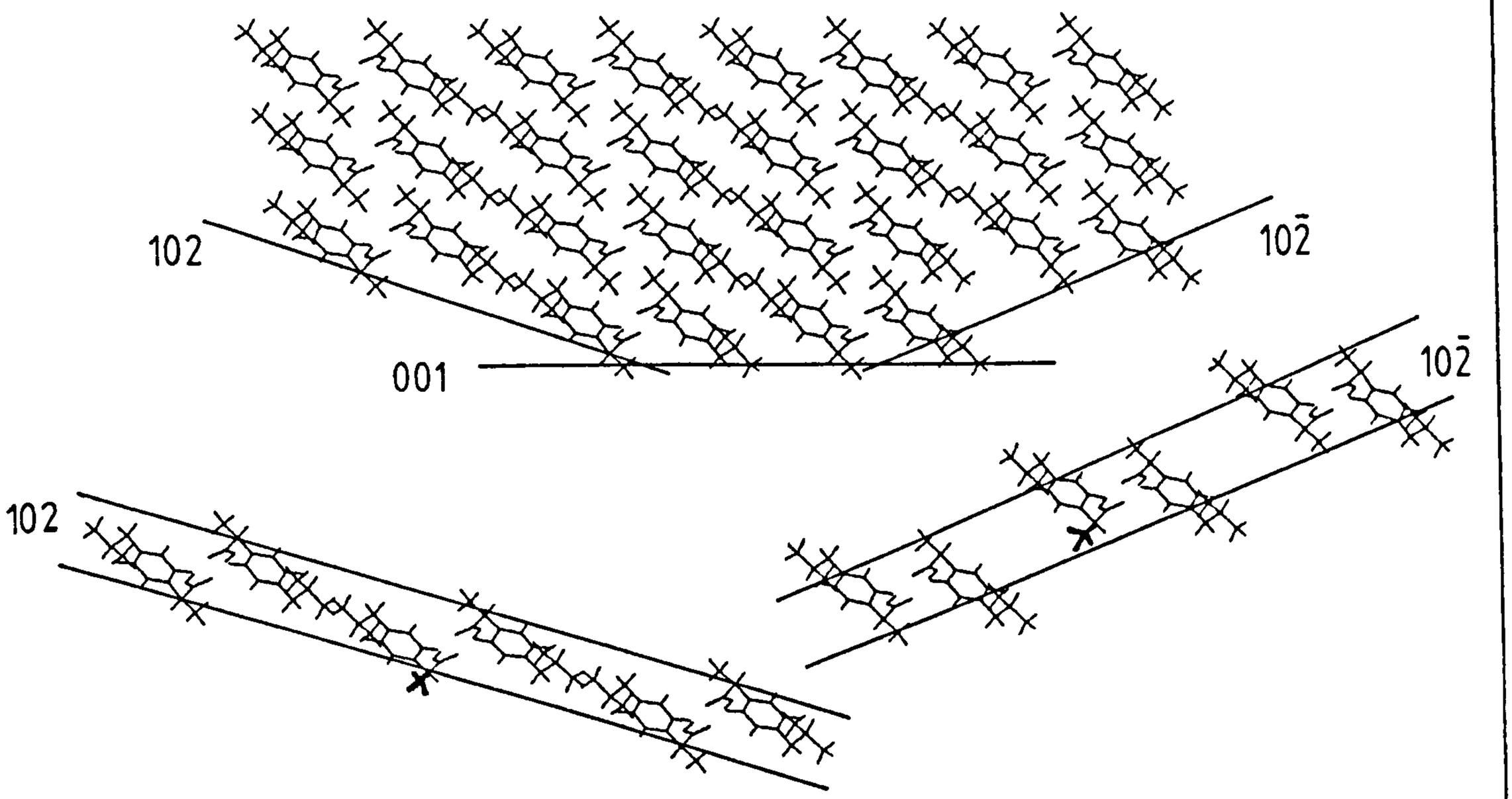

Figure 3.28: Surface structures of the (102) and (10$\bar{2}$) faces with S(+)-ibuprofen dimer incorporated

3.2.5.6 Summary

Two separate mechanisms are proposed for morphological modifications resulting from growth of ibuprofen from polar hydrogen bonding and non-polar solvents:-

Interactions with more polar solvents appear to be predominantly due to a hydrogen bonding effect, with steric factors also contributing at {001} surfaces.

Non-polar solvents appear to reduce the rate of growth at the {001} face due to the presence of enantiomeric dimers in solution adsorbing preferentially at this surface. This may be the source of the additional lattice strain observed in ibuprofen crystals grown from a non-polar solvent, resulting in increased dissolution rates and mosaic spread. Incorporation of enantiomeric dimers into the crystal lattice, appears to be the likely cause, and the increased time taken for dimers to orientate at the growth interface, and/or exchange with the correct dimers if necessary may also contribute. Growth of good quality crystals from hexane solution is more difficult than from polar solvents, requiring slower cooling rates, possibly due to the longer time taken for the above processes, although this is difficult to compare when growth conditions are different.

3.3 ASSESSMENT OF PLASTICITY AND FRACTURE PROPERTIES OF IBUPROFEN CRYSTALS USING MICROINDENTATION TECHNIQUES

In section 1.4.4 the effect of the crystal deformation mechanism on compactibility was discussed. Plastic deformation (or slip) occurs only on specific slip planes within the crystal structure. Microscopic observations of crystal surfaces indented with the Knoop indenter provided information on the active slip systems and on the fracture behaviour of ibuprofen. Crystal hardness measurements were also performed using Knoop microindentation testing. Effective Resolved Shear Stress (ERSS) calculations were then performed to analyse hardness results.

3.3.1 Identification of Potential Slip Systems and Cleavage Planes from Crystal Structure Analysis

As described in section 2.6.2.1, potential slip systems can be identified on the basis of large interplanar spacings (d_{hkl}) and small Burgers vector ($\underline{b}$), provided there is no impediment to slip. The planes with highest d_{hkl} values were previously determined in section 3.2.1 using the program MORANG to identify likely growth forms. In table 3.7, potential slip systems are identified on the basis of d_{hkl} values and molecular overlap between layers.

{hkl}	d_{hkl} (Å)	Comments
100	14.472	Relatively planar surface (see figure 3.18) coupled with high d_{hkl} and low intermolecular interactions combine to make this the cleavage plane.
001	10.587	d_{hkl} quite high, and E_{att} relatively low. However, the surface is ridged (figure 3.22) and will restrict slip to particular directions. Also a potential cleavage plane.
$1\bar{1}0$	6.925	Hydrogen bonding present between planes and molecular overlap will prevent slip (figure 3.27).
$01\bar{1}$	6.324	Hydrogen bonding also present between layers, but overlap less than for {110} planes therefore restricted movement possible (figure 3.26).
$11\bar{1}$	5.599	Similar to $\{1\bar{1}0\}$ - a lot of overlap between layers therefore slip unlikely.
$\bar{1}\bar{1}1$	5.601	as above
$10\bar{2}$	5.567	Not affected by hydrogen bonding; movement relatively unaffected by molecular overlap (figure 3.28).
102	4.731	as above
$2\bar{1}0$	5.330	Molecular overlap prevents slip as for $\{1\bar{1}0\}$.
020	3.943	Strongly hydrogen-bonded, and high degree of overlap, but slip potentially possible in some directions (figure 3.27).

TABLE 3.7: IDENTIFICATION OF POTENTIAL SLIP PLANES

Burgers vectors were then calculated for potential slip

directions lying in the slip plane and are given in table 3.8.

Slip plane	$\underline{b}$ [uvw]	|b| (Å)	Comment
100	010	7.886	
	001	10.730	Not obstructed
	011	13.316	or hydrogen
	$01\bar{1}$	13.316	bonded
001	100	14.667	
	010	7.886	Not obstructed
	110	16.653	or hydrogen
	$1\bar{1}0$	16.653	bonded
$01\bar{1}$	100	14.667	Hydrogen bonds must be broken.
	011	N/A	Molecular obstructions present.
$10\bar{2}$	010	7.886	No bonds or obstruction.
	$20\bar{1}$	29.50	Too high to be likely.
102	010	7.886	No bonds or obstruction.
	$20\bar{1}$	29.50	Too high to be likely.
020	100	14.667	No bonds or obstruction.
	001	N/A	
	101	N/A	Molecular
	$10\bar{1}$	N/A	obstruction.

TABLE 3.8: BURGERS VECTORS FOR POSSIBLE SLIP DIRECTIONS

The slip system activated is also dependent on the

plane of indentation, and the indenter angle. For instance, slip on particular systems is easiest to activate when the long axis of the indenter is parallel to the planes on which slip occurs. The slip systems listed above, can however be used as a guide to the possible sources of slip traces observed around indentations.

3.3.2 Microscopic Observations of Structural Changes around Knoop Indentations

Observation of the cracks and dislocation traces around indentations was performed to obtain information regarding the actual cleavage and slip planes respectively. Changes in the slip traces with indenter angle were looked for as these may have indicated a change from one slip system to another.

3.3.2.1 {001} face

Examination of the crystal surface around indentations on the {001} crystal faces predominantly showed cracking along [010], as shown on plate 3.13. This seemed to be due to cleavage on the {100} planes, since their intersection with the {001} surface lies along the same direction. Occasionally, thermal etching revealed additional slip traces in the same direction, although the presence of cracks tended to conceal this.

Plate 3.13: Knoop indentation on the (001) face showing cracking along [010].

(Sample unetched)

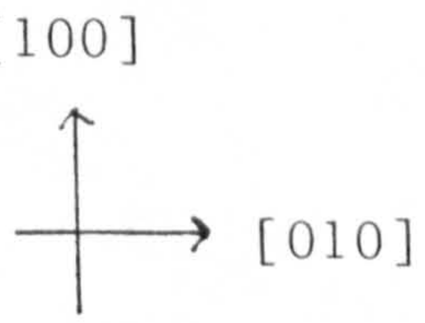

although the presence of cracks tended to conceal this. An example of the observed slip traces is shown in the lower left hand side of the indentation in plate 3.14; the cracks on the right were present before thermal etching, traces on the left appeared after etching.

Additional, shorter slip traces were observed along [100] when the long axis of the indenter was approximately 30° from [010]. Some indication of this can be seen in plate 3.14, and more clearly in plate 3.15. Slip on either {020} or $\{01\bar{1}\}$ planes could generate traces at this orientation.

{001} samples, allowed to etch thermally, also exhibited further development of cracks along [010], not always directly attached to an indentation, which occurred over time. Plate 3.16 shows an indentation after storage at 30°C for fourteen days, in which these slower developing cracks can be observed. This slow stress relaxation may be the source of the strain recovery (expansion) of ibuprofen compacts observed on storage [5] and may be due to time-dependent resolution of elastic stresses introduced during indentation, or further dislocation movement e.g. release of piled up dislocations.

3.3.2.2 {100} face

The predominant direction of slip traces or cracks after indentation of {100} samples was also [010], as

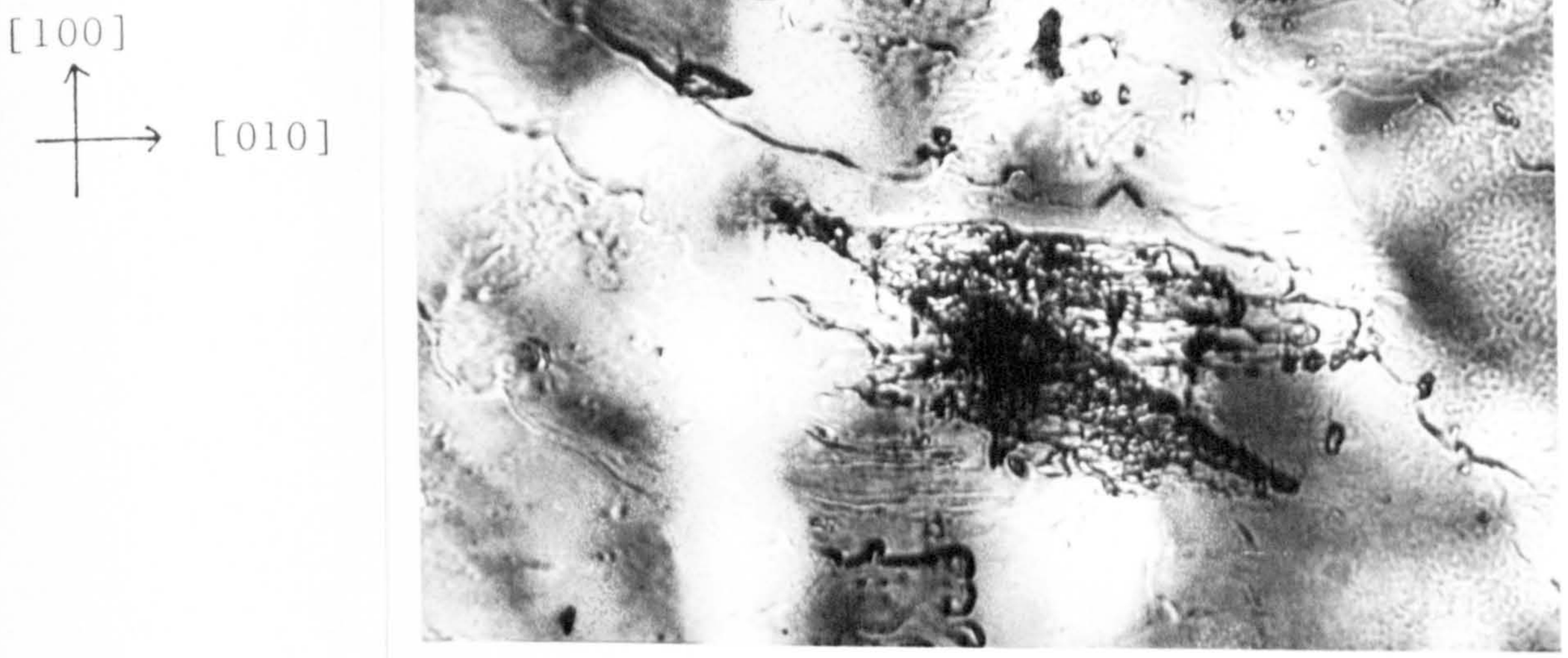

Plate 3.14: Knoop indentation on the (001) face showing cracking along [010], and etched slip traces at the same orientation. Shorter cracks also observed along [100]. (Sample thermally etched).

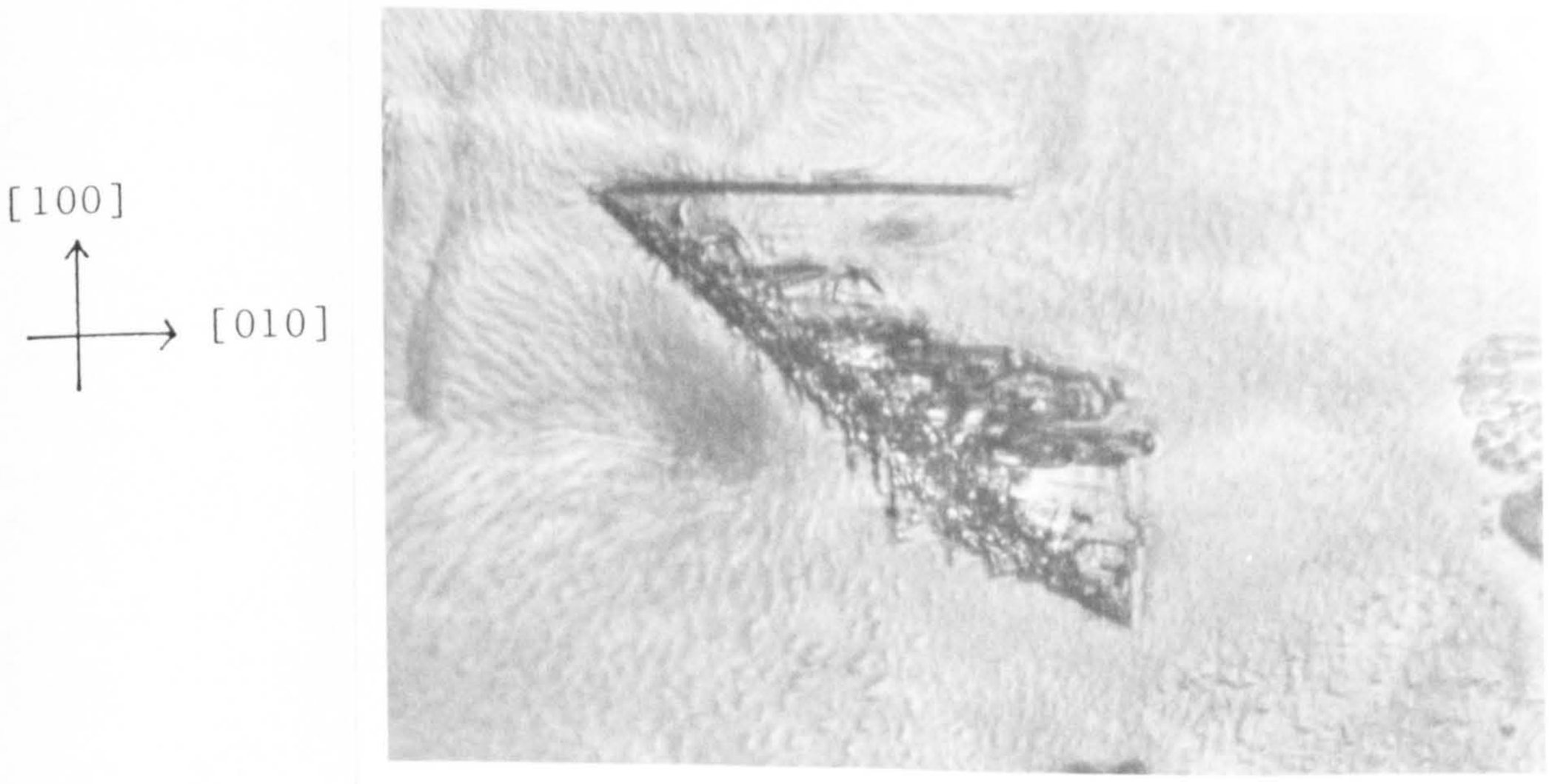

Plate 3.15: Knoop indentation on the (001) face showing slip traces along [010]. Slip traces along [100] appeared after thermal etching for 30 days.

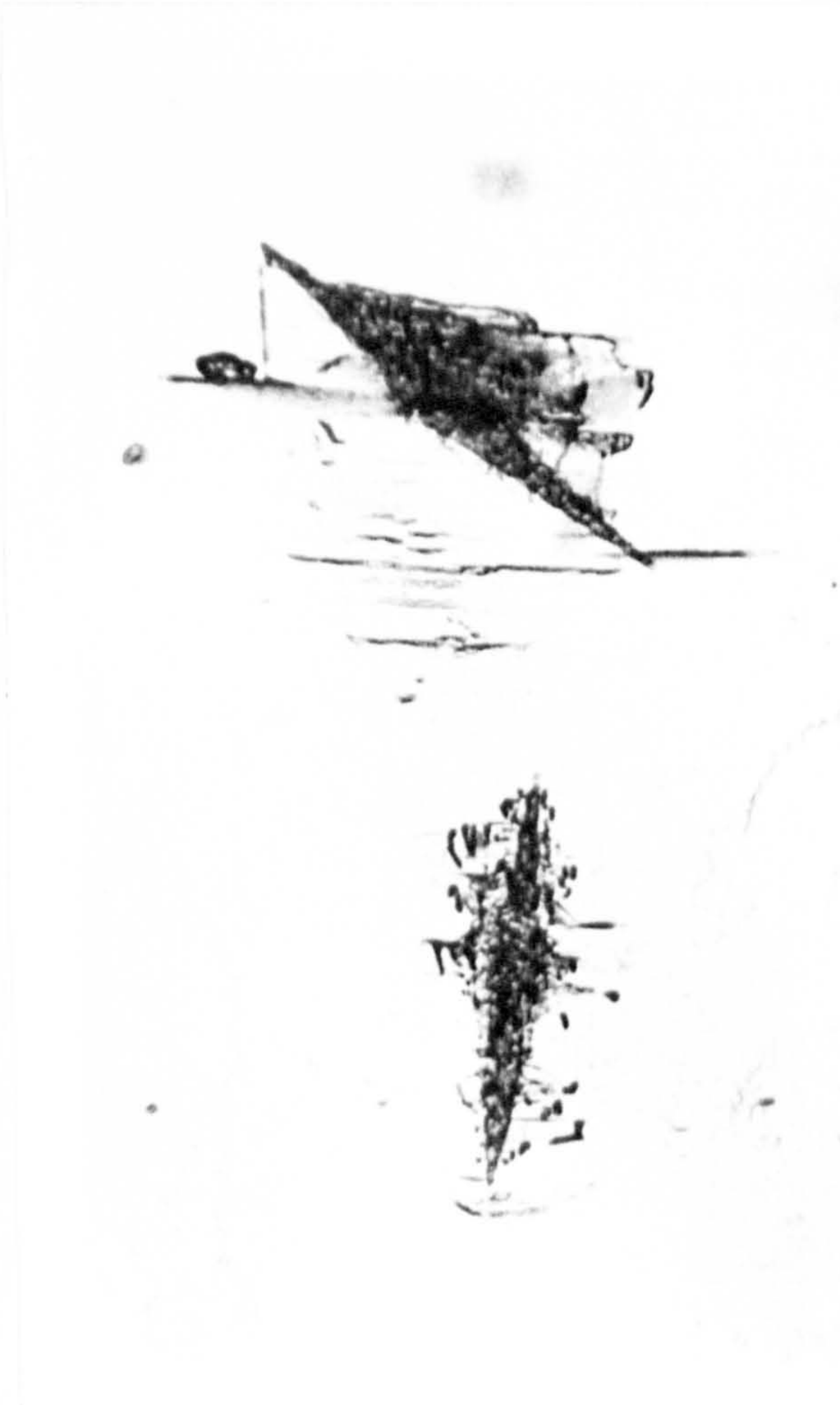

Plate 3.16: Knoop indentation on the (001) face showing cracking produced by relaxation of residual stresses.

(Sample stored and thermally etched for 14 days).

[100]

[010]

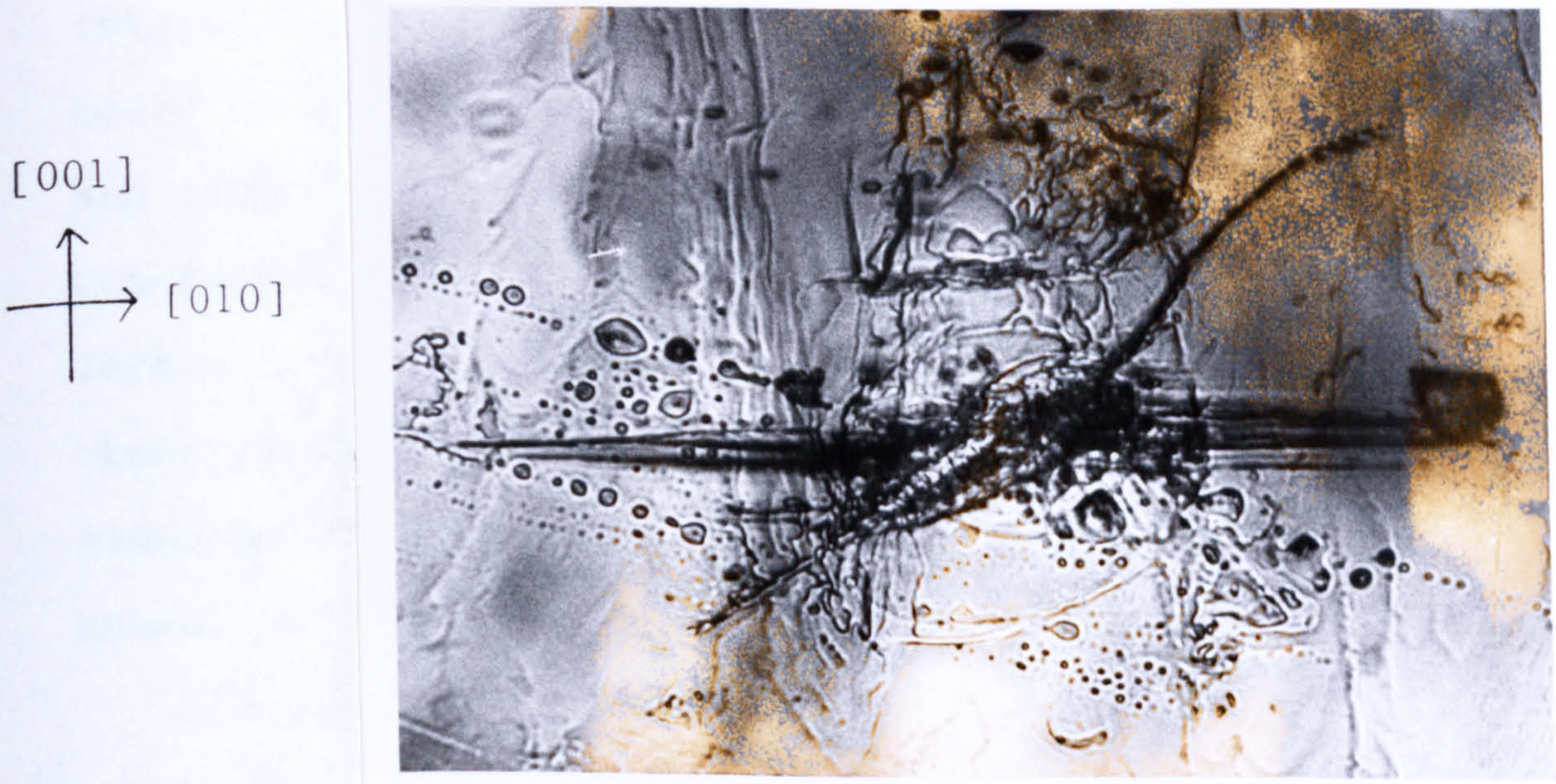

Plate 3.17: Knoop indentation on the (100) face showing slip traces along [010]

(Sample photographed immediately after indentation).

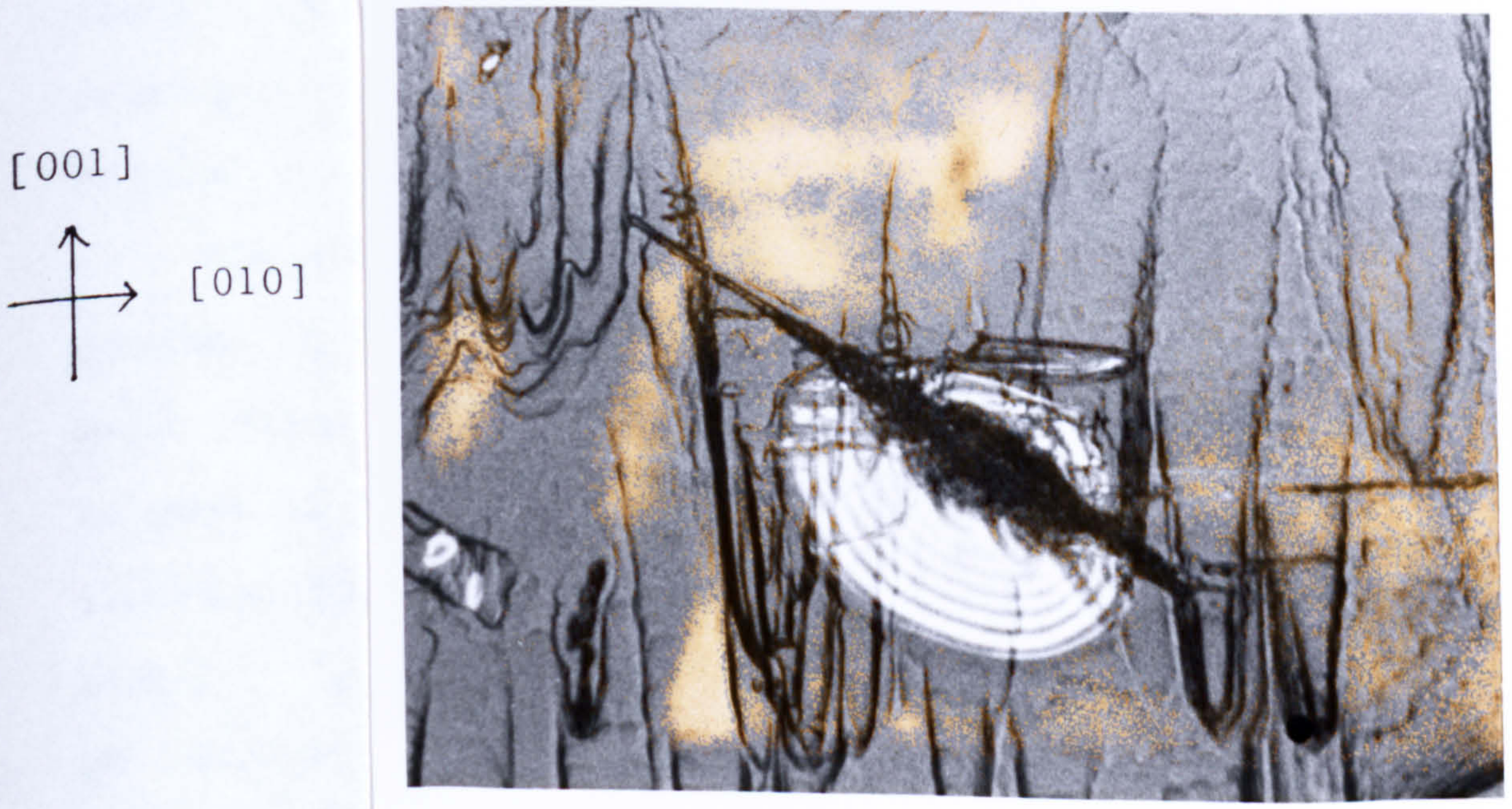

Plate 3.18: Knoop indentation on the (100) face showing conchoidal cracking, and slip traces along [010] which appeared after thermal etching.

instance to correspond with slip or possibly cleavage respectively on {001} planes. since they intersect with the {100} surface at this angle and have a high interplanar spacing. Other possible slip planes which could produce slip traces at this orientation are {102} and $\{10\bar{2}\}$, which have much lower interplanar spacings. Conchoidal cracking, due to lifting off of surface layers on removal of the indenter was also frequently observed on {100} samples, since the major cleavage plane was parallel to the surface. An example of this is shown in plate 3.18.

In plate 3.18, slip traces were again observed, along [010], which appeared to be detached from the indentation itself, and which were only observed after storage (and simultaneous thermal etching). Detached slip traces were also seen after storage in one instance at 55° to [010], when the indentation was parallel to [001] (plate 3.19). This may again have been due to cracking caused by residual stresses, or stress relaxation by slip on $\{01\bar{1}\}$ planes.

Plate 3.20 shows an example of slip trace alignments at a second orientation. When {100} samples were indented with the long axis of the indenter at 45° to both [010] and [001], slip traces parallel to the indenter axis were occasionally observed after thermal etching. These may also have been due to slow recovery of elastic stresses, but none of the likely slip planes intersect the surface at this angle and the observed

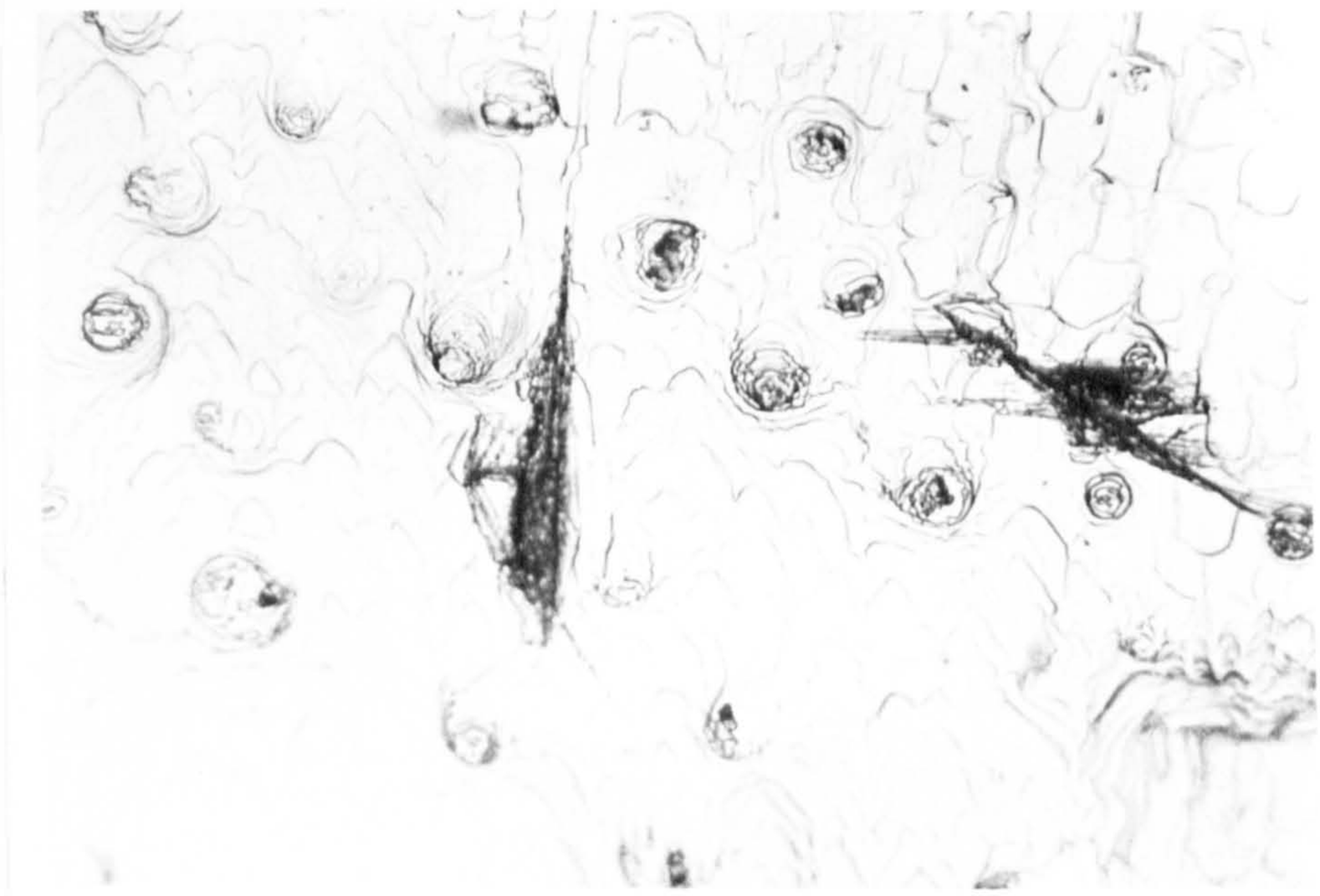

Plate 3.19: Knoop indentations on the (100) face showing slip traces along [010] and, with the long axis of the indenter parallel to [001], at 55° to the indenter axis.

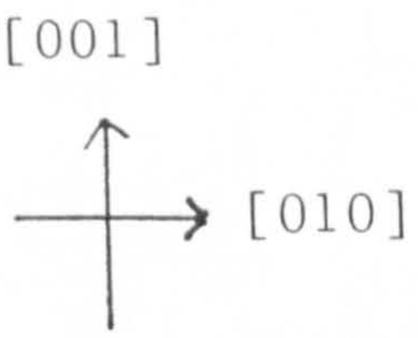

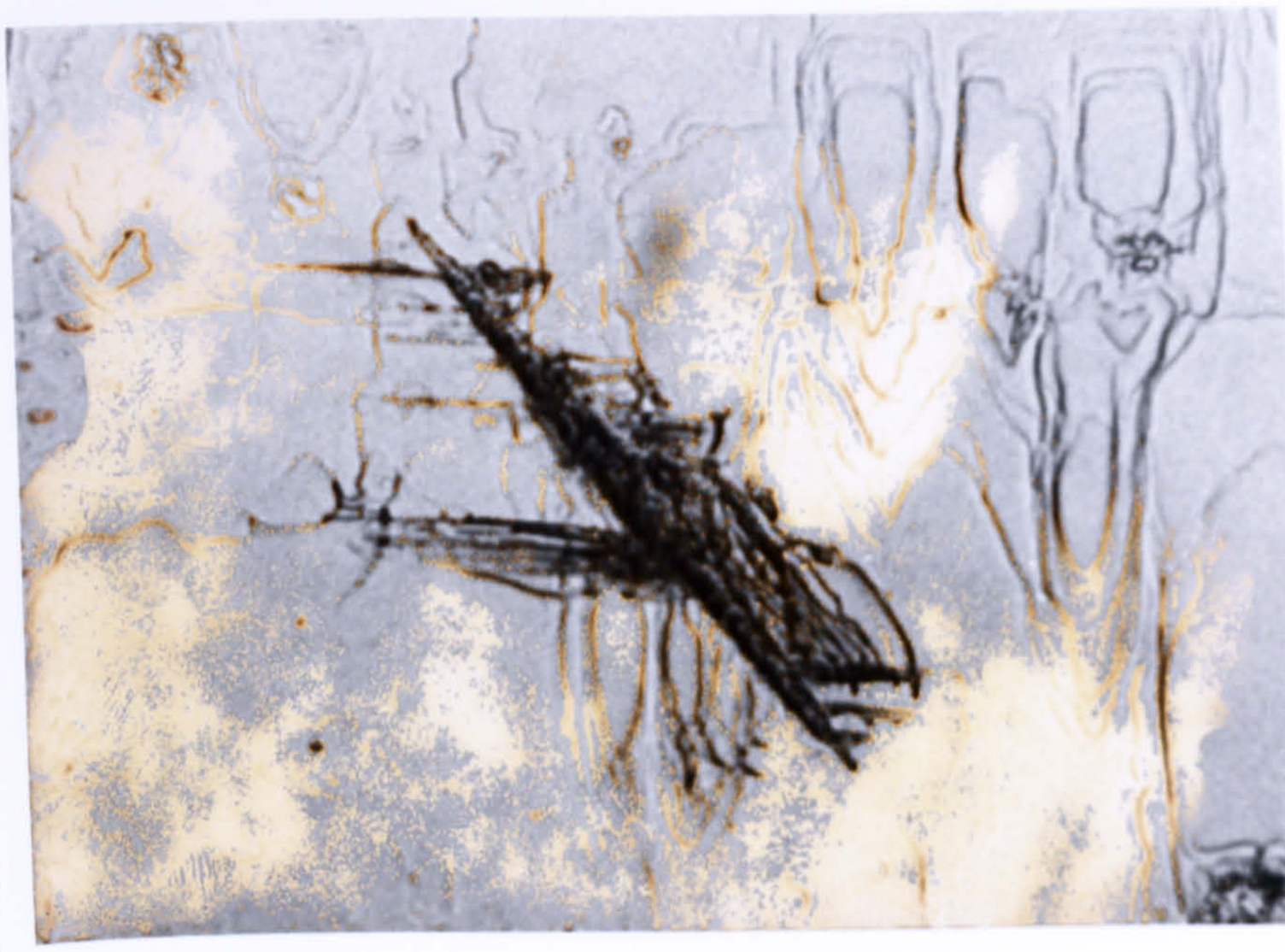

Plate 3.20: Knoop indentations on the (100) face showing slip traces along [010] and parallel to the long axis of the indenter.

(Sample etched for 14 days).

traces seem more likely to have been associated with conchoidal cracking on the underlying planes.

3.3.2.3 $\{1\bar{1}0\}$ face

Indentation on the $\{1\bar{1}0\}$ planes produced features aligned in two main directions. These were identified as cracking along [001], corresponding to the intersection of the {100} cleavage plane; and dark traces along [110] into the crystal bulk, following the angle of intersection of the {001} planes with $\{1\bar{1}0\}$. Both of these are shown in plate 3.21. The curved bands seen at the top and bottom of the indentation were indicative of cleavage taking place down into the crystal bulk, with the fringeing effect arising from optical interference due to slight movement of adjacent crystal planes and introduction of a thin air gap between them. The dark traces along [110] also appear to have considerable depth, and are again likely to be due to internal cracking, since slip will not produce optical effects such as this.

Storage of the samples for two months at 30°C showed slip traces generated by dislocation movement on {100} from the internal cracks (with subsequent etching) as shown in plate 3.22. Internal cracking along [110] appears to have produced surface cracks detached from the indentations.

Plate 3.21: Knoop indentations on the $(1\bar{1}0)$ face showing slip traces in the [001] (with fringeing) and [110] directions.

(Sample photographed immediately after indentation).

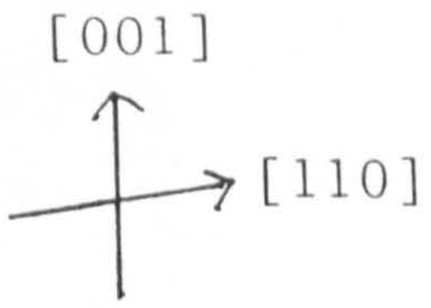

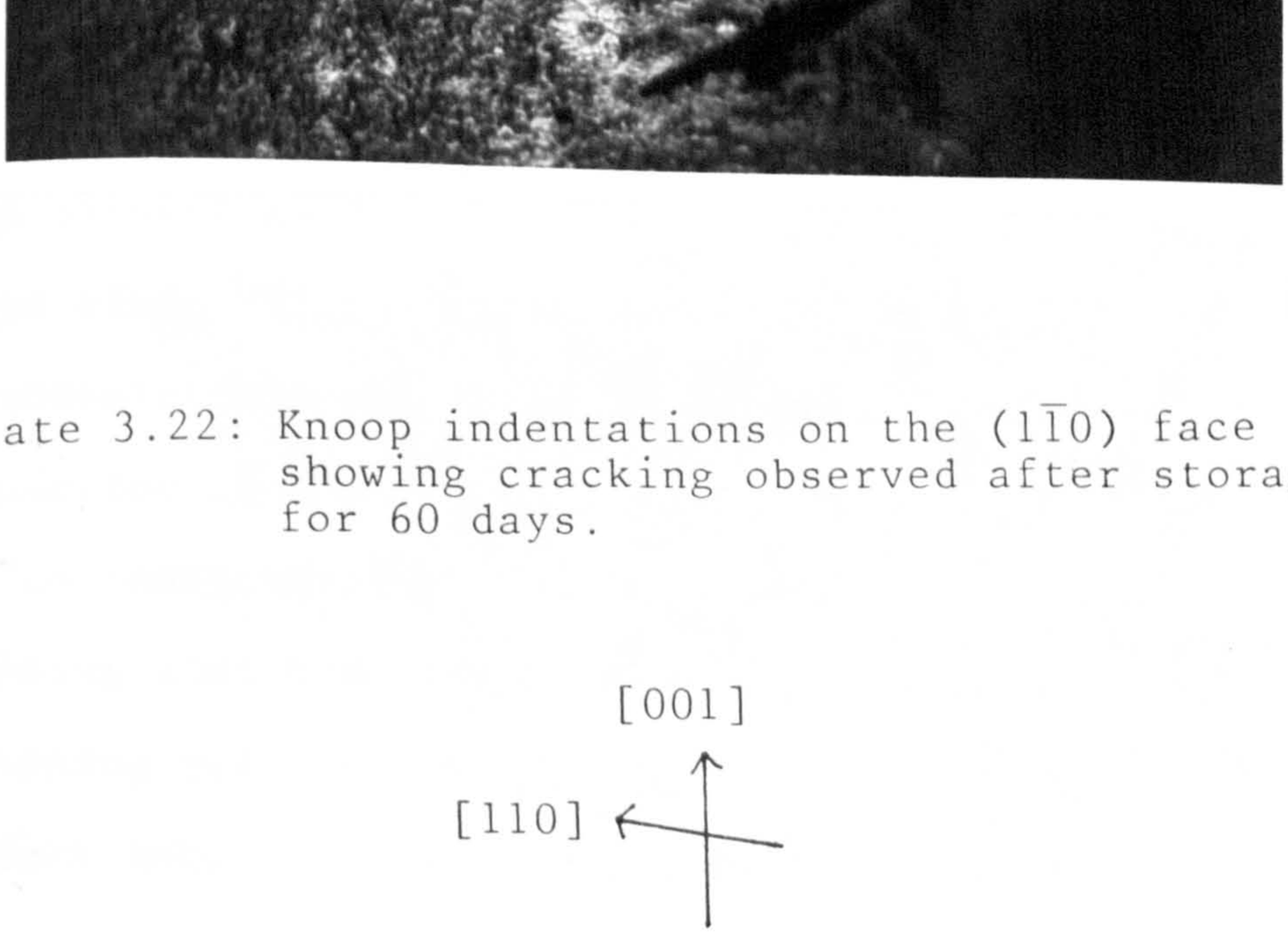

Plate 3.22: Knoop indentations on the $(1\bar{1}0)$ face showing cracking observed after storage for 60 days.

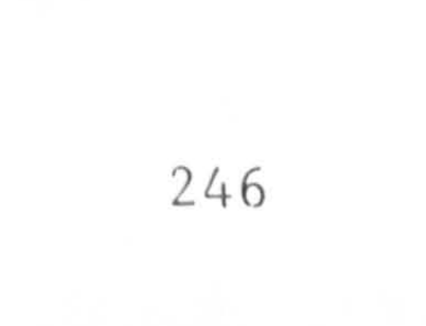

The directions of the traces on the {1$\bar{1}$0} face indicate that the activated slip planes are {100} and possibly {001}, cracking concealing any slip traces which may have been produced by slip on the latter planes. Slip on other proposed systems such as {102} would not have produced traces at these orientations.

3.3.2.4 {111} face

Indentation on the {1$\bar{1}$1} plane shows similar deep curved bands to those on the {1$\bar{1}$0} planes (plate 3.23), which seemed to correspond to cleavage on {100}. Occasionally, very short traces were also observed along [110], as also illustrated in plate 3.23. These corresponded to the intersection of the {001} planes.

Thermal etching of indented samples for one to two months allowed etch pits to develop, these also being aligned along [011], but were not necessarily connected with indentations (plate 3.24). Traces parallel to the intersection of the {100} cleavage plane also appeared close to indentations, but these were not etched, suggesting that they had appeared at some point late in the etching process. These can be seen in plate 3.25, at the right hand side of the centre indentation.

Measurements of crystal hardness were also made during indentation, and were used to obtain further evidence of the active slip systems. This will be

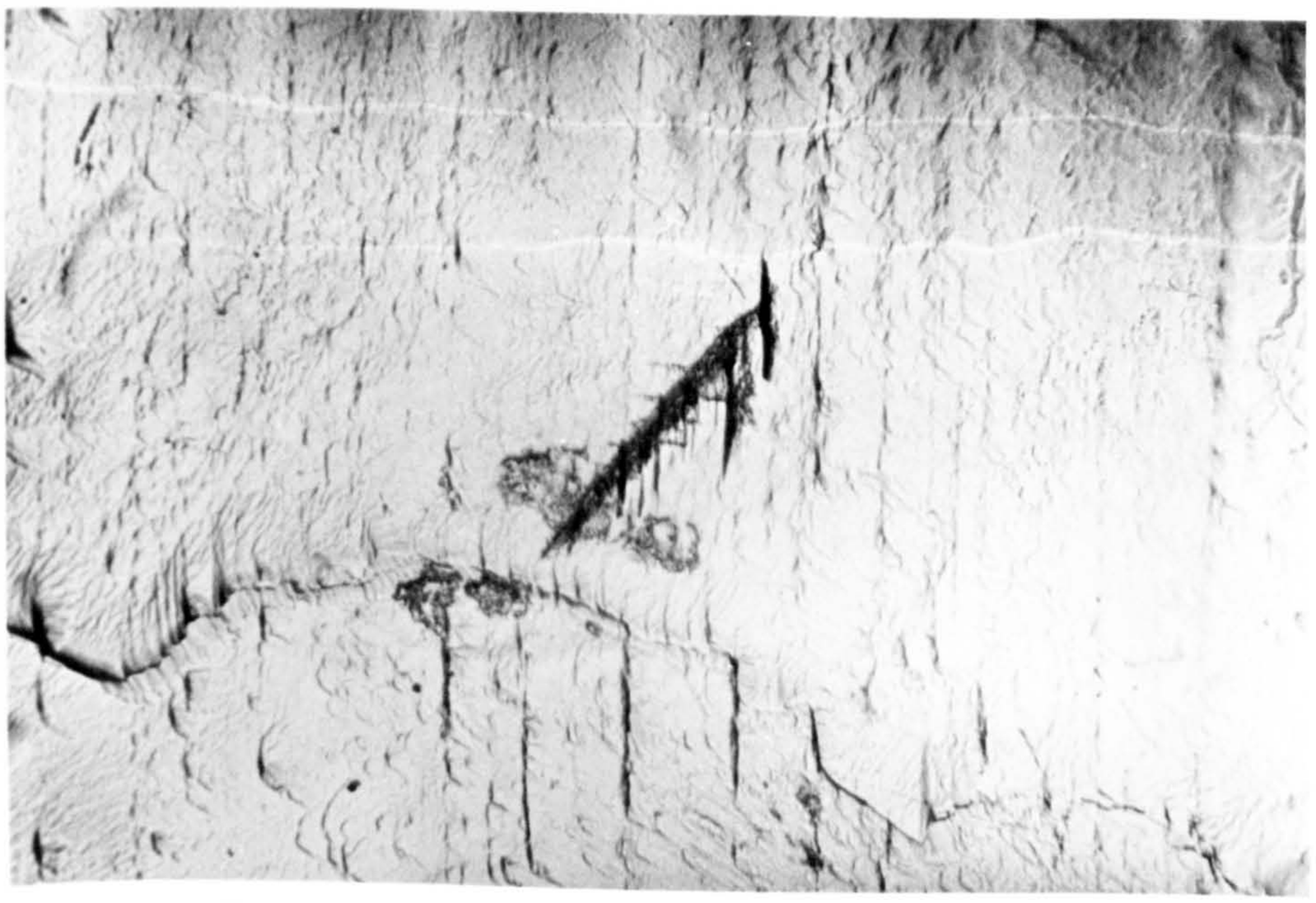

Plate 3.23: Knoop indentation on the $(1\bar{1}1)$ face showing cleavage in the [011] direction and slip traces along [110].

(Sample photographed immediately after indentation).

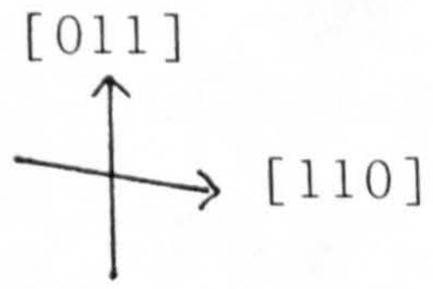

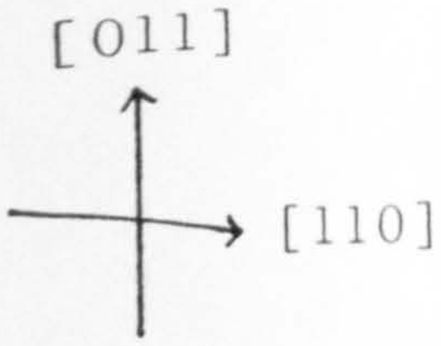

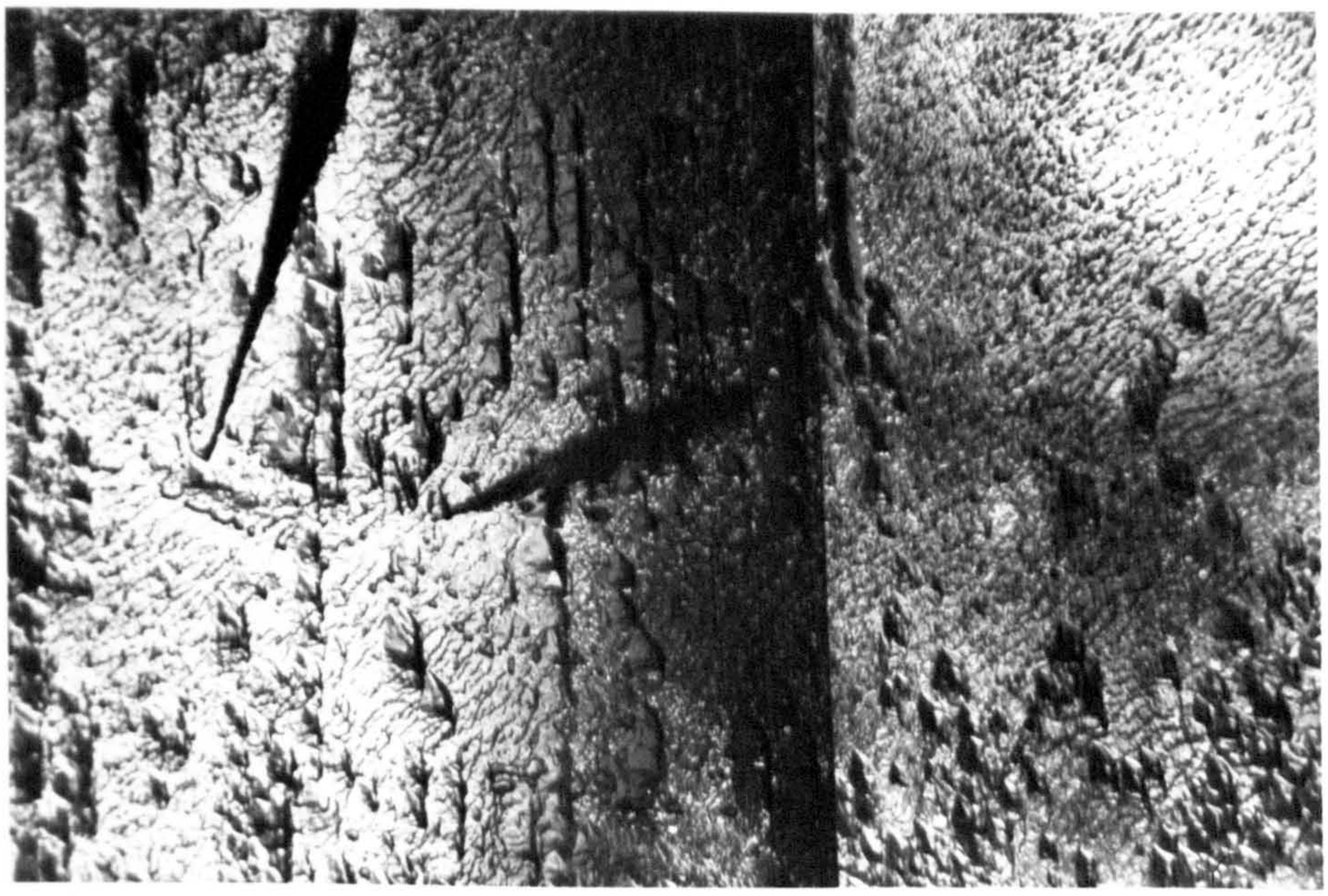

Plate 3.24: Knoop indentation on the $(1\bar{1}1)$ face showing etch pit alignments produced during storage & etching for 30 days.

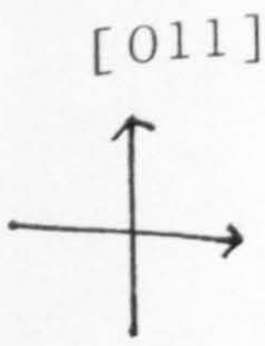

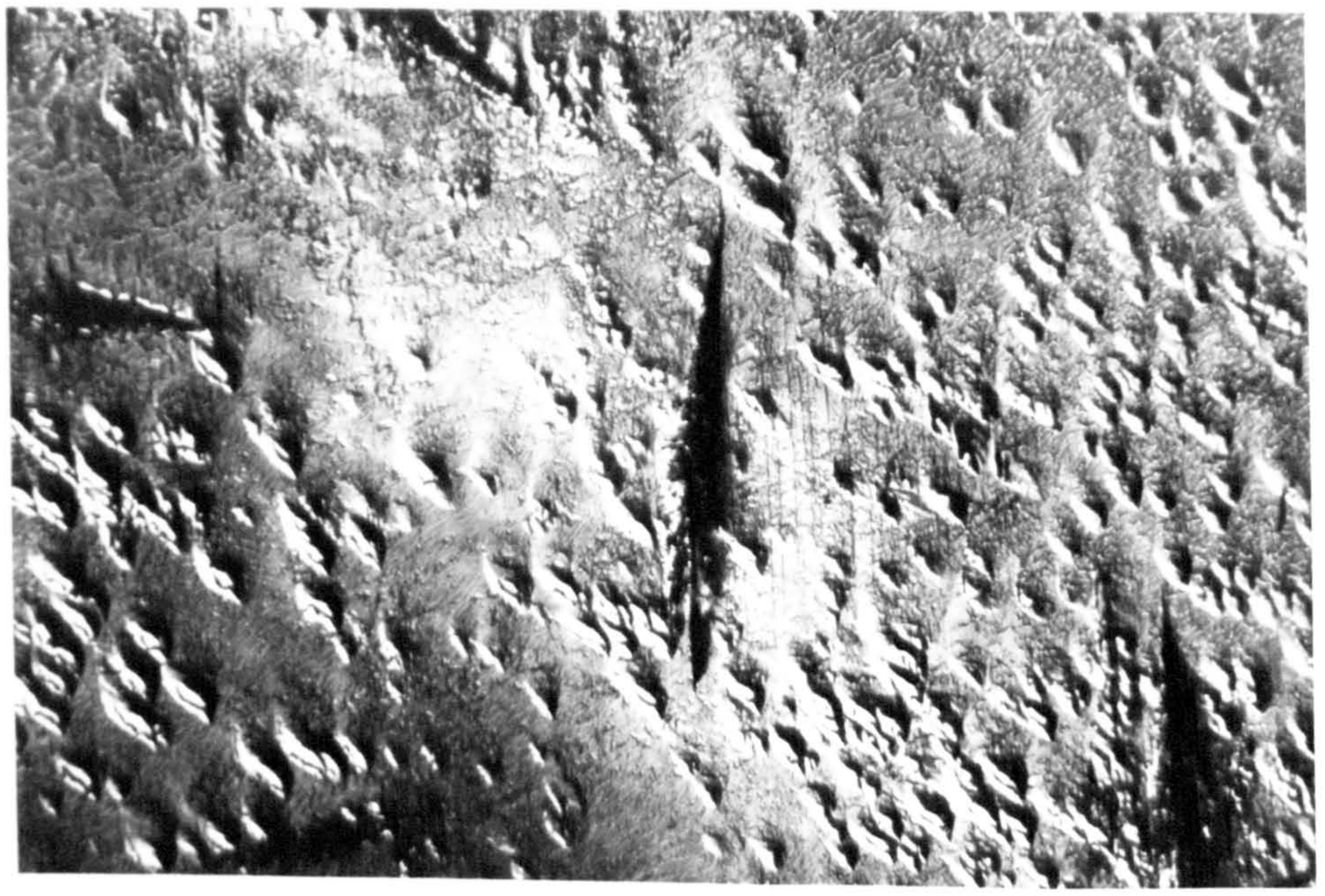

Plate 3.25: Knoop indentations on the $(1\bar{1}1)$ face showing traces parallel to the cleavage plane, not apparently etched, but which appeared during storage.

reported in the following section.

3.3.3 Hardness Measurements using the Knoop indenter

Knoop hardness was determined on the {100}, {001}, $\{1\bar{1}0\}$ and $\{1\bar{1}1\}$ crystal forms. Three samples of good quality of each were tested: one grown from hexane and two from acetonitrile for each of {100} and {001}. $\{1\bar{1}0\}$ and $\{1\bar{1}1\}$ habit faces from hexane-grown crystals were too small to be of use. Initial examination of the results showed insignificant differences between hardness results of the two types of crystal therefore the results were considered together. Knoop hardness curves illustrated show mean hardness values for the {001}, {100}, $\{1\bar{1}0\}$ and $\{1\bar{1}1\}$ growth forms respectively. Standard deviations are plotted as bars.

3.3.3.1 {001} face

Knoop hardness results for the {001} face are shown in figure 3.29. They show that [010] was the softest direction, and [100] the hardest. No other minima or maxima were observed in the results, but "shoulders" were observed at $\pm$10 to 30° from [010] indicating a possible change in the active slip system at these points. Alternatively, cracking (particularly in the hexane-grown samples) may have led to an overestimate of the length of the indentations aligned along [010], decreasing the apparent hardness value at this orientation. The standard deviation of the measurements

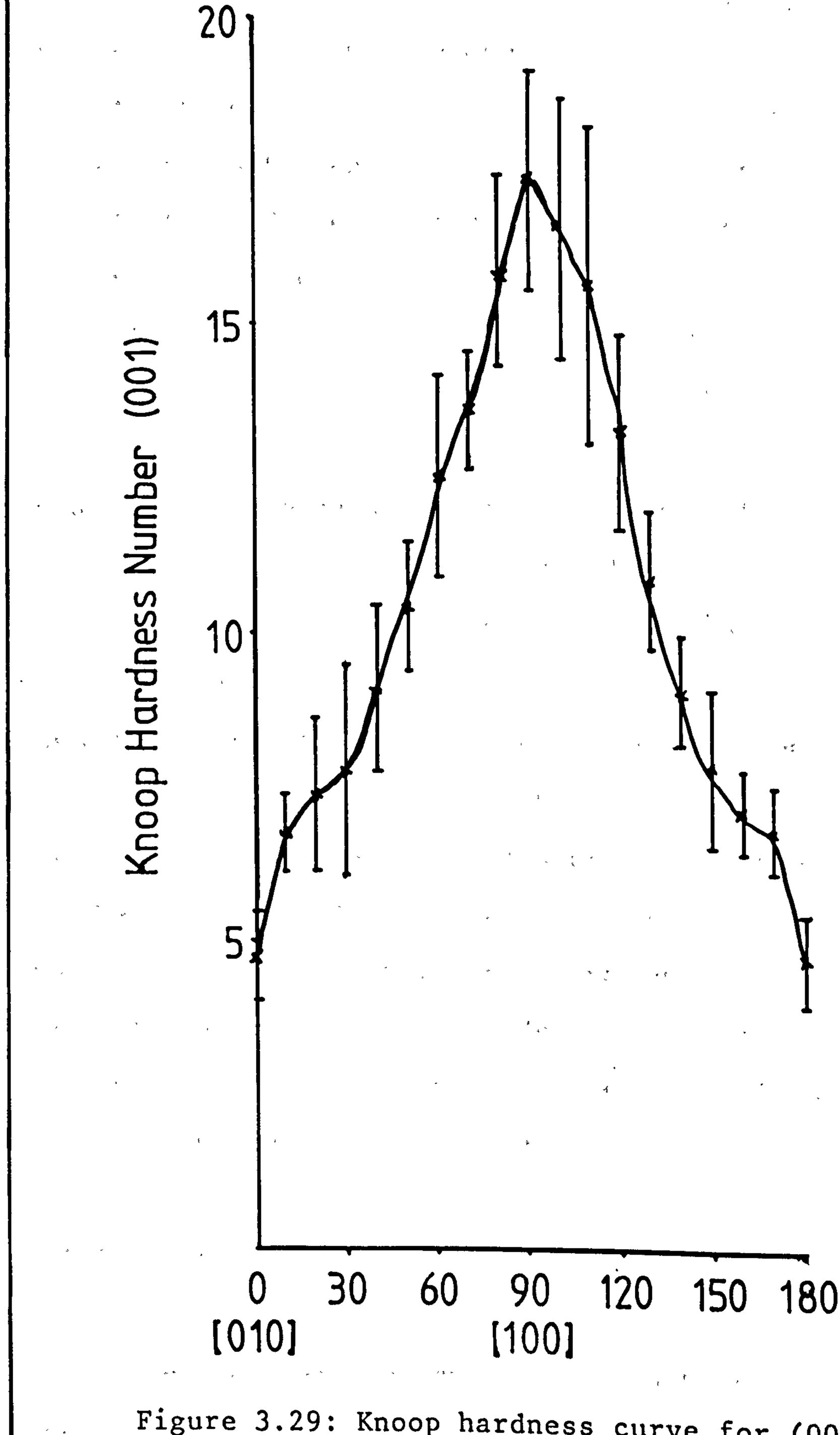

Figure 3.29: Knoop hardness curve for (001)

at this orientation is however small, indicating measurement errors were unlikely to be the cause.

The direction of minimum hardness, [010], corresponds to the direction of the slip traces observed on this face, and to the angle at which {100} planes intersect with the indented surface. Of the other possible slip planes, only {102} and $\{10\bar{2}\}$ would intersect at the same angle, but have lower interplanar spacings, and are therefore less likely to be the active system.

Maximum hardness occurs when the long axis of the indenter is parallel to [100]. At this indenter angle, slip and/or cleavage on {100} planes would be most difficult to activate.

Slip traces parallel to [100] were also observed with the indenter approximately 35° from [010], indicating a possible secondary slip system which could involve either {020} or $\{01\bar{1}\}$ planes, both of which would be difficult to initiate, due to hydrogen-bonding between planes, but may explain the "shoulders" on the hardness curve. Slip on $\{01\bar{1}\}$ would be the more likely of the two, due to the higher d_{hkl} value.

3.3.3.2 {100} face

More complex hardness curves are observed on the {100} face, as illustrated in figure 3.30. The softest direction is again along [010], with one smaller minimum

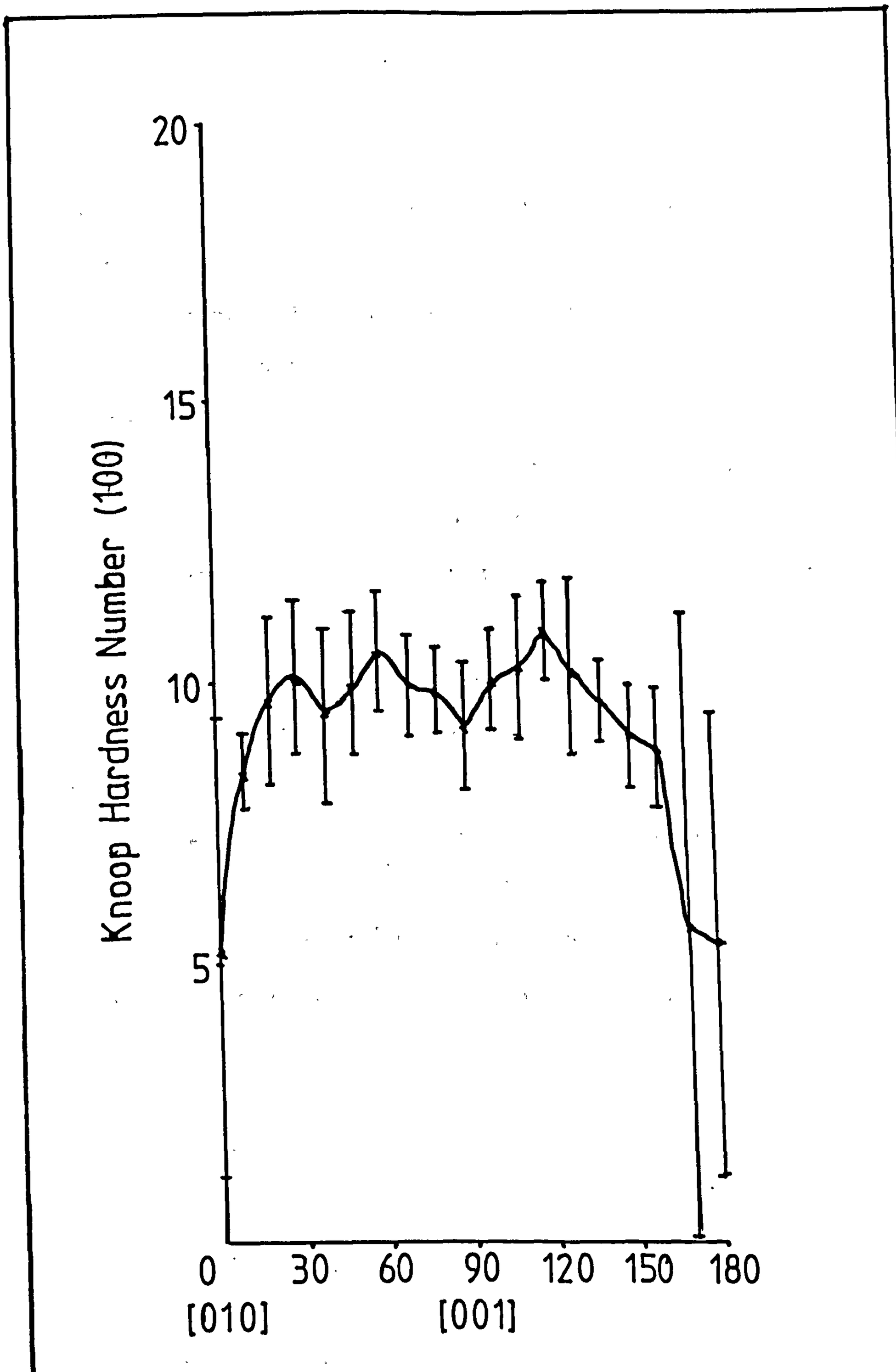

Figure 3.30: Knoop hardness curve for (100)

in the [001] direction.

Microscopic observation also showed slip traces aligned along [010], which suggested the activation of slip systems involving {001}, {102} or $\{10\bar{2}\}$ planes, with {001} being most likely due to the high interplanar spacing. $\{10\bar{2}\}$ planes however intersect at a similar angle to the surface, as illustrated in figure 3.31, and may also be involved. The standard deviation of the results around [010] suggests that cracking in the hexane-grown samples may have contributed to measurement errors.

The smaller minimum in the [001] direction is less easy to explain in terms of potential slip planes. It may be an artefact of slip on the major system. However, slip traces were observed at this indenter angle in one instance (plate 3.19) at 55° to [001] which may be associated with slip on $\{0\bar{1}1\}$ planes, which intersect at this angle, despite a high attachment energy. ERSS calculations are required for confirmation.

3.3.3.3 $\{1\bar{1}0\}$ face

Two minima are observed in the Knoop results shown in figure 3.32, the major one in the [001] direction, and a smaller minimum in the [110] direction. Observations indicated these were likely to be associated with slip on {100} and {001} planes respectively. Slip on the {001} planes does not seem to

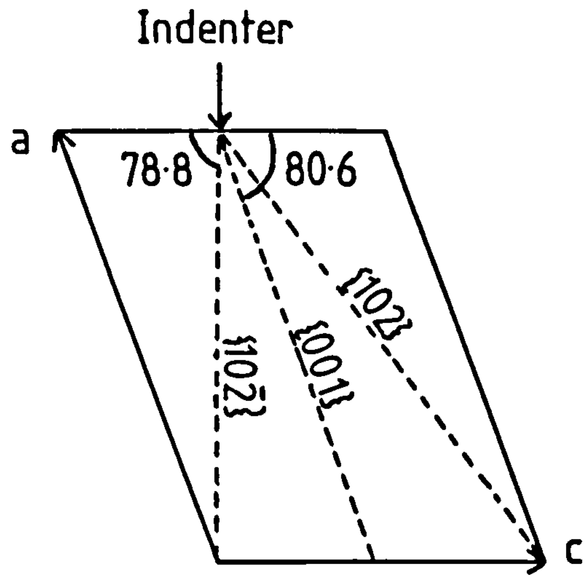

Figure 3.31: Orientation of the (102) and (10$\bar{2}$) planes

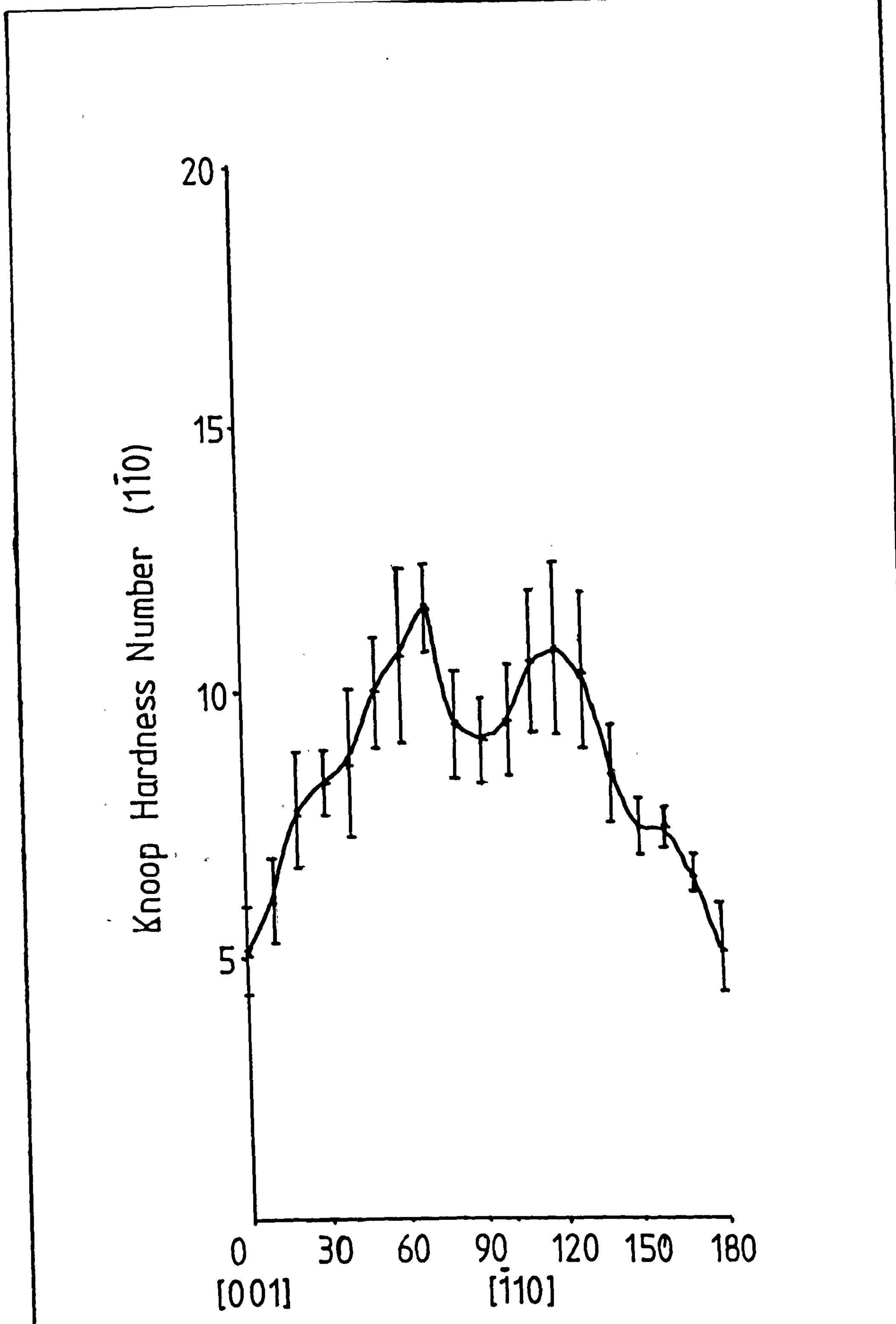

Figure 3.32: Knoop hardness curve for (1$\bar{1}$0)

be as easily activated by indentation on $\{1\bar{1}0\}$ as on $\{100\}$, leading to a higher hardness value on the $\{1\bar{1}0\}$ face. This is likely to be because the $\{001\}$ planes are at a larger angle to the face normal in this case.

3.3.3.4 $(1\bar{1}1)$ face

One minimum is observed in the Knoop hardness plot, shown in figure 3.33, on the $\{1\bar{1}1\}$ face in the $[0\bar{1}1]$ direction. This is again parallel to the intersection of the $\{100\}$ planes, and the direction of the slip traces observed on this face. The traces parallel to $[110]$ do not seem to be reflected in the Knoop hardness results. Slip on the $\{001\}$ planes was difficult to generate at this orientation, and $[1\bar{1}0]$, the angle of their intersection with the $\{1\bar{1}1\}$ surface, was the hardest direction.

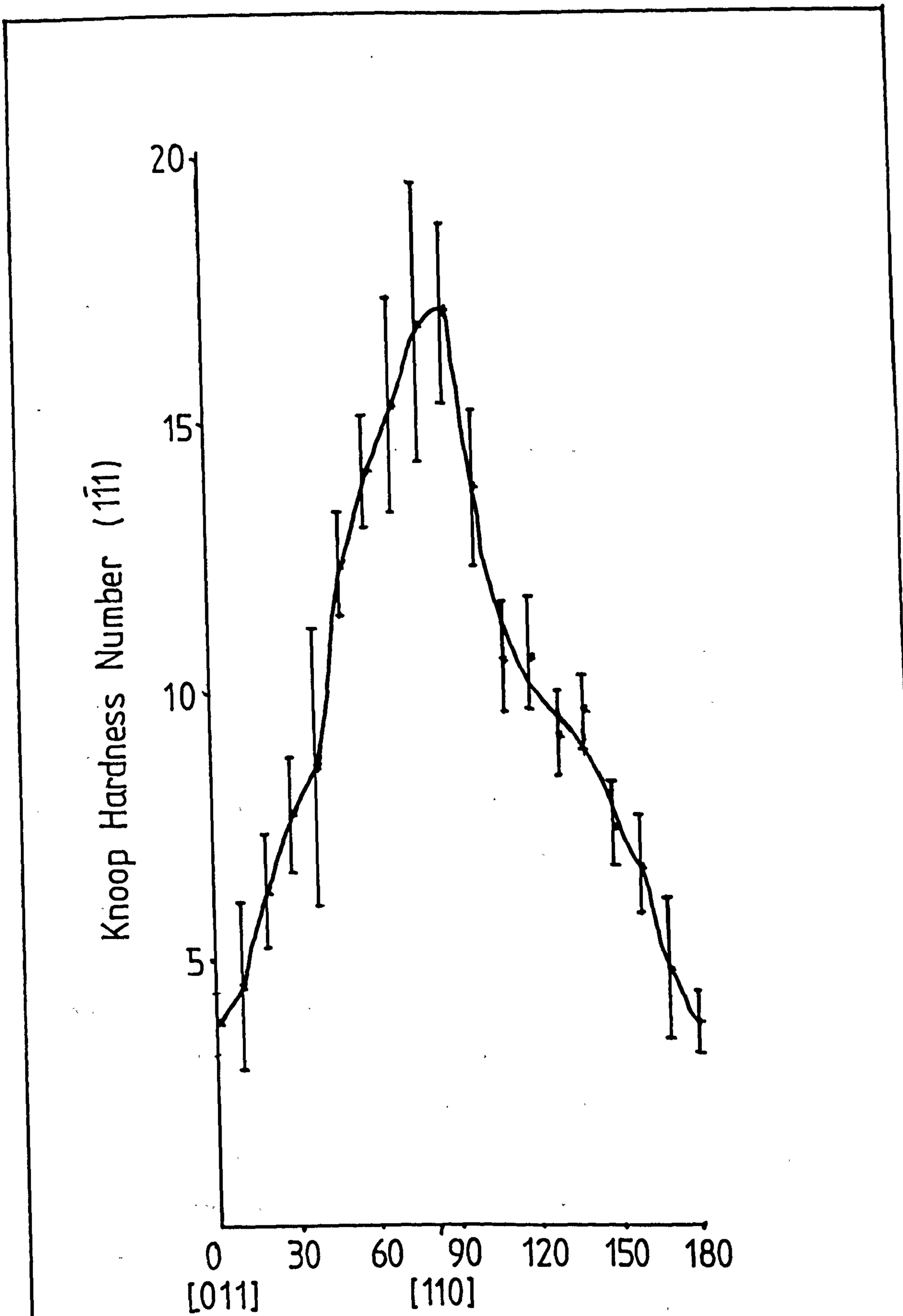

Figure 3.33: Knoop hardness curve for (1$\bar{1}$1)

3.3.4 Analysis of Hardness Anisotropy from ERSS Calculations

Calculation of effective resolved shear stresses (ERSS) was developed in order to explain hardness anisotropy in inorganic materials. Slip in organic molecular solids has not been as comprehensively studied, but it is likely that the deformation systems are more complex, due to molecular overlap and the conformation changes of molecules at the surface of slip planes. Organic materials also tend to fracture more readily [70]. ERSS calculations only take into account deformation by slip, although they have also been applied to twinning [134]. Elastic deformation and brittle fracture may also occur during indentation, which can affect hardness results, and cannot be dealt with in terms of ERSS at present.

Both brittle fracture and time-dependent relaxation of elastic stresses were observed on indentation of ibuprofen crystals which may make analysis of hardness on the sole basis of ERSS curves problematic. However, assuming the general principles which govern likely slip systems are similar i.e. high d_{hkl} and/or low E_{att} and low b, it should be possible to determine at least whether proposed slip systems are possible or not. Potential molecular obstructions, and the presence of strong intermolecular interactions which may make slip less easy than predicted, were identified by the use of

crystal packing diagrams. Consideration of these factors in the selection of likely slip systems should avoid some of the problems outlined above.

Although a low value of ERSS indicates a hard crystal direction and vice versa, since the ERSS values obtained are not absolute (since F/A in equation 2.8 is ignored) it is more difficult to compare ERSS curves directly for different slip systems especially if switching between slip systems occurs. The shape of the ERSS curves should indicate likely hard and soft directions for the proposed slip systems, but consideration of d_{hkl}, $\underline{b}$, intermolecular interactions and molecular overlap is also necessary when determining the active slip system from ERSS analysis.

From the preceding experimental observations, the dominant slip planes appeared to be {100} and {001} since slip traces on different faces were aligned parallel to their intersection with the indented surface. Minima in the hardness results also occurred when the long indenter axis was parallel to the intersection of these planes. However additional slip traces and features on the hardness curves were also present. ERSS curves were determined for all potential slip systems in order to identify which were most likely.

3.3.4.1 {001} face

The major slip traces on the {001} face were aligned along [010]. Of the slip systems presented in table 3.8, these traces could be produced only by slip on either {100} or $\{10\bar{2}\}$ planes. Calculated ERSS curves for all the possible Burgers vectors for these slip planes are shown in figure 3.34. Of the {100} slip systems, {100}[001] gives generally highest values, and is closest in shape to the inverse of the hardness values. $\{10\bar{2}\}$[010] is unlikely to be an active slip system, since it is most resistant to slip when the long indenter axis is aligned along [010], the softest crystallographic direction. Slip on {100}[010] may contribute to the formation of shoulders on the Knoop hardness curves for this face (and to be dominant at [100] where it has the highest value of all systems investigated), but the maxima in the ERSS curves are not quite at the same angles as the shoulders, and this is not therefore conclusive.

Additional slip traces were observed parallel to [100], consistent with slip on {020} or $\{01\bar{1}\}$ planes. ERSS curves for these are illustrated in figure 3.35, with ERSS curves for slip on {001} planes, which could also be activated, but would not produce any slip traces on the {001} surface, since emergent dislocations only appear on crystal surfaces which intersect the slip plane, unlike this case where they are parallel. Slip on

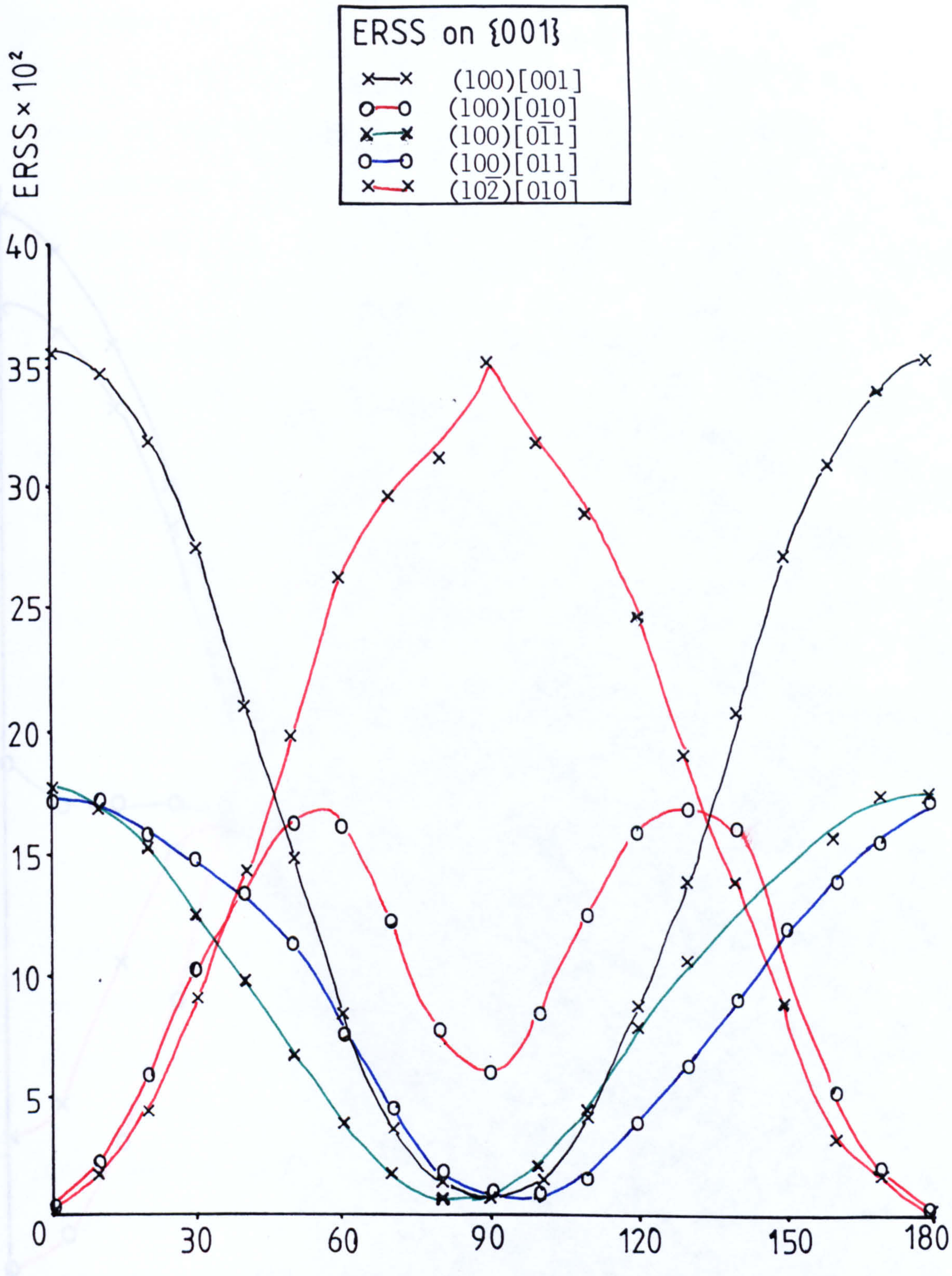

Figure 3.34: ERSS curves for major slip systems on (001) face

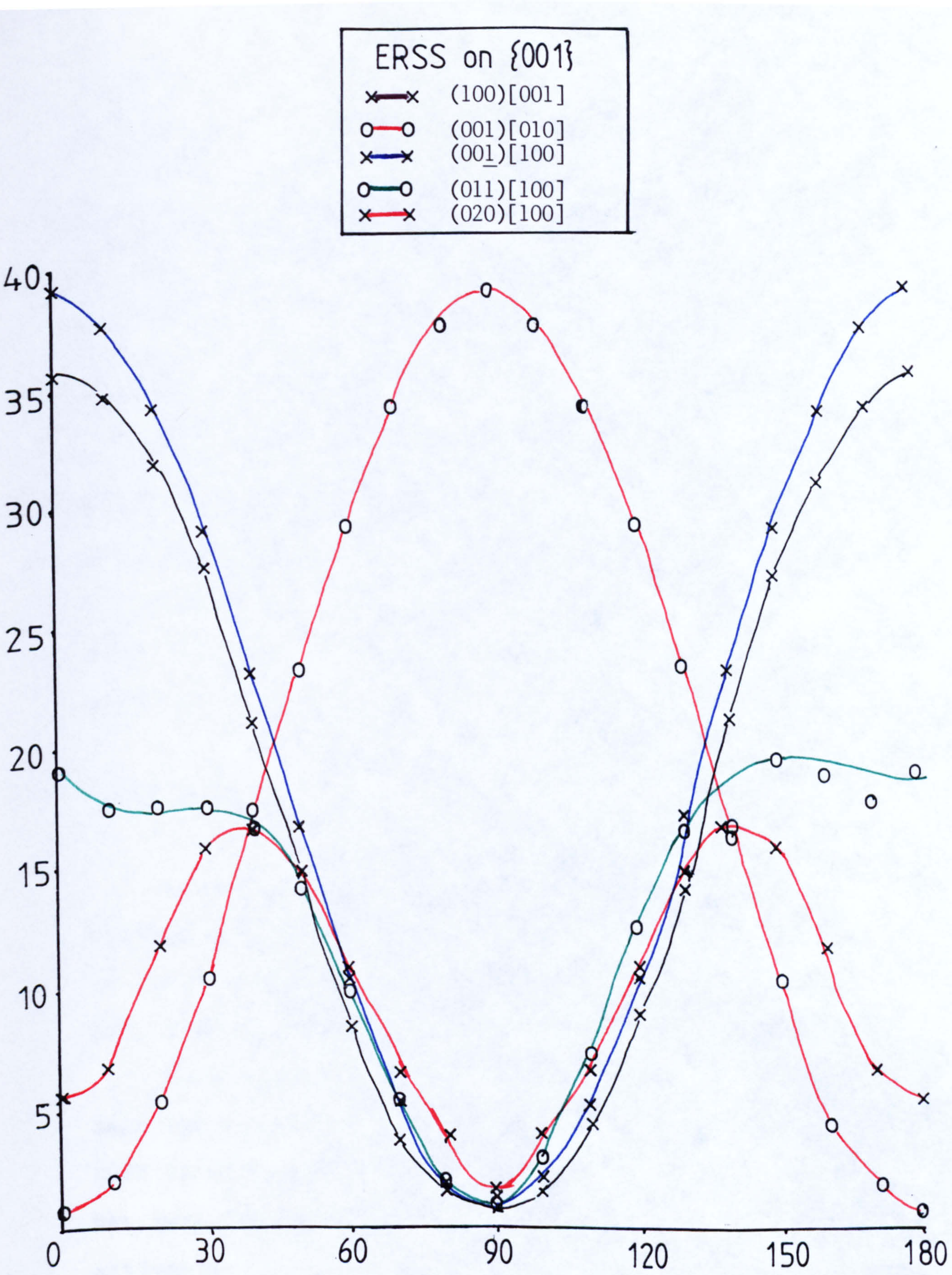

Figure 3.35: ERSS curves for other potential slip systems on (001)

both $\{01\bar{1}\}[100]$ or $\{020\}[100]$ could contribute to the shoulders on the hardness curves (and dominate in the [100] direction) although the ERSS values are below those of the dominant system $\{100\}[001]$. In this case, an additive effect may be taking place. The higher d_{hkl} of the $\{01\bar{1}\}$ planes makes slip more likely than on $\{020\}$.

The ERSS curve for $\{001\}[100]$ closely follows that for $\{100\}[001]$ on this plane of indentation, and it is therefore impossible to determine whether it is activated or not, again because the planes are parallel to the surface. Slip on $\{001\}[010]$ is not likely to take place since the maximum in ERSS occurs in the hardest direction.

3.3.4.2 {100} face

On the {100} face, the dominant slip traces were aligned along [010] and could have been produced by slip on $\{001\}$ or $\{10\bar{2}\}$ planes. ERSS curves for all possible slip systems are shown in figure 3.36.

The minimum in the hardness curves appears to have been due to slip on $\{001\}[100]$, since the maximum in ERSS occurs parallel to [010]. Again $\{10\bar{2}\}[010]$, which has very low ERSS at this angle does not seem to be activated.

What were believed to be additional slip traces were occasionally observed at 55° to 60° from [010]. Of

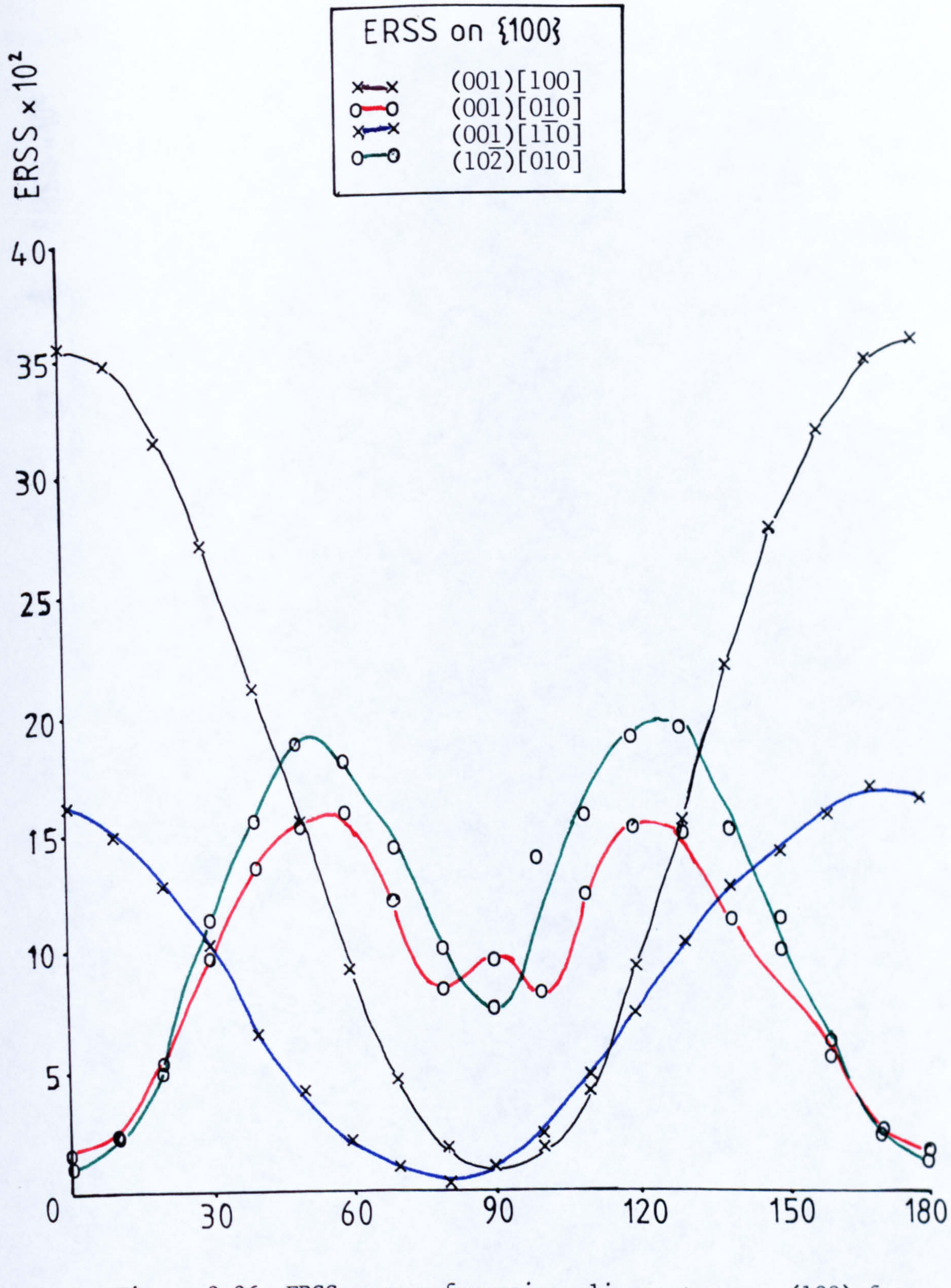

Figure 3.36: ERSS curves for major slip systems on (100) face

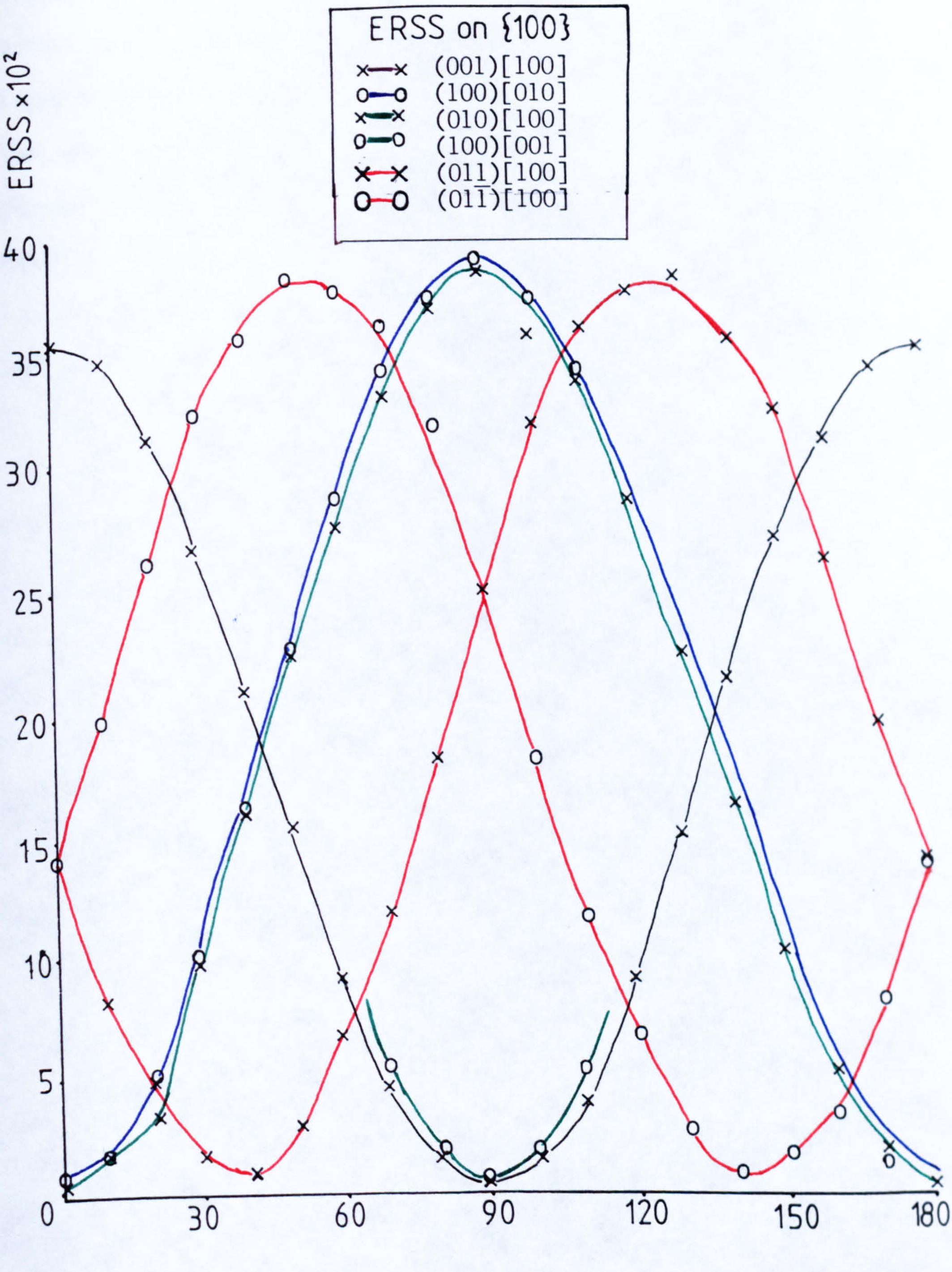

Figure 3.37: ERSS curves for other potential slip systems on (100)

the likely slip planes, only {01$\bar{1}$} or {011} could produce slip traces at this angle. Calculated ERSS curves are illustrated in figure 3.37. The maxima in the respective ERSS curves at the angles of interest suggest slip on these planes is most likely at these angles. However, hardness results do not show a minimum at these angles, and it would appear that hydrogen-bonding between layers acts to prevent slip (in agreement with high E_{att} for these planes), and an insignificant amount of slip takes place on these planes.

ERSS curves were also calculated for slip on {020} and {100} planes in order to investigate the secondary minimum in the hardness results parallel to [001]. Slip on {100}[001] is not activated at this orientation, but {100}[010] gave a maximum ERSS value, as did {020}[010]. Since no slip traces were observed parallel to [001] slip on {020} planes seems unlikely, and the secondary minimum seems to be due to slip on {100}[010], parallel to the indented surface.

3.3.4.3 {1$\bar{1}$0} and {1$\bar{1}$1} faces

ERSS curves could not be determined for these faces as the necessary stereographic projections of crystal directions could not be obtained due to a fault in the plotting program, as described earlier (section 2.4.1). However the slip traces observed, and Knoop hardness curves are consistent with slip on {100} and {001}

planes. No slip traces were observed which could have been associated with slip on any other of the proposed systems.

3.3.4.4 Summary

ERSS curves calculated for the {100} and {001} faces suggest that two major slip systems are activated by indentation, possibly on both faces. namely;

{100}[001]

and {001}[100].

Slip on {100}[010] also appears to be activated on the {100} face, giving rise to a secondary minimum in the hardness results for this face.

The combination of slip traces on both faces suggested that slip on $\{01\bar{1}\}$ and {011} planes may also have been taking place. Calculated ERSS curves are consistent with this, despite very high calculated values which are not reflected in the hardness curves. The relatively infrequent appearance of slip traces, and this scaling down of the calculated ERSS suggests slip on $\{01\bar{1}\}[100]$ or {011}[100] is hindered by the molecular interactions between the planes, or possibly by molecular obstruction. A small degree of slip on these systems would however be sufficient to explain the formation of shoulders on the hardness results, and the apparent flattening of the hardness curves for the {100} face between the minima.

Despite the need to take account of bonding between layers, and the presence of molecular obstruction to slip, use of ERSS calculations to analyse hardness anisotropy in organic molecular solids appears possible. The active slip systems were those with highest d_{hkl} and smallest Burgers vector, consistent with plastic slip in inorganic materials. The lower interactions between planes in organic materials, which have Van der Waals and electrostatic interactions rather than ionic bonding, appears to increase the number of active slip systems - there are normally only one or two in inorganic materials.

3.3.5 Summary and Discussion

Determination of the slip systems operating during micro-indentation testing should demonstrate how a material will deform under pressure e.g. compaction/ tableting. ERSS calculation, combined with Knoop hardness measurements and microscopic observations, appears to be a valid technique for identifying these active slip systems.

Knoop hardness measurements were not able to differentiate between ibuprofen samples grown from different solvents, which have been shown elsewhere to compress differently. It was, however, noted during testing that hexane-grown samples cracked more easily than those grown from acetonitrile, leading to possible measurement errors in section 3.3.3.1 and 3.3.3.2 , and were generally more brittle, requiring more careful handling. Macroscopic cracking also occurred readily with hexane-grown crystals, as illustrated in plates 3.26 and 3.27.

Brittle materials are more likely to deform by fracture than by plastic deformation during compaction at typical tableting pressures, potentially leading to weaker compacts [70] as outlined in section 1.4.4. These materials also become harder, and more difficult to compress as the particle size decreases[135], resulting in a decrease in compact strength. Kaneniwa et al[71], also showed that by increasing the particle size of a

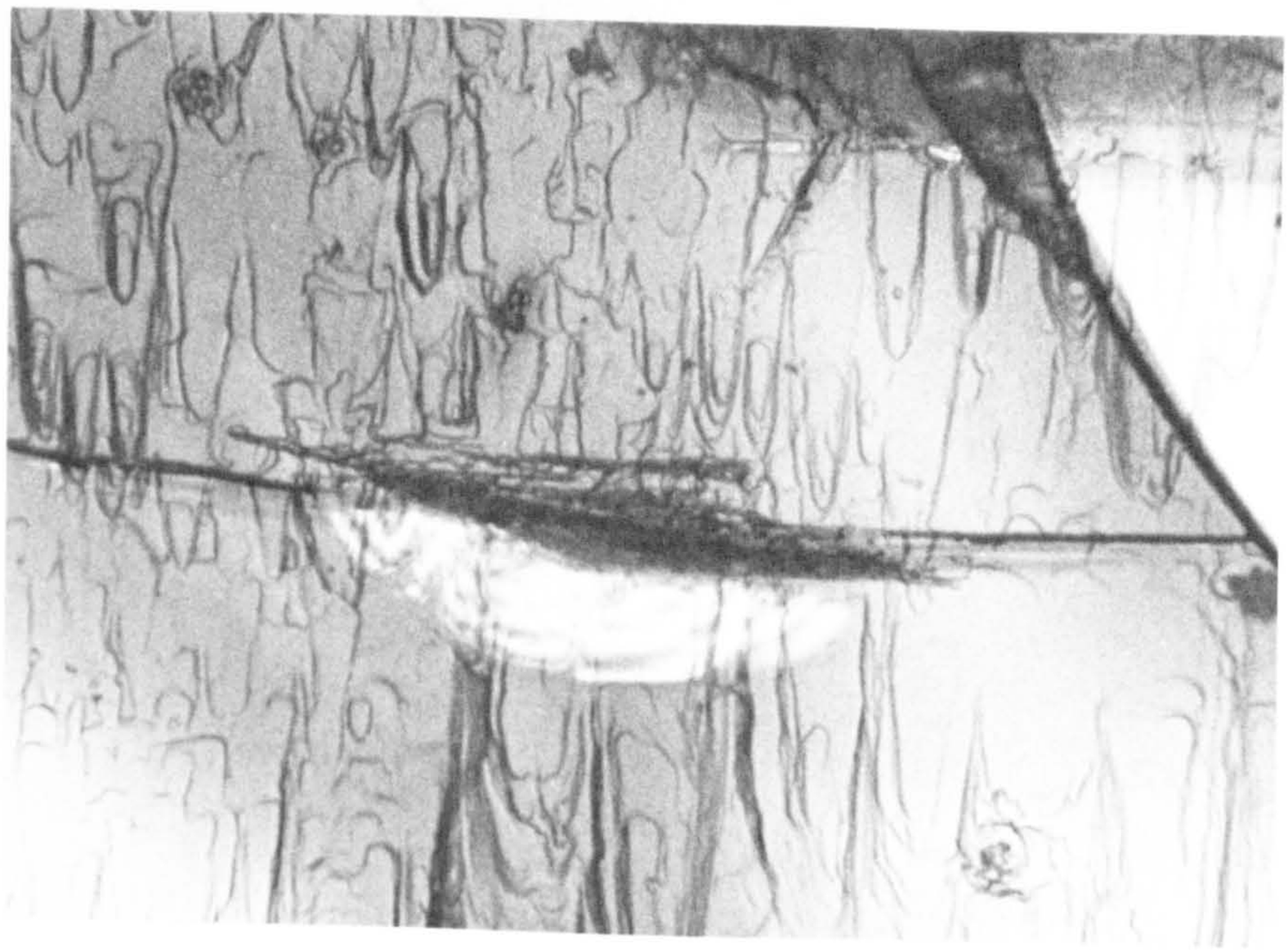

Plate 3.26: Cracking around an indentation on the (001) face of a hexane-grown crystal.

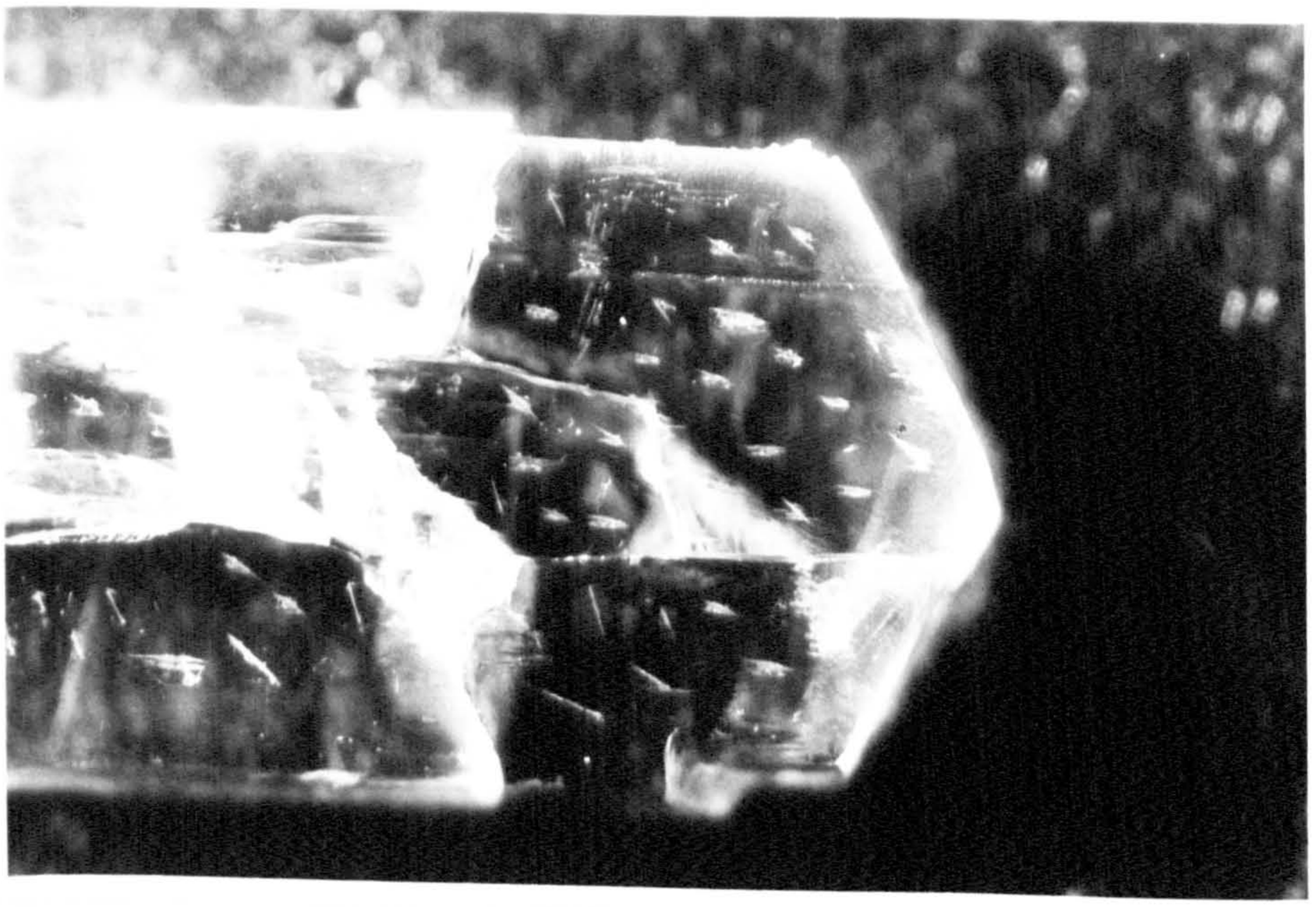

Plate 3.27: Macroscopic cracking on a hexane-grown crystal after indentation.

compound known to deform by brittle fracture, stronger compacts were produced, whereas compact tensile strength was independent of particle size for materials deforming plastically. By this reasoning, at equivalent particle sizes, ibuprofen crystallised from polar solvents should form stronger compacts than crystals grown from non-polar solvents. Small brittle particles below a critical size appear to be ductile (deforming by gross yielding rather than slip), and are squashed flat at high pressures. This, or increased localised asperity melting, which would occur by the same mechanism, may be a possible reason for increased adhesion to the die walls of tablets produced commercially. If applied stresses cannot be relieved by plastic deformation, or by further brittle fracture, then asperity melting becomes possible [69].

Gordon and Amin [1] found that ibuprofen recrystallised from polar solvents showed improved tableting performance compared to that recrystallised from hexane or heptane; sticking of compacts to the die walls and compact lamination were reduced, and improved tablet bonding was observed. This appeared to be due at least in part to an increase in plasticity, associated with crystallisation from a solvent from which crystal growth occurred by deposition of monomers rather than dimers. This introduced less strain to the crystal system, demonstrated by the decreased asterism observed in crystals grown from acetonitrile, and decreased

distortion of x-ray topographs. Hüttenrauch [136] also found that well-crystallised samples of lactose and cellulose (which deformed plastically) produced stronger compacts than less well-crystallised samples of the same material. The well-crystallised samples had a greater potential for what was termed "activation". Plastic deformation appeared to increase the dislocation density of the well-crystallised material and hence its internal energy, the resulting stress being released by interparticulate bonding and/or slip. Conversely, in samples showing lower crystallinity, dislocations would tend to pile-up and/or be pinned by impurities, and the crystals are therefore more likely to fracture under pressure or exhibit work-hardening.

Individual dislocations could not be detected by X-ray topography to further confirm the slip systems proposed. X-ray topographs did indicate however that hexane grown crystals were more strained, and also that the {001} type planes were most strained. Adsorption of the "wrong" dimers and slowing of growth at this face would appear to be the cause.

CONCLUSIONS

4 CONCLUSIONS

Various factors appear to contribute to the alteration in compaction behaviour of ibuprofen crystals grown from different solvents. The change in crystal morphology from long, thin plates to a more equant shape occurs by a proposed change in the growth mechanism: growth from polar solvents occurs by deposition of monomer units, whereas from non-polar solvents, carboxylic acid dimers seem to be the growth unit. This leads to an increase in internal strain in crystals grown from non-polar solvents, particularly in the {001} growth sector which would be most affected by the change in growth mechanism. No change was observed in crystal hardness, but the increase in strain did lead to increased reactivity, observed during dissolution testing.

Crystals with a greater degree of internal disorder tend to be less able to deform plastically, and this was observed with ibuprofen crystals grown from hexane, which tended to be more brittle. This may be a major source of the incidence of capping and lamination observed on compaction of ibuprofen. Additionally, brittle materials are more likely to deform by local asperity melting (or gross yielding) at high pressures, explaining the increased incidence of sticking of tablets of hexane-crystallised ibuprofen in tablet dies.

The change in habit may also affect the incidence

of capping and lamination, since it has been observed that flat platey crystals are more likely to take up a preferred orientation within the tablet bed, resulting in a layering effect within the compact, rather than a homogeneous, well-bonded one.

Crystallisation on an industrial scale, at conditions of high supersaturation, will not necessarily produce the same crystal morphologies as those obtained in this work. However, the variation in crystal morphology observed followed similar trends to those previously observed at conditions of high supersaturation [1], and therefore are likely to be applicable in general terms in the industrial situation.

The defect concentration of crystals grown at high supersaturation is, on the other hand, likely to differ considerably from that of the relatively low defect crystals grown in this work. However, it was necessary to use low defect crystals in order to identify the slip systems operating during plastic deformation. The effect of the nature and concentration of crystal defects on the compaction of ibuprofen crystals is a a subject for further study.

FURTHER WORK

5 FURTHER WORK

Future work on the subject of the problems of compaction of industrially produced ibuprofen crystals might include a detailed study of the fracture mechanics of ibuprofen crystals, comparing crystals grown from solvents of varying polarity. Dislocation characterisation by x-ray topography, involving growth of very high quality crystals, may permit a better understanding of the deformation processes. The source of fringeing observed in the topographs may be elucidated if better quality crystals were available. Further work on the physical properties of ibuprofen crystals might include solution calorimetry to determine precisely the effect of lattice strain on heat of formation, entropy etc., and further dissolution experiments to determine the rate constants for the transport and surface controlled reactions, and the influence of lattice strain on them. Additionally, and perhaps most importantly, compaction measurements of crystals grown from polar solvents would be of interest.

APPENDIX

Appendix

Structure of S(+)-Ibuprofen

```
 A,B,C =   12.462   8.035   13.539
ALPHA,BETA,GAMMA =   90.000 112.890 90.000    SPGR =  P21
66    SYMOPS= 257
 1 O    -0.96442  -0.90200  -0.77656
 2 O    -1.08433  -0.73300  -0.89622
 3 O    -0.26847   0.07143   0.04999
 4 O    -0.14976  -0.75969  -0.83159
 5 C    -0.98678  -0.64068  -0.80225
 6 C    -0.89047  -0.64068  -0.80225
 7 C    -0.90086  -0.52813  -0.89366
 8 C    -0.88367  -0.54743  -0.69834
 9 C    -0.95632  -0.40807  -0.70356
10 C    -0.94632  -0.32631  -0.61743
11 C    -0.87604  -0.37981  -0.51657
12 C    -0.81026  -0.52262  -0.51095
13 C    -0.81480  -0.60468  -0.59986
14 C    -0.86405  -0.28780  -0.40935
15 C    -0.76727  -0.16459  -0.37199
16 C    -0.74106  -0.10065  -0.26509
17 C    -0.78360  -0.02076  -0.44988
18 C    -0.24401  -0.07008  -0.10053
19 C    -0.34153  -0.19578  -0.06593
20 C    -0.45756  -0.11468   0.05094
21 C    -0.34018  -0.28813  -0.03133
```

22	C	-0.26673	-0.42216	-0.01646
23	C	-0.26237	-0.51112	-0.10445
24	C	-0.33306	-0.46643	-0.20486
25	C	-0.40624	-0.33004	-0.22297
26	C	-0.40818	-0.24134	-0.13516
27	C	-0.333676	-0.56308	-0.30494
28	C	-0.43896	-0.68360	-0.35162
29	C	-0.43399	-0.81782	-0.27508
30	C	-0.44775	-0.75281	-0.45608
31	H	-1.06500	-0.97510	-0.81200
32	H	-0.16870	0.13090	0.08660
33	H	-0.80998	-0.70679	-0.78252
34	H	-0.83188	-0.43893	-0.87655
35	H	-0.90513	-0.60061	-0.96165
36	H	-0.98135	-0.46202	-0.91339
37	H	-1.00497	-0.35951	-0.78183
38	H	-1.00301	-0.21991	-0.62707
39	H	-0.75143	-0.56627	-0.43287
40	H	-0.76219	-0.71442	-0.59438
41	H	-0.94368	-0.21989	-0.42797
42	H	-0.85480	-0.37260	-0.34684
43	H	-0.69164	-0.22539	-0.37435
44	H	-0.66950	-0.01487	-0.23682
45	H	-0.81669	-0.03985	-0.26273
46	H	-0.72014	-0.20570	-0.21200
47	H	-0.71204	-0.06502	-0.42161
48	H	-0.79016	-0.07029	-0.52562
49	H	-0.86241	-0.04480	-0.46076

50	H	-0.32107	-0.28587	0.12913
51	H	-0.52531	-0.20659	0.02894
52	H	-0.45310	-0.05330	0.12282
53	H	-0.47802	-0.02459	-0.01226
54	H	-0.21182	-0.45940	0.06447
55	H	-0.20409	-0.61642	-0.09153
56	H	-0.46340	-0.29422	-0.30351
57	H	-0.45883	-0.12765	-0.14966
58	H	-0.33513	-0.47647	-0.36466
59	H	-0.25917	-0.63744	-0.27936
60	H	-0.51698	-0.61408	-0.36535
61	H	-0.50858	-0.89730	-0.30923
62	H	-0.35597	-0.88734	-0.26135
63	H	-0.43024	-0.76837	-0.20019
64	H	-0.52234	-0.83229	-0.49023
65	H	-0.44969	-0.65760	-0.51232
66	H	-0.36933	-0.82414	-0.43622

REFERENCES

1 R.E.Gordon & S.I.Amin (1986) European Patent 0 120 587 B1.

2 L.Addadi, Z.Berkovitch-Yellin, I.Weissbuch, M.Lahav & L.Leiserowitz (1983) Mol.Cryst.Liq.Cryst. 96, 1-17

3 Z.Berkovitch-Yellin, J.van Mil, L.Addadi, M.Idelson, M.Lahav & L.Leiserowitz (1985) J.Am.Chem.Soc. 107, 3111-3122

4 J.L.Wang, Z.Berkovitch-Yellin & L.Leiserowitz (1985) Acta Cryst. B 41, 341-348

5 M.E.Aulton, D.N.Travers & P.J.P.White (1973) J.Pharm.Pharmacol. 25 suppl 79p-86p

6 E.N.Hiestand & D.P.Smith (1984) Powder Tech. 38, 145-149

7 M.A.Peacock, J.D.H.Donnay & G.Donnay (1960) in Techniques of Organic Chemistry Vol. I. Physical Methods Part II. Ed A.Weissberger 3rd edn. Interscience, New York.

8 R.M.Hooper and K.J.Roberts (1982) University of Strathclyde, unpublished work

9 J.W.Gibbs (1878) Trans.Comm.Acad.Arts Sci. 3, 343-356

10 G.Wulff (1901) Z.Krist.,34, 449-455

11 J.D.H.Donnay and D.Harker (1937) Am.Mineralogist 22 463-511

12 P.Hartman & W.G.Perdok (1955) Acta cryst. 8, 49-52

13 P.Hartman (1973) in Crystal growth: an introduction, Ed.P.Hartman, North-Holland, Amsterdam, 367-392

14 M.Born (1923) Atomtheorie des festen Zustandes, 2nd edn. p538. Leipzig; Berlin: Teuber.

15 P.Hartman & P.Bennema (1980) J.Cryst.Growth 49, 145-152

16 G.Filippini, C.M.Gramaccioli & M.Simonetta (1979) J.Chem.Phys. 71, 71-85

17 G.S.Pawley & S.L.Chalpot (1980) Phys.Status Solidi (b) 99, 517-522

18 A.J.Pertsin and A.I.Kitaigorodskii (1987) in, The Atom-atom Potential Method. Applications to Organic

Molecular Solids ch.1., Springer-Verlag

19 J.B.Bates and W.R.Busing (1974) J.Chem.Phys. 60(2), 2414-2419

20 W.C.Burton, N.Cabrera and F.C.Frank (1951) Proc.Roy.Soc.Lond. A243, 299-358

21 F.C.Frank (1949) Disc.Faraday Soc. 5, 48-54

22 K.A.Jackson (1958) Liquid metals and solidification, American Society for Metals, Cleveland, Ohio, 174-186

23 J.R.Bourne and R.J.Davey (1976) J.Cryst.Growth 36, 278-286

24 P.Bennema and G.H.Gilmer (1973) in Crystal Growth: An Introduction, Ed. P.Hartman, North-Holland, Amsterdam, ch.10

25 H.J.Human, J.P.Van der Eerden, L.A.M.J.Jetten and J.G.M.Odekerken (1980) presented at ICCG-6, Moscow

26 S.W.H. de Haan, V.J.A.Meeusen, B.P.Veltman, P.Bennema, C.van Leeuwen and G.H.Gilmer (1974) J.Cryst.Growth 24/25, 491-494

27 J.R.Bourne and R.J.Davey (1976) J.Cryst.Growth 36, 287-296

28 J.R.Bourne & R.J.Davey (1977) J.Cryst.Growth 39, 267-274

29 R.J.Davey (1982) in Current Topics in Materials Science, Vol.8, ed. E.Kaldis. North-Holland Publishing Co., Amsterdam

30 A.E.D.M.Van der Heijden, R.M.Geertman & P.Bennema (1991) J.Phys.D: Appl.Phys. 24, 123-126

31 B.R.Pamplin (1980) Crystal Growth 2nd edn., Pergamon Press, London, Chapter 1

32 H.E.Buckley (1935) Z.Krist 91, 375-381

33 H.E.Buckley (1952) Crystal Growth, Chapman & Hall, London

34 S.N.Black, R.J.Davey and M.Halcrow (1986) J.Cryst.Growth 79, 765-774

35 L.Addadi, Z.Berkovitch-Yellin, N.Domb, E.Gati, M.Lahav and L.Leiserowitz (1982) Nature 296, 21-26

36 Z.Berkovitch-Yellin, L.Addadi, M.Idelson,

L.Leiserowitz and M.Lahav (1982) Nature 296, 27-34

37 Z.Berkovitch-Yellin, L.Addadi, M.Idelson, M.Lahav and L.Leiserowitz (1982) Angew.Chemie suppl. 1336-1345

38 L.Addadi, Z.Berkovitch-Yellin, I.Weissbuch, M.Lahav, L.Leiserowitz and S.Weinstein (1982) J.Amer.Chem.Soc. 104, 2075-2077

39 J.L.Wang, Z.Berkovitch-Yellin & L.Leiserowitz (1985) Acta Cryst. B41, 341-348

40 D.Hull (1975) Introduction to dislocations 2nd edn., Pergamon Press, London

41 A.R.Lang (1973) in Crystal Growth: an introduction Ed. P.Hartman, North-Holland, Amsterdam.

42 J.M.Burgers (1939) Proc.Kom.Ned.Acad.Wet., 47, 293-378

43 H.K.Chan & D.J.W.Grant (1989) Int.J.Pharm. 57, 117-124

44 P.York & D.J.W.Grant (1985) Int.J.Pharm. 25, 57-72

45 W.G.Johnston (1961) Progress Ceram.Sci. 2, 1-7

46 J.M.Thomas & B.D.Renshaw (1967) J.Chem.Soc. A. 2058-2062

47 J.M.Thomas & B.D.Renshaw (1969) J.Chem.Soc. A. 2749-2752, 2753-2755, 2756-2759

48 J.M.Thomas & J.O.Williams (1967) Trans.Farad.Soc. 63, 1922-1928

49 I.D.Begg, P.J.Halfpenny, R.M.Hooper, R.S.Narang, K.J.Roberts & J.N.Sherwood (1983) Proc.Roy.Soc.Lond. A386, 431-442

50 A.G.Mitchell, B.L.Milaire, D.J.Saville & R.V.Griffiths (1971) J.Pharm.Pharmacol. 23, 534-535

51 R.Huttenrauch (1978) Acta Pharm.Technol. Suppl. 16, 55-127

52 W.C.Duncan-Hewitt & D.J.W.Grant (1986) Int.J.Pharm. 28, 75-84

53 E.N.Hiestand, G.E.Amidon, D.P.Smith and B.D.Tiffany (1981) Proc.Int.Powd.Bulk Solids & Handling Proc., Rosemount, Illinois, 383-387

54 P.York (1983) Int.J.Pharm. 14, 1-28

55 M.P.Summers. R.D.Enevers & J.E.Carless (1977) J.Pharm.Sci. 66. 1172-1175

56 K.Ridgway & R.Rupp (1969) J.Pharm.Pharmacol. 21 suppl.. 30s-39s

57 K.Ridgway & J.B.Scotton (1970) J.Pharm.Pharmacol. 22 suppl. 24s-28s

58 D.L.Simmons. N.D.Gyanchandani & P.Picotte (1972) Can.J.Pharm.Sci. 7. 121-123

59 Y.Nakai. E.Fukoaka & H.Nakagawa (1978) Yakugaka Zasshi 98. 23-30

60 Y.Nakai. E.Fukoaka & H.Nakagawa (1978) Yakugaka Zasshi 98. 184-190

61 H.Nakagawa. E.Fukoaka & Y.Nakai (1979) Yakugaka Zasshi 99. 936-943

62 R.Tindle. J.W.Kennerley & R.P.Scherer (1984) Proc. 4th Pharm.Tech.Conf.Edinburgh Vol III p 175-195

63 K.Ridgway. J.Glasby & P.H.Rosser (1969) J.Pharm.Pharmacol. 21 suppl. 24s-29s

64 M.E.Aulton (1977) Manuf.Chem. 48(5). 28-36

65 K.Ridgway, E.Shotton & E.Glasby (1969b) J.Pharm.Pharmacol. 21 suppl., 19s-23s

66 J.Ichikawa, K.Imagawa & N.Kaneniwa (1988) Chem.Pharm.Bull. 36(7), 2699-2702

67 K.Ridgway & M.E.Aulton (1971) J.Pharm.Pharmacol. 23 suppl., 111s-120s

68 S.Malamataris, S.bin Baie & N.Pilpel (1984) J.Pharm. Pharmacol. 36, 616-617

69 E.N.Hiestand, J.E.Wells, C.B.Peot & J.F.Ochs (1977) J.Pharm.Sci. 66, 510-519

70 W.C.Duncan-Hewitt & G.C.Weatherley (1989) Pharm.Res. 6(5), 373-378

71 N.Kaneniwa, K.Imagawa & J.Ichikawa (1988) Chem.Pharm.Bull. 36, 2531-2537

72 A.H-L.Chow, P.K.K.Chow, W.Zhongshan & D.J.W.Grant (1985) Int.J.Pharm. 24, 239-258

73 K.Y.Chow, J.Go, M.Mehdizadeh & D.J.W.Grant (1984) Int.J.Pharm. 20, 3-24

74 P.Knoop, C.G.Peters & W.B.Emerson (1939)
J.Res.Nat.Bur. Stand. 23, 39-63

75 D.Tabor (1970) Rev.Phys.Technol. 1(3), 145-179

76 J.M.Thomas & G.D.Renshaw (1965) Trans.Farad.Soc.
61, 791-796

77 J.M.Thomas & G.D.Renshaw (1968)
J.Chem.Soc.Chem.Comm. 987, 1247-1248

78 C.A.Brookes & R.P.Burnand (1973) in The Science of
Hardness Testing and its Research Applications, Eds
J.H.Westbrook & H.Conrad, American Society for
Metals, Cleveland, Ohio

79 H.M.Burt & A.G.Mitchell (1981) Int.J.Pharm. 9,
137-152

80 A.H.-L.Chow & D.J.W.Grant (1989) Int.J.Pharm. 51,
129-135

81 K.J.Roberts, J.N.Sherwood, D.K.Bowen & S.T.Davies
(1983) Materials Letters 2(2), 104-110

82 M.M.Mitrovic, R.I.Ristic & I.Ciric (1990) Appl.Phys
A 51(5), 374-378

83 D.K.Tanner (1976) X-ray Diffraction Topography, Pergamon Press, London

84 A.R. Lang (1978) in Modern diffraction and imaging Techniques in Materials Science Ed. S.Amelinckx, North-Holland, Amsterdam

85 British Pharmacopeia (1988)

86 Dictionary of Organic Compounds 5th edn. (1982) Chapman and Hall, London

87 P.V.Marshall (1987) Ph.D.Thesis, University of Bradford

88 Manufacturers data

89 R.M.Hooper, B.J.McArdle, R.S.Narang & J.N.Sherwood (1980) in Crystal Growth, Ed. Pamplin, Pergamon Press, London, Chapter 10

90 P.Hartman (1963-1965) in Physics and Chemistry of the Organic Solid-state, Vol.I, Eds. D.Fox, M.M.Labes & A.Weissberger, Interscience, New York

91 L.J.Gilmore (1984) J.Appl.Cryst. 17, 42-46

92 P.R.Mallinson and K.W.Muir (1985) J.Appl.Cryst. 18, 51-53

93 A.Guinier (1978) in Diffraction and Inaging Techniques in Materials Science, Eds. S.Amelinckx, R.Gevers & J.Van Landuyt, North-Holland, Amsterdam

94 A.Authier (1978) in Modern Diffraction and Imaging Techniques in Material Science, Ed.S.Amelinckx, North-Holland, Amsterdam

95 P.J.Halfpenny (1982) Ph.D.Thesis, University of Strathclyde

96 H.M.Burt & A.G.Mitchell (1980) Int.J.Pharm. 5, 239-251

97 H.M.Burt & A.G.Mitchell (1979) Int.J.Pharm. 3, 261-274

98 J A Brinell & A Wahlberg (1901) J.Iron & Steel Inst. 59, 243-248

99 H.Weingraber (1948) Die Technik 3, 417-420

100 R.Smith & J.Sandland (1925) J.Iron & Steel Inst. 1, 285-293

101 C.A.Brookes & B.Moxley (1975) J.Phys E: Scientific Instruments 8, 456-460

102 J.H.Westbrook & H.Conrad (Eds) (1973) The Science of Hardness testing and its research applications, The American Society for Metals, Cleveland, Ohio

103 H.O'Neil (1934) The hardness of metals and its measurement. Sherwood Press, Cleveland, Ohio

104 C.A.Brooke (1983) in Science of hard materials, Eds. Viswandham, Rowcliffe and Gurland, Plenum Press, New York

105 H.O'Neill (1967) Hardness measurements of metals and alloys 2nd edn. Chapman and Hall, London

106 F.W.Daniels and C.G.Dunn (1949) Trans.A.S.M. 41, 419-427

107 A.W.Cottrell (1953) Dislocations and Plastic Flow in Crystals, Oxford University Press, Oxford

108 J.J.Gilman & W.G.Johnstone (1959) J.Appl.Phys. 30(2), 129-135

109 N.Cabrera (1957) Semiconductor Surface Physics, Ed.R.H.Kingston, Univ.Pennsylvania Press,

Philadelphia

110 C.A.Brookes, J.B.O'Neill & B.A.W.Redfern (1971) Proc.Roy.Soc. Lond.A 322, 73-88

111 C.K.Johnstone (1976) Oakridge National Laboratories

112 P.Bladon & R.Breckenridge (1989) University of Strathclyde

113 B.Stokes, R.Keown and K.Dyson (1968) J.Appl.Cryst. 1, 68-70

114 R.Docherty, K.J.Roberts & E.Dowty (1988) Comp.Phys.Comm. 51, 423-430

115 E.Dowty (1980) Am.Mineral. 65, 465-469

116 G.Clydesdale, R.Docherty & K.J.Roberts (1991) Comp.Phys.Comm. 64, 311-328

117 A.A.Freer (1989) personal communication

118 A.T.Hagler, E.Huler & S.Lifson (1973) J.Am.Chem.Soc. 96(17), 5319-5327

119 C. Zhangfeng (1990) personal communication

120 J.Bunyan, N.Shankland & D.B.Sheen (1991) in

Particle Design Via Crystallisation, AIChE Special Symposium Series 284(87), 44-57

121 S.Lifson, A.T.Hagler and P.Dauber (1979) J.Am.Chem.Soc. 101, 5111-5121

122 H.Umeyama, S.Nakagawa & I.Moriguchi (1979) J.Phys.Chem. 83(15), 2048-2052

123 J.Hildebrand & R.Scott (1949) Solubility of non-electrolytes. 3rd edn.. Reinhold publishing Corp. New York

124 J.Hildebrand & R.Scott (1962) Regular Solutions, Prentice-Hall, Englewood Cliffs, New Jersey

125 Kirk-Othmer Encyclopaedia of Chemical Technology, 2nd edn. Supplement volume, p889-910, Interscience (1971)

126 A.T.Florence, E.G.Salole & J.B.Stenlake (1974) J.Pharm.Pharmac.26, 479-480

127 K.Y.Chow, J.Go, W.Zhongshan, M.Mehdizadeh, & D.J.W.Grant (1985) Int.J.Pharm. 25, 41-56

128 K.D.Ertel, R.A.Heasley, C.Koegel, A.Chakrabarti & J.T.Carstensen (1990) J.Pharm.Sci. 79, 552

129 A.T.Hagler, E.Huler & S.Lifson (1974)
J.Am.Chem.Soc. 96, 5319-5327

130 N.Shankland, D.B.Sheen and K.J.Roberts, (1991)
unpublished results

131 A.T.Gray (1991) Personal Communication

132 J.Jacques, A.Collet & S.H.Wilen (1981) Enantiomers,
Racemates & Resolutions, Wiley, New York

133 R.I.Ristic, J.N.Sherwood & K.Wojciechowski (1988)
J.Cryst.Growth 91, 163-166

134 H.Gallacher, A.Littlejohn, D.B.Sheen & J.N.Sherwood
(1987) Cryst.Latt.Def.& Amorph.Mat. 16, 137-143

135 K.Kendall (1978) Nature 272, 710-711

136 R.HÖttenrauch (1977) Proc. 1st
Inter.Conf.Pharm.Tech., Paris, p114-120

137 A.A.Freer, J.M.E.Bunyan, N.Shankland & D.B.Sheen
(1992) submitted to Acta Cryst.